Naphthylisoquinoline Alkaloids: Structural Elucidation, Metabolism, and Functional Analysis of their Bioactivities

DISSERTATION ZUR ERLANGUNG DES

NATURWISSENSCHAFTLICHEN DOKTORGRADES

DER BAYERISCHEN JULIUS-MAXIMILIANS-UNIVERSITÄT WÜRZBURG

vorgelegt von

Johan Henrik Faber

aus

Kopenhagen,

Dänemark

Würzburg 2006

Eingereicht am: _____

bei der Fakultät für Chemie und Pharmazie

1. Gutachter: _____

2. Gutachter: _____

der Dissertation

1. Prüfer: _____

2. Prüfer: _____

3. Prüfer: _____

des Öffentlichen Promotionskolloquiums

Tag des Öffentlichen Promotionskolloquiums: _____

Doktorurkunde ausgehändigt am: _____

Die vorliegende Arbeit wurde in der Zeit von Februar 2002 bis September 2005

am Institut für Organische Chemie der Universität Würzburg angefertigt

Herrn Prof. Dr. Dr. h.c. G. Bringmann danke ich für

die hervorragende Unterstützung dieser Arbeit,

die freundliche Atmosphäre

und die exzellenten Arbeitsbedingungen

Teile der im Rahmen dieser Arbeit erzielten Ergebnisse waren bereits Gegenstand von Publikationen[31,104,117,126,132,147,154,211,241] sowie von Postern und Vorträgen

Dedicated to my family

Contents

RESULTS AND DISCUSSION

1 Introduction

Historically, man has used plants to supply almost all of his basic needs such as foods clothing, shelter, and medicines.[1,2] Plants have formed the basis of sophisticated traditional medicine systems that have been in existence for thousands of years.[1] For example Hippocrates (5th century B.C.) mentioned 300 to 400 medicinal plants in his writings and Diosocorides (1st century B.C.) wrote *De Materia Medica*, a medicinal plant treatise that outlined the medical use of numerous of plant species. Many hundred of plant remedies are also described in the Papyrus of Ebers, discovered in Egypt, which was written about 1550 B.C.[2,3] Furthermore, traditional Chinese medicine uses multiple plant prescriptions and has served the health needs of the Chinese population for over 5000 years.[4] The Bible also describes over 30 plant species, including frankincense and myrrh, which are reported to have antiseptic and healing properties.[3] The history of medicinal plant use in North America's began with the native indigenous cultures,[5] and medicinal plants played an important role in the medical practices among the Americans of European origin from about 1620 to 1920 A.D.[1]

The introduction of acetylsalicylic acid as an analgesic in 1897 by Bayer & Company marked the beginning of the era of synthetic pharmaceuticals.[6] Synthetic Chemistry dominated the 20th century and allowed the pharmaceutical industry to become tremendously successful in the prevention and treatment of disease, although the compounds synthesized most often were structurally based on natural products.

Over the past 10 to 15 years alternative drug discovery methods such as rational drug design[7,8] and combinatorial chemistry[9,10] have placed great pressure on natural product drug discovery programs and during this period most major pharmaceutical companies have terminated or considerably scaled down their natural products operations.[11] Recently, a very interesting methodology has been developed based on the utilization of high-energy γ-irradiation derived from a ^{60}Co source as an initiator of random free radical recombinations in aqueous solutions of bioactive compounds.[12,13] However, despite the promise of these alternative drug discovery methods, there is still a shortage of lead compounds progressing into clinical trials.

This development has contributed to a steady decline in the output of the R&D programs of the pharmaceutical industry the recent years.[14] The number of new active substances also known as new chemical entities, hit a 20-year low of 37 in 2001.[15] Further evidence of this drop in productivity is evident from the report that only 16 new drug applications had been

received by the U.S. Food and Drug Administration (FDA) in 2001, down from 24 the previous year.[15]

The use of plants in the traditional medicine system continue to play an essential role in health care, and it has been estimated by the World Health Organization (WHO) that approximately 80% of the world's inhabitants rely mainly on such traditional medicines for their primary health care.[16] Plant products also play an important role in the health care systems of the remaining 20% of the population, mainly residing in developed countries, and at least 119 chemical substances, derived from 90 plants species, can be considered as important drugs currently in use in one or more countries.[16] Of these 119 drugs, 74% were discovered as a result of chemical studies directed at the isolation of the active substances from plants used in traditional medicine.[16]

An important example of such a plant derived drug is the antimalarial drug quinine (**1**) (Figure 1), which formed the basis for the synthesis of several quinoline derivatives. The most commonly used antimalarial drugs chloroquine (**2**) and mefloquine (**3**) are representatives of these derivatives (Figure 1). Quinine (**1**) was originally isolated in 1820 by French pharmacist Caventou and Pelletier from the bark of *Cinchona* species (*e.g.*, *C. officinalis*), which had long been used by indigenous groups in the Amazon region for the treatment of fevers, and was introduced into Europe in the 1600s for the treatment of malaria. The excessive application of these antimalarial drugs has led to a resistance of global extent.[17] Malaria is a life-threatening parasitic disease, which annually causes over one million deaths and currently is a menace to 40% of mankind. In 1989 the WHO declared the control of malaria to be a global priority,[18] which makes the investigation of new antimalarial compounds of utmost importance.

Artemisia annua (Quinghaosu) has been revealed to be an important plant in the search for urgently needed new drugs against malaria. The plant has long been used in the treatment of fevers in traditional Chinese medicine, and has yielded the antimalarial drug artemisinin (**4**) (Figure 1), effective against most chloroquine (**2**) resistant *Plasmodium* strains.[19]

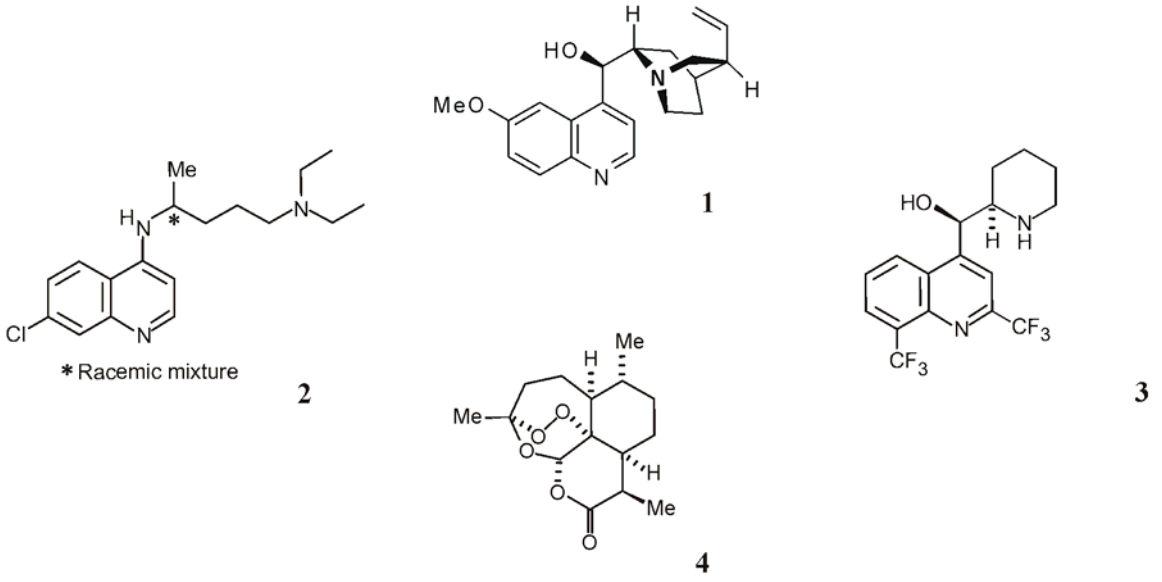

Figure 1. Four important antimalarial drugs: the plant derived quinine (**1**), the quinoline derivatives chloroquine (**2**), mefloquine (**3**), and the likewise plant derived artemisinin (**4**).

Extracts of the plant species Ancistrocladaceae and Dioncophyllaceae, two closely related tropical liana families,[20] have been widely applied in traditional medicine in several countries, including the treatment of malaria.[21] Examination of these extracts has revealed that the profound biological activity is due to the presence of naphthylisoquinoline alkaloids, for which the phytochemical incidence seems to be restricted to these two small plant families.[22] The structurally unique naphthylisoquinoline alkaloids are characterized by a biaryl system consisting of a naphthalene and an isoquinoline moiety. Many of these alkaloids display atropisomerism, since the biaryl axis usually is rotationally hindered due to the presence of bulky *ortho*-substituents, ancistrocladinine (**5**) (Figure 2) was one of the first naphthylisoquinoline alkaloids ever to be fully structural elucidated.[23]

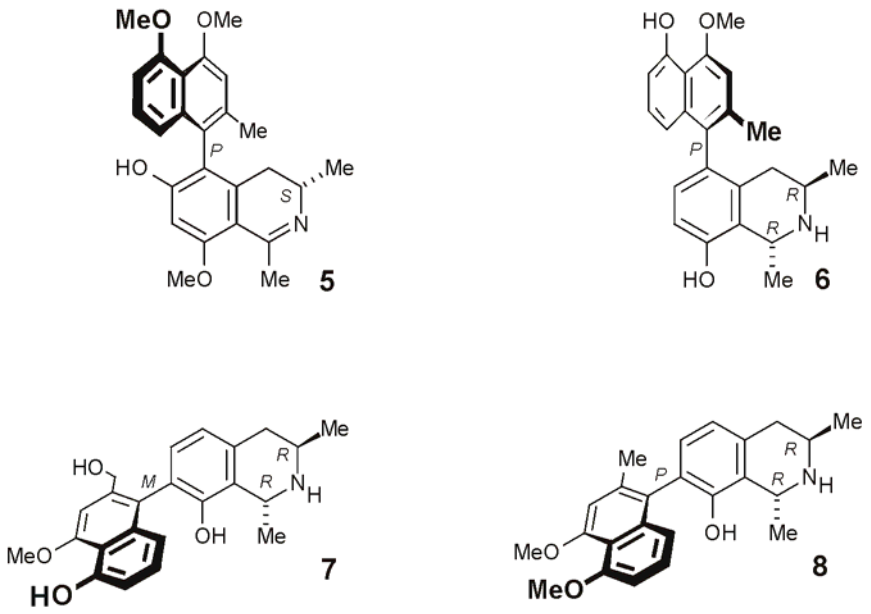

Figure 2. Structures of the naphthylisoquinoline alkaloids ancistrocladinine (**5**), dioncophylline C (**6**), dioncopeltine A (**7**), and dioncophylline A (**8**).

Recently, it has been demonstrated that these secondary metabolites are biosynthesized by an acetate – polymalonate pathway unique for isoquinoline alkaloids.[24] The broad structural variety within the naphthylisoquinoline alkaloids arises from their probable biosynthetic formation through oxidative phenolic coupling of the two bicyclic systems, which can generate a multitude of possible structures.[25] Many of the about 120 alkaloids of this type so far isolated, exhibit very promising biological activities, such as spasmolytic activity,[26] anti-HIV activity,[27-29] antileishmanial activity,[30,31] antitrypanosomal properties,[32] molluscicidal activity,[33,34] larvicidal activity,[35] insecticidal activity,[36-39] and fungicidal activity.[40]

However, of the greatest pharmacological significance is the distinct antiplasmodial activity against *Plasmodium falciparum*, the pathogenic agent of the pernicious *malaria tropica*. The two most active representatives, dioncophylline C (**6**) (IC_{50} = 15 ng/mL)[41] and dioncopeltine A (**7**) (IC_{50} = 21 ng/mL)[42] (Figure 2) are almost as active as chloroquine (**2**) (IC_{50} = 7 ng/mL)[41] in *in vitro* assays against *P. falciparum*. In a rodent model (OF1 mice infected with *P. berghei*), intravenous application of dioncophylline C (**6**) (ED_{50} = 1.90 mg kg^{-1} d^{-1}) and dioncopeltine A (**7**) (ED_{50} = 10.71 mg kg^{-1} d^{-1}) achieved a complete clearance of parasites from the circulation of *P. berghei* infected mice.[43]

These findings make the search for further new compounds of this type potentially rewarding since the naphthylisoquinoline alkaloids represent a promising class of lead structures of novel antimalarial drug candidates.

The mechanism of the antimalarial activity displayed by this compound class has been postulated to be similar to that of chloroquine (**2**), inhibiting the degradation of toxic heme metabolite ferriprotoporphyrin IX (FPIX) (**9**) (Figure 3) in the food vacuole of the malaria parasite,[44] but they are also strongly active against chloroquine (**2**) resistant strains.[45] Still a lot of research remains to be done in order to acquire an in depth understanding of the mode of action of the antimalarial activity shown by the naphthylisoquinoline alkaloids.

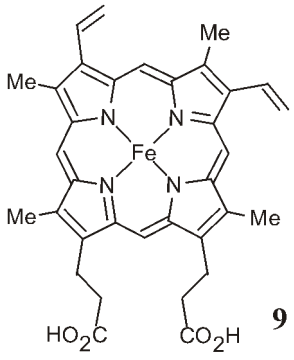

9

Figure 3. Structure of ferriprotoporphyrin IX (FPIX) (**9**) a heme metabolite toxic to the malaria parasite.

In contrast to the bioactivity screening of the naphthylisoquinoline alkaloids, virtually nothing is known about the biotransformation and toxicokinetics of these compounds. An incubation experiment with dioncophylline A (**8**) (Figure 2) has been performed with rat liver microsomes.[46] From subsequent GC-MS analysis of the incubation mixture hints were obtained of the formation of an *O*-demethylation product of **8**. However, an unequivocally assignment of the exact identification of the *O*-demethylation site was not established. A better understanding of the pharmacokinetics of the compounds and more extended experiments are needed to unravel the underlying mode of action of the antiplasmodial activity displayed by these alkaloids.

The process of drug development from drug discovery to marketed drugs has been estimated to take en average period of 10 years and cost more than 800 million dollars.[47] Furthermore, it has been estimated that only one in 5000 lead compounds will successfully advance through clinical trials and be approved for use. The first step in the process is the lead identification. Secondly comes the preclinical phase, which includes: scale-up of bioactive

lead compound, optimization, mode of action analysis, toxicology, absorption, distribution, metabolism, and excretion investigations.[48] Some of the important goals of pre-clinical studies are to secure the availability of the compound and to identify all hazards and risks associated with the treatment, before starting the final steps of the process: the clinical trials in humans.[49]

The main aims of this project were apart from isolation and identification of novel bioactive compounds, to optimize the scale-up isolation process of already known naphthylisoquinoline alkaloids and carry out pre-clinical investigations of these compounds in collaboration with cooperation partners within the interdisciplinary project SFB 630 entitled: Recognition, Preparation, and Functional Analysis of Agents Against Infectious Diseases.

In detail the present work was devoted to the following aims:

I. Phytochemical and chemotaxonomic investigations of Ancistrocladaceae species:

- Phytochemical investigation of the leaves from the East African liana *Ancistrocladus tanzaniensis*.
- Phytochemical investigation of the leaves from a novel and botanically yet undescribed Congolese *Ancistrocladus* species collected in the habitat Yeteto.

I. Large scale isolation of bioactive naphthylisoquinoline alkaloids from *T. peltatum*, using the new method fast centrifugal partition chromatography (FCPC).

II. γ-ray synthesis of antiplasmodial bioactive naphthylisoquinoline analogs, by irradiation using a ^{60}Co source of commercial available isoquinoline and other aromatic compounds, followed by an antiplasmodial activity guided isolation of the irradiation products.

III. Characterization of interactions between naphthylisoquinoline alkaloids and FPIX (**9**) and comparison of these interactions with chloroquine (**2**)-FPIX (**9**) interactions, using CD, UV, NMR, and MS spectroscopy.

IV. Phase 1 and 2 drug metabolism investigations of antiplasmodially active naphthylisoquinoline alkaloids using rat liver microsomes.

2 Mode of Action of Quinoline Antimalarial Drugs

Malaria is an infectious disease causing more than 500 million incidences and 1.3 million deaths[50] every year mainly in Sub-Saharan Africa. The cheapest and readily available antimalarial drug is chloroquine (**2**), which is a representative of the quinoline derivatives an important series of chemically related antimalarial agents.[51,52] Adverse reactions in a large number of patients[53] combined with the growing resistance of the most dangerous malarial parasite *Plasmodium falciparum*[54] to quinoline antimalarials (*e.g.*, quinine (**1**), chloroquine (**2**), mefloquine (**3**), and amodiaquine (**10**), (Figure 4)[55] make the investigation of the mode of action of these drugs a major issue.

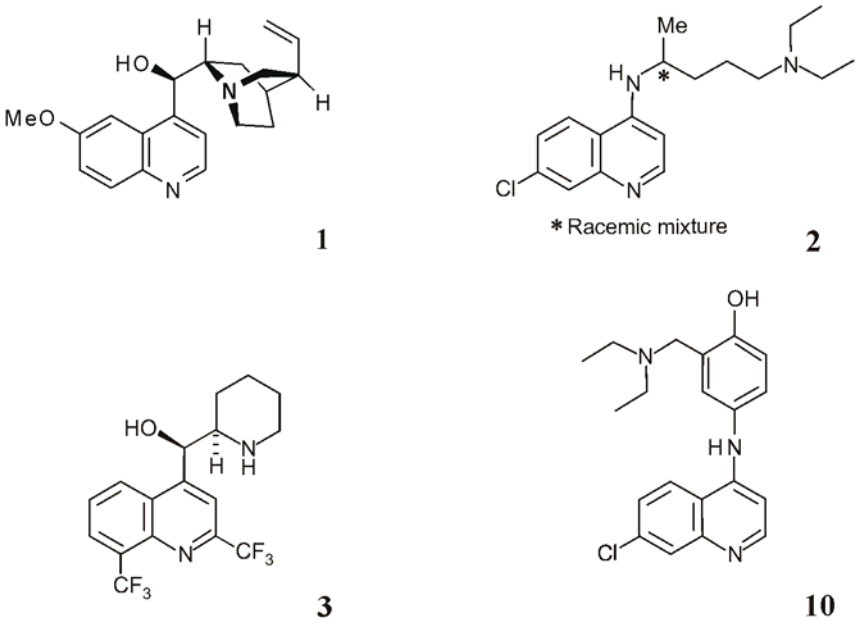

Figure 4. Some of the most commonly used antimalarial drugs: quinine (**1**), chloroquine (**2**), mefloquine (**3**), and amodiaquine (**10**).

During the pathogenic blood stage of the malaria infection, the parasite resides for almost its entire life cycle inside the red blood cells of the host.[52] The cytosol of these cells are ingested into a specialized acidic organelle called a food vacuole, where hemoglobin is enzymatically digested.[56] In the process, large quantities of ferriprotoporphyrin IX (FPIX) (**9**) (Figure 6) are released into the food vacuole. The metabolite which is noxious to the parasite,[52] is converted into a insoluble and crystalline form called malaria pigment equivalent to hemozoin,[57] which is nontoxic to *P. falciparum* and appears as dark black spots in the red blood cells of infected patients.[56]

It has become increasingly evident that the mode of action of most antimalarial drugs is to interfere with hemozoin formation inside the food vacuole of the parasite.[58- 62] Quinoline antimalarial drugs act by inhibiting FPIX (**9**) crystal growth.[63] Inhibition is stage-specific for parasites actively degrading FPIX (**9**)[64] and the quinolines concentrate to millimolar levels in the food vacuole, despite circulating in the plasma at nanomolar concentrations.[65,66] The weak base properties of chloroquine (**2**) (pK_{a1}= 8.1; pH_{a2} = 10.2) would explain its selective accumulation in the food vacuole.[66] At neutral pH, chloroquine (**2**) is uncharged and can diffuse freely through membranes; at acidic pH (*viz.*, in the food vacuole) it is in its double protonated, membrane impermeable form and thus trapped inside the food vacuole. [66,67]

Complex formation between chloroquine (**2**) and FPIX (**9**) was first reported in the 1960s by Cohen et al.[68] In 1980 Fitch and coworkers proposed that FPIX (**9**) is the molecular drug target of chloroquine (**2**) and other quinoline antimalarials and further examined the equilibrium association of these compounds with FPIX (**9**).[69] Although this proposal initially met with considerable skepticism, subsequent investigations have provided that interactions of these drugs with FPIX (**9**) do indeed lie at the heart of their antimalarial activity.[70]

2.1 UV Spectroscopy

The original observation that chloroquine (**2**) forms a complex with FPIX (**9**) in solution was based on changes in the UV absorption spectrum of FPIX (**9**) upon titration with a solution of chloroquine (**2**).[68] In aqueous solutions buffered at pH 7, FPIX (**9**) exhibits a Soret absorption band with a peak at 390 nm and a shoulder at 360 nm (see Figure 5).

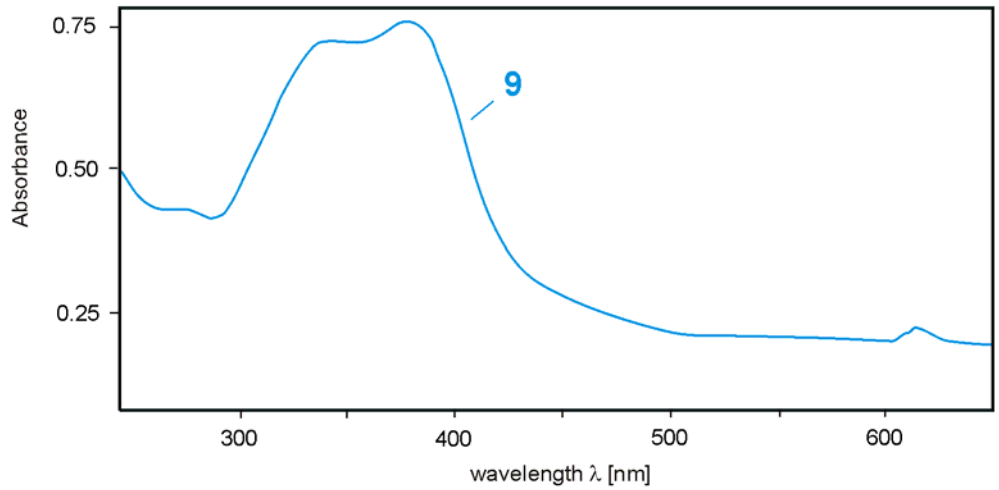

Figure 5. UV absorption spectrum of FPIX (**9**, 0.168 mM) (pH 6.5).

These spectral characteristics reflect that FPIX (**9**) (Figure 6) predominately forms a μ-oxo dimer in aqueous solutions at pH ≥ 6.5.[71,72] A crystal structure of this μ-oxo dimer is available and it was proved to consist of two FPIX monomers (**9**) bridged by an Fe-O-Fe bond (**11**) (Figure 6).[72] However, it has been found that more species exist in aqueous solution.[73-75] Among these species are the monomeric form FPIX (**9**) and a precursor for hemozoin represented by structure **12** a dimer where the propionic acid side chain of each FPIX (**9**) portion is chelated with the Fe center of the adjacent FPIX (**9**) moiety (Figure 6).[73]

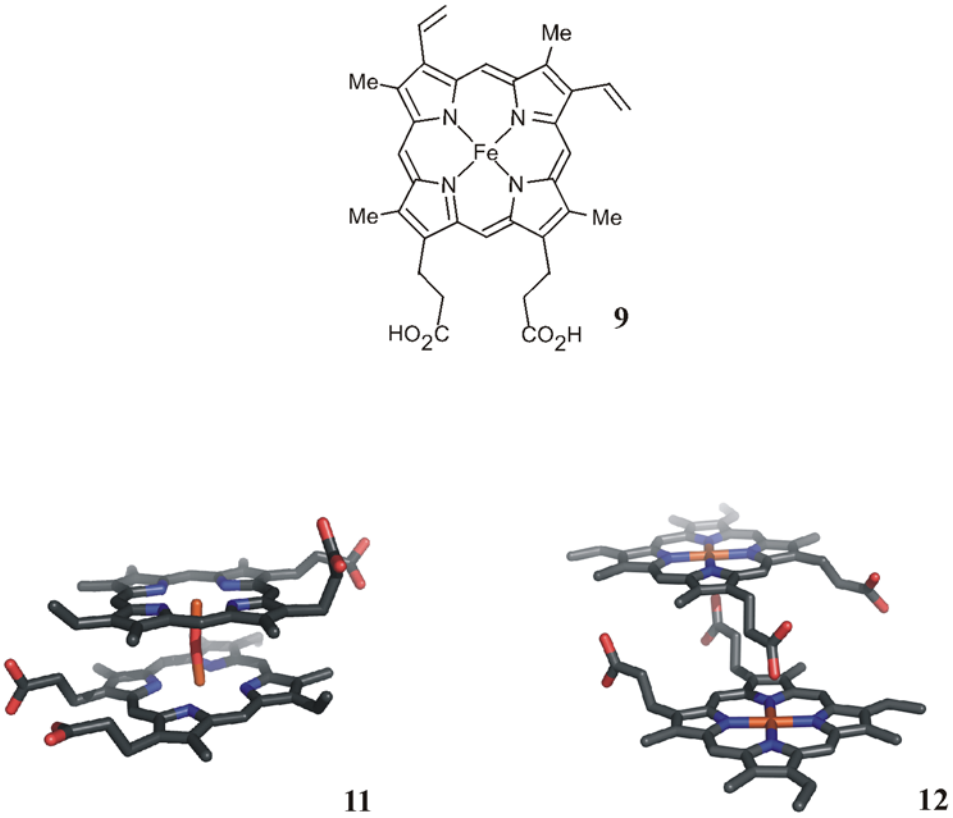

Figure 6. The structures of FPIX (**9**), the FPIX μ-oxo dimer (**11**), and the FPIX chelate dimer (**12**). The drawings of the last two structures were provided by K. F. Schwedhelm.

The complex formation in aqueous solution between quinoline antimalarial drugs and FPIX (**9**) results in a decrease in the intensity of 360 nm shoulder relative to the 390 nm peak of the Soret band as well as subtle changes in structure of the absorption spectrum in the longer wavelength, *i.e.,* around 600 nm.[76-78] These spectral changes are thought to derive from π–π complexation of the porphyrin quinoline ring systems.[76,79]

The study of FPIX (**9**) in aqueous solutions is rather complex due to the presence of several species. Essentially to circumvent this problem several studies of FPIX (**9**) have been performed in nonaqueous, mixed solvent or detergent solutions.[80-85] Several studies have used buffered 40% (v/v) aqueous DMSO to investigate the interaction between quinoline antimalarial drugs and FPIX (**9**), in which FPIX (**9**) is believed to be present in its monomeric form.[76,80,86,87] In this solvent system the Soret band of FPIX (**9**) exhibits a considerable hypochromic effect upon interaction with quinoline antimalarial drugs such as chloroquine (**2**) (Figure 7).[76] This hypochromic effect is more noticeable in buffered 40% (v/v) aqueous DMSO in comparison with purely aqueous medium, on account of the fact that FPIX (**9**) is

essentially dimeric under the later conditions which itself gives rise to large hypochromic effect.[70]

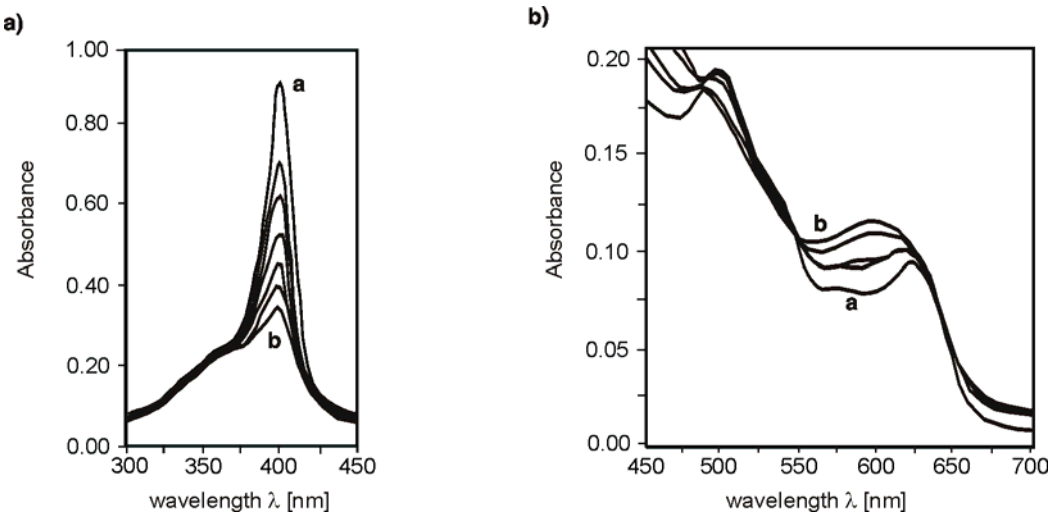

Figure 7. UV spectroscopic changes observed when FPIX (**9**) is titrated with chloroquine (**2**) studied in buffered 40% (v/v) aqueous DMSO: a) The UV bands of chloroquine (**2**) have been removed by titration of the reference cell with chloroquine (**2**). Spectra have been corrected by dilution, b) Changes in the visible region of FPIX (**9**). The sample is three times more concentrated than that used in a). In each case the inset **a** is FPIX (**9**) in the absence of chloroquine (**2**), inset **b** is a large molar excess of chloroquine (**2**) added. The figure is reproduced from Ref. [76] with permission from T. J. Egan.

The marked changes in the UV absorption spectrum of FPIX (**9**) upon interaction with chloroquine (**2**) and other quinoline antimalarials have been extremely valuable in detecting and monitoring these interactions. The quenching in of the Soret band can be used to determine association constants and stoichiometry for the complex formation.[77,78,80,86-88] There are significant discrepancies between different studies of association constants reported in various media in terms of the absolute magnitudes of constants and the stoichiometry. Thus these studies indicate that the solvent plays a major role in the strength of complex formation.

2.2 Structures of FPIX (9)-Quinoline Antimalarials in Solution

The knowledge of the structures of FPIX (**9**)–quinoline complexes derive from NMR and computational investigations. No crystal structures of such complexes are available.

A general FPIX μ-oxo dimer (**11**)–quinoline drug complex has emerged from early one dimensional NMR studies. These models were based on analysis of how paramagnetic Fe(III) center of FPIX (**9**) broadened aromatic versus aliphatic protons or carbon resonances of

quinine (**1**) and chloroquine (**2**).[89-92] These data suggested that noncovalent π–π interactions between the FPIX (**9**) tetrapyrrole and quinoline rings were likely quite significant in determining the stability of the FPIX (**9**)–quinoline drug complexes, and that interplanar distance between the FPIX (**9**) and the drug was between 3 and 5 Å.[89-92]

An approach was pursued by de Dios and coworkers, in which the first atomic resolution structures of FPIX (**9**) in complex with several antimalarial drugs were determined by NMR spectroscopy.[93] The distances between the Fe(III) center of FPIX (**9**) and the protons of the drugs were obtained by NMR studies from the effect of the paramagnetic center on T_1 ^{1}H-relaxtion rates using the Solomon-Bloembergen equation. These distances were used as restrains in calculation. The study established a 2:1 stoichiometry of the FPIX (**9**)–quinoline drug complexes, thus it was assumed that FPIX (**9**) exist as a μ-oxo dimer. In that and further NMR investigations, relaxation rates and spin states of investigated complexes were determined experimentally and found to be $S = 1/2$ for the complex of FPIX μ-oxo dimer (**11**)–chloroquine (**2**).[93-95] Furthermore, it was demonstrated that the structures do not significantly change at different pH values.[93]

There is considerable consensus in the structures proposed by different NMR studies, all giving evidence for a non-covalent interaction between FPIX (**9**) and quinoline antimalarial drugs.[90,93,96,97] The NMR based model proposed by de Dios and coworkers suggested a possible role of the side chain of chloroquine (**2**) lying in close proximity to the porphyrin ring system and stabilizing the complex (Figure 8).[93]

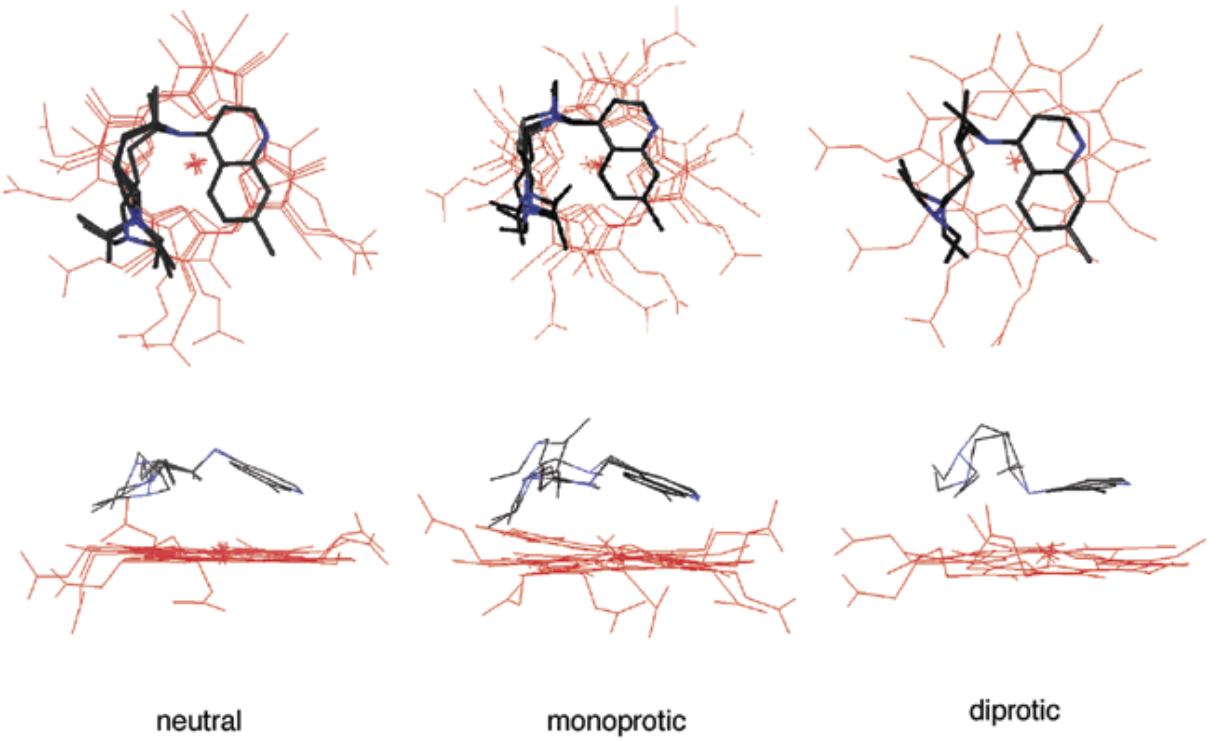

Figure 8. Axial (top) and side (bottom) views of superpositioned lowest-energy complexes formed between FPIX μ-oxo dimer (**11**) and neutral (left), +1 (middle), +2 (right) forms of chloroquine (**2**). Blue denotes nitrogen atoms in chloroquine (**2**), and red denotes the FPIX (**9**) backbone. In these images, protons and the second FPIX (**9**) monomer of the μ-oxo dimer are omitted for clarity. The figure is reproduced from Ref. [93]

2.3 Further Spectroscopic Investigations

The interaction of FPIX (**9**) with quinoline antimalarial drugs has so far been studied by applying a wide range of methods.[70,98,99] Mössbauer spectroscopy was used to observe the interaction between FPIX (**9**) and antimalarial drugs.[100] It was shown that chloroquine (**2**) binds to the FPIX μ-oxo dimer (**11**) form and a twofold mode of action for the antimalarial activity displayed by the drug was suggested, according to which chloroquine (**2**) binds to FPIX μ-oxo dimer (**11**) and inhibits hemozoin crystal formation and, additionally, soluble FPIX μ-oxo dimer (**11**)–chloroquine (**2**) complexes exert oxidative stress on the parasite from inside the food vacuole. Likewise through Mössbauer spectroscopy, the spin state of Fe(III) in pure FPIX μ-oxo dimer (**11**) was characterized.[71,101] It was found that the FPIX μ-oxo dimer (**11**) can form $S = 3/2$, $S = 5/2$ spin admixed species with weak axial quinoline ligands. Circular dichroism was used to determine the stoichiometry of the FPIX (**9**)–chloroquine (**2**) complex.[102] According to that study, a molar ratio of 2:1 for the FPIX (**9**)–chloroquine (**2**)

complex was found at basic pH values. The same stoichiometry was reported in the initial investigations on the FPIX (**9**)–chloroquine (**2**) interaction[62] and for the analogs complex formed by quinine (**1**) and urohemin using UV spectroscopy.[91] Electrospray ionization mass spectroscopy studies on complexes formed between FPIX (**9**) and antimalarial drugs showed non-covalent interactions between the molecules[75] and *m/z* values have been obtained corresponding to a FPIX μ-oxo dimer (**11**)–chloroquine (**2**) complex.[74] Further evidence of a non-covalent interaction was recently given by polarization-resolved resonance Raman spectroscopy[103,104] conducted on FPIX (**9**) in complex formation with chloroquine (**2**). Resonance Raman and UV spectroscopy also provided insight of the electronic structure of high-spin FPIX (**9**).[105]

Despite the significant advances in the understanding of FPIX (**9**)–quinoline interactions over the past decade, the relationship between formation of such complexes and the ability of the quinoline antimalarial drugs to inhibit the formation of malaria pigment *in vivo* remains elusive.

3 Isolation and Characterization of Naphthylisoquinoline Alkaloids from *Ancistrocladus tanzaniensis* Cheek & Frimodt-Møller (Ancistrocladaceae)

3.1 Introduction

The chemotaxonomic investigation of the leaves of *A. tanzaniensis* was a continuous work of my Master thesis[106] carried out the Danish University of Pharmaceutical Sciences in cooperation with P. W. Dalsgaard.

3.2 *A. tanzaniensis*

Ancistrocladus tanzaniensis Cheek & Frimodt-Møller is one of the *ca.* 17 species from the monogeneric family Ancistrocladaceae,[107] and the only second one identified in East Africa.[108,109] *A. tanzaniensis* was discovered in 1997 in the Uzungwa Mountains in Tanzania, at 1200 m above sea level, in contrast to all other *Ancistrocladus* species, which so far have been found at habitats of less than 1000 m altitude.[107,109] The plant material was collected in the Uzungwa Mountains in Tanzania by H. Ndangalsi and F. Mbago in December 2000.

3.3 Isolation and Structural Elucidation of Naphthylisoquinoline Alkaloids from *A. tanzaniensis*

3.3.1 Extraction and Isolation

Air dried leaves of *A. tanzaniensis* were ground and sequentially extracted with petroleum ether, CH_2Cl_2, and MeOH. The CH_2Cl_2 extract was concentrated in vacuo and analytical HPLC analysis (UV profile, retention time) revealed the extract to contain naphthylisoquinoline alkaloids. Intensive treatment with preparative reversed-phase HPLC afforded the isolation of pure material of **13**-**18** (Figure 9).

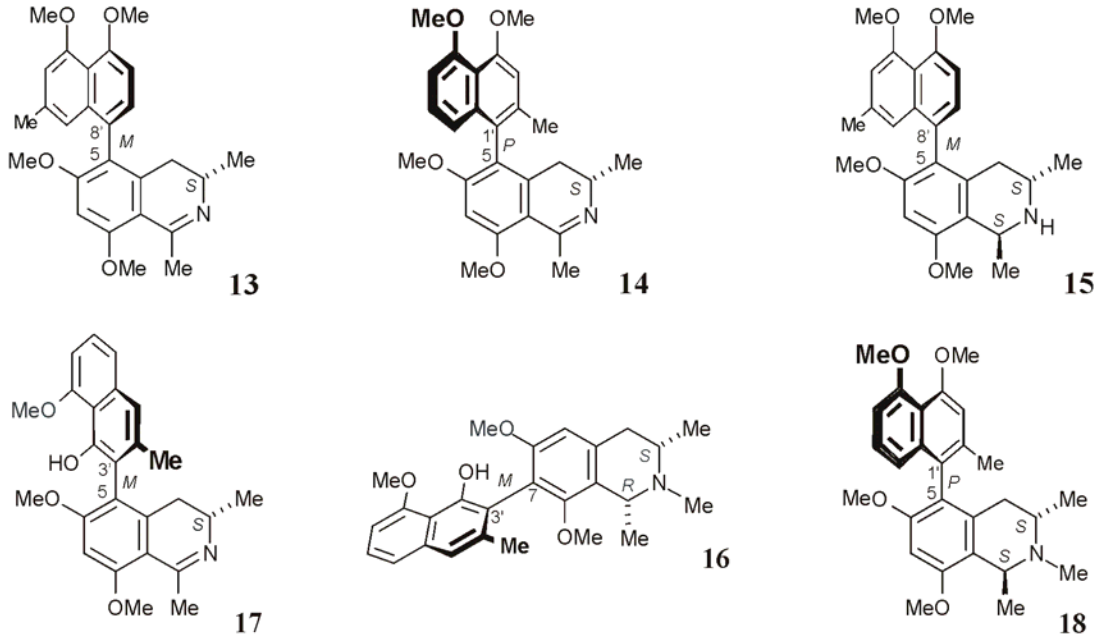

Figure 9. Structures of the naphthylisoquinoline alkaloids **13-18** isolated from *Ancistrocladus tanzaniensis.*

3.3.2 Structural Elucidation of Ancistrotanzanine B (13)

3.3.2.1 Spectroscopic Characterization

The third fastest eluting alkaloid in reversed-phase HPLC was deduced to correspond to the molecular formula of $C_{26}H_{29}NO_4$, from its HRMS (ESI) and from the ^{13}C NMR spectral data. Its ^{1}H NMR spectrum revealed a three-proton singlet at low field for CH_3-1 (2.86 ppm), which, when combined with the absence of both a three-proton doublet at *ca.* 1.5 ppm and an H-1 signal at *ca.* 4 ppm (as typical of naphthyl-1,3-methyltetrahydroisoquinolines), hinted at the presence of a naphthyldihydroisoquinoline alkaloid (Figure 10).[22] This assumption was confirmed by the chemical shift of the C-1 peak (173.9 ppm) in the ^{13}C NMR spectrum.

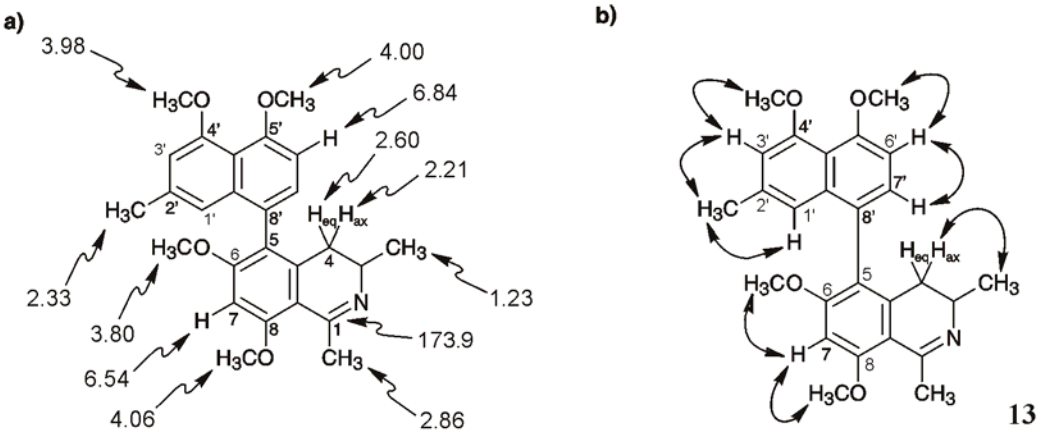

Figure 10. Selected NMR data of ancistrotanzanine B (**13**): a) ^{1}H and ^{13}C NMR shifts (δ in ppm); b) NOE interactions indicative of the constitution.

From the "normal" shifted signal of CH_3-2' (2.33 ppm), and the aromatic spin pattern system of three singlets and two doublets, the biaryl axis was excluded from being located at C-1' or C-3', leaving only C-8' or C-6' for the positioning of the biaryl axis. Of these, the latter could be eliminated by NOE interactions between H-6' (a doublet at 6.84 ppm) and the (normal-shifted) methoxy group (4.00 ppm) at C-5', revealing that the coupling position in the naphthalene moiety was located at C-8'.

Since only one out of four methoxy groups (3.80 ppm) was found to be high-field shifted (in contrast to those at 3.98, 4.00, and 4.06 ppm), the axis had to be located at C-5 of the isoquinoline unit, which was confirmed by NOE interactions between H-7 (δ 6.54) and the protons of OCH_3-6 and OCH_3-8. In conclusion, the second compound was a 5,8'-coupled naphthyldihydroisoquinoline with the constitution **13**, as shown in Figure 10.

3.3.2.2 The Absolute Configuration

Compound **13** has two stereogenic elements, the center at C-3 and the rotationally hindered biaryl axis between C-5 and C-8'. The absolute configuration at the stereocenter was assigned by a ruthenium-catalyzed oxidative degradation procedure[110,111] carried out by M. Schraut, ultimately leading to the Mosher derivative of (*S*)-3-aminobutyric acid (**19**) (Scheme 1), thus establishing the configuration at C-3 to be *S*.

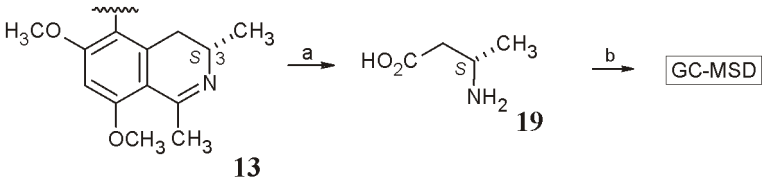

Scheme 1. Oxidative degradation of **13** and analysis of the resulting amino acids for the determination of the absolute configuration of naphthylisoquinoline alkaloids after esterification and derivatization: (a) $RuCl_3$, $NaIO_4$; (b) MeOH, $SOCl_2$ (MSD: Mass-sensitive detection).

The configuration at the biaryl axis relative to that of the stereogenic center at C-3 was deduced from NOE interactions between the protons of the aromatic methyl group (CH_3-2') and H-1' with those of the methyl group at C-3 and with H-4_{ax}, which are both below the isoquinoline plane, indicating a close spatial proximity of these atoms, and a similar specific interaction was found between H-4_{eq} and H-7'. Given the known absolute *S*-configuration at the C-3 stereogenic center, these interactions clearly indicated an absolute *M*-configuration at the axis as shown in Figure 11.

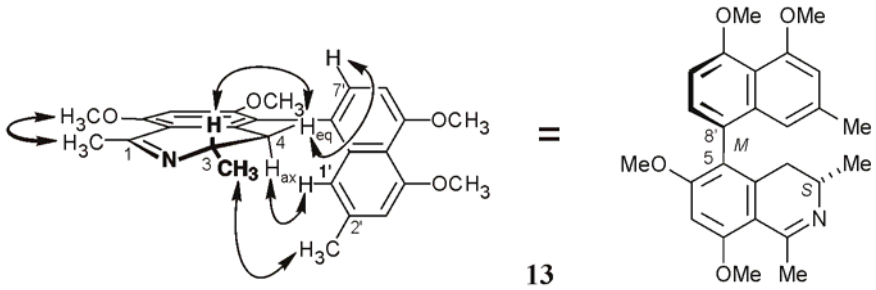

Figure 11. Configuration at the biaryl axis of **13** relative to the stereogenic center through NOE interactions.

This conclusion that the biaryl axis has the *M*-configuration was confirmed by the CD spectrum of **13**, which was opposite to that of the likewise 5,8'-coupled, but *P*-configured alkaloid ancistroealaine A (**20**) (Figure 12).[30]

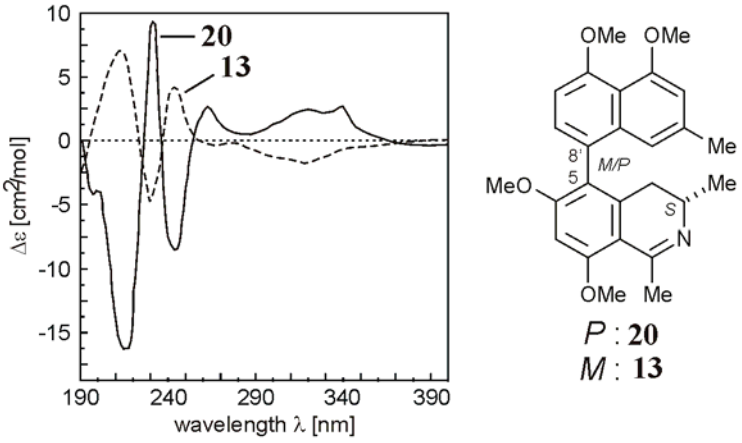

Figure 12. CD spectra of **13** and ancistroealaine A (**20**) both recorded in MeOH.

This naphthylisoquinoline alkaloid **13** was thus a new compound and was named ancistrotanzanine B. With its constitution identical to that of **20** and the same configuration at C-3, it can also be addressed as 5-*epi*-ancistroealaine A.

3.3.3 Structural Elucidation of 6-*O*-Methylancistrocladinine (14)

3.3.3.1 Spectroscopic Characterization

The molecular formula of the second, slightly less polar new alkaloid was $C_{26}H_{29}NO_4$ as deduced from HRMS (ESI). Its ^{1}H NMR data (Figure 13) indicated the presence of a naphthyldihydroisoquinoline alkaloid with four methoxy groups, resonating at 3.80, 3.99, 4.02, and 4.06 ppm. With a spin system of three neighboring protons, giving rise to two doublets (6.66 and 6.82 ppm) and one pseudo triplet (7.23 ppm), and from their H,H-COSY interactions, the position of the biaryl axis again had to be in the ring that bears the methyl group (CH_3-2').

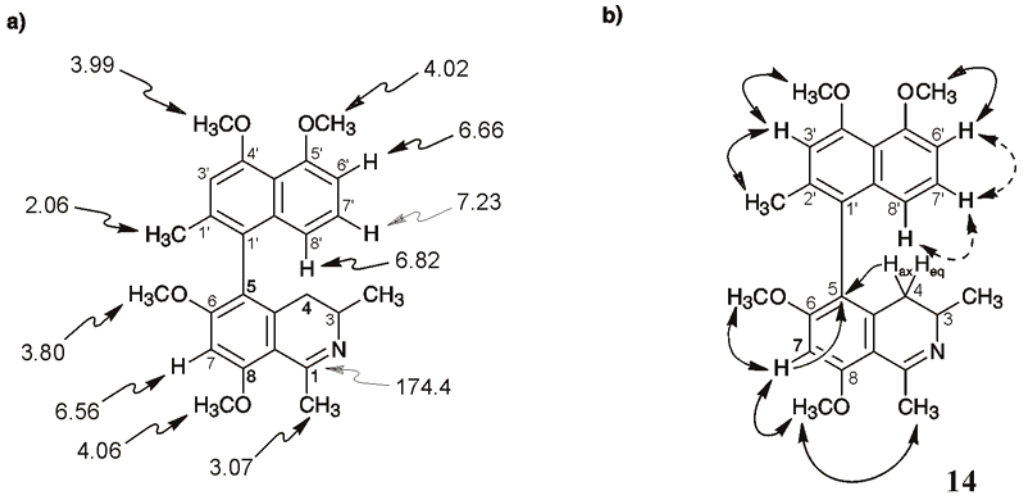

Figure 13. Selected NMR data of 6-*O*-methylancistrocladinine (**14**): a) ^{1}H and ^{13}C NMR shifts (δ in ppm), b) HMBC (single arrows), and NOE (double arrows) interactions indicative of the constitution.

The high-field shift of the latter (2.06 ppm, Figure 13) confirmed this result. Whether the coupling site was C-1' or C-3' became evident from NOE correlations between CH_3-2' and H-3' and between H-3' and OCH_3-4' (Figure 13). This finding was in agreement with NOE correlations between H-8' and H-4_{eq} and between H-4_{ax} and CH_3-2' (Figure 14), which were possible only if the alkaloid was 5,1'-linked. In the isoquinoline portion, the axis was indeed found to be located at C-5, as shown by HMBC effects of both, H_{ax}-4 and H-7, with the quaternary C-5 atom. The 5,1'-coupling type was further confirmed by the fact that only one out of four methoxy groups, OCH_3-6, was high-field shifted (3.80 ppm). This was corroborated by NOE interactions of H-7 (6.56 ppm) with the protons of both of the two methoxy groups at C-6 and C-8, and further of OCH_3-8 with CH_3-1 (Figure 13). The presence of a double bond between C-1 and the nitrogen atom was deduced from the chemical shift (3.07 ppm) of the CH_3-1 signal in the ^{1}H NMR spectrum, from its multiplicity (singlet), from the chemical shift of the ^{13}C NMR peak of C-1 (174.4 ppm), and from the absence of an H-1 signal, which normally appears around 4.20 ppm in 1,2,3,4-tetrahydroisoquinolines.[22] These findings permitted to attribute the constitution **14** shown in Figure 13 to the alkaloid.

3.3.3.2 The Absolute Configuration

The absolute configuration at C-3 of **14** was again determined to be *S* by ruthenium-mediated oxidative degradation carried out by M. Schraut,[110,111] which gave (*S*)-3-aminobutyric acid (**19**) as the main product.

This in combination with the relative configuration at the axis, as evident from the above mentioned specific NOE interaction between H-4_{eq} and H-8', and between CH_3-2' and H-4_{ax} (Figure 14) showed that the axis had to be *P*-configured. In consequence, the compound had to possess the full stereostructure **14** as displayed in Figure 14, thus being the as yet unknown 6-*O*-methyl analog of the known[112] alkaloid ancistrocladinine (**5**) (see Figure 2 for structure).

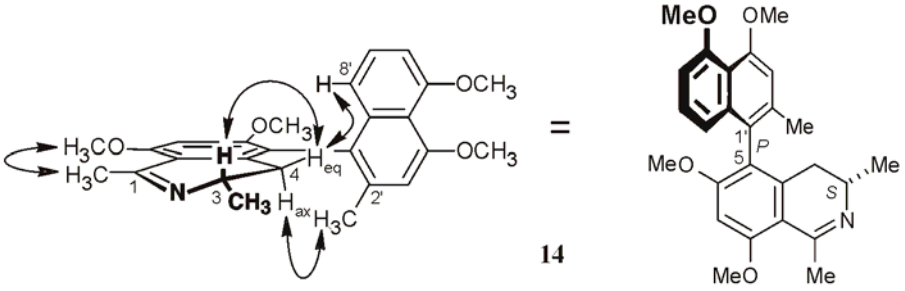

Figure 14. The configuration at the biaryl axis of **14** relative to the stereogenic center given by NOE interactions.

The *P*-configuration of 6-*O*-methylancistrocladinine (**14**) at the biaryl axis was further corroborated by comparison of its CD spectrum with that of the corresponding atropo-diastereomer, 6-*O*-methylhamatinine (**21**) (see Figure 17 for structure),[113] which was found to be opposite, as expected.[25]

3.3.4 Structural Elucidation of Ancistrotectoriline (15)

3.3.4.1 Spectroscopic Characterization

The NMR, CD, and mass spectra of the third compound and its optical rotation were very similar to those published for ancistrotectoriline (**15**), an alkaloid from the Asian liana *A. tectorius*,[114] but with some differences in the ^{1}H NMR and ^{13}C NMR shifts (Figure 15). The most significant differences between the values of the isolated compound and those from the literature[114] were: 4.60 instead of 4.12 ppm for H-1; 118.2 instead of 114.6 ppm for C-9 and 126.4 instead of 136.2 ppm for C-9'. Still, the one- and two-dimensional NMR experiments led to the conclusion that the compound isolated here was the same as that isolated by Dr. Y. Ye's group, with the constitution and relative configuration as shown in Figure 15. As a final proof an authentic sample of ancistrotectoriline (**15**) kindly provided by Dr. Y. Ye's group showed full agreement with our sample in the direct NMR comparison and a single set of signals for a 1:1 mixture of ancistrotectoriline (**15**) isolated from *A. tectorius* and ancistrotectoriline (**15**) isolated from *A. tanzaniensis*. The obtained NMR data of the mixture

were found to be identical to those we had recorded for ancistrotectoriline (**15**) isolated from *A. tanzaniensis*.

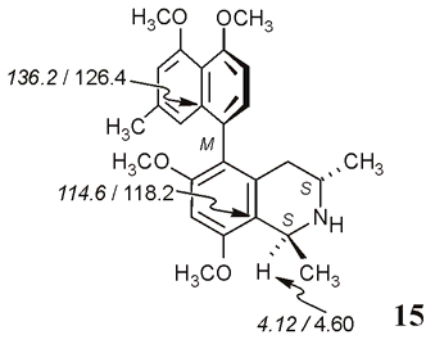

Figure 15. Selected NMR data of ancistrotectoriline (**15**), ^{1}H and ^{13}C NMR shifts (δ in ppm), previously published values[114] in *italic*.

3.3.4.2 Absolute Configuration

The absolute configuration at C-1 and C-3 of **15**, however, had been assigned only tentatively in the literature.[114] M. Schraut carried out ruthenium(III)-catalyzed periodate oxidation analysis of the compound, which afforded L-alanine and (*S*)-3-aminobutyric acid (**19**),[110,111] confirming the configuration at the two stereogenic carbons as 1*S*,3*S*, as previously assumed.[114]

This result was in agreement with NOE interactions between H-3 and CH_3-1 on one hand and between H-4_{ax} and CH_3-3 and H-1 on the other (Figure 16), indicating a relative *trans*-configuration at C-1 *versus* C-3, which had previously been deduced only from chemical shifts.[114] The relative stereoarray at the biaryl axis in **15** was established by NOE interactions between H-7' and H-4_{eq} (hence both were above the isoquinoline "plane") and between H-1' and H-4_{ax} (both below this "plane"), from which, in conjunction with the absolute *S*-configuration at C-1 and C-3 established above, the *M*-configuration at the biaryl axis was deduced. This absolute axial configuration of **15** was confirmed by the close resemblance of its CD spectrum with that of the related *M*-configured ancistrobrevine B[115] (not shown) and was in agreement with the likewise CD-based assignment in the literature,[114] allowing a full structural assignment for ancistrotectoriline (**15**), now found to occur in *A. tectorius* but also in *A. tanzaniensis*.

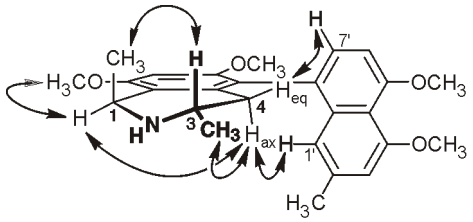

15

Figure 16. Configuration at the biaryl axis of **15** relative to the stereogenic centers through NOE interactions.

3.3.5 Isolation and Identification of Ancistrotanzanine C (16)

Ancistrotanzanine C (**16**) (Figure 17) had successfully been isolated from *A. tanzaniensis* and subsequently structurally elucidated during my Master thesis[106] and later on by M. Dreyer from *A. heyneanus*.[116] With reference material from previous isolation work the compound could unambiguously be identified by coelution. HPLC-DAD-UV and HPLC-MS experiments confirmed the presence of a naphthylisoquinoline alkaloid with the molecular mass of *m/z* 407, all spectroscopic data were found to be identical to those previously published.[117] The compound was isolated in larger amounts by preparative HPLC for bioactivity testing.

3.3.6 Isolation and Identification of Ancistrotanzanine A (17)

The most apolar naphthylisoquinoline alkaloid in the reversed-phase HPLC chromatogram was found to correspond to a molecular weight of *m/z* 419 by HPLC-MS experiments. The isolated alkaloid coeluted with an authentic sample of ancistrotanzanine A (**17**) (Figure 17) kindly provided by M. Dreyer. He had previously, likewise from the leaves of *A. tanzaniensis*, isolated and structurally elucidated this alkaloid with the hitherto unprecedented 5,3'-coupling type between the naphthalene and isoquinoline portions.[118] Milligram quantities were isolated for in depth NMR experiments (NOESY, ^{13}C, and HMBC) to the contribution for the structural elucidation of the novel alkaloid.

3.3.7 Isolation and Identification of *O,N*-Dimethylancistrocladine (18)

The in reversed-phase HPLC fastest eluting naphthylisoquinoline alkaloid corresponded to a molecular formula of $C_{27}H_{33}NO_4$ (*m/z* 435) according to HRMS (ESI). A coelution was

carried out with authentic material of *O,N*-dimethylancistrocladine (**18**) (Figure 17) kindly provided by M. Dreyer. At the same time he had isolated, likewise from the leaves of *A. tanzaniensis*, and structurally elucidated this 5,1' fully *O*-and *N*-methylated naphthyltetrahydroisoquinoline alkaloid. Isolation of the alkaloid in larger quantities by preparative HPLC was carried out for the NMR experiments (NOESY, ^{13}C, and HMBC) to the contribution for the structural elucidation of the novel alkaloid.

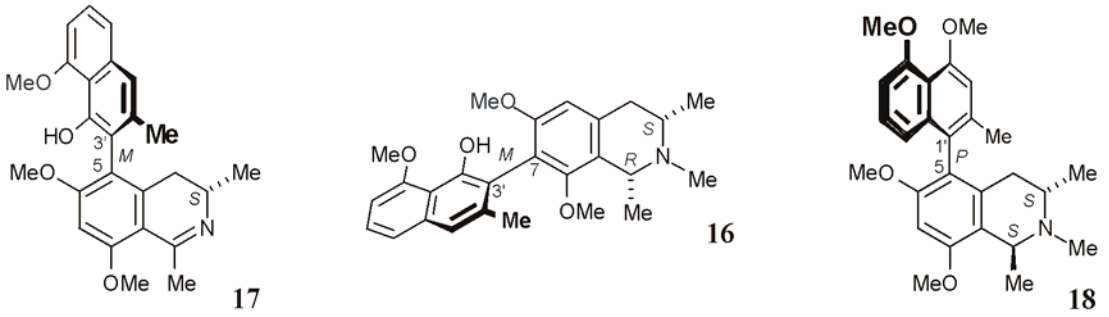

Figure 17. Structures of the known naphthylisoquinoline alkaloids ancistrotanzanines A (**17**) and C (**16**) and *O,N*-dimethylancistrocladine (**18**) isolated from leaf material of *Ancistrocladus tanzaniensis*.

3.4 Bioactivity Testing

The bioactivity screening of the compounds against 3D7 strain *P. falciparum* was carried out at the Danish University of Pharmaceutical Sciences by Prof. Dr. S. B. Christensen and coworkers, whereas the additional screenings were carried out at the Swiss Tropical Institute by Dr. R. Brun and coworkers. Compounds **13**, and **15-17** exhibited moderate antiplasmodial activities against the K1 strain (Basel) of *P. falciparum* (resistant to chloroquine (**2**) and pyrimethamine), less than that of the standard chloroquine (**2**), but showed virtually no antiplasmodial activity against the chloroquine (**2**)-sensitive 3D7 strain (Copenhagen) of *P. falciparum* (Table 1).

The most significant activity was found against *Leishmania donovani*, the pathogen of visceral leishmaniasis. In comparison to the highly active naphthylisoquinoline alkaloid ancistroealaine A (**20**, 4.1 µg/mL),[30] its atropo-diastereomer ancistrotanzanine B (**13**) was more active by a factor of 2.5 (1.6 µg/mL), and a similarly high antileishmanial activity was found for ancistrotanzanine C (**16**) and ancistrotanzanine A (**17**). Weak antitrypanosomal activities were exhibited by all compounds against the pathogen of African sleeping sickness,

T. b. rhodesiense, while **17** and **13** were some four times less active than the standard against *T. cruzi* (Chagas' disease). The compounds were found to show only weak or no cytotoxicities.

Table 1. Bioactivities of compounds **13**-**18**.

	IC_{50} [µg/mL]					
	13	**14**	**15**	**16**	**17**	**18**
P. falciparum (strain: K1)[a]	0.3	2.2	0.5	0.1	0.3	3.6
Standard: chloroquine 0.055[b]						
P. falciparum (strain: 3D7)[c]	5	5.4	14	4.2	n.d.[d]	34.1
Standard: chloroquine 0.01[b]						
T. cruzi	1.5	60.5	17.8	14	1.7	65.3
Standard: benznidazole 0.42[b]						
T. b. rhodesiense	0.7	5.2	2.1	1.3	0.7	5.4
Standard: melarsoprol 0.001[b]						
L. donovani	1.6	30	>10	3	1.8	n.d.[d]
Standard: miltefosin 0.305[b]						
Cytotoxicity L6 (MIC)	8.1	21.4	6.5	n.d.[d]	6.4	n.d.[d]

[a] Basel. [b] All values in µg/mL. [c] Copenhagen. [d] Not determined.

3.5 Chemotaxonomic Considerations

From a chemotaxonomic point of view, all of the compounds isolated from *A. tanzaniensis* have an oxygen function at C-6 and the *S*-configuration at C-3. They are thus representatives of the so-called "Ancistrocladaceae-type" alkaloids.[22] With these phytochemical characteristics, *A. tanzaniensis* closely resembles the only other known East African *Ancistrocladus* species, *A. robertsoniorum*,[119,120] and also the South-East Asian members of the Ancistrocladaceae (among them, the ancistrotectoriline-producing *A. tectorius*).[22,114] It is clearly different from Central and West African *Ancistrocladus* species, many of which produce typical "Dioncophyllaceae-type" alkaloids like dioncophylline A (**8**) and dioncophylline C (**6**) (*R*-configurated at C-3 and devoid of an oxygen function at C-6[22]) and also mixed, hybrid types (*e.g.*, *R* at C-3 and oxygenated at C-6).[121]

In addition to these relationships with other plants, which help to define the chemotaxonomic position of *A. tanzaniensis*, the discovery of ancistrotanzanine A (**17**), with its previously unknown 5,3'-linkage by M. Dreyer, makes this "new" plant species unique within the tropical plant families Ancistrocladaceae and Dioncophyllaceae from a phytochemical point of view.

4 Isolation of Naphthylisoquinoline Alkaloids from a Congolese *Ancistrocladus* Species Collected in the Habitat Yeteto (Ancistrocladaceae)

4.1 The Congolese *Ancistrocladus* Species

Samples of a probably new *Ancistrocladus* species were collected in the Democratic Republic of Congo, in the swamp region of the rainforest Yeteto near the town Ikela, by Prof. Dr. V. Mudogo. From the Congo Basin, only three species *A. congolensis*, *A. likoko*, and *A. ealaensis,* all botanically described by J. Leonard,[122] are known so far.[109] Due to the lacking availability of species from this region and because most herbarium specimens lack flowers or fruits, it is difficult to estimate the variability of the species or to get a sound knowledge about the distribution range and ecological preferences. It is likely that more new species and more new records will come to light if fertile collections become available. In some - but not all - characters, the samples investigated from Ikela approach *A. ealaensis*, therefore, further investigations, including DNA analysis, are necessary to clarify the presumed species status.[123]

4.2 Isolation and Structural Elucidation of the Naphthylisoquinoline Alkaloids from the Leaves of the Congolese *Ancistrocladus* Species Collected in the Habitat Yeteto

4.2.1 Introduction

The isolation and structural elucidation and characterization of ancistrocladinium B (**22**) were carried out in close cooperation with S. Pedersen, who started the chemotaxonomical investigation of the leaves of the Congolese *Ancistrocladus* species during an exchange stay within the our group as a part of her Master thesis.[124]

4.2.2 Extraction and Isolation

Air-dried and powdered leaves of the collected plant material were exhaustively extracted with CH_2Cl_2/MeOH, 6:4. The extract was submitted to liquid-liquid separation, FCPC (Fast Centrifugal Partition Chromatography), and preparative HPLC, which permitted isolation of two alkaloids. Their UV profiles hinted at the presence of naphthylisoquinoline alkaloids, but the second maximum of each of the compounds was found to be shifted bathochromically by

30–40 nm in comparison to those previously reported for other naphthylisoquinoline alkaloids (typically *ca.* 306 nm).[125-127]

4.2.3 Structural Elucidation of Ancistrocladinium B (22)

In the more apolar region of the analytical HPLC chromatogram, two baseline-separated peaks in a ratio of 46:54 were detected. Isolation of two respective chromatographic fractions on a preparative scale and subsequent analysis by HPLC and NMR showed the two samples to be nearly identical, each of them again consisting of the previous two compounds, indicating their interconversion at room temperature. This was unambiguously proven by immediate analytical HPLC analysis of the freshly resolved single peaks obtained by preparative HPLC, revealing an equilibration by gradual interconversion of the two peaks even at room temperature. These findings were in agreement with HPLC-MS experiments, which gave rise to identical mass spectra for both peaks, thus proving the presence of two slowly interconverting compounds, possibly atropo-diastereomers.

The only example of a naphthylisoquinoline alkaloid with a configurationally semi-stable biaryl axis that has so far been reported, is dioncophylline E (7,3'-coupled; **23**) (Figure 18).[128] All other known representatives of this class of secondary metabolites form rotational isomers that are – depending on the substitution pattern in the proximity of the biaryl linkage – either configurationally fully stable, such as dioncopeltine A (**7**)[129] and dioncophylline C (**6**),[130] or rotate very rapidly at room temperature, as in the case of dioncophylline B (**24**) (Figure 18).[131] The apparent semi-stability of the axial configuration gave a clear hint that this alkaloid had to be new, very probably even being based on a novel coupling type.

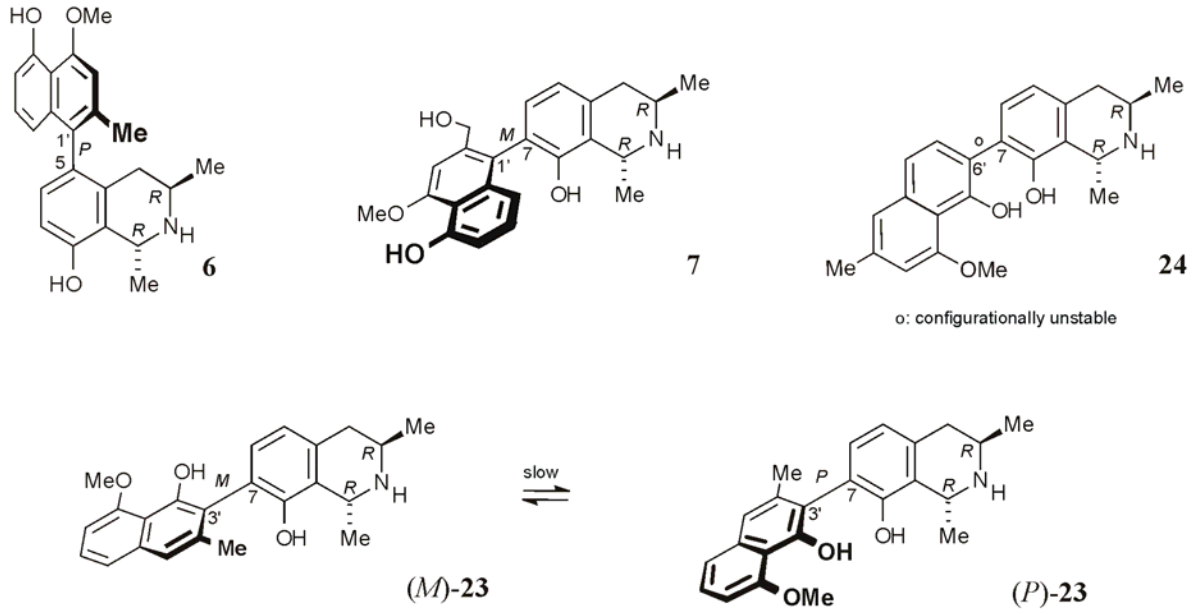

Figure 18. Structures of the configuration stable **6** and **7**, the configurational unstable dioncophylline B (**24**), and the two configurational semi-stable atropoisomers of dioncophylline E (**23**) (O: configurationally unstable axis).

4.2.3.1 Spectroscopic Characterization

HRMS (ESI) of a solution of the equilibrium mixture of the two atropo-diastereomers, showed that **22** is a cationic compound, with a molecular formula of $C_{25}H_{28}NO_4^+$. The NMR experiments were carried out on two chromatographical fractions enriched in each of the two atropo-diastereomers, which thus enabled a structural assignment for each of the two peaks observed in the HPLC chromatogram.

The ^{1}H NMR spectrum recorded of a fraction enriched in the in reversed-phase HPLC faster eluting peak A showed a three-proton singlet at low field for C*H*$_3$-1 (δ 2.56), which, in combination with the absence of a three-proton doublet at *ca.* δ 1.5 and an H-1 signal at *ca.* δ 4 (as typical of naphthyl-1,3-dimethyltetrahydroisoquinolines[22]), hinted at the presence of a naphthyldihydroisoquinoline alkaloid. This assumption was confirmed by the chemical shift of the C-1 peak (δ 174.54) in the ^{13}C NMR spectrum, to which the protons of C*H*$_3$-1 showed HMBC couplings. The presence of three methoxy groups was established by the signals resonating at δ 3.97, 4.00, and 4.04, each integrating for three protons. Two of them were

assigned to be situated at C-6 and C-8 in the isoquinoline moiety, by NOE correlations in the series {CH_3-1–OCH_3-8–H-7–OCH_3-6–H-5–H_{eq}-4–H-3}, which was further confirmed by HMBC couplings of the singlet signals of H-7 (δ 6.76) to both, C-8 and C-6, and of H-5 (δ 6.81) to C-6.

This assignment unambiguously left N-2 as the only possible coupling position of the biaryl to the isoquinoline moiety, thus, hinting at the presence of a dihydroisoquinolinium cation. The quaternary alkaloid **22** was isolated as its trifluoroacetic acid salt, but the identity of the authentic, natural counter-ion was not established.

The remaining OMe group was established to be located at C-4' by an NOE interaction with H-3'. In the naphthalene moiety, the aromatic spin pattern of two singlets and two doublets, and the normal, not high field shifted signal of CH_3-2' (δ 2.47), left C-6' or C-8' to be the coupling position of the biaryl axis. The latter was excluded by an NOE correlation sequence in the series {H-7'–H-8'–H-1'–CH_3-2'–H-3'–OCH_3-4'}. This attribution was in agreement with HMBC long-range couplings, found crosswise from H-8' to C-1' and from H-1' to C-8', and between the signal of O*H*-5' and the quaternary C-6', thus unequivocally revealing the coupling position in the naphthalene moiety to be at C-6'.

The NMR data obtained of a fraction enriched in the more slowly eluting peak B were very similar to those obtained for peak A but with some differences in the ^{1}H NMR and ^{13}C NMR shifts. The most significant differences between the values of peak B and those of peak A were: δ 174.66 instead of δ 174.54 for C-1; δ 2.50 instead of δ 2.56 for CH_3-1; δ 4.36 instead of δ 4.49 for H-3 and δ 6.75 instead of δ 6.76 for H-7.

Investigations of the NMR experiments recorded on fractions enriched in either peak A or peak B, clearly hinted at the presence of two compounds possessing the same constitution.

In conclusion the slowly interconverting compounds are the two atropo-diastereomeric forms of a hitherto unprecedented *N*,6'-coupled naphthylisoquinoline alkaloid with the constitution **22** shown in Figure 19. The novel compound **22** was henceforth named ancistrocladinium B.[132]

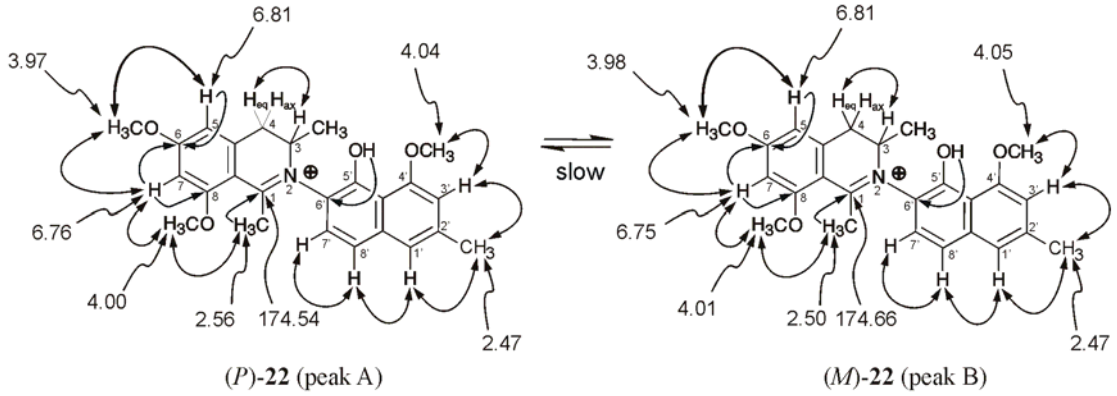

(*P*)-**22** (peak A) (*M*)-**22** (peak B)

Figure 19. Ancistrocladinium B (*P*)-**22** (peak A) and (*M*)- **22** (peak B); ^{1}H and ^{13}C NMR shifts (δ in ppm), HMBC (single arrows), and NOE (double arrows) interactions used for the determination of the constitution.

4.2.3.2 The Absolute Configuration

The absolute configuration at C-3 was determined to be *S* for both atropisomers, again by the ruthenium-mediated oxidative degradation,[110,111] here performed directly on the equilibrium mixture of peak A and B, affording (*S*)-3-aminobutyric acid (**19**), analyzed by GC of its Mosher derivative carried out by M. Schraut.

NOESY investigations by NMR experiments on fractions enriched in the chromatographically reversed-phase HPLC more rapid atropisomer originating from peak A (retention time 16.8 min, ratio 75:25) or the slower one originating from peak B (retention time 18.1 min, 0:100), enabled us to assign the relative configuration at the axis for each of the two epimers. For the proton signals of peak A, *i.e.*, the epimer with the low-field shifted signal of H-3 (δ 4.49), an atropisomer-specific NOE correlation was observed between that H-3 and H-7'. In combination with the known *S*-configuration at C-3, this interaction revealed an absolute *P*-configuration at the chiral axis as shown in Figure 20. A similar specific NOE interaction was observed between the protons of CH_3-3 and H-7' for the chromatographically slower peak B, which is the epimer with the high-field shifted signal of H-3 (δ 4.36). This interaction allowed attributing the absolute axial *M*-configuration to the slower atropisomer as shown in Figure 20.

Figure 20. Configuration at the biaryl axis of (*P*)-**22** and (*M*)-**22** relative to the stereogenic center through NOE interactions.

The assumption that ancistrocladinium B (**22**) consists of an atropo-diastereomeric mixture, was further corroborated by the individual CD spectra of the two atropisomers recorded online, by using the HPLC-CD technique in the stopped-flow mode[133] performed by T. Gulder. The two spectra were found to be virtually opposite, as anticipated from the fact that the hetero-biaryl system and its particular dihedral angle at the axis between the chromophores strongly dominates the CD curves.[120] The presence of the new coupling type in **22** precluded a configurational assignment of the two atropisomers by empirical comparison of their experimental CD spectra with that of a configurationally known similar alkaloid. The attribution of the two peaks to the atropo-diastereomers of **22** was therefore achieved by quantum chemical CD calculations performed by M. Reichert.[134] With the stereogenic center at C-3 assigned as *S* (see above), the computational efforts concentrated on the absolute configuration at the chiral axes. The two independent conformational analyses for the two atropo-diastereomers, (*P*,3*S*)-**22** and (*M*,3*S*)-**22**, resulted in five and six minimum geometries, respectively, which were optimized at the semiempirical PM3[135] level. For each single conformer thus obtained, the respective CD spectrum was computed by using the OM2[136] method. For (*P*,3*S*)-**22** the corresponding five, and for (*M*,3*S*)-**22** the respective six spectra were summed up following the Boltzmann statistics, *i.e.*, according to the heats of formation. The resulting two overall CD curves were then UV-corrected[137] and compared with the experimental ones (Figure 21).

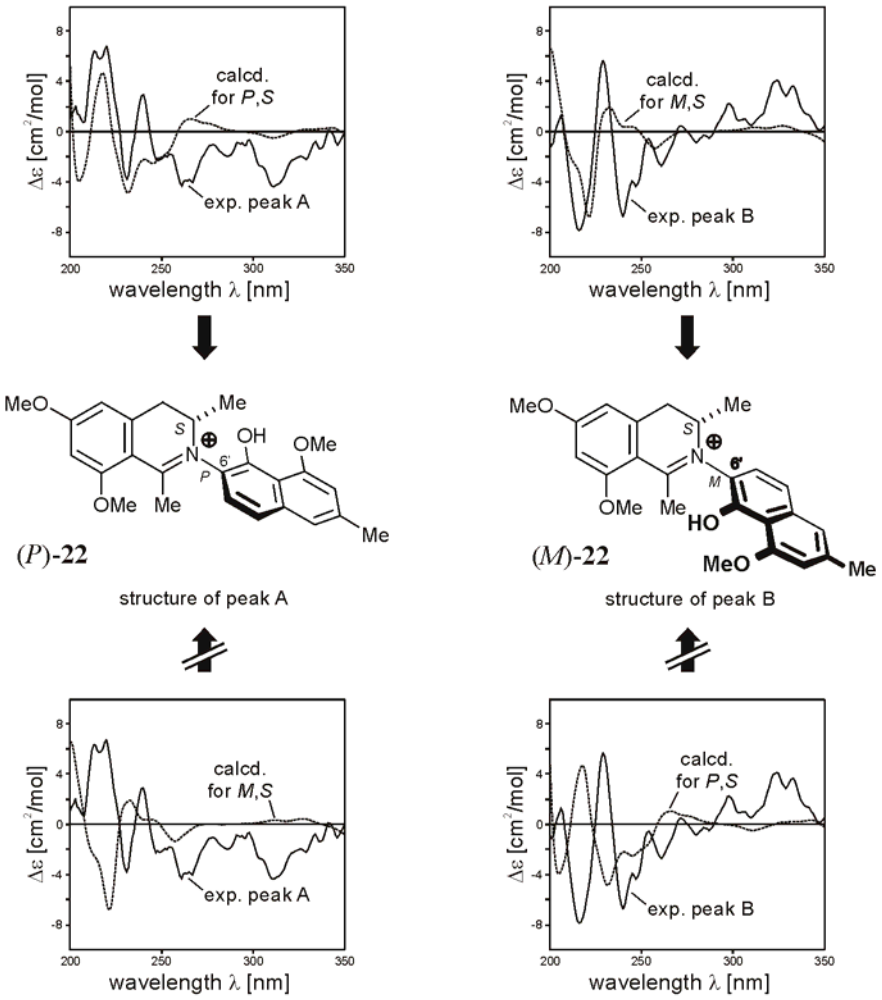

Figure 21. Assignment of the absolute configuration to the two atropo-diastereomers of ancistrocladinium B (**22**) by comparison of the experimental LC-CD spectra (stopped-flow mode) of peak A (left) and B (right) with the spectra calculated for (*P*,3*S*)-**22** and (*M*,3*S*)-**22**, by using the OM2 Hamiltonian.

The experimental CD spectrum of peak A (faster eluting in HPLC) agreed well with the one simulated for (*P*,3*S*)-**22** (Figure 21, left), as did the CD curve of peak B (more slowly eluting in HPLC) with the one calculated for (*M*,3*S*)-**22** (Figure 21, right). From this pairwise match the absolute configuration of the two atropo-diastereomers was unambiguously determined, leading to the same results as those deduced from the observed NOE correlations for the two signal sets in ^{1}H NMR (Figure 20).

4.2.3.3 Kinetic Characterization of the Axial Stability of Ancistrocladinium B (22)

The configurational semi-stability of the axis of this novel naphthylisoquinoline alkaloid **22** made it rewarding to measure its rotational barrier by investigating the temperature-dependent atropo-diastereomerization.

The process of interconversion of the two atropisomers may be expressed as a reversible isomerization equilibrium:

$$(P)\text{-}\mathbf{22} \underset{k_r}{\overset{k_f}{\rightleftharpoons}} (M)\text{-}\mathbf{22} \qquad \text{(eq. 1)}$$

In order to obtain the rate constants for the two isomerization directions, k_f and k_r, The decrease of the diastereomeric excess of freshly resolved chromatographical fractions enriched in the respective (*P*)- or (*M*)-atropisomer was analyzed by HPLC-UV (Figure 22), by determining the area under the curve for each of the chromatographical peaks over time.

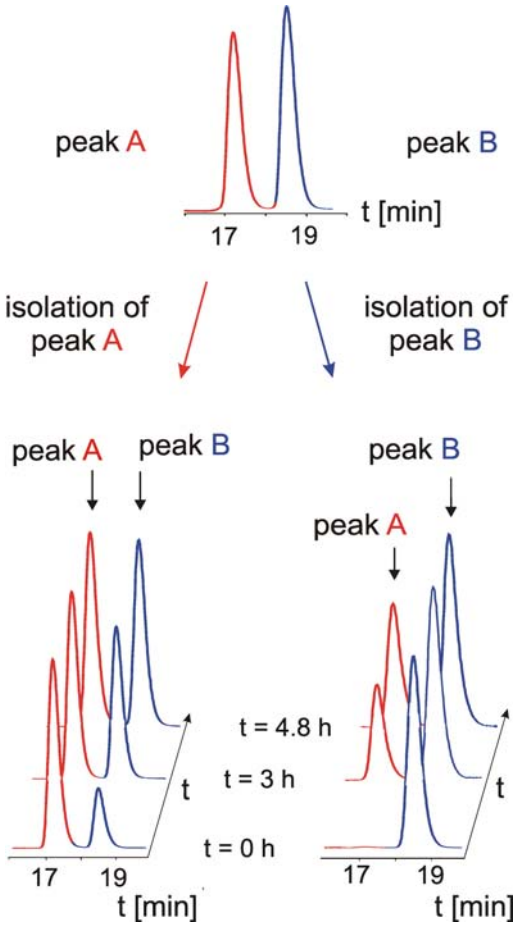

Figure 22. Determination of the atropoisomerization rates of ancistrocladinium B (**22**) by resolution of its two atropo-diastereomers (peaks A and B), followed by their separate thermal equilibration over time in MeOH/H_2O (1:1) at 60°C, analyzed by analytical HPLC on an achiral C_{18} phase.

According to procedures established in the literature, the rate constants can subsequently be determined from the slope of logarithmic plots (Table 2, and Figure 22).[138-140] The analyses were carried out at four different temperatures for the reversible isomerization in both directions (k_r and k_f). The equilibrium constant (K_{eq}) was likewise determined for each of the temperatures (Table 2), and is defined as:

$$K_{eq} = \frac{k_f}{k_r} = \frac{[(M) - 22]}{[(P) - 22]} \qquad \text{(eq. 2)}$$

The ratio k_f/k_r was given using the relative concentration estimated by the area under the respective peak for each of the atropo-diastereomers obtained by HPLC-UV analysis, recorded of a mixture in equilibrium. The individual values of k_f and k_r were thereby determined.

The corresponding free energy of activation ($\Delta G^{\neq}$) for the experimentally determined k_f- and k_r values (Table 2) were obtained using the Eyring equation.

$$\Delta G^{\neq} = RT[23.76 - \ln(k/T)] \qquad \text{(eq. 3)}$$

From kinetics, the difference between the free energies of activation ($\Delta\Delta G^{\neq}$) for the two isomerization directions is equal to the Gibbs free energy at equilibrium, ΔG°, which may also be determined from the ratio k_f/k_r. From thermodynamic considerations, ΔG° was additionally found directly from the equilibrium constant (K_{eq}), determined by HPLC-UV and from ΔH° and ΔS°, obtained by plotting R ln K_{eq} versus $1/T$ for the investigated temperatures. The validity of k_f and k_r was affirmed since the independent kinetic and thermodynamic methods led to near identical ΔG° values (Table 2). The data in Table 2 was obtained for the atropoisomerization of **22** followed from (*P*)-**22** to (*M*)-**22**. While studying the isomerization in the reverse direction, from (*M*)-**22** to (*P*)-**22**, a deviation of less than 3% between the two test series performed. At 25 ºC the Gibbs free energy, obtained from the slope of Eyring plots was found to be $\Delta G^{\neq}_f$ = 107.2 kJ mol^{-1} and $\Delta G^{\neq}_r$ = 107.7 kJ mol^{-1}, for (*P*)-**22** and (*M*)-**22**, respectively. The difference of 0.5 kJ mol^{-1} in favor of the isomerization from (*P*)-**22** to (*M*)-**22** is in agreement with the equilibrium constant found at room temperature, leading to a ratio of 46:54 for (*P*)-**22** to (*M*)-**22**. The isomerization barrier is thus >100 kJ mol^{-1}, *i.e.*, just above the defined energy barrier of well-separable stable isomers,[141] and thus in good accordance with the observed slow interconversion of the two atropo-diastereomers at room temperature.[25]

Table 2. Kinetic parameters of the atropoisomerization of **22** studied from (*P*)-**22** to (*M*)-**22**.

	Temperature K			
	305	325	334	349
k_f [a]	2.426×10^{-6}	2.180×10^{-5}	6.377×10^{-5}	2.857×10^{-4}
k_r [a]	2.020×10^{-6}	1.845×10^{-5}	5.403×10^{-5}	2.454×10^{-4}
K_{eq} [a]	1.201	1.182	1.180	1.164
$\Delta G^{\neq}_f$ [a]	107.5	108.8	108.9	109.6
$\Delta G^{\neq}_r$ [a]	108.0	109.3	109.4	110.1
$\Delta\Delta G^{\neq}$ [a]	0.47	0.46	0.46	0.44
ΔG° [b]	0.46	0.45	0.46	0.44

[a] k in s^{-1}; $\Delta G^{\neq}_f$: free energy of activation for the (*P*)-**22** to (*M*)-**22** isomerization direction; $\Delta G^{\neq}_r$: free energy of activation for the (*M*)-**22** to (*P*)-**22** isomerization direction; $\Delta\Delta G^{\neq}$ and ΔG°: equilibrium free energy; all values in kJ mol^{-1}. [b] Calculated from $\ln K_{eq} = \Delta G^{\circ} / RT$.

A satisfying agreement was also found with the results from DFT calculations using the B3LYP hybrid functional, leading to a calculated value of $\Delta G^{\neq}_f$ = 112.6 kJ mol^{-1} for the atropoisomerization from (*P*)- to (*M*)-**22**, and $\Delta G^{\neq}_r$ = 113.9 kJ mol^{-1} for the axial rotation from (*M*)- to (*P*)-**22**, thus again reproducing the slight preference of the *M*-atropodiastereomer in the atropisomeric equilibrium at room temperature. The difference between the observed activation enthalpies and the calculated ones can be explained by the fact that the calculations were carried out *in vacuo*, although the solvents used will certainly affect the experimentally obtained values.

4.2.3.4 Continuous Characterization Work

I. Kajahn from our group succeeded in recording ^{1}H NMR spectra of pure isolated peak A and B of ancistrocladinium B (**22**), obtained by LC-NMR. The spectra were in good agreement with the ones presented in this work. Furthermore, she carried out an additionally kinetic characterization of the axial stability of ancistrocladinium B (**22**) at other temperatures. The results of the kinetic characterization work, was found to be in good agreement with the ones presented above.[132]

4.2.4 Isolation and Characterization of Ancistrocladinium A (25)

In the more polar region of the HPLC chromatogram a peak was observed, possessing a UV profile which hinted at the presence of a naphthylisoquinoline alkaloid. However, as for ancistrocladinium B (**22**) the second maximum coming from high frequencies was found to be bathochromically shifted with 30-40 nm in comparison to previously reported naphthylisoquinoline alkaloids.[125-127] HRMS (ESI) revealed the alkaloid to correspond to a molecular weight of $C_{26}H_{30}NO_4^+$. The presence of an additional isoquinolinium salt was thus obvious and further confirmed by ^1H and ^{13}C NMR experiments. A coelution was carried with an authentic sample of ancistrocladinium A (**25**) (Figure 23) kindly provided by I. Kajahn. She had before, from the leaves of *A. benomensis*, isolated and structurally elucidated the alkaloid to represent the *N*,8'-coupling type between the naphthalene and isoquinoline portions. Milligram quantities were isolated for biological activity test.

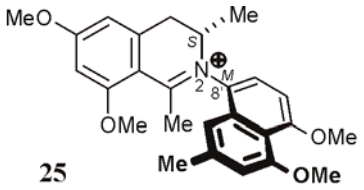

25

Figure 23. Structure of ancistrocladinium A (**25**) isolated from leaf material of the investigated Congolese *Ancistrocladus* species (habitat: Yeteto).

4.3 Bioactivity of the Alkaloids

The pronounced antiprotozoal activities of naphthylisoquinoline alkaloids against pathogens belonging to the genera *Plasmodium*, *Leishmania*, and *Trypanosoma*[30,32,43,44,126] warranted a screening of ancistrocladinium A (**25**) and B (**22**) against these parasites (Table 3). The bioactivity screening against *L. major* was carried out at the Institute for Molecular Infection Biology at the University of Würzburg by Dr. A. Ponte-Sucre and coworkers, whereas the additional bioactivity screenings were carried out at the Swiss Tropical Institute by Dr. R. Brun and coworkers. The alkaloids exhibited moderate antiplasmodial activities against the K1 strain of *P. falciparum*, although, not reaching the splendid IC_{50} values obtained for other naphthylisoquinoline alkaloids.[30,32] The results are, however, most useful for ongoing QSAR (Quantitative Structure-Activity Relationship) investigations,[142,143] since the compound is based on as yet unscreened coupling types. Ancistrocladinium B (**22**)

exhibited a moderate activity against the pathogens *T. cruzi* and *T. b. rhodesiense,* whereas ancistrocladinium A (**25**) displayed a 5-fold higher activity against the pathogen *T. rhodesiense*, but was inactive against *T. cruzi*. The most significant activities were detected against Old World *Leishmania* species. Thus, both, ancistrocladinium A (**25**) and B (**22**), were highly active against *L. donovani*, the pathogen responsible for visceral leishmaniasis. Against *L. major,* the pathogen that causes cutaneous leishmaniasis, ancistrocladinium B (**22**) displayed an activity 15-fold higher than that of the gold standard miltefosine. The compounds were highly toxic against L-6 myoblast cells (available in Basel) and J774.1 macrophages (kept in Würzburg), but the indexes describing the cytotoxicity of the compounds against the cell lines in relation to their activity against the parasites (IC_{50}cytotoxicity/IC_{50}activity), for ancistrocladinium A (**25**) against *L. donovani* and ancistrocladinium B (**22**) against *L. major*, suggest pharmacological profiles better than the one found for miltefosine in experiments performed in parallel.

Table 3. Bioactivities of ancistrocladinium A (**25**) and B (**22**)

	IC_{50} [µg/mL]	
	22	**25**
P. falciparum (strain: K1)[a] Standard: chloroquine 0.041[b]	0.862	0.25
T. cruzi (strain: tulahuen C4)[a] Standard: benznidazole 0.53[b]	1.24	>30
T. b. rhodesiense (strain: STIB 900)[a] Standard: melarsoprol 0.00046[b]	0.39	0.075
L. donovani (strain: MHOM-ET-67/L82) [a] Standard: miltefosine 0.05[b]	1.1	0.722
Cytotoxicity[a] Cells: rat skeletal myoblast L-6	2.01	25.0
L. major (strain: MHOM/IL/81/FE/BNI)[c] Standard: miltefosine 13.00[b]	2.69	3.08
Cytotoxicity[c] Cells: J774.1 macrophages	7.93	22.15

[a] Basel. [b] All values in µg/mL. [c] Würzburg.

4.4 Isolation and Structural Elucidation of the Naphthylisoquinoline Alkaloids from the Roots of the Congolese *Ancistrocladus* Species Collected in the Habitat Yeteto

4.4.1 Introduction

The phytochemical and chemotaxonomical investigation of the roots of the Congolese *Ancistrocladus* species (habitat Yeteto) was performed in cooperation with J. Spuziak and Prof. Dr. V. Mudogo from the Université de Kinshasa during his scientific visits in our group.

4.4.2 Extraction and Isolation

Root material of the Congolese *Ancistrocladus* species were powdered and sequentially extracted with *n*-hexane, CH_2Cl_2, and MeOH-H_2O. The CH_2Cl_2 and MeOH-H_2O extracts were concentrated *in vacuo*, and the remaining crude residues thereof were further resolved by FCPC and sequenced in fractions which were evaporated *in vacuo* and further purified with preparative HPLC. The procedure afforded pure material of **20**, **21**, **26–32**, **34**, and **35**.

4.4.3 Structural Elucidation of 5'-*O*-Demethylhamatine (26)

4.4.3.1 Spectroscopic Characterization

The molecular formula of the first quite polar compound was $C_{24}H_{27}NO_4$ as evidenced by HRMS (ESI). ^{1}H NMR investigations indicated the presence of a naphthyltetrahydroisoquinoline alkaloid with two methoxy groups, which were found to be normally shifted (3.93 and 4.13 ppm), thus excluding the possibility that they were in proximity to the axis. The position of the biaryl axis in the naphthalene moiety was suggested from the high-field-shifted position of the CH_3-2' (2.14 ppm) and the spin pattern of the aromatic protons (one triplet, two doublets, and two singlets) to be located at C-1' or C-3'. The latter was excluded since the more downfield shifted methoxy group (4.13 ppm) was assigned to OCH_3-4' by NOE correlations to H-3', which furthermore showed NOE correlation to C*H*$_3$-2'. Consequently the biaryl axis had to be situated at C-1'. This was confirmed by the crosspeaks found in the NOESY spectra in the series {H-8'–H-7'–H-6'}.

The highfield shifted methoxy group at 3.93 ppm was assigned to be located at C-8, since NOE correlations were observed for the signal with both H-7 and C*H*$_3$-1. Therefore, the biaryl axis had to be located at C-5 in the isoquinoline portion, which was fully in agreement with HMBC long-range couplings observed to C-5 (118.6 ppm) with both, the signals of the

protons H_{eq}-4 and H-7, and across the biaryl axis with CH_3-2'. In conclusion, the naphthylisoquinoline alkaloid was established to be of 5,1'-coupling type and to possess the constitution shown in Figure 24a, with free OH-functions at C-6 and C-5'.

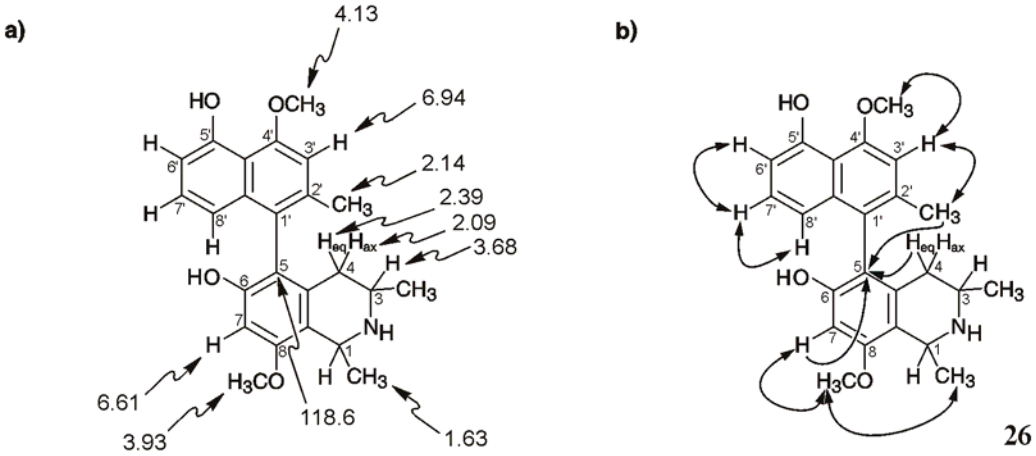

Figure 24. Selected NMR data indicative of the constitution of 5'-*O*-demethylhamatine (**26**): a) ^{1}H and ^{13}C NMR shifts (δ in ppm), b) HMBC (single arrows) and NOE (double arrows) interactions used for the determination of the constitution.

4.4.3.2 The Absolute Configuration

The relative configuration of the methyl groups at C-1 and C-3 was deduced from NOE correlation between CH_3-1 (1.63 ppm) and H-3 (3.68 ppm) revealing the two methyl groups to be oriented *trans* relative to each other. The absolute configurations at C-1 and C-3 were determined to be 1*S*,3*S* by ruthenium-catalyzed oxidative degradation[110] carried out by M. Schraut, affording L-alanine and (*S*)-3-aminobutyric acid (**19**). An NOE interaction between H-3 and the methyl group at C-2' (Figure 25) revealed that these two spin systems were on the same side of the molecule, thereby allowing the assignment of the stereo array of the axis to be *M*-configured as shown in Figure 25. The new alkaloid was found to be the 5'-*O*-demethyl analog of hamatine (**27**)[144-146] (see Figure 33 for structure) and was thus named 5'-*O*-demethylhamatine.[147] The resemblance of the CD spectrum of **26** with that of **27**, in which the biaryl axis is also *M*-configured[148] further confirmed the absolute configuration.

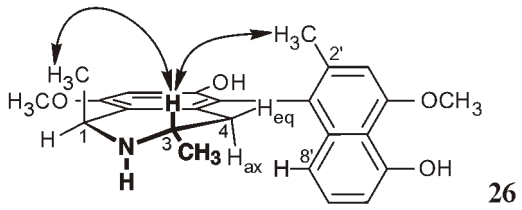

26

Figure 25. Configuration at the biaryl axis of **26** relative to the stereogenic centers through NOE interactions.

4.4.4 Structural Elucidation of 5'-*O*-Demethylhamatinine (28)

4.4.4.1 Spectroscopic Characterization

The molecular formula ($C_{24}H_{25}NO_4$) of the second alkaloid (**28**) was deduced from HRMS (ESI) and from the ^{13}C NMR spectral data. The ^{1}H NMR spectrum indicated the presence of a naphthyl-1,3-dimethyldihydroisoquinoline alkaloid characterized by the lack of the H-1 quartet at *ca.* 4 ppm and the downfield shifted CH_3-1 signal at 2.79 ppm.[22] This assumption was corroborated by the chemical shift of the C-1 peak (175.0 ppm) in the ^{13}C NMR spectrum. The "high-field", as opposed to normally shifted, signal of C*H*$_3$-2' (2.16 ppm), and the aromatic spin pattern system of one triplet, two doublets, and two singlets indicated the position of the biaryl axis to be in the ring that bears the methyl group (CH_3-2'), leaving only C-1' or C-3' for the coupling site. Of these, the latter could be eliminated by NOE interactions between H-3' (a singlet at 6.94 ppm) and both C*H*$_3$-2' and the (normally-shifted) methoxy group (4.13 ppm) at C-4', revealing that the coupling position in the naphthalene moiety was located at C-1'. This conclusion was further confirmed by NOE interactions between H-8' (6.62 ppm) and both H_{ax}-4 (2.23 ppm) and CH_3-3 (1.20 ppm), which, in turn, suggested a biaryl linkage at C-5 of the isoquinoline moiety. Further evidences for this assignment was given by HMBC long-range couplings from H-7 (6.70 ppm), and H_{eq}-4 (2.51 ppm) to C-5, and NOE correlations observed between the "normally" shifted signal of OC*H*$_3$-8 (4.05 ppm) and both H-7 and C*H*$_3$-1, which clearly excluded the possibility of the axis being located at C-7. In conclusion, the second compound was found to be a 5,1'-coupled naphthyldihydroisoquinoline, and to possess the constitution depicted in Figure 26.

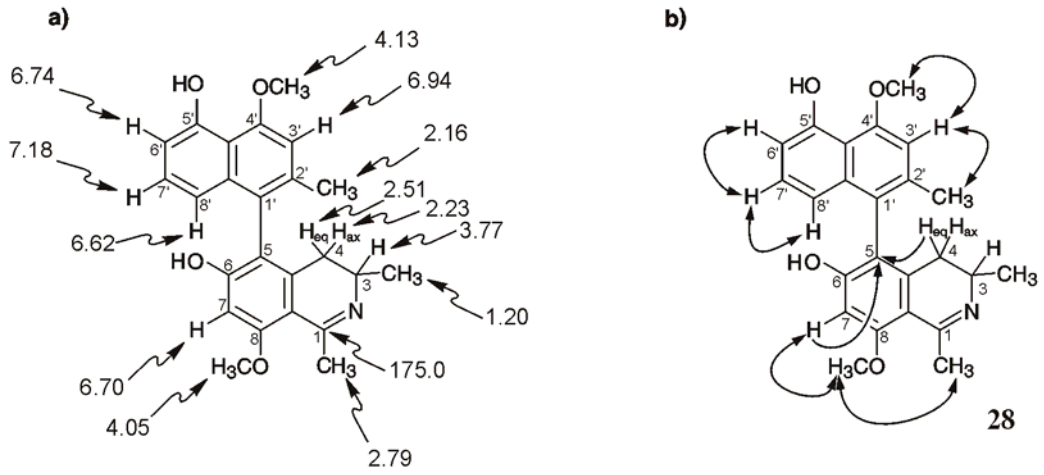

Figure 26. Selected NMR data indicative of the constitution of 5'-*O*-demethylhamatinine (**28**): a) ^{1}H and ^{13}C NMR shifts (δ in ppm), b) HMBC (single arrows) and NOE (double arrows) interactions used for the determination of the constitution.

4.4.4.2 The Absolute Configuration

The oxidative degradation procedure[110] carried out by M. Schraut, determined the absolute configuration at C-3 as 3*S*. Thus the axis was established to be *M*-configured by the above mentioned NOE interactions between H-8' and the protons of the methyl group at C-3 (Figure 27). This stereochemical assignment is in agreement with the very similar CD spectra of (**28**) and that of the known alkaloid hamatinine (**29**) (see Figure 33 for structure).[113] The compound (**28**) has not previously been identified and was henceforth named 5'-*O*-demethylhamatinine,[147] since it represents the 5'-*O*-demethyl analog of hamatinine (**29**).

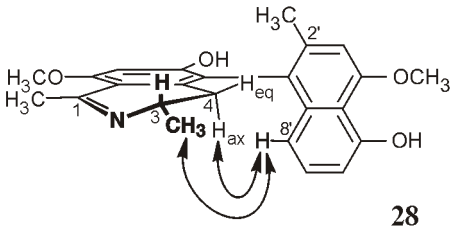

Figure 27. Configuration at the biaryl axis of **28** relative to the stereogenic center through NOE interactions.

4.4.5 Structural Elucidation of 6-*O*-Demethylancistroealaine A (30)

4.4.5.1 Spectroscopic Characterization

Compound **30** showed a chromatographical behaviour very similar to that of **31** but reversed-phase preparative HPLC enabled a good separation.

The quickest eluting alkaloid (**30**) of the two in reversed-phase HPLC was found to possess a molecular formula of $C_{25}H_{27}NO_4$, as deduced from HRMS (ESI). The ^{1}H NMR spectrum of **30** revealed a three-proton singlet at low field for CH_3-1 (2.80 ppm), which, when combined with the absence of both a three-proton doublet at *ca.* 1.5 ppm and a H-1 signal at *ca.* 4 ppm, again hinted at the presence of a naphthyldihydroisoquinoline alkaloid.[22] This assumption was confirmed by the chemical shift of the C-1 peak (175.8 ppm) in the ^{13}C NMR spectrum. Two *ortho*-coupled aromatic protons affording two doublets at 6.94 and 7.11 ppm (H-6' and H-7'), one singlet at 6.68 ppm (H-7), and two broadened singlets at 6.71 and 6.82 ppm (H-1' and H-3'), indicated the biaryl axis to be located at C-8' or C-6' in the naphthalene portion. This conclusion was in agreement with the "normally" shifted signal of CH_3-2' (2.33 ppm), which showed NOE interactions with both H-1' and H-3'. NOE interactions observed between the doublet at H-6' and the protons from OCH_3-5' (3.96 ppm) left C-8' as the only possible location of the biaryl axis in naphthalene moiety. The signals from two additional methoxy groups were observed at 3.94 and 4.05 ppm. The more highfield shifted one showed NOE interactions to the singlet of H-3', which enabled the assignment of the signal to originate from OCH_3-4'. The last methoxy group was likewise found to be "normally" shifted (4.05 ppm), thus the biaryl axis had to be located at C-5 in the isoquinoline moiety. This assignment was in agreement by NOE correlations between H-7' and CH_3-3 and between H-1' and H-3 (Figure 28b), which were possible only if the alkaloid was 5,8'-linked. In the isoquinoline portion, the axis was indeed found to be located at C-5, as shown by HMBC long-range couplings with the quaternary C-5 with both H_{eq}-4 and H-7, and – across the biaryl linkage – with H-7'. The NOE interactions in the series {CH_3-1–OCH_3-8–H-7} established the naphthylisoquinoline to possess the structure **30** shown in Figure 28.

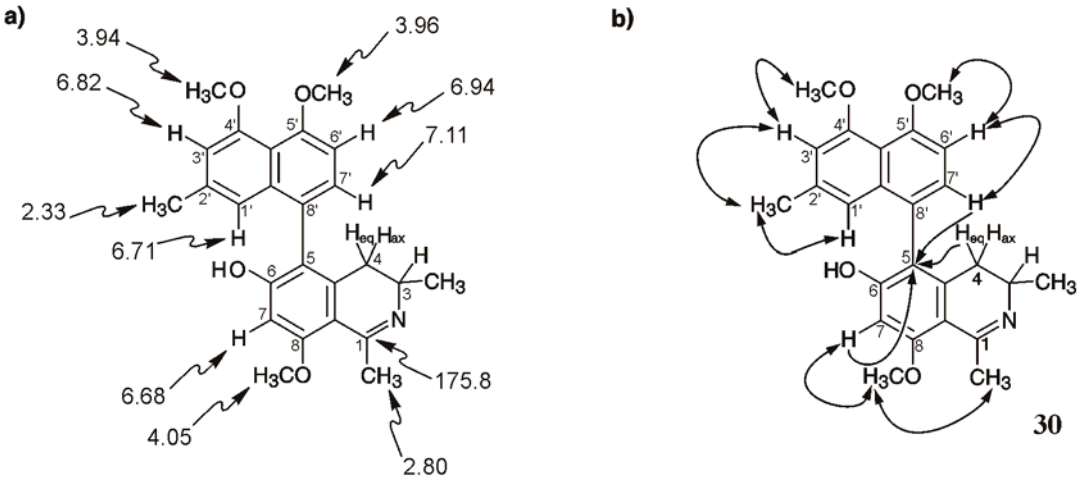

Figure 28. Selected NMR data indicative of the constitution of 6-*O*-demethylancistroealaine A (**30**): a) ^{1}H and ^{13}C NMR shifts (δ in ppm), b) HMBC (single arrows) and NOE (double arrows) interactions used for the determination of the constitution.

4.4.5.2 The Absolute Configuration

As for **26** and **28**, application of the oxidative degradation method[110] performed by M. Schraut established the absolute configuration at C-3 to be *S*. The previously mentioned NOE interactions between H-7' and CH_3-3 and between H-1' and H-3 revealed the *P*-configuration of the biaryl axis (Figure 29). This absolute axial configuration of **30** was confirmed by the close resemblance of its CD spectrum with that of the known alkaloid ancistroealaine A (**20**) (see Figure 33 for structure).[30] The alkaloid was thus found to be novel and represents the 6-*O*-demethyl analog of ancistroealaine A (**20**), and was thus named 6-*O*-demethylancistroealaine A.[147]

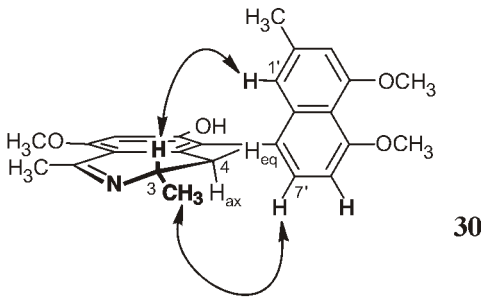

Figure 29. Configuration at the biaryl axis of **30** relative to the stereogenic center through NOE interactions.

4.4.6 Structural Elucidation of 6,5'-*O,O*-Didemethylancistroealaine A (31)

4.4.6.1 Spectroscopic Characterization

Not only did compounds **30** and **31** show great chromatographical similarity, but the spectral data of the two also revealed a close relation of the compounds. HRMS (ESI) showed compound **31** to possess a molecular formula of $C_{24}H_{25}NO_4$; in comparison with the structure of **30**, this correlates to the loss of 14 mass units, *i.e.*, CH_2, suggesting that the alkaloid was an *O*-demethylated derivative of **30**. The NMR data were in good in agreement with those of **30**, and again the presence of a naphthyldihydroisoquinoline alkaloid was indicated by a low-field shifted signal of C-1 at 175.7 ppm in the ^{13}C NMR, and the signal of CH_3-1 at 2.79 ppm in the ^1H NMR. Throughout the NMR investigations only minor negligible changes in the chemical shifts were observed, the only significant difference being the presence of just two methoxy groups, thus substantiating the assumption that **31** represents a *O*-demethylation analog of **30**. NOE correlations between the methoxy groups resonating at 4.04 and 4.10 ppm and H-7 and H-3', respectively, enabled the assignment of the two methoxy groups to C-8 and C-4'. Thereby, leaving the only possible site for the *O*-demethylation to be at C-5'. This conclusion was further confirmed since H-6' showed HMBC long-range couplings to both C-4' and C-5', the signals of which were both downfield shifted, thus again indicating that an oxygen function remained at position C-5', but now as a hydroxy group instead of a methoxy group. The spin pattern system of the aromatic protons consisting of two doublets and three singlets combined with the "normal" shifted signal of CH_3-2' (2.34 ppm), left C-6' and C-8' to be the coupling position for the biaryl axis in respect to the naphthalene moiety. The NOE correlations in the series {H-1'–CH_3-2'–H-3'–OCH_3-4'} and H-1' with both, H-3 and H_{eq}-4, unambiguously proved the naphthylisoquinoline alkaloid to be of the 5,8'-coupling type. Thus, at least from its constitution, the compound is the 5'-*O*-demethyl analog of 6-*O*-demethylancistroealaine A (**30**) (Figure 30a).

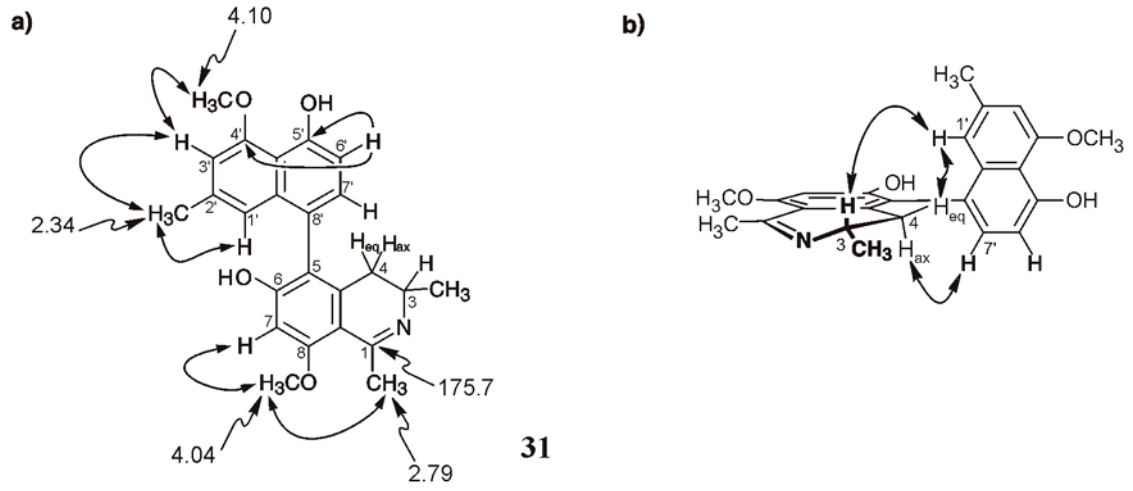

Figure 30. Selected NMR data of 6,5'-*O,O*-didemethylancistroealaine A (**31**): a) ^{1}H and ^{13}C NMR shifts (ppm), HMBC (single arrows) and NOE (double arrows) interactions relevant for the constitution, b) configuration at the axis relative to the stereogenic center through NOE interactions.

4.4.6.2 The Absolute Configuration

The formation of 3-(*S*)-aminobutyric acid (**19**) by ruthenium-catalyzed oxidation[110] of **31** carried out by M. Schraut, proved that the alkaloid is *S*-configured at C-3. It was thus possible to assign the stereo array of the axis to be *P*-configured, from the previously mentioned NOE interactions between H-1' with both H-3 and H_{eq}-4 and additionally between H-7' and H_{ax}-4 (Figure 30b). This assignment was further confirmed, since the CD spectrum of ancistroealaine A (**20**)[30] was – as expected – very similar to that of **30**, revealing the compound to possess the structure **31** (Figure 30b) *i.e.*, the – also novel – 5'-*O*-demethyl derivative of **30**; it was thus named 6,5'-*O,O*-didemethylancistroealaine A.[147]

4.4.7 Structural Elucidation of 5-*epi*-6-*O*-Methylancistrobertsonine A (32)

4.4.7.1 Spectroscopic Characterization

The fifth new compound and 6-*O*-methylhamatinine (**21**) were difficult to separate by reversed-phase HPLC. The use of fast centrifugal partition chromatography (FCPC), a liquid-liquid chromatographical procedure, enabled a preparative-scale separation of 65% of the alkaloids present in the crude extract in a pure state, with complete recovery of the remaining contaminated material.

The resolved fifth compound, corresponding to a molecular formula of $C_{27}H_{33}NO_4$ according to HRMS (ESI), showed the ^{1}H NMR spectrum of a fully *O*- and *N*-methylated naphthyltetrahydroisoquinoline alkaloid, with four methoxy groups (3.98, 3.95, 3.93, and 3.65 ppm), three *C*-methyl groups (2.27, 1.52, and 1.07 ppm), and finally a three-proton singlet with a chemical shift (2.54 ppm) characteristic of an *N*-CH_3 group. The position of the latter was unequivocally assigned by NOE interactions with all proximal protons H-1, C*H*$_3$-1, H-3, and C*H*$_3$-3, and further by HMBC long-range correlations of the CH_3-protons with both, C-1 and C-3. In the aromatic region two doublets and three singlets were found, each corresponding to one proton. The H,H-COSY experiment revealed only two – rather than three – protons to be adjacent to each other, and thus the spin pattern system hinted at an either 6'- or 8'- coupling site in the naphthalene portion. This was supported by the "normal" chemical shift of CH_3-2' (2.27 ppm), revealing the methyl group to be unaffected by the anisotropic field of the isoquinoline ring. NOE interactions between H-6' and OC*H*$_3$-5', combined with the long-range coupling between H-1' and the quaternary carbon atom C-8' (127.5 ppm) as evidenced by HMBC, located the biaryl axis to be at C-8' in the naphthalene portion.

The signal from H-1' was assigned by NOE interactions with H_{ax}-4 and by the NOE correlations in the series {H-1'–CH_3-2'–H-3'–OCH_3-4'}. Long-range couplings between the quaternary C-5 to both, H-7 (6.72 ppm) and across the biaryl axis to H-7' (7.09 ppm) as evidenced by HMBC, combined with NOE interactions in the series {H_{ax}-4–CH_3-3–CH_3-N–CH_3-1–OCH_3-8–H-7–OCH_3-6} showed the biaryl axis to be located at C-5 of the isoquinoline ring. These findings established the naphthylisoquinoline alkaloid to possess the constitution **32** shown in Figure 31a.

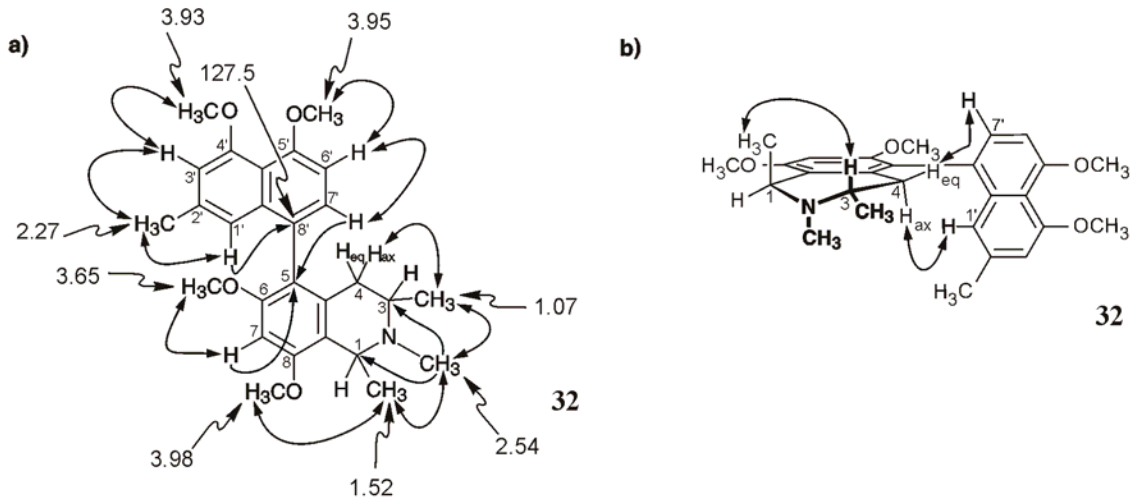

Figure 31. Selected NMR data of 5-*epi*-6-*O*-methylancistrobertsonine A (**32**): a) ^{1}H and ^{13}C NMR shifts (ppm), HMBC (single arrows) and NOE (double arrows) interactions relevant for the constitution, b) configuration at the axis relative to the stereogenic centers at C-1 and C-3 through NOE interactions.

4.4.7.2 The Absolute Configuration

An NOE interaction between CH_3-1 and H-3 indicated a relative *trans*-configuration at C-1 versus C-3. Ruthenium-mediated oxidative degradation[110] carried out by M. Schraut of **32** yielded *N*-methylalanine and (*S*)-3-methylaminobutyric acid as the main products. Accordingly, **32** is *S*-configured both at C-1 and C-3. NOE interactions of H_{ax}-4 with H-1' and H_{eq}-4 with H-7' revealed the axis to be *M*-configured (Figure 31b). This is agreement with the almost mirror image CD spectrum of **32** compared to that of ancistrobertsonine A[119] (**33**, see Figure 32), which is *P*-configured at the – CD-dominating[149] – biaryl axis. Compound **32** had hitherto not been described in the literature, and was named 5-*epi*-6-*O*-methylancistrobertsonine A,[147] since it represents the respective derivative of ancistrobertsonine A (**33**).

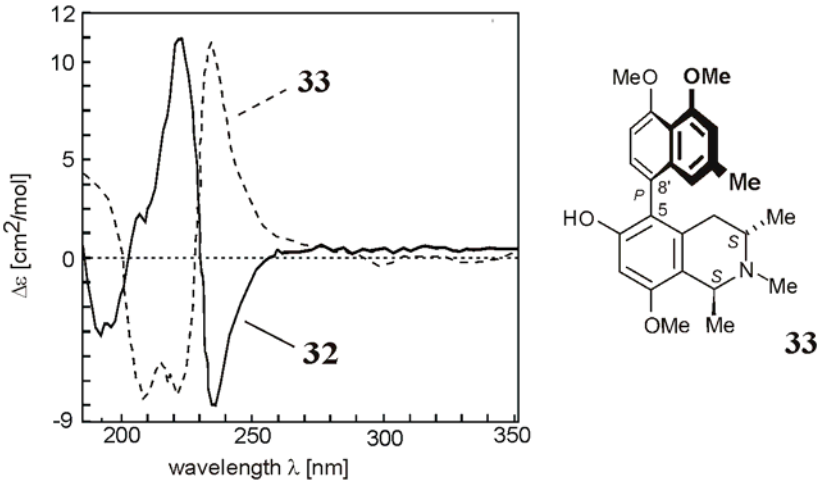

Figure 32. CD spectra of **32** and ancistrobertsonine A (**33**).

4.4.8 Identification and Isolation of Known Naphthylisoquinoline Alkaloids

Analyses of the crude extract including HPLC-UV, HPLC-MS, and co-elution with authentic reference material easily permitted the identification of the known naphthylisoquinoline alkaloids; 6-*O*-demethylancistrobrevine A (**34**), described for the first time as isolated from *A. abbreviatus*[22], however, except for its melting point and $[\alpha]_D^{20}$ data no further spectroscopic, physical, or chromatographical data were reported; hamatine (**27**) and ancistrocladine (**35**), which were isolated for the first time from *A. hamatus*[146] and *A. heyneanus*,[150] respectively (subsequently they were both identified in several *Ancistrocladus* species, both Asian[144,145] as well as African[115,119]); hamatinine (**29**) and 6-*O*-methylhamatinine (**21**), both previously isolated from *A. cochinchinensis*;[151] ancistroealaine A (**20**) prepared fully synthetically[152,153] and isolated from the Central African species *A. ealaensis*,[30] see Figure 33. All of the compounds were isolated in milligram quantities to be available for bioactivity and other testing. The recorded spectroscopic and physical data of compounds **20** and **27**-**35** were identical to those reported in the literature. A huge discrepancy was found between the recorded $[\alpha]_D^{20}$ of **34** and the previously reported one,[22] *i.e.*, $[\alpha]_D^{20}$ = +55 vs. $[\alpha]_D^{20}$ = -80. However, good agreement was found with the specific rotation reported for ancistrobrevine A (structure not shown), *i.e.*, $[\alpha]_D^{20}$ = +54,[22] thus hinting that the one obtained within this work is the correct one, and the previous reported $[\alpha]_D^{20}$ value -80 were a mistake.

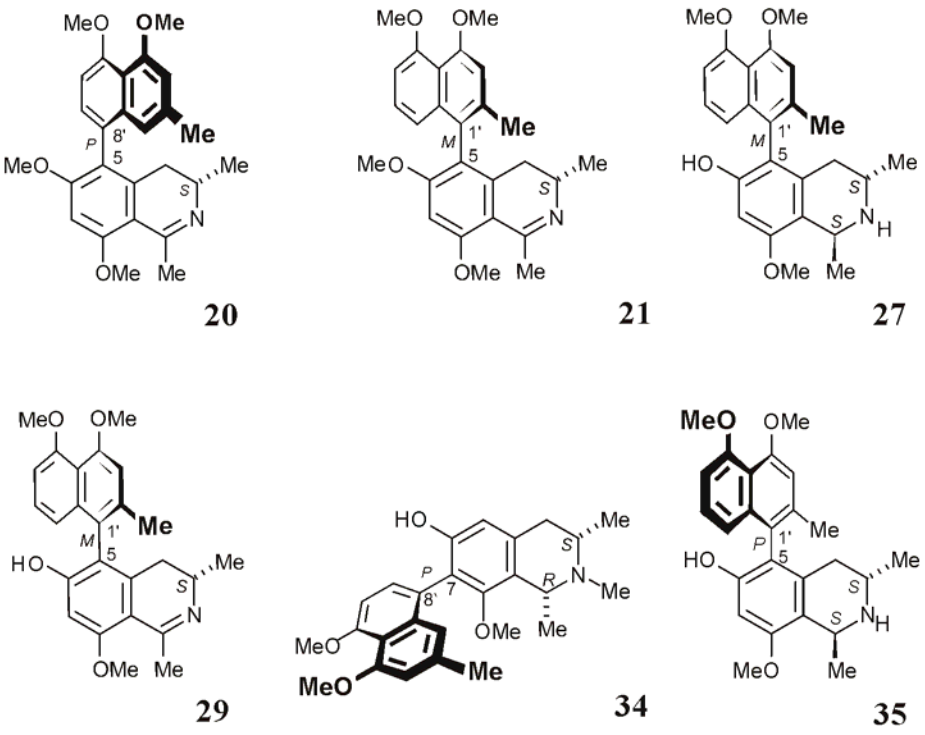

Figure 33. Structures of the known naphthylisoquinoline alkaloids **20**, **21**, **27**, **29**, **34**, and **35** isolated from root material of the investigated Congolese *Ancistrocladus* species (habitat: Yeteto).

4.5 Bioactivity of the Alkaloids

The newly isolated compounds **26**, **28**, and **30-32** along with the known 6-*O*-demethylancistrobrevine A (**34**) were screened for their activities against pathogens belonging to the genera *Plasmodium*, *Leishmania*, and *Trypanosoma* (Table 4). These bioactivity screenings were carried out at the Swiss Tropical Institute by Dr. R. Brun and coworkers. The additionally known naphthylisoquinoline alkaloids had already in previously work been screened for their activities against these pathogens. All of the naphthylisoquinoline alkaloids **26**, **28**, **30-32**, and **34** tested were found to exhibit weak antiplasmodial activities against the K1 strain of *Plasmodium falciparum* (resistant to chloroquine (**2**) and pyrimethamine). The antitrypanosomal activities exhibited by **26**, **28**, and **30-32** were found to be moderate to weak against the pathogens of African sleeping sickness (*Trypanosoma brucei rhodesiense*), and Chagas' disease (*T. cruzi*). Compound **32** was found to display an activity against *Leishmania donovani* (visceral leishmaniasis) within the range of the most active naphthylisoquinolines tested.[126] By contrast the two *O*-demethylated derivatives **30** and **31** of the highly

antileishmanially active ancistroealaine A (**20**)[30] exhibit only weak activity against *L. donovani*; thus indicating a high *O*-methylation rate as an important feature for the antileishmanial activity of the naphthylisoquinoline alkaloids.

Table 4. Bioactivities of the novel compounds **26**, **28**, **30-32**, and **34**.

	IC_{50} [µg/mL]					
	26	**28**	**30**	**31**	**32**	**34**
P. falciparum (strain: K1)	1.0	2.8	1.8	2.1	1.9	2.1
Standard: chloroquine 0.041[a]						
T. cruzi	18.2	15.2	10.5	6.4	14.6	9.5
Standard: benznidazole 0.53[a]						
T. b. rhodesiense	2.0	9.8	13.9	9.7	6.9	5.0
Standard: melarsoprol 0.00046[a]						
L. donovani	4.4	n.e.[b]	17	21.2	1.6	19.4
Standard: miltefosine 0.05[a]						
Cytotoxity	70.2	>90	>90	>90	68.0	25.3

[a] All values in µg/mL. [b] No effect.

4.6 Chemotaxonomic Considerations

From a chemotaxonomic point of view, all of the compounds reported have an oxygen function at C-6 and the *S*-configuration at C-3. These phytochemical characteristics show close relations of the present as yet undescribed Congolese *Ancistrocladus* species, to the known members of Ancistrocladaceae from Central and East Africa, [30,119-121,126] and to those from Asia. [125,144-148] The species is clearly different from those Central and West African, which have been found to produce the "Dioncophyllaceae-type" alkaloids, characterized by *R*-configuration at C-3 and the lack of an oxygen function at C-6 and also mixed, hybrid types (*e.g.*, *R* at C-3 and oxygenated at C-6).

The close relationship with the Asian Ancistrocladaceae species was further confirmed by online screening for the presence ancistrocladinium A (**25**) and B (**22**) in crude extracts of other *Ancistrocladus* species, using the analytical "triad" HPLC-MS, HPLC-NMR, and HPLC-CD. The screening was carried out by I. Kajahn and T. Gulder. The analysis led to the successful identification of ancistrocladinium A (**25**) in *A. cochinchinensis*, and *A. tectorius*

(both from Vietnam), and ancistrocladinium B (**22**) in *A. benomensis* (from Malaysia) and *A. heyneanus* (from India). Their chromatographical and spectroscopic (MS, ^{1}H NMR, and CD) data were found to be identical to those of the authentic isolated material.

5 Isolation of Naphthylisoquinoline Alkaloids from *Triphyophyllum peltatum* (Dioncophyllaceae)

5.1 *Triphyophyllum peltatum*

Besides Ancistrocladaceae, the only other plant family known to produce naphthylisoquinoline alkaloids, are the closely related Dioncophyllaceae.[22,154] This small palaeotropical family consists of only three monotypic genera; *Triphyophyllum*, *Habropeltatum*, and *Dioncophyllum*. All three species are lianas climbing up high trees, by means of hooked leaves[155] and have unique large thin seeds with a large membranous wing, which during maturation exceed the size of the fruit they are borne from (Figure 34).[156] *T. peltatum*, which is endemic to the Ivory Coast in West-Africa, has been found to be carnivorous as a juvenile plant.[157]

Figure 34. Characteristic hooked leave and seeds of the "part-time" carnevivorous liana *T. peltatum.* Pictures provided by Dr. H. Rischer.

Among the three Dioncophyllaceae species, *T. peltatum* is phytochemically by far the best investigated one. Moreover, it has the highest content of naphthylisoquinoline alkaloids, while *H. dawei* and *D. thollonii* produce large amounts of related but nitrogen-free naphthoquinones and teralones.[158] Nearly 20 different naphthylisoquinoline alkaloids have been isolated from *T. peltatum* so far.[158] Some of these structurally and biosynthetically unique secondary metabolites display highly potent *in vitro* and *in vivo* antiplasmodial activities, like dioncopeltine A (**7**) and dioncophyllines B (**24**) and C (**6**), (Figure 36).[43,44,159]

5.2 Extraction and Isolation

5.2.1 Extraction by Soxhlet Apparatus

Soxhlet extraction, where the samples are washed with repeated volumes of fresh solvent, leads to an extremely efficient extraction process. The advantages of the method in comparison to other extraction methods are numerous, including avoiding steps of phase

partitioning and utilizing small volumes of solvent. For large-scale extraction of plant material of *T. peltatum* a sequentially soxhlet extraction procedure, based on the solvents of different polarities, *i.e.*, PE, $CHCl_3$, CH_2Cl_2, MeOH, has been developed by Dr. D. Feineis and coworkers within our group.[160] The procedure leads to good prefractionations of naphthylisoquinoline alkaloids present in the plant material, achieved already at the first extraction step.[160]

5.2.2 Fast Centrifugal Partition Chromatography (FCPC)

For further large scale purification of the naphthylisoquinoline alkaloids present in the crude extract of *T. peltatum* obtained by soxhlet extraction, a preparative chromatographic method was developed using fast centrifugal partition chromatography (FCPC).

The FCPC chromatography instrument is a continuous development of the liquid-liquid chromatography methodology based on immiscible liquid phases.[161,162] Though closely related, the FCPC instrument is different from the most comment liquid-liquid chromatography method, *i.e.*, the high speed counter current chromatography (HSCCC). Both methods employ fractionation by a hybrid technique of liquid-liquid counter-current distribution and liquid chromatography, in conjunction with the use of centrifugal force.[163] Whereas HSCCC instruments are equipped with capillary columns upon which centrifugal force field is generated from both rotational and synchronous planetary motion,[164] the FCPC columns contains disks engraved with hundreds of separation channels, connected with ducts and are arranged in a circle around the rotor of a centrifuge so that the channels are oriented parallel to the direction of the centrifugal field (Figure 35).[161-163]

The FCPC column is filled with the liquid stationary phase prior to the separation process. While the rotor of the centrifuge is in motion (up to 1400 rpm), the mobile liquid phase is pumped into the column, thereby providing vigorous mixing between stationary and mobile phases, as well as retention of a very large fraction of the stationary phase.[161] The FCPC has a higher loading capacity in comparison to the HSCCC and usually also a higher partition efficiency, although still not reaching the resolution achievable by HPLC techniques.[163]

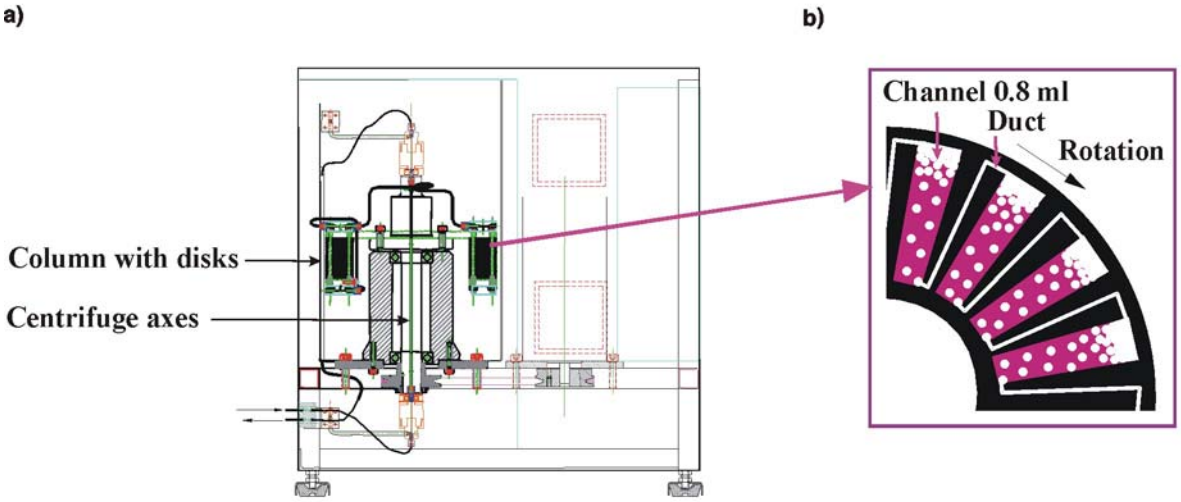

Figure 35. a) Front view of FCPC apparatus, b) basic channel design engraved into the disks of the column.

FCPC has several distinctive properties: (a) it depends for its efficiency solely upon the distribution coefficient (K_D) of a compound between the stationary and mobile phases, (b) it accomplishes excellent separation by taking advantage of the high volume of stationary phase (50% to 90% of total volume), (c) it eliminates the irreversible adsorptive loss of samples onto the solid support used in conventional column chromatography and HPLC, (d) it uses remarkably small amounts of expensive solvents, (e) it permits quantitative recovery of applied sample regardless of resolution of components, *i.e.*, a failed separation can be easily and rapidly re-run on an appropriately modified system without loss of precious starting material, and (f) it can be scaled-up from analytical- to preparative-scale separation in a completely straightforward manner.[164,165]

To achieve a good separation with FCPC it is important that the compound of interest can be equally distributed between two immiscible phases so the distribution coefficient (K_D) is between 0.5 and 2 ($K_D = C_{lower\ phase} / C_{upper\ phase}$).[164,165] Inspired by the ARIZONA system[166] and previous isolation work by G. Lang[167] within our group, small amounts of the extract of *T. peltatum* were solved in the biphasic solvent system of *n*-heptane – ethyl acetate (EtOAc) – methanol (MeOH) – water in different solvent combinations. Subsequently HPLC analysis conducted of the upper phases and the lower phases showed that the solvent system *n*-heptane – EtOAc – MeOH – water in a ratio of 8:2:8:2 with the use of the lower phase as the mobile phase was most suitable for the resolution of the naphthylisoquinoline alkaloids in the sequential extracts of *T. peltatum*.

By the use of this system up to 1 g of raw extract was injected in each run into the FCPC and within a chromatographic run of one hour, fractions of several hundred milligrams enriched in the respective naphthylisoquinoline alkaloids were obtained in a purity of up to 90% as estimated by NMR. Thus, the FCPC has a much higher throughput than procedures using preparative HPLC to resolve crude extracts, on the other hand HPLC provides a much better resolution.

5.2.3 Preparative HPLC

The fractions obtained by FCPC treatment of the crude plant extracts of *T. peltatum* were further resolved by preparative HPLC.

5.2.4 Isolation from Roots of *T. peltatum*

By conducting the isolation procedure using the FCPC on crude extracts of root material from *T. peltatum* several bioactive naphthylisoquinoline alkaloids were isolated in larger amounts: dioncophylline A (**8**);[168] dioncophylline B (**24**);[131] dioncophylline C (**6**);[130] dioncopeltine A (**7**);[129] dioncolactone A (**36**)[129] (Figure 36), all of the alkaloids were isolated for the first time from root material of *T. peltatum*. The recorded spectroscopic data of **6-8**, **24**, and **36** were found to be in good agreement with those reported in the literature.

5.2.5 Isolation from Leaves and Twigs of *T. peltatum*

From crude extracts of leaves and twigs from *T. peltatum*, the isolation in smaller amounts of known bioactive naphthylisoquinoline alkaloids was successfully achieved by preparative HPLC: habropetaline A (**37**), identified for the first time in *Habropeltatum dawei* by HPLC-CD, HPLC-NMR, and HPLC-MS/MS[133] and subsequently isolated from *T. peltatum*;[169] and dioncophyllinol B (**38**) isolated for the first time from root material of *T. peltatum*[170] (Figure 36). The recorded spectroscopic data of **37** and **38** were found to be identical to those reported in the literature.

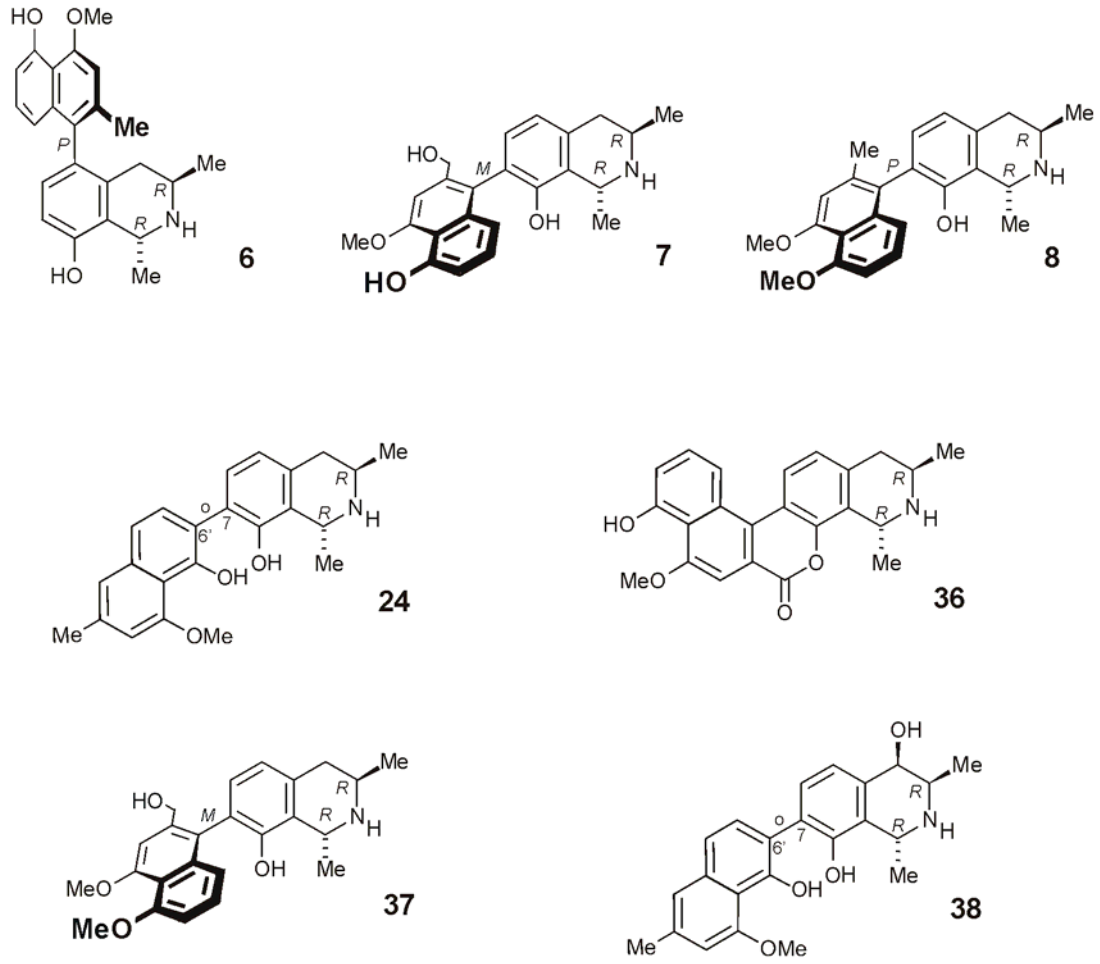

Figure 36. Naphthylisoquinoline alkaloids isolated from *T. peltatum*; dioncophylline C (**6**), dioncopeltine A (**7**), dioncophylline A (**8**), dioncophylline B (**24**), dioncolactone (**36**), habropetaline A (**37**), and dioncophyllinol B (**38**).

6 γ-Ray Synthesis of Antiplasmodial Bioactive Naphthylisoquinoline Analogs

6.1 Introduction

6.1.1 Radiation Chemistry

The wide field of radiation chemistry was initiated by the discovery of X-rays by Röntgen, radioactivity by Becquerel and the particle nature of electrons by Thomson at the end of the 19th century. At the beginning of the 20th century, one of the early experiments using radiation showed that hydrogen and oxygen are formed by the irradiation of water.[171] Later on, radiation chemistry was defined as the science of the chemical effects brought about by the absorption of ionizing radiation on matter.[172] Irradiation with high-energy photons usually results in the ejection of an electron from the matter leading to the formation of radicals.[173]

6.1.1.1 Radiation Chemistry of Organic Compounds in Aqueous Solutions

It has been found that during irradiation of an aqueous solution most of the energy is absorbed by the water itself.[174,175] Firstly, a water molecule absorbs energy and is transformed into an exited state or an electron is ejected and a water ion is formed.[174,175] These species are immediately transformed into radical and ionic primary irradiation products. The most abundant primary products are solvated electrons, hydroxyl radicals and hydrogen atoms.[176] Free electrons are transformed into solvated electrons, excited state water degrades into a hydrogen and a hydroxyl radical, and water radicals are converted into a hydroxyl radical and a proton.

Solvated electrons react mainly as reducing agents, whereas hydrogen atoms can react as reducing agents, *e.g.*, by addition to double bonds, or as oxidizing agents by abstraction of hydrogen atoms from saturated bonds. The hydroxyl radicals can react as oxidizing agents by abstraction of electrons or hydrogen atoms or by addition to unsaturated bonds. Hydrogen abstraction occurs for example in alcohols; in alkanes hydrogen abstraction or breaking of C-C bonds is observed.[173] With the formation of these products, new radicals are often formed, leading to chain reactions and more efficient use of deposed energy.

Irradiation of organic compounds in aqueous or organic solution has been found to lead to the formation of organic radicals either through direct ionization or via the primary radiolysis of water.[177]

For the irradiation of aromatic compounds in water it has been reported that the addition of primary water radiolysis products to double bonds can take place, forming cyclohexadienyl and hydroxycyclohexadienyl radicals.[177,178] These organic radicals combine and disproportionate to give a complex mixture of products such as phenol, biphenyl, cyclohexadiene, phenylcyclohexadienes, dicyclohexadienes and others.[179,180]

The most abundant products after irradiation of benzene are dimeric compounds such as biphenyl, phenylcyclohexadiene, phenylcyclohexene and non-aromatic bi-cyclic compounds or compounds with a higher molecular weight (three or more rings) but with an equivalent composition. The average molecular weight increases with the absorbed dose.[181,182]

6.1.1.2 γ-Ray Synthesis

γ-ray synthesis was first introduced by Prof. Dr. G. Folkers, U. Kessler and A. Wuhrmann from Swiss Federal Institute of Technology [12,183,184] as a new method to create chemical libraries, which could be used for high-throughput screening technologies. Later on, the method was used at the Institute of Pharmacy at the University of Würzburg by Prof. Dr. U. Holzgrabe and coworkers for the development of new acetylcholinesterase inhibitors.[13] In these preliminary experiments it was shown that γ-ray synthesis might be an attractive complementary method for combinatorial chemistry or natural compounds, the classical sources for new lead compounds in drug discovery.[184]

6.1.2 Strategy for γ-Ray synthesis

3D QSAR investigations of the naphthylisoquinoline alkaloids[142,143] have predicted that simplified naphthylisoquinoline structures (structures not shown), without any stereogenic centers, can display antiplasmodial bioactivities in the same range as found for the most potent naturally occurring alkaloids. The starting material for the γ-ray synthesis should be substances consisting of pharmacophoric elements that can be expected to be rearranged through irradiation in a new way.[13] These considerations inspired the choice of compounds **39**–**42** as the starting materials (Figure 37) for the γ-ray synthesis of antiplasmodial compounds; all substances are commercially available. Samples for irradiation were prepared containing either one or two compounds in equimolar concentrations, which led to a total of ten samples plus one sample containing only solvent. The irradiation of the samples was carried out at PPS Laboratories (Paul Scherrer Institute, Villigen, Switzerland), by A.

Wuhrmann using a ^{60}Co source at 50 kGy and one at 500 kGy, in order to determine the effect of low and high doses.

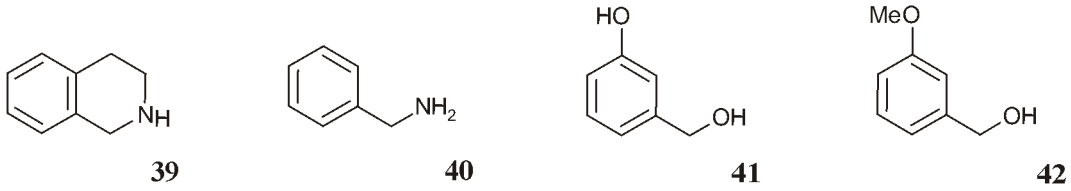

39 **40** **41** **42**

Figure 37. Starting materials for the γ-ray synthesis: 1,2,3,4-tetrahydroisoquinoline (**39**), benzylamine (**40**), 3-hydroxy-benzyl-alcohol (**41**), and 3-methoxy-benzyl-alcohol (**42**).

The solvent was chosen as a mixture of MeOH-water 9:1 on the basis of the solubility of the substances and with the intention of obtaining polar products.

6.2 Bioactivity Guided Isolation of γ-Ray Products

Isolation of antiplasmodial irradiation products was performed by a bioactivity guided fractionation of the irradiated samples, directed by their efficacy against *P. falciparum*. The general work-procedure is depicted in Figure 38.

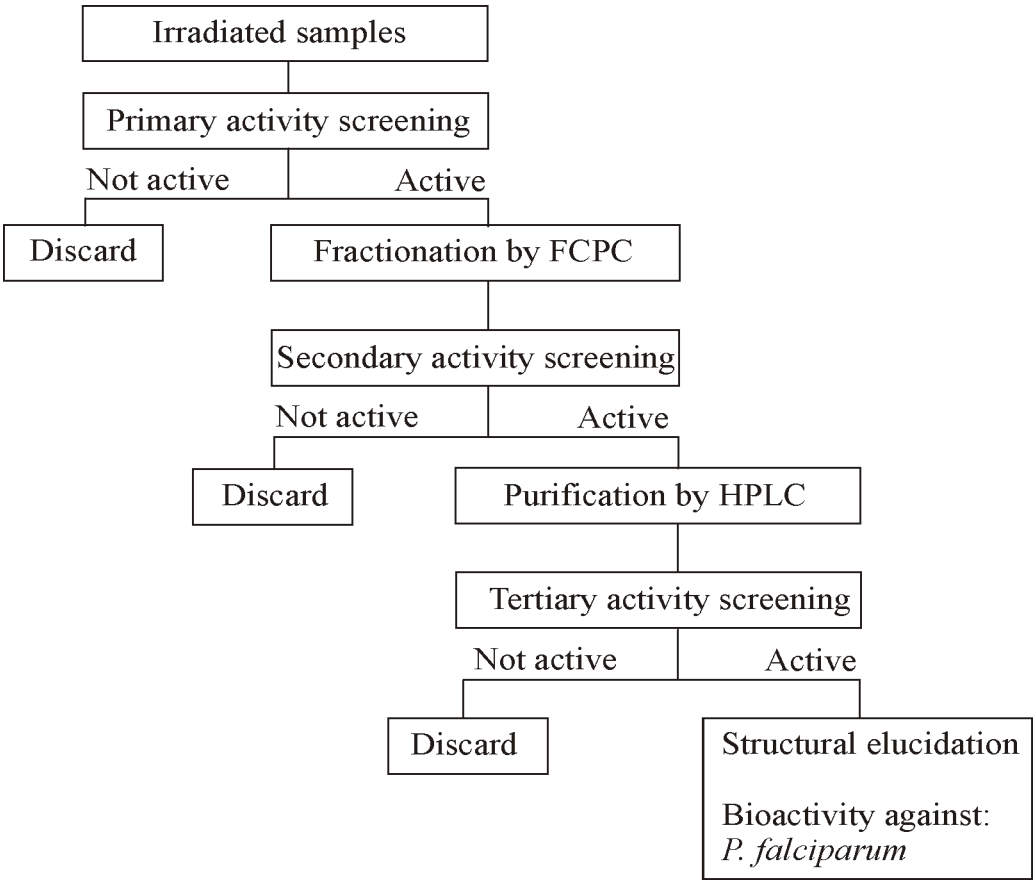

Figure 38. Work-procedure of the bioactivity guided isolation of antiplasmodial irradiation products.

6.2.1 Bioactivity of Starting Material and Primary Activity Screening

For sake of comparison, the starting compounds (**39**–**42**) and all the irradiated samples were initially tested at the Danish University of Pharmaceutical Sciences by Prof. Dr. S. B. Christensen and coworkers for their antiplasmodial activity against *P. falciparum* (strain 3D7) in a modified Desjardins test,[185] at different concentration intervals (Chapter Ex. 5.2). The obtained IC_{50} values (Table 5) were assigned as if the reaction mixtures contained unchanged starting material only, with an activity lower than 50 μM being defined as inactive.

Table 5. IC_{50} [μM] against *P. falciparum* (strain: 3D7) of the starting compounds and the samples irradiated with 50 and 500 kGγ.

	IC_{50} [μM] *P. falciparum* (strain: 3D7)[a]								
Samples	**39**	**40**	**41**	**42**	**39 + 40**	**39 + 41**	**39 + 42**	**40 + 41**	**41 + 42**
Preparation									
Control	~50	>50	>50	>50	n.d.[b]	n.d.[b]	n.d.[b]	n.d.[b]	n.d.[b]
500 kGγ	>50	>50	>50	>50	>50	>50	>50	>50	>50
50 kGγ	~20	>50	~40	>50	~15	>50	>50	>50	>50

[a] Standard: chloroquine 0.003 μM. [b] Not determined.

The bioactivity screening revealed the irradiated samples containing 1,2,3,4-tetrahydroisoquinoline (**39**) and the mixture of **39** with benzylamine (**40**) (**39 + 40**) to display higher antiplasmodial activity against *P. falciparum* than found for the control screening of the starting material.

Furthermore, the screening showed the higher irradiation dose to have a negative effect on the antiplasmodial activity, although HPLC analysis showed that quantitatively more products had been formed. Later it was found that the antiplasmodially active products were found in lower concentrations in the samples irradiated with the higher dose in comparison to the samples irradiated with the lower dose.

HPLC and HPLC-MS analyses of the samples containing **39** showed that 34% of the starting material to be remained in the sample after irradiation at 50 kGy. Twelve peaks for irradiation products were observed (peaks A-L, see Figure 39), all with an absorbance intensity >15% at 220 nm in comparison to the remaining starting material. Additionally the HPLC-MS analyses revealed three of these peaks to have a mass higher than that of the starting material (peaks C, H, and L, see Figure 39).

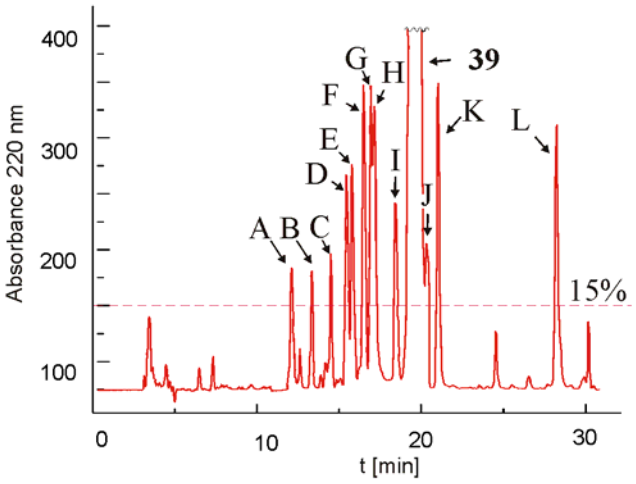

Figure 39. HPLC chromatogram of the irradiated sample containing **39**; the dashed line marks the 15% level of intensity of **39** recorded by 220 nm. HPLC-MS analyses revealed peaks C, H, and L to originate from compounds with a higher mass than the starting material. Peaks C and H were identified as compound **43** and **44**, respectively.

Similar analyses of the sample containing the mixture **39** + **40** irradiated at 50 kGy, showed that 20% and 25% were remaining of the two starting materials, respectively. Again twelve peaks originating from irradiation products exhibited an absorbance intensity >15% at 220 nm in comparison to the remaining starting material of **39**. Of these, four had a mass higher than that of the starting material, and two were found to be present in both samples.

6.2.2 Fractionation by FCPC and Secondary Activity Screening

Both of the active irradiated samples were each fractionated in one run by direct injection of the irradiated sample on to the FCPC. The eluents were collected in 10 mL fractions, which were subsequently analyzed by HPLC. This enabled the division of the chromatographical eluent of the **39** reaction mixture into eight fractions (*i.e.*, F1-F8) and the one of the mixture **39** + **40** into ten fractions (*i.e.*, F1-F10). The solvents of the fractions were evaporated and the residues were subsequently screened for their antiplasmodial activity (Table 6).

Table 6. IC_{50} [μM] against *P. falciparum* (strain: 3D7) of the fractions obtained by chromatography treatment using FCPC of the samples **39** and the mixture **39** + **40** irradiated at 50 kGy.

	IC_{50} [μM] *P. falciparum* (strain: 3D7)[a]									
Fraction	F1	F2	F3	F4	F5	F6	F7	F8	F9	F10
Samples										
39	>50	>50	~15	~30	>50	>50	>50	>50	n.d.[b]	n.d.[b]
39 + 40	>50	~50	~20	~15	~30	>50	>50	>50	>50	>50

[a] Standard: chloroquine 0.003 μM. [b] Not determined.

The screening revealed two fractions of **39** (*i.e.*, fractions F3 and F4) and three fractions of the mixture **39** + **40** (*i.e.*, fractions F3, F4, and F5) to display higher antiplasmodial activity than the starting compounds. These fractions were chosen for further seperation; all other fractions were discarded. HPLC-UV and HPLC-MS analyses showed these fractions to contain starting material and additionally four compounds with masses higher than that of the starting material, *i.e.*, two compounds in the fractions of **39** and four compounds in the mixture **39 + 40**, two of which were identified to be identical to those present in the fractions of **39** (Table 6).

6.2.3 Fractionation by HPLC and Tertiary Activity Screening

For the further purification of the active compounds, the fractions were resolved by preparative HPLC, analyzed by HPLC and HPLC-MS, and subsequently pooled into four subfractions (*i.e.*, SF1-SF4) each containing only one compound. The subfractions (*i.e.*, SF1-SF4) were screened for their activity against *P. falciparum* (Table 7).

Table 7. IC_{50} [μM] against *P. falciparum* (strain: 3D7) of the subfractions SF1-SF4 obtained by preparative HPLC of the fractions from the FCPC procedure.

	IC_{50} [μg/mL]			
Subfraction	SF1	SF2	SF3	SF4
P. falciparum (strain: 3D7)[a]	<10	~30	<10	<10

[a] Standard: chloroquine 0.003 μM.

The screening revealed subfractions SF1, SF3, and SF4 to contain antiplasmodially active compounds, whereas subfraction SF2 contained a near to inactive compound. From the subfractions SF1, SF3, and SF4 compounds **43**, **44**, and **45** were structurally elucidated, respectively.

6.2.4 Structural Elucidation of 3,4-Dihydro-1-Isoquinolinone (43)

3,4-Dihydro-1-isoquinolinone (**43**) was found to be present in both bioactive irradiation samples, *i.e.*, of **39** and in the mixture **39** + **40**. The molecular formula C_9H_9NO was deduced by HRMS (ESI) and from the number of signals in the ^{13}C NMR spectrum. In the aliphatic region of the ^{1}H NMR spectrum two triplet signals were found both integrating for two protons, these signals showed correlations to each other in the H,H-COSY experiment and were assigned to H_2-3 (3.43 ppm) and H_2-4 (2.81 ppm). In the aromatic region two doublets H-5 (7.29 ppm) and H-8 (7.89 ppm) and two triplets H-6 (7.44 ppm) and H-7 (7.26 ppm) indicated the presence of four ortho disposed protons, a conclusion which was confirmed by the H,H-COSY experiment. This assumption was confirmed by NOE correlations found in the series {H_2-2–H_2-3–H-5–H-6–H-7–H-8}. Thus, the compound could only possess the structure of 3,4-dihydro-1-isoquinolinone (**43**) as shown in Figure 40. The assignment was further confirmed by the chemical shift of C-1 (173.9 ppm) in the ^{13}C NMR spectrum, to which H_2-3 and H-8 showed long-range couplings in the HMBC experiments.

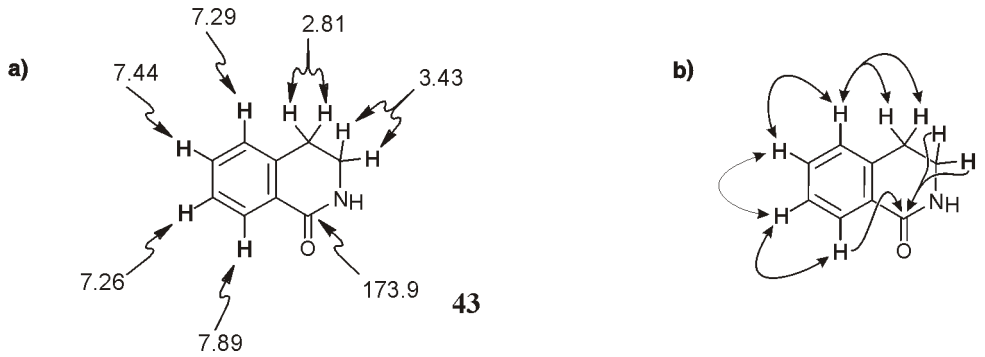

Figure 40. Selected NMR data of 3,4-dihydro-1-isoquinolinone (**43**): a) ^{1}H NMR and ^{13}C NMR shifts (δ in ppm), b) HMBC single arrows and NOE (double arrows) interactions for the determination of the constitution.

3,4-Dihydro-1-isoquinolinone (**43**) was synthesized for the first time in 1936.[186] Several bioactivities have been reported for the compound, such as an anti-inflammatory properties[187] and the induction of apoptosis.[188]

6.2.5 Structural Elucidation of 3,4-Dihydro-1-Isoquinolineamine (44)

The second irradiation product, was likewise present in both bioactive irradiation samples, *i.e.*, of **39** and in the mixture **39** + **40** and was found to correspond to a molecular formula of $C_9H_{10}N_2$ as deduced from its HRMS (ESI) and ^{13}C NMR spectral data. The ^{1}H NMR spectrum revealed a close similarity between compound **43** and **44** with the same spin pattern system of two triplets H_2-3 (3.50 ppm) and H_2-4 (2.94 ppm) in the aliphatic region and in the aromatic region two doublets H-5 (7.30 ppm) and H-8 (7.93 ppm) and two triplets H-6 (7.48 ppm) and H-7 (7.35 ppm). The H,H-COSY experiment of **44** showed the same correlations between the spin systems as found for **43**, and furthermore similar NOE correlations were found in the series {H_2-2–H_2-3–H-5–H-6–H-7–H-8}. Thus the irradiation product was identified to possess the structure 3,4-dihydro-1-isoquinolineamine (**44**) (Figure 41). The assignment was further confirmed by the presence of the downfield shifted signal of C-1 (168.5 ppm) in the ^{13}C NMR spectrum, to which H_2-3 and H-8 showed long-range couplings in the HMBC experiments.

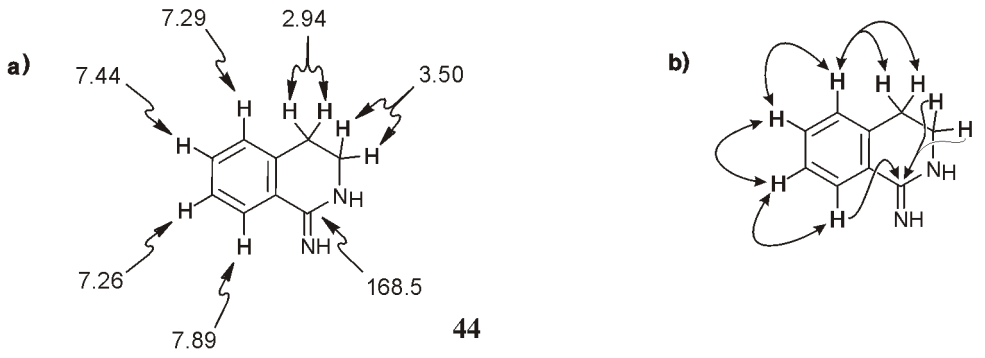

Figure 41. Selected NMR data of 3,4-dihydro-1-isoquinolineamine (**44**): a) ^{1}H NMR and ^{13}C NMR shifts (δ in ppm), b) selected HMBC (single arrows) and NOE (double arrows) interactions.

3,4-dihydro-1-isoquinolineamine (**44**) was synthesized for the first time in 1969,[189] and has been reported to possess antihypertensive activity,[190] and nitric oxide synthase inhibitor activity.[191]

6.2.6 Structural Elucidation of 1,2,3,4-Tetrahydro-1,2-Diazirino-Isoquinoline (45)

The third irradiation product was only present in the mixture **39** + **40**, the HRMS (ESI) data of **45** were found to be near to identical with the one of **44**, thus **45** likewise corresponded to the molecular formula $C_9H_{10}N_2$. Despite this obvious similarity, the NMR data of **45** were very different from the ones of **43** and **44**. In the aliphatic region two multiplets were observed both integrating for two protons for H_2-3 (3.08 ppm) and H_2-4 (2.92 ppm), additionally a downfield shifted signal of H-1 (5.22 ppm) was found as a singlet integrating for one proton. The signals in the aromatic region were highly overlapping. Resolution of these signals, which could enable a structural assignment, failed, although ^{1}H NMR experiments were recorded in various solvents ($CDCl_3$, MeOD, acetone-d_6, pyridine-d_5). Integration of the region with the overlapping signals showed that they corresponded to four protons. The H,H-COSY experiments revealed couplings between the multiplets in the aliphatic region and between the overlapping signals in the aromatic region. NOE correlations were found between the signal of H_2-4 and the overlapping signals in the aromatic region and furthermore between these signals and the signal of H-1. The HMBC experiment revealed long-range couplings between H_2-3 and C-1 (72.5 ppm); furthermore HMBC correlations were found from the overlapping signals in the aromatic region to C-1. The overlapping signals in the aromatic region prevented an unequivocal structural assignment of this irradiation product. However, the diastereotopic nature of the methylene protons indicated that the compound was chiral. Taking into account also the molecular formula, the structure 1,2,3,4-tetrahydro-1,2-diazirino-isoquinoline (**45**) (Figure 42) is the most probable for this irradiation product.

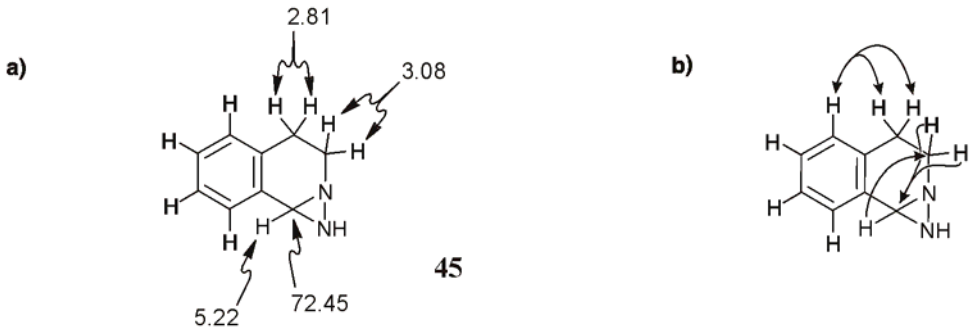

Figure 42. Selected NMR data of 1,2,3,4-tetrahydro-1,2-diazirino-isoquinoline (**45**): a) ^{1}H NMR and ^{13}C NMR shifts (δ in ppm), b) selected HMBC (single arrows) and NOE (double arrows) interactions.

1,2,3,4-tetrahydro-1,2-diazirino-isoquinoline (**45**) had been synthesized previously.[192]

6.3 Bioactivity of the Irradiation Products 43–45

The radiochemically synthesized compounds **43-45** were tested for their bioactivities against pathogens belonging to the genera *Plasmodium*, *Leishmania*, and *Trypanosoma* (Table 8). The bioactivity screenings were carried out at the Swiss Tropical Institute by Dr. R. Brun and coworkers. Compounds **43-45** exhibited only weak antiplasmodial activity against the K1 strain (Basel) of *P. falciparum*. The very limited amount isolated precluded an IC_{50} characterization of the activity displayed by the compounds against the chloroquine (**2**)-sensitive 3D7 strain (Copenhagen) of *P. falciparum*. The antitrypanosomal activities exhibited by the compounds were found to be moderate to weak against the pathogens of African sleeping sickness (*Trypanosoma brucei rhodesiense*), and Chagas' disease (*T. cruzi*). Compound **43** was found to display significant activity against *Leishmania donovani* (visceral leishmaniasis), and is remarkably only by a factor of three less active than the most active naphthylisoquinolines tested.[126]

Table 8. Bioactivities of the compounds **43-45**.

	IC_{50} [μg/mL]		
	43	**44**	**45**
P. falciparum (strain: K1)	2.0	2.6	3.4
Standard: chloroquine 0.041[a]			
T. cruzi	18.2	15.2	10.5
Standard: benznidazole 0.53[a]			
T. b. rhodesiense	1.8	2.0	2.6
Standard: melarsoprol 0.00046[a]			
L. donovani	6.6	n.e.[b]	12
Standard: miltefosine 0.05[a]			
Cytotoxity	70.0	82.0	43.8

[a] All values in μg/mL. [b] No effect.

6.4 Evaluation of the Method

γ-ray synthesis has proved to be a suitable tool for the generation of a small compound library. FCPC/HPLC bioassay guided fractionation as deconvolution tool was used in this study to identify compounds possessing high antiplasmodial activity against *P. falciparum*. However, the bioactivity screening was both time and resource consuming; a faster screening method would be an advantage. HPLC-MS results showed that the irradiation procedure leads

to compounds with masses in the range of 180-500 mass units. This meets the mass criterion of Lipinski's "rule of five" for drug-like molecules,[193] and thus makes the method suitable as a complementary tool to traditional random chemistry methods.

The mechanism of reaction leading to the identified compounds is not obvious and cannot be explained by the traditional reactions known from radiation chemistry.[174-182] For compounds **44** and **45** an additional nitrogen atom has been incorporated and the only source for such a nitrogen donor in the mixture must have been from the starting material **39** itself. The fact that compound **45** only occurred in the irradiated mixture of compound **39** and **40** and not in the irradiated sample containing only **39**, indicates that there is an intermolecular interaction between the two starting materials. Further experiments, *e.g.* different solvents, radiolabelling of reactants, need to be carried out in order to clarify the mechanism of synthesis of the irradiation products.

7 Antimalarial Drug–Heme Interactions

7.1 Introduction

The antimalarial drug–heme interactions study was carried out as a part of the SFB 630 project in cooperation with the research group of Prof. Dr. A. Haase and Dr. C. Faber from the Department of Experimental Physics 5 at the University of Würzburg. Their group used paramagnetic relaxation studies by NMR to study the interactions between antiplasmodial active naphthylisoquinoline alkaloids and FPIX (**9**) and between the antimalarial drug chloroquine (**2**) and FPIX (**9**). Furthermore, they used the Evans method to characterize the spin state of FPIX (**9**) in complex formation with these compounds. I contributed to the study with the isolation of antiplasmodial active naphthylisoquinoline alkaloids as described in Chapter 5 and with the work presented within this Chapter.

As already mentioned many of the naphthylisoquinoline alkaloids exhibit strong bioactivity against *Plasmodium* species *in vitro*[41,42,194] and *in vivo*.[43] Investigations have shown that their mode of action seems to be similar to that of chloroquine (**2**), inhibiting the degradation of toxic heme metabolites in the food vacuole of the malaria parasite.[44] This inspired the examination of the ability of five naphthylisoquinoline alkaloids, ancistrocladine (**35**), korupensamine A (**46**), dioncophylline C (**6**), dioncopeltine A (**7**), and dioncophylline A (**8**) (Figure 43), to interact with FPIX (**9**) (Figure 44).

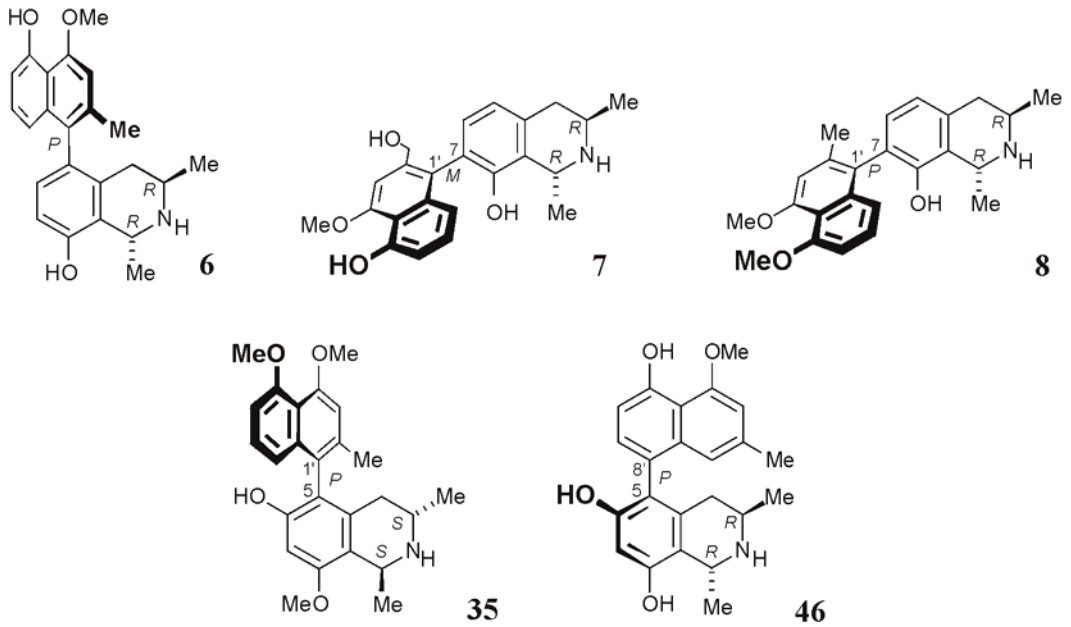

Figure 43. The naphthylisoquinoline alkaloids dioncophylline C (**6**), dioncopeltine A (**7**), dioncophylline A (**8**), ancistrocladine (**35**), and korupensamine A (**46**), examined for their interaction with FPIX (**9**).

Circular dichroism (CD) studies in the UV region conducted on an aqueous equimolar mixture of dioncophylline C (**6**) and FPIX (**9**) gave the first clear evidence of complexation between the two species. Being achiral FPIX (**9**) does not show any CD effect (Figure 44) whereas the chiral dioncophylline C (**6**) shows Cotton effects in the region from 210-310 nm (Figure 44). CD studies recorded on a mixture of the two compounds revealed the presence of a negative peak in the area of 390 nm (Figure 44), which is in the same region where UV spectroscopy investigations of FPIX (**9**) show a flat Soret band.[195] These results indicate the formation of chiral complex between dioncophylline C (**6**) and FPIX (**9**).

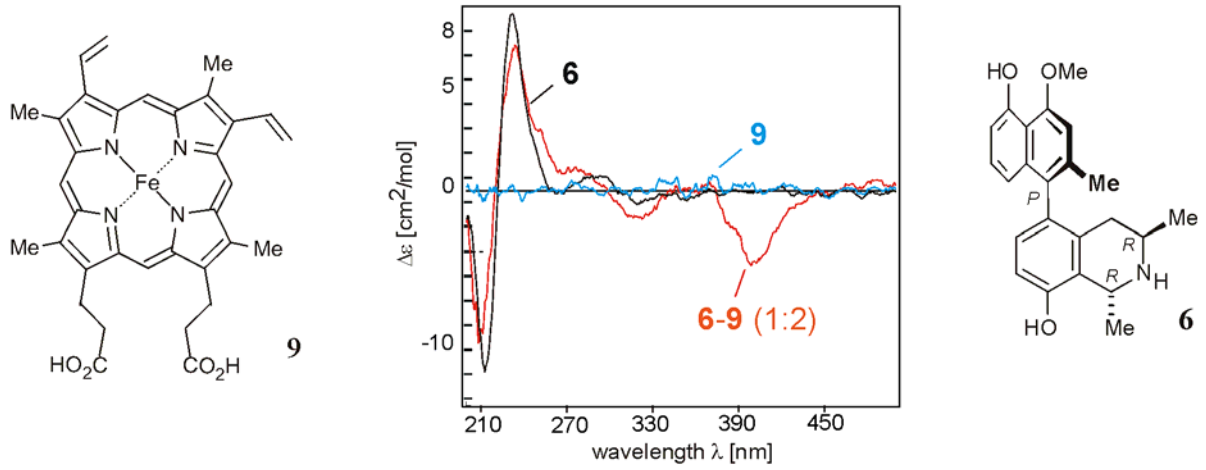

Figure 44. CD spectra of dioncophylline C (**6**) (black line), FPIX (**9**) (blue line), and an equimolar (2 mM) mixture of the two (red line).

Solubility tests showed that 2 mM stock solutions of both **6** and **9** could easily be prepared at physiological conditions (pH 7.4). However, on mixing the two a precipitate formed, which was only found to be soluble at pH <10 for concentrations >1 mM, and in sub mM concentrations for pH >10. The FPIX (**9**) solutions in the concentrations necessary for CD measurement (≥ 1 mM) are darkly colored leading to irreproducible results. Unfortunately, due to these limitation the CD spectral changes were not found to be reliable for further complex characterization analysis.

7.2 UV Titration

The binding of different quinoline antimalarial drugs, such as chloroquine (**2**) and mefloquine (**3**), to FPIX (**9**) has previously been shown to affect the spectral characteristics of FPIX (**9**).[74,196,197] Therefore the effect of the effect of the naphthylisoquinoline alkaloids on the absorption spectrum of FPIX (**9**) was examined, for further complex characterization. At the much lower concentrations needed for UV titration studies (~0.2 mM) in comparison to CD investigations, the solubility of mixtures of FPIX (**9**) with each of the naphthylisoquinoline alkaloids tested, *i.e.* ancistrocladine (**35**), korupensamine A (**46**), dioncophylline C (**6**), dioncopeltine A (**7**), and dioncophylline A (**8**) was sufficient at both pH levels investigated (pH 6.5 and pH 10.5).

Full absorption spectra were taken in the range 250-550 nm following each addition of a predetermined amount of dioncophylline C (**6**) to a solution of FPIX (**9**) (0.168 mM) in the range of 0.1-10 molar equivalents (Figure 45).

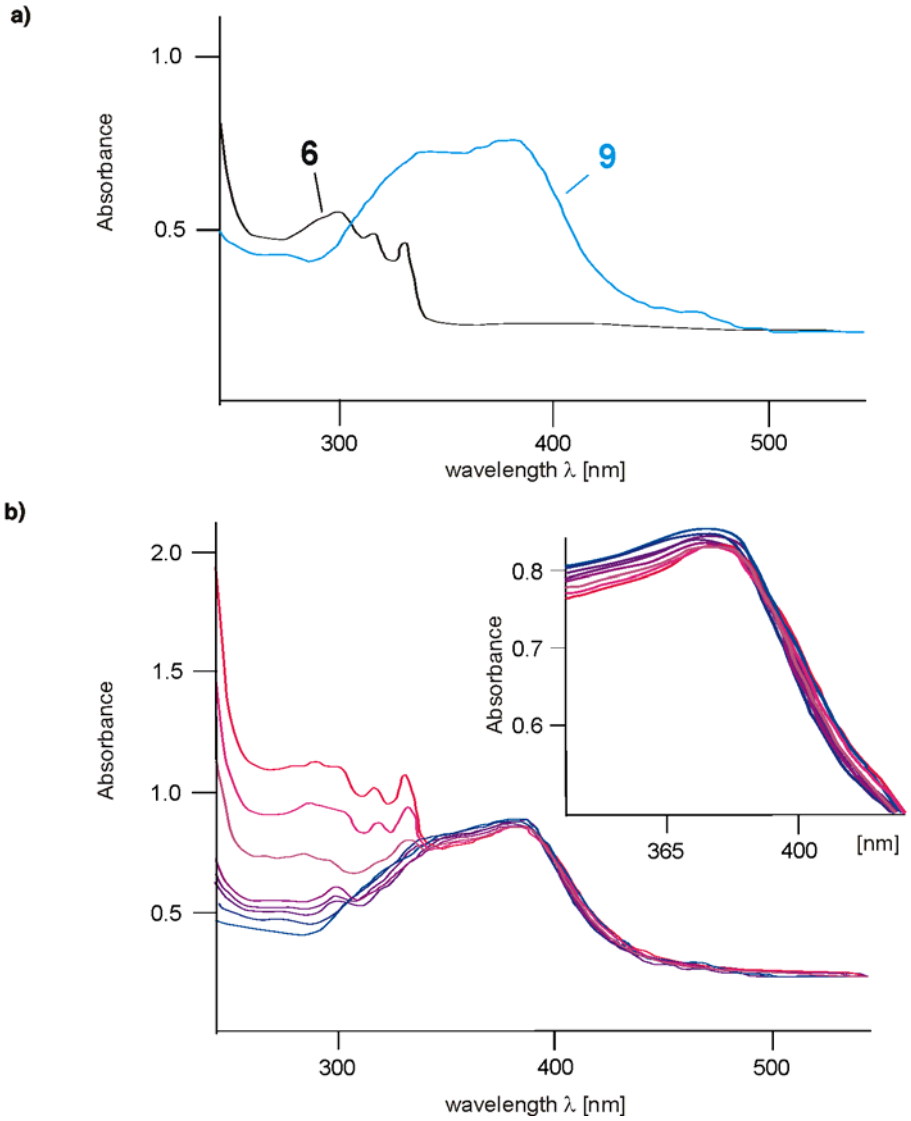

Figure 45. a) UV absorption spectra of dioncophylline C (**6**, 0.4 mM) and FPIX (**9**, 0.168 mM) (pH 6.5), b) UV difference absorption spectra of FPIX (**9**) solutions (0.168 mM) titrated with dioncophylline C (**6**) in the 0.1-10 molar equivalents, going from low concentrations of dioncophylline C (**6**) (blue) to high concentrations (red) (pH 6.5), showing the decrease of the absorption at 365 nm by increasing dioncophylline C (**6**) concentrations. Inset: zoom of the recorded UV absorption spectra.

The data showed a complex titration behavior, especially for the high-wavelength region of the Soret band (370-435 nm). Thus, the absorption intensity of higher-wavelength difference absorption bands would invert during titration, *i.e.*, first increase with added dioncophylline C (**6**) and then decrease (or vice versa), as though a process subsequent to the complex formation produced an inverted impact at the same wavelength. A comparable titration

behavior was found for all of the naphthylisoquinoline alkaloids investigated for their interactions with FPIX (**9**) (Figure 46).

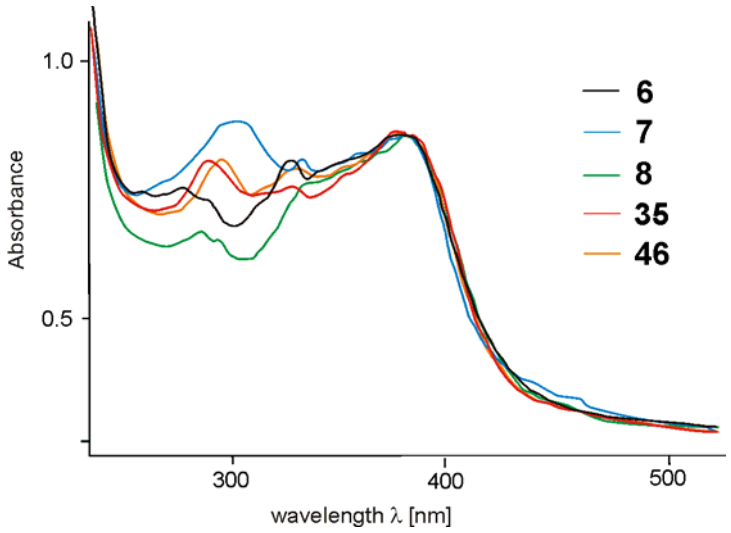

Figure 46. UV absorption spectra of FPIX (**9**) solutions (0.168 mM) added 0.4 mM of dioncophylline C (**6**, black line), dioncopeltine A (**7**, blue line), dioncophylline A (**8**, green line), ancistrocladine (**35**, red line), and korupensamine A (**46**, orange), respectively, all solutions buffered at pH 6.5.

Only small changes were observed between the UV analyses carried out pH 6.5 and 10.5 (Figure 47) and can be assigned the changes of the Soret band of FPIX (**9**) as previously reported[71] and experimentally observed (data not shown).

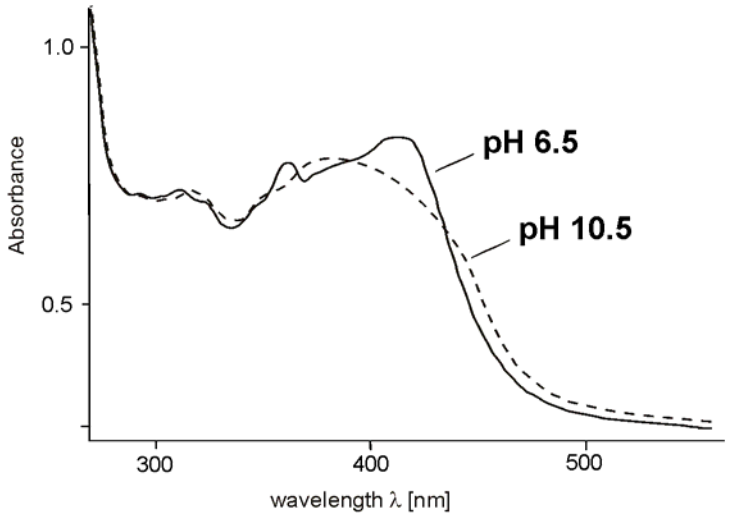

Figure 47. UV absorption spectra of 0.168 mM FPIX (**9**) added 0.4 mM of dioncophylline C (**6**) buffered at pH 6.5 (black line) and pH 10.5 (dashed line).

The intensity of response was invariably small and no significant shift changes or "new" extremes of the UV bands were observed. Titration plots were constructed from data at each of the wavelengths above 330 nm representing a difference maximum or minimum, *i.e.*, 347, 365, and 390 nm. Of these, only the data corresponding to the absorption band centered around 365 nm (Figure 45 and 46) produced both useful and reproducible titration plots for both pH levels investigated, *i.e.*, pH 6.5 and 10.5 (Figure 47).

7.2.1 Job's Plot

Job's method of continuous variations is a commonly used technique for determining the composition of coordination compounds.[198] Basically, the method uses intensive property in a series of solutions of constant total molarities, but of varying metal-to-ligand ratio. For the characterization of the FPIX (**9**)–naphthylisoquinoline complex formation UV spectroscopy was employed to measure the optical property of mixtures of the two components, compensated for free FPIX (**9**) and free naphthylisoquinoline absorbance. For each experiment two equimolar stock solutions, one of FPIX (**9**) and one of each of the naphthylisoquinoline alkaloids, were prepared. A set of working solutions was then obtained by mixing V_L of the naphthylisoquinoline with (V_T-V_L) mL of the FPIX (**9**) stock solution, where V_T is a fixed total volume and V_L is a variable, $0 \leq V_L \geq V_T$. The absorbances of these solutions were then measured at the fixed wavelength of 365 nm and plotted as a function of mole fraction of ligand: V_L/V_T. The position of maxima on these plots, in relation to the mole-fraction axis, *e.g.* dioncophylline C (**6**):FPIX (**9**) ratio, were found to be in the area 0.66 for all naphthylisoquinoline alkaloids tested and for both pH levels investigated (Figure 48, exemplified for dioncophylline C (**6**) at pH 6.5). This indicates[199] a nominal complex stoichiometry of one naphthylisoquinoline alkaloid molecule to two FPIX monomers (**9**) (1:2).

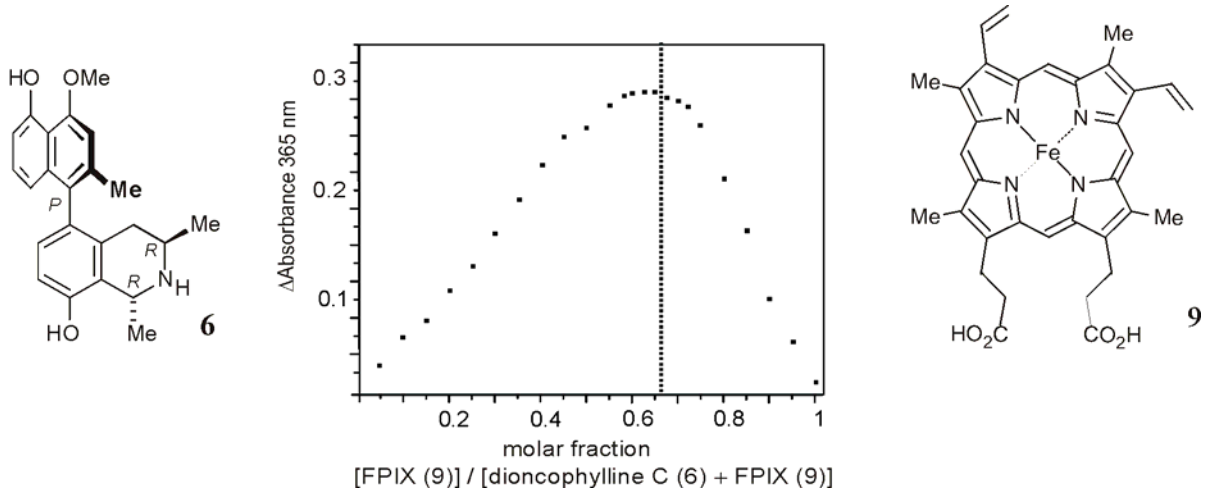

Figure 48. Job's plot (continuous variations plot) for the complexation of dioncophylline C (**6**) and FPIX (**9**) obtained by recording absorbance differences at 365 nm and plotted as a function of mole fraction of FPIX (**9**), indicating the 1:2-complex stoichiometry.

7.2.2 Binding Constant

For determination of the binding constant of the complex formation between FPIX (**9**) and dioncophylline C (**6**) aliquots of a stock solution of **6** (0.168 mM) were added to a solution of FPIX (**9**) (0.168 mM). The complex formation was monitored by the decrease of the UV absorbance of the Soret band of **9** at λ = 365 nm. The corresponding binding constant (Table 9) was subsequently analyzed using a nonlinear curve fitting with a 2:1 association model (Figure 49).[200,201]

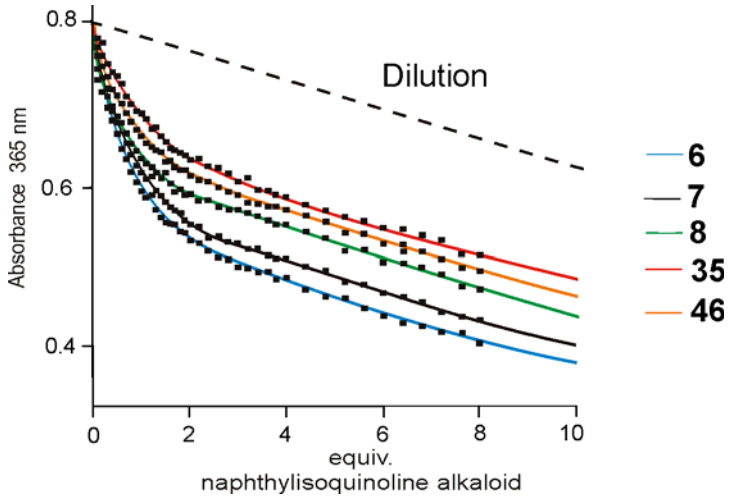

Figure 49. Binding isotherm at λ = 365 nm for the titration of 0.168 mM FPIX (**9**) titrated with 0.168 mM of dioncophylline C (**6**, black line), dioncopeltine A (**7**, blue line), dioncophylline A (**8**, green line), ancistrocladine (**35**, red line), and korupensamine A (**46**, orange), all solutions buffered at pH 6.5. The solid lines represent the calculated curve fit for the experimental data (■), whereas the dotted line indicates the expected change in absorption due to simple dilution of the sample during titration.

According to this UV titration, in water at pH = 6.5 the complexation of dioncophylline C (**6**) to FPIX (**9**) has an association constant of $4.71 \cdot 10^{4}$ M^{-1}. This gives a dissociation constant K_D of $(2.12 \pm 1.6) \cdot 10^{-5}$ M (Table 9), which is comparable but still a factor of approximately 10 weaker than the values previously reported for the complexation between FPIX (**9**) and the antimalarial drug chloroquine (**2**), *i.e.*, $3.16 \cdot 10^{-6}$ M[202] and $(2.5 \pm 1.8) \cdot 10^{-6}$ M[203] and as determined within our group by Y. Reichert by the use of UV titration, *i.e.* $3.92 \cdot 10^{-6}$ M.[204]

For the UV titration in water at pH = 10.5 the complexation of dioncophylline C (**6**) to FPIX (**9**) was determined to have a dissociation constant of $(2.19 \pm 2.1) \cdot 10^{-5}$ M (Table 9). Thus, the dissociation constants determined at pH 6.5 and 10.5 are in the same magnitude and only differ by a factor of 1.04, which indicates that the complexation is comparable at the two conditions investigated. Comparable dissociation constants were determined for the additional naphthylisoquinoline alkaloids analyzed (Table 9).

Table 9. Dissociation constants determined for the complexation of FPIX (**9**) naphthylisoquinoline alkaloids **6**, **7, 8**, **35** and **46** at pH 6.5 and pH 10.5.

	K_D (10^{-5} M)				
	6	**7**	**8**	**35**	**46**
9[a] (pH 6.5)	2.12±1.6	1.47±0.8	2.77±1.4	6.67±0.8	2.94±0.7
9[b] (pH 10.5)	2.50±1.2	2.03±0.9	3.35±0.6	8.02±1.6	4.00±1.4

[a]pH buffered to 6.5. [b] pH adjusted to 10.5.

The determined dissociation constants for the complexation of naphthylisoquinoline alkaloids with FPIX (**9**) indicate that this might be the explanation for the mode of action of their antiplasmodial activity. The order of the reported activities exposed by the compounds against *P. falciparum*, *e.g.*, **7>6**>**46**>**8**>**35**, (Table 14) is comparable to order of the determined K_D values for the complexation with FPIX (**9**), *e.g.*, **7>6**>**8>46**>**35** (Table 9). Korupensamine A (**46**) is the only exception of this tendency, since it has been found to be an factor of 2 more active against *P. falciparum* than dioncophylline A (**8**) (Table 14), however, by comparing the dissociation constants determined for the two compounds, **46** was revealed to be a slightly weaker ligand for the complexation with FPIX (**9**).

7.3 Mass Spectrometry

Electrospray ionization mass spectrometry (ESI MS) provides a rapid sensitive tool for probing noncovalent interactions.[205-207] Most studies of this type are based on the ability of ESI to transfer noncovalent solution-phase assemblies intact into the gas phase. The validity of this strategy has been supported in numerous studies, especially for experiments on protein-protein and protein-ligand interactions,[208] including studies on heme containing proteins.[209] The relative binding strengths between the drugs and Fe(III)-heme was assessed using low-energy collision-induced dissociation. This approach has previously been shown to be useful in determining the structure-activity relationship of antimalarial agents, namely, artemisinin-type drugs,[75] terpene isonitriles,[74] chloroquine (**2**),[74] and neocryptolepine derivatives.[210]

To further investigate the nature of the complexes formed between different naphthylisoquinoline alkaloids and FPIX (**9**), mixtures were subjected to electrospray ionization mass spectrometry (ESI-MS) performed by Dr. M. Büchner and Dr. A. Sickmann.

Under the conditions employed (5 mM in MeOH-H_2O 3:1, *ca*. 0.05% NH_4OH), the analyses of the FPIX (**9**) solution revealed the presence of prominent peaks at *m/z* 616.2 corresponding to free monomeric FPIX (**9**), 1231.3 corresponding to a chelate dimer of **9** presumably represented by structure **12**, and 1249.4 corresponding to a μ-oxo dimer of **9** presumably represented by structure **11** (Figure 50). Interestingly MS/MS investigations conducted on the *m/z* 1249.4 peak [$\mathbf{11}^+$] (spectrum not shown) selectively led to the fragmentation peak *m/z* 1231.3 of the FPIX chelate dimer (**12**) and with no traces of the fragmentation peak of the monomer *m/z* 616.2 peak (**9**), thereby indicating a rapid and flexible conversion between the two dimer forms, with structure **12** as the more stable form of the two. HRMS (ESI) analyses revealed the obtained results to differ by no more than 5 ppm from the theoretical masses of the assigned structures (Table 10).

Due to the isotopic distribution over a broad *m/z* region caused by Fe and Cl, the monoisotopic signals were to small in intensity for an accurate mass measurement. Therefore, typically the most intense signal (X+n) of this isotopic distribution was taken and compared with the repective calculated value. The calculations of the repsective mass values of the isotopic distribution were performed as described in Chapter Ex. 1.1.

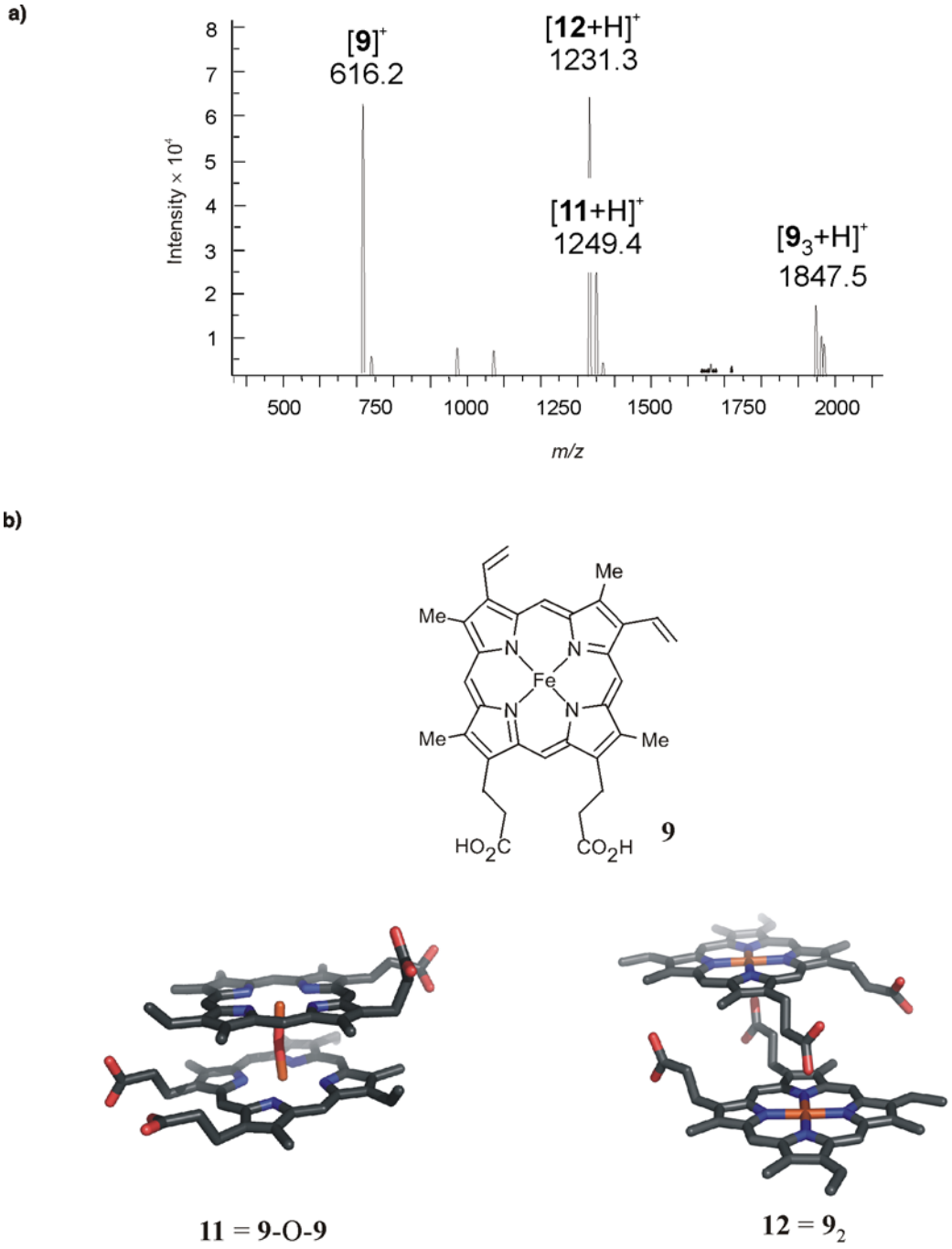

Figure 50. Mass spectrometric analysis of a FPIX (**9**) solution: a) mass spectrum, b) the assigned structures FPIX (**9**), the FPIX μ-oxo dimer (**11**), and the FPIX chelate dimer (**12**). The drawings of the last two structures were provided by K. F. Schwedhelm.

Table 10. Analysis for the structural assignment of the most significant peaks obtained HRMS (ESI) analysis of a FPIX (**9**) solution.

Peak assignment	Molecular formula	Isotopic pattern	Calcd. For	Found	Δ ppm
[**9**]	C34H32FeN4O4	Monoisotopic	614.18142	614.18266	1.5
[**12**+H]$^+$	C68H63Fe2N8O8	X + 4	1231.34666	1231.34882	2.2
[**11**+H]$^+$	C68H65Fe2N8O9	X + 4	1249.35723	1249.36053	3.2

Mixtures of FPIX (**9**) with dioncophylline C (**6**) yielded significant *m/z* 979.4 and 1594.5 peaks (Figure 51), which were assigned to correspond to the complexation of **6** to a monomer of FPIX (**9**) and to the FPIX chelate dimer (**12**), respectively. The assignment was confirmed by HRMS (ESI) measurements (Table 11). MS/MS analyses of each of the two peaks revealed the peak at *m/z* 980.4 to fragment into the monomer of FPIX (**9**) and dioncophylline C (**6**), whereas the peak at *m/z* 1594.5 fragmented into the FPIX chelate dimer (**12**) and dioncophylline C (**6**) (chromatograms not shown). All of the other naphthylisoquinoline alkaloids tested, *i.e.*, dioncophylline A (**8**), dioncopeltine A (**7**), ancistrocladine (**35**), and korupensamine A (**46**) showed the same kind of complexation behavior (spectra not shown). It is important to note that, under the experimental conditions employed, there was no evidence for the formation of a complex between the naphthylisoquinoline alkaloids investigated and the FPIX μ-oxo dimer (**11**).

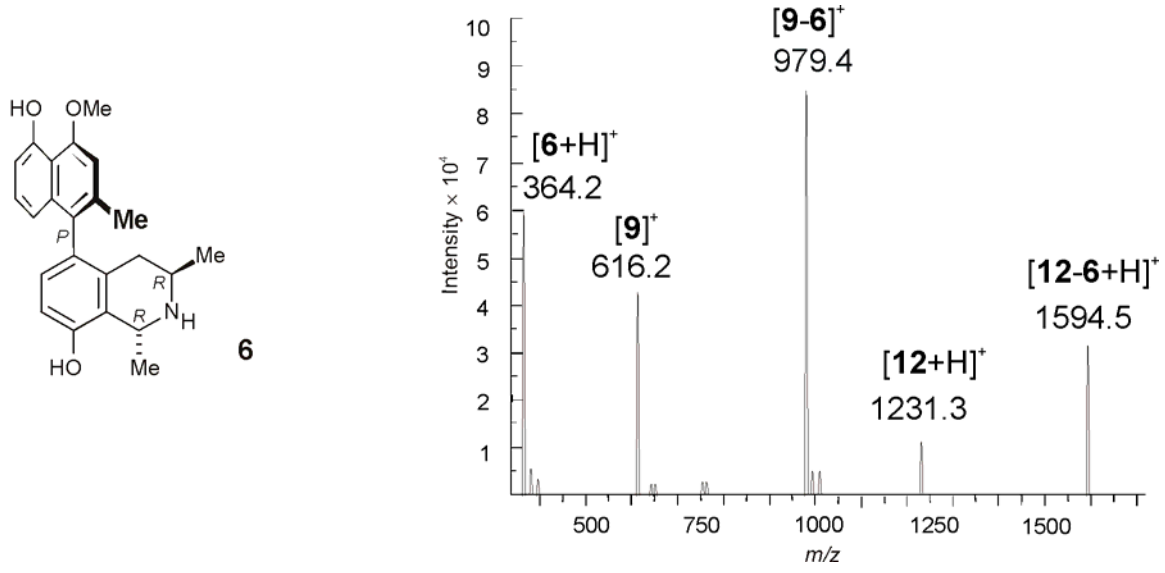

Figure 51. Mass spectrometric analysis of the interactions of dioncophylline C (**6**) with FPIX (**9**).

Table 11. Analysis for the strutural assignment of the most significant peaks obtained by HRMS (ESI) analysis of a solution of FPIX (**9**) and dioncophylline C (**6**).

Peak assignment	Molecular formula	Isotopic pattern	Calcd. for	Found	Δ ppm
[**9**–**6**]$^+$	C57H57FeN5O7	X + 2	979.36034	979.35960	0.8
[**12**–**6**+H]$^+$	C91H88Fe2N9O11	X + 5	1595.53300	1595.52909	4.0

Mixtures of FPIX (**9**) with chloroquine (**2**) yielded significant *m/z* 935.4, 1550.5, 1568.5 peaks, which correspond to, complexation of **2** to a monomer of **9**, to the FPIX chelate dimer (**12**), and to the FPIX μ-oxo dimer (**11**), respectively (Figure 52). The assignment was confirmed by HRMS (ESI) measurements (Table 12)

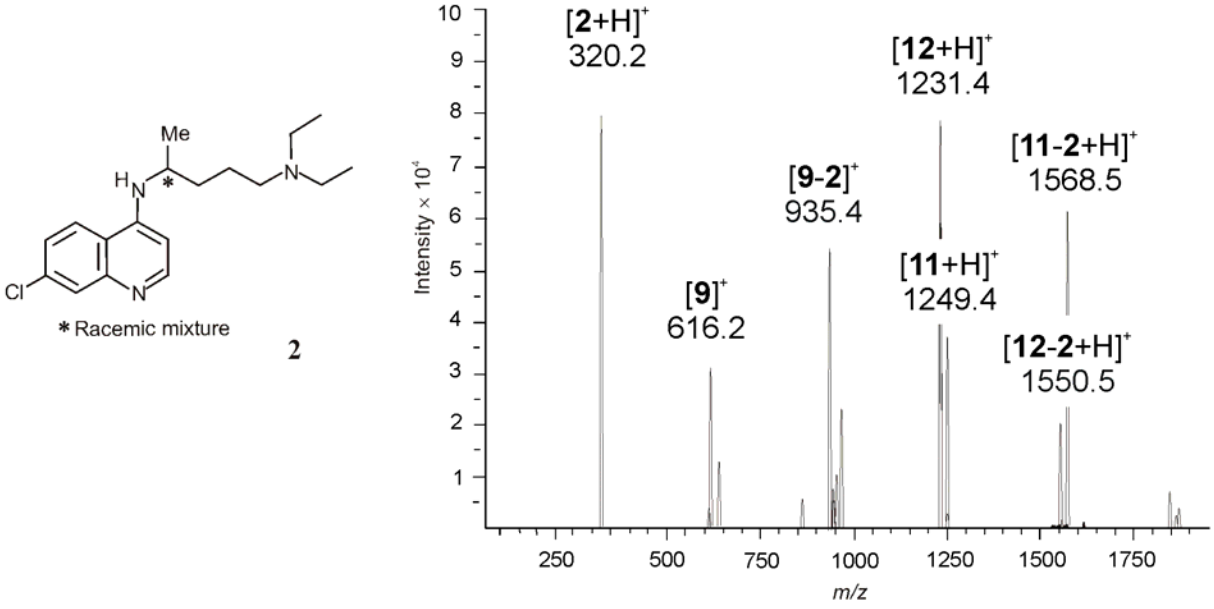

Figure 52. Mass spectrometric analysis of the interactions of chloroquine (**2**) with FPIX (**9**).

Table 12. Analysis of the strutural assignment of the most significant peaks obtained by HRMS (ESI) analysis of a solution of FPIX (**9**) and chloroquine (**2**).

Peak assignment	Molecular formula	Isotopic pattern	Calcd. for	Found	Δ ppm
[**9**–**2**]$^+$	C52H58FeClN7O4	monoisotopic	933.36295	933.36591	3.2
[**12**–**2**+H]$^+$	C86H88Fe2ClN11O8	X + 4	1550.52846	1550.53151	3.0
[**11**–**2**+H]$^+$	C86H91Fe2ClN11O9	X + 4	1568.54175	1568.53903	2.7

Furthermore, intensive HRMS (ESI) studies revealed peaks corresponding to a double protonated tetramer, *i.e.*, chloroquine (**2**)$_2$–FPIX μ-oxo dimer (**11**)$_2$ (Figure 53 and Table 12).

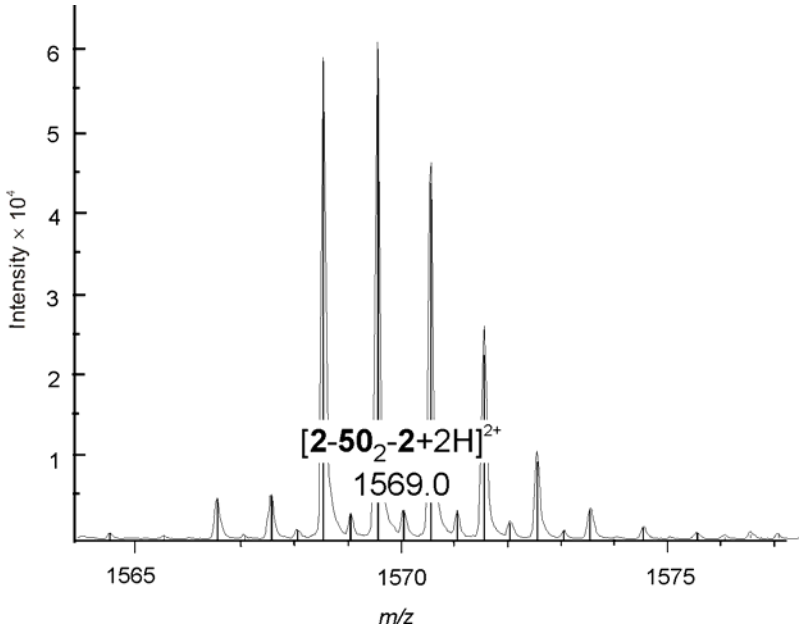

Figure 53. Mass spectrum of a 250 μM MeOH/H_2O (v/v 3:1) solution of the chloroquine (**2**) FPIX (**9**) mixture. The isotopic pattern at *m*/*z* 1569.04372 reveals the formation of the doubly charged complex [chloroquine (**2**)$_2$–FPIX μ-oxo dimer (**11**)$_2$+2H]$^{2+}$. The signals are overlapped by the more intensive signals of the singly charged complex [chloroquine (**2**)–FPIX μ-oxo dimer (**11**)+H]$^+$.

Table 13. Analysis of the peaks obtained by HRMS (ESI) of a solution of FPIX (**9**) and chloroquine (**2**) assigned to correspond to the doubly charged complex formation of chloroquine $(\mathbf{2})_2$–FPIX μ-oxo dimer $(\mathbf{11})_2$.

Peak assignment	Molecular formula	Isotopic pattern	Calcd. For	Found	Δ ppm
$[\mathbf{2}_2–\mathbf{11}_2+2H]^+$	C172H182Fe4Cl2 N22O18	X + 9	1569.04072	1569.04079	0.0

In the previously reported MS studies of the interaction between chloroquine (**2**) and FPIX (**9**) the complexation of chloroquine (**2**) with FPIX μ-oxo dimer (**11**) was the only interaction product that was detected.[74] By using the reported method of keeping the components in a solution of H_2O and CH_3CN[74] no signals were detected on our instrument, whereas a good ionization was obtained by replacing CH_3CN with MeOH. However, it should be mentioned that experiments carried out during a paramagnetic relaxation rate study carried out by the research group of Dr. C. Faber, revealed that the complexation of chloroquine (**2**) and FPIX (**9**) was strongly affected by adding MeOH to aqueous solutions of the complex.[211] The same tendencies were found by paramagnetic relaxation studies of the complexation between naphthylisoquinoline alkaloids and FPIX (**9**).[211,212] Thus, the question still stands on how comparable the obtained MS data are with the interactions between FPIX (**9**) and different ligands *in vivo*, inside the plasmodium infected erythrocytes.

Nevertheless, the results of the mass spectrometry analyses indicate that the interactions of naphthylisoquinoline alkaloids with FPIX (**9**) may involve an operate mechanism different to that of the antimalarial drug chloroquine (**2**).

7.4 Structural Investigations of Antimalarial Drug–FPIX Complex Formation studied by NMR

By the use of an NMR method proposed by Evans[213,214] the spin states of the paramagnetic iron atoms in the dioncophylline C (**6**)–FPIX (**9**) and chloroquine (**2**)–FPIX (**9**) complexes were determined by the research group of Dr. C. Faber. For the characterization of the dioncophylline C (**6**)–FPIX (**9**) complex the pH level was necessarily adjusted to pH 10.5 using 0.05 NaOD (Chapter 7.1) in order to obtain clear solutions at the high concentrations required for NMR experiments (~2 mM). A solution of dioncophylline C (**6**) was titrated to a solution of FIPIX (**9**). The investigations showed a constant spin state at $S = 3/2$. Thereby

suggesting the paramagnetic iron atoms to be unaffected by complex formation between dioncophylline C (**6**) and FIPIX (**9**). Similar titration analysis performed with chloroquine (**2**) and FPIX (**9**) at pH 6.5 and pH 9 revealed a change in chemical shift when chloroquine (**2**) was in excess and indicated a low spin state of $S = 1/2$ of the paramagnetic iron atoms in the complex of chloroquine (**2**) and FPIX (**9**).

Furthermore, the research group of Dr. C. Faber determined the longitudinal relaxation rates $R_{complex}$ and effective correlation times τ_C for the dioncophylline C (**6**)–FPIX (**9**) and chloroquine (**2**)–FPIX (**9**) complexes. The parameters were derived from titration experiments of solutions of the antimalarial ligands to solutions of FPIX (**9**) studied by NMR experiments at three different magnetic field strengths. Along with $R_{complex}$ and the spin state *S*, τ_C is the third parameter necessary for the determination of intermolecular distances, which they used to calculate structural models for the FPIX (**9**)–antimalarial drug complexes in aqueous solution.

Complex structures were calculated with molecular dynamics simulations with intermolecular distance restraints between antimalarial ligands and the Fe(III) center in FPIX (**9**). For the calculations of the dioncophylline C (**6**)–FPIX (**9**) complex, they made use of the stoichiometry and dissociation constant for the complex formation determined by UV as described in Chapter 7.2.1 and 7.2.2, respectively. The derived structure of the dioncophylline C (**6**)–FPIX (**9**) (Figure 54a) complex showed high similarity to the complex formed by chloroquine (**2**)–FPIX (**9**) (Figure 54b).

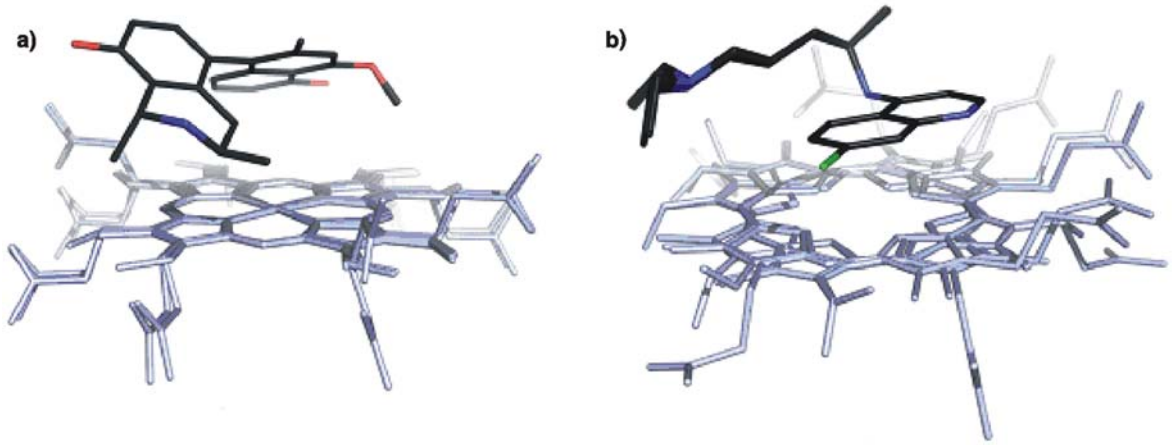

Figure 54. a) Calculated 3D structures of the dioncophylline C (**6**)–FPIX (**9**), b) calculated 3D structures of the chloroquine (**2**)–FPIX (**9**) complex; for reasons of clarity, only seven out of 30 structures used for analysis are overlaid by superimposing the structure of dioncophylline C (**6**) and chloroquine (**2**), respectively. The drawings of the structures were provided by K. F. Schwedhelm.

7.5 β-Hematin Inhibition

A prominent route for the detoxification of free FPIX (**9**) in malaria parasites is sequestration into crystals of hemozoin,[215] the characteristic malaria pigment.[57,216] Recently, chloroquine (**2**) and related drugs have been demonstrated to inhibit synthetic hemozoin (β-hematin) formation and therefore it is assumed that the compounds inhibit the hemozoin formation in the malaria parasite. [63,217-219]

Several methods have been developed for detecting and measuring inhibition of β-hematin.[63,217-219] Many of these tests have disadvantages in being time consuming and require incubation,[60,220] reaction,[221] or drying processes[217,222] between 12 and 48 h. Another requires specialized equipment for analysis of H^3-labelled β-hematin[223] and some make use of materials that are not commercially available, such as histidine-rich protein 2[219] or a peptide bionucleating template dendrimer.[224]

Recently, an assay for β-hematin inhibition suited for high-throughput screening has been developed,[225] which makes use of the incapability of pyridine solutions to disrupt β-hematin while capable of solubilizing solid FPIX (**9**) from a mixture of the two. The assay was

reported to show trends in inhibitory activities for the test compounds which were in agreement with other methods for quantification.[225] Furthermore, the materials are cheap and the UV detection easily available. This method was used to screen dioncophylline C (**6**), dioncopeltine A (**7**), dioncophylline A (**8**), ancistrocladine (**35**), and korupensamine A (**46**) for their β-hematin formation inhibition activity (Figure 55).

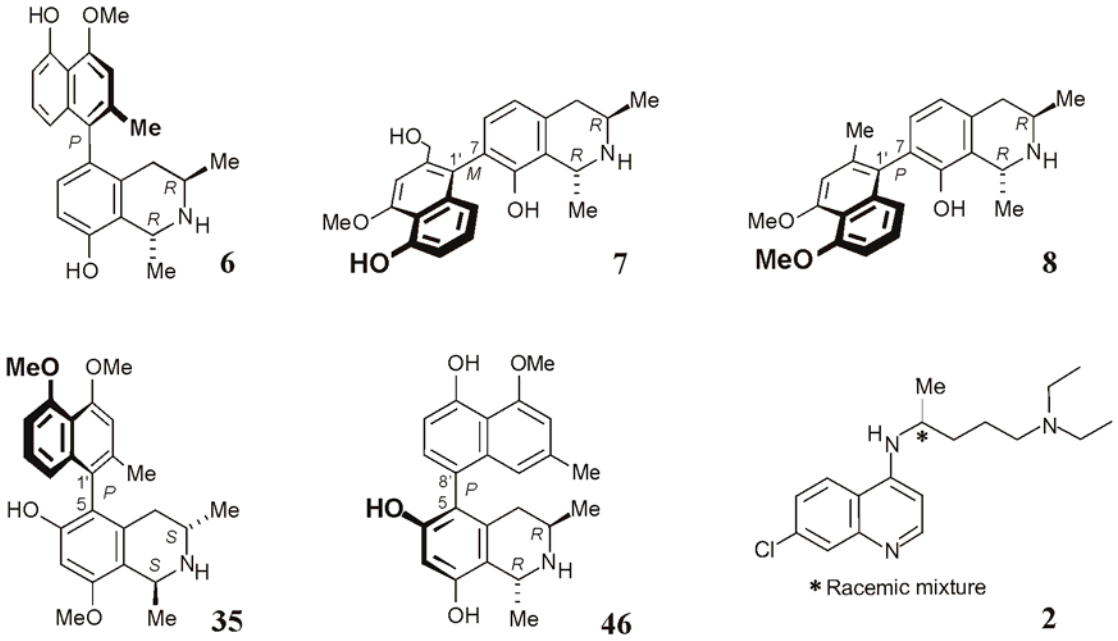

Figure 55. The naphthylisoquinoline alkaloids dioncophylline C (**6**), dioncopeltine A (**7**), dioncophylline A (**8**), ancistrocladine (**35**), and korupensamine A (**46**), and chloroquine (**2**) screened for their β-hematin formation inhibition activity.

To determine the IC_{50} values for the β-hematin formation inhibition activity displayed by each of the naphthylisoquinoline alkaloids investigated, increasing numbers of molar equivalents were added to a series of tubes containing FPIX (**9**) dissolved in sodium hydroxide. The β-hematin formation process was then initiated by addition of sodium acetate solution to give a final concentration of 4.5 M and pH of 4.5. All solutions were equilibrated at 60 °C before initiation of the process. After 60 min of incubation at 60 °C, a 5% (v/v) pyridine solution in water was added to the reaction mixture at room temperature. This was then agitated and briefly treated in an ultrasonic bath to permit all of the unreacted FPIX (**9**) to dissolve. The samples were centrifuged by 150 × g for 5 min and subsequently the supernatant was carefully transferred to a cuvette and the absorbance measured at 405 nm, where the Soret band of the remaining FPIX (**9**) in solution shows absorbance (Figure 56). All tests were carried out in triplicate with a standard deviation below 5%.

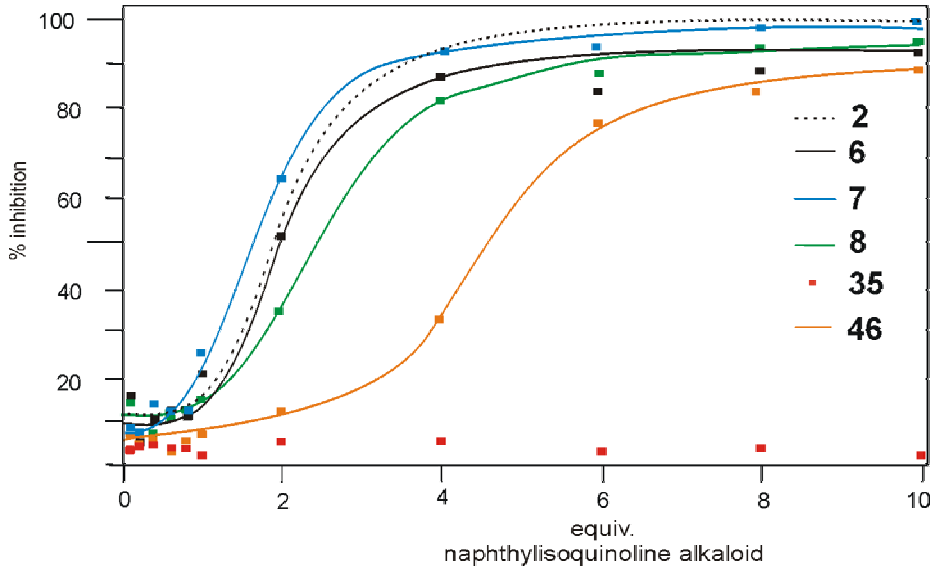

Figure 56. The inhibition rate in % of the β-hematin formation versus naphthylisoquinoline alkaloid concentration from which the IC_{50} value was obtained. The solid lines are best fit of the data to a sigmoidal dose response curve for the experimental data (■); dioncophylline A (**8**, green line), dioncophylline C (**6**, black line), dioncopeltine A (**7**, blue line), korupensamine A (**46**, orange), ancistrocladine (**35**, red squares), and chloroquine (**2**, dotted line).

As already indicated by the UV studies of the complex formation, the region above 390 nm of the Soret band of FPIX (**9**) was found to be rather unstable and produce unreliable results by titration with naphthylisoquinoline alkaloids (Chapter 7.2), which was confirmed by measuring the UV absorbance of the incubations at 405 nm, since there were some difficulties in obtaining consistency in the results. This was especially true for the measurements of samples containing concentrations higher than 2 molar equivalents of the naphthylisoquinoline alkaloids.

The results of these incubations are shown in Figure 56. The inhibition curve was fitted to a sigmodial dose response curve, from which the IC_{50} values for inhibition of the β-hematin formation were obtained (Table 14).

Table 14. β-hematin inhibition and antiplasmodial (*P. falciparum*) activity for the tested naphthylisoquinoline alkaloids and chloroquine (**2**).

	IC_{50}	
Naphthylisoquinoline alkaloid	Phiβ (equiv.)[a]	*P. falciparum* (mg/mL)
Dioncopeltine A (**7**)	1.57 ± 0.02	0.0048
Chloroquine (**2**)	1.91 ± 0.30	0.0041
Dioncophylline C (**6**)	2.01 ± 0.04	0.0063
Dioncophylline A (**8**)	2.48 ± 0.02	0.144
Korupensamine A (**46**)	4.52 ± 0.05	0.072
Ancistrocladine (**35**)	>10[b]	0.899

[a] This study ±standard error of the mean on three determinations.

[b] No effect in the investigated molar equivalent range, *i.e.*, 0.1-10.

Dioncophylline C (**6**), dioncopeltine A (**7**), and dioncophylline A (**8**) were found to display high inhibition activity against the β-hematin formation all with IC_{50} below 2.5 molar equivalents. These values are in the same range as the reported values of the most active antimalarial drugs tested with this assay so far, *i.e.*, amodiaquine (**10**) and chloroquine (**2**) (see Figure 4 for structures), displaying IC_{50} values for inhibition of the β-hematin formation of 1.45 and 1.91 molar equivalents,[225] respectively. Korupensamine A (**46**) was found to be at little less active with a determined IC_{50} of 4.52 molar equivalents for the inhibition of the β-hematin formation. Ancistrocladine (**35**) was found to be inactive in the investigated molar equivalent range, *i.e.*, 0.1-10. At molar equivalent concentrations higher than 10 of the naphthylisoquinoline alkaloids, an insoluble precipitate was formed in the samples, unfortunately this problem could not be solved by lowering the start concentration, since inaccuracy was observed for measurement of concentrations below 0.15 mM of FPIX (**9**).

The determined IC_{50} values are overall in good agreement with the determined association constants (Chapter 7.2.2) of the respective naphthylisoquinoline alkaloids to FPIX (**9**), except for ancistrocladine (**35**) for which no IC_{50} could be determined. Likewise, there seem to be good agreement between the determined IC_{50} values for the inhibition of the β-hematin formation by the compounds and with the individual *in vitro* determined IC_{50} values displayed by the compounds against *P. falciparum* (Table 14). In occurrence with the antiplasmodial activities of the substances investigated, dioncopeltine A (**7**) is the strongest inhibitor of the β-hematin formation, and also in agreement is the finding of dioncophylline C (**6**) to be the second-strongest inhibitor. Dioncophylline A (**8**) was found to be a stronger inhibitor of the β-

hematin formation in comparison to korupensamine A (**46**); this is in contrast to the antiplasmodial activities of the two compounds, but comparable to the order of the dissociation constants to FPIX (**9**) determined for the two compounds (Chapter 7.2.2).

The results clearly indicate that there is an inhibition of the β-hematin formation displayed by the most antiplasmodially active naphthylisoquinoline alkaloids. There seems to be some correlation between the antiplasmodial activities determined for the compounds and their ability to inhibit β-hematin formation, which thus might be an explanation – at least partial- for their antiplasmodial activity. However, the IC_{50} values for the inhibition of the β-hematin formation obtained by the assay do not correlate with the IC_{50} values for the antiplasmodial activity determined for the screened compounds. Thus, the assay should only be used as a fast and easy indicator of possible antiplasmodial activity of the compounds.

8 Metabolism Study of Naphthylisoquinoline Alkaloids

8.1 Introduction

The phase 1 and *in vivo* metabolism study of dioncophylline A (**8**) was performed in close cooperation with M. Sieber as a part of his Diplom-Arbeit and with the research group of Prof. Dr. W. Dekant at the Department of Toxicology at the University of Würzburg.

8.1.1 Phase 1 and Phase 2 Drug Metabolism

There are many routes by which drugs may be metabolized or biotransformed in the body. These include oxidation, reduction, hydrolysis, hydration, conjugation, and condensation reactions.[226] A detailed understanding of these pathways is essential, as the route of metabolism of a drug can determine its ultimate pharmacological or toxicological activity.[227] Drug metabolism can be formally divided into two phases: phase 1 (functionalization reactions) and phase 2 (conjugative reactions).[226-229] The chemical reactions normally associated with phase 1 and phase 2 drug metabolism[226] are given in Table 15.

Table 15. Reactions classed as phase 1 or phase 2 metabolism.

Phase 1	**Phase 2**
Oxidation	Glucuronidation/glucosidation
Reduction	Sulfation
Hydrolysis	Methylation
Hydration	Acetylation
Dethioacetylation	Amino acid conjugation
Ismoerization	Glutathione conjugation
	Fatic acid conjugation
	Condensation

The reactions of phase 1 are thought to act as a preparation of the drug for the phase 2 reactions, *i.e.*, phase 1 "functionalizes" the drug by producing or uncovering a chemically reactive functional group on which the phase 2 reactions can occur.[226,228] The phase 2 reactions are the true "detoxification" pathways and give products that usually account for the bulk of the inactive products of a drug.[226,228] Many of the reactions of both phase 1 and phase 2 are capable of being performed on the same compound and, thus, there is a possibility of

interaction of the various metabolic routes in term of competing reactions for the same substrate.[226-229]

In the human body, the liver serves as the main organ involved in drug metabolism. Of particular importance for the phase 1 metabolism reactions are the cytochrome P450 enzymes. This enzyme complex is responsible for the majority of the hepatic metabolic reactions.[230-232]

8.1.2 In Vitro Assays for Phase 1 and Phase 2 Drug Metabolism Studies

Several procedures have been developed for *in vitro* phase 1 and phase 2 drug metabolism studies.[233-236] In most cases the drug is incubated with liver microsomes, which are known to contain high levels of cytochrome P450.[233,235] When the cofactors NAHPH and molecular oxygen are added to these liver microsomes in buffered aqueous solution, most phase 1 metabolic reactions (for which the cytochrome P450 enzymes are responsible) can take place *in vitro*.[233-235] For phase 2 metabolic reactions additional adding of "activated" substrate derivative is necessary, *e.g.*, uridine-diphosphoglucoronic acid (UDPGA) for glucuronidation reactions.[226,233,235]

8.1.3 Metabolism of Naphthylisoquinoline Alkaloids

As previously stated the naphthylisoquinoline alkaloids represent a new and promising class of lead structures for novel antimalarial drug candidates.[41,142,159,194] In contrast to the antimalarial activity of the naphthylisoquinoline alkaloids, virtually nothing is known about the biotransformation and toxicokinetics of these compounds. The only metabolism investigation of this compound class reported in the literature is a preliminary experiment dealing with the metabolic fate of dioncophylline A (**8**) studied by GC-MS analysis,[46] the results of which were later confirmed by HPLC-MS.[237] In the present work, the phase 1 biotransformation of dioncophylline C (**6**), dioncopeltine A (**7**), and dioncophylline A (**8**) (Figure 57), as well as their phase 2 biotransformation were investigated.

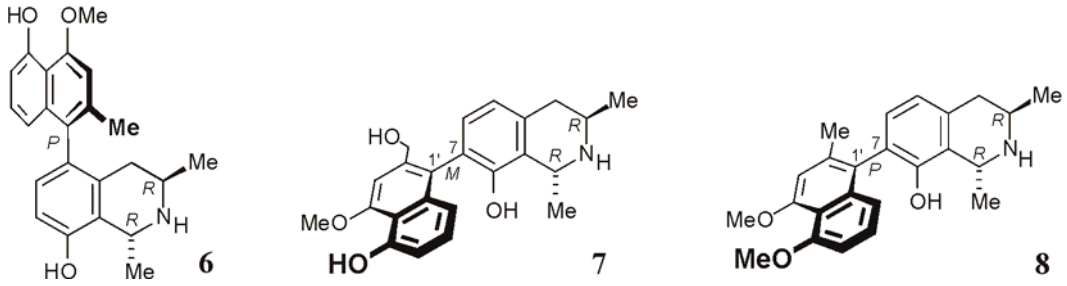

Figure 57. The naphthylisoquinoline alkaloids dioncophylline C (**6**), dioncopeltine A (**7**), and dioncophylline A (**8**) investigated for their phase 1 and 2 biotransformation.

8.2 Phase 1 Metabolism Study of Dioncophyllines A (**8**) and C (**6**), and Dioncopeltine A (**7**)

8.2.1 Liver Microsomal Incubation Assay for Phase 1 Investigations

Complete incubation systems contained rat liver microsomal protein in phosphate buffer (pH 7.4) and an NADPH-generating system. The mixtures were preincubated at 37 °C, then a stock solution of the respective naphthylisoquinoline alkaloid was added in predetermined concentration steps and the mixtures were incubated in preset time intervals. The reaction was terminated by addition of cold methanol. After centrifugation, supernatants from incubation solutions were analyzed by HPLC-UV and HPLC-MS.

8.2.2 Incubation of Dioncophylline A (**8**)

In the case of dioncophylline A (**8**), a time and protein concentration-dependent formation of two new peaks was observed (Figure 58). In the absence of enzymatically active microsomal protein or required cofactors no new peaks were formed (data not shown).

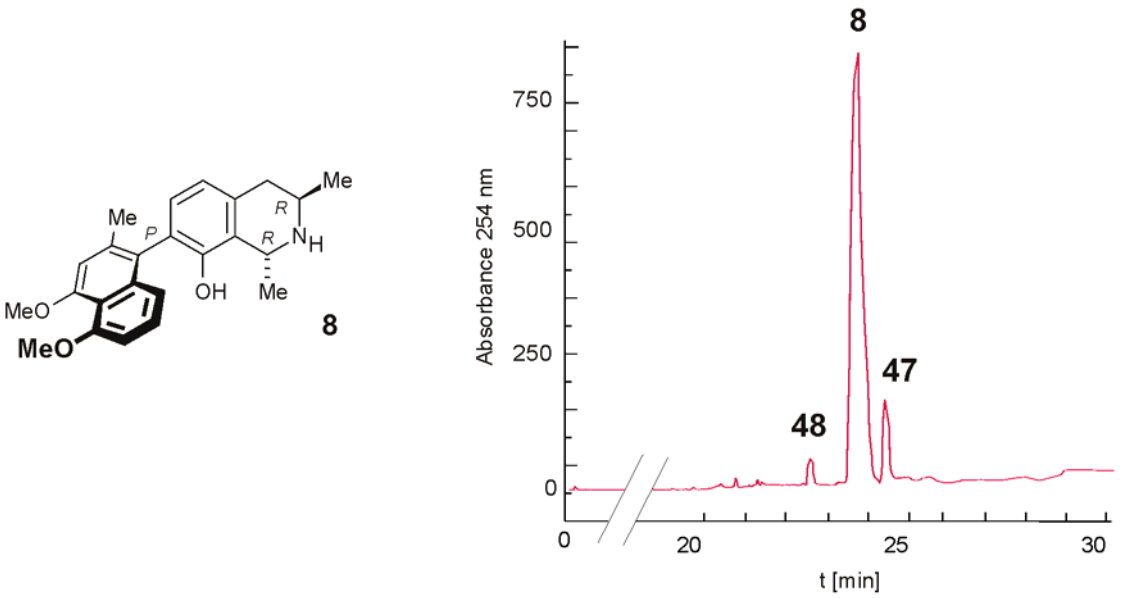

Figure 58. HPLC-UV (254 nm) analysis of a microsomal incubation solution on a reversed-phase column, showing the peaks of dioncophylline A (**8**) and the two metabolites 5'-*O*-demethyldioncophylline A (**47**) (eluting later) and **48** (eluting earlier).

The peaks of the two formed compounds showed UV spectra characteristic of a naphthylisoquinoline core structure[117] and their UV spectra were very similar to that of dioncophylline A (**8**). Both peaks were isolated and subjected to mass spectrometry (Figure 59 and 60).

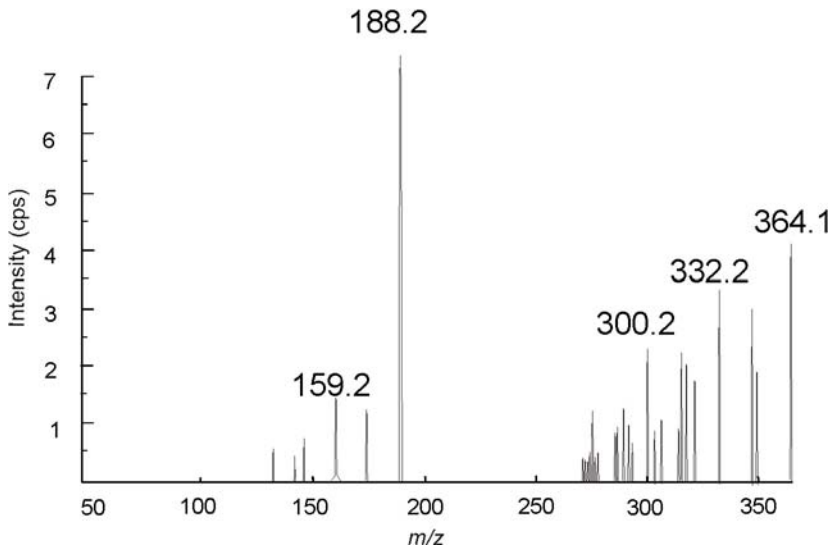

Figure 59. Mass spectrum of 5'-*O*-demethyldioncophylline A (**47**) ($[M+H]^+$ = 364). The peak at *m/z* 188 corresponds to the naphthalene moiety of the molecule.

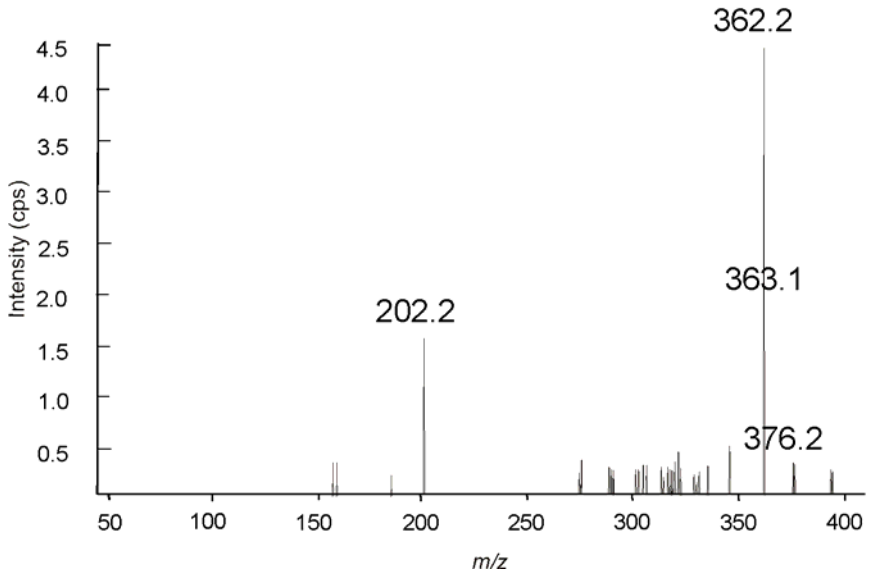

Figure 60. Mass spectrum of the minor metabolite **48** ($[M+H]^+$ = 394). The structure is deduced from HPLC-MS/MS data. The peak at *m/z* 202 corresponds to the naphthalene moiety of the molecule, the signal at *m/z* = 376 indicates a loss of water (*m/z* 18) from the molecular ion.

In HPLC-MS/MS analysis, the faster eluting metabolite gave a mass spectrum identical to that of 5'-*O*-demethyldioncophylline A (**47**). Furthermore, the signals in the ^{1}H NMR spectrum were found to be shifted identical to those reported for **47** in the literature.[238] The *O*-demethylation site of dioncophylline A (**8**) was unambiguously assigned to the 5'-position, since an NOE experiment revealed cross peaks between the singlet of H-3' (δ 2.47) and the signal of the methoxy group at the 4'-position (δ 3.99) (Figure 61a).

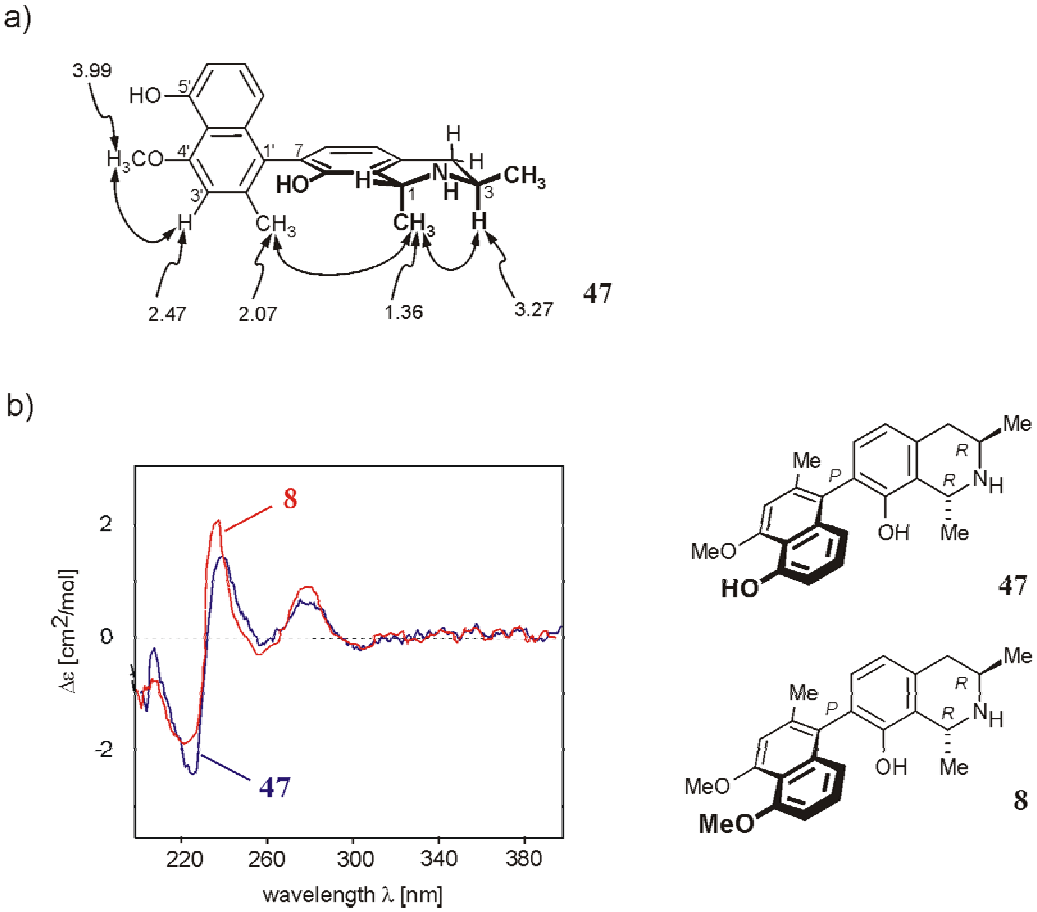

Figure 61. a) NOE interactions of 5'-*O*-demethyldioncophylline A (**47**), unambiguously proving that enzymatic *O*-demethylation of dioncophylline A (**8**) occurs in the 5'-position (and not at C-4'), b) CD spectra of the metabolite **47** (blue line) and **8** (red line) possess the same polarity and thus demonstrate that the biaryl axis is not changed by metabolism.

The relative configuration of the methyl groups at C-1 and C-3 was deduced from an NOE correlation between C*H*$_3$-1 (δ 1.36) and H-3 (δ 3.27) revealing these two groups to be oriented *trans* relative to each other. The biaryl axis of the metabolite was established to be *P*-configured, because its CD spectrum showed a close resemblance with that of the likewise *P*-configured dioncophylline A (**8**) (Figure 61b), thus the absolute axial configuration was found to be unaffected by the metabolic process. This was confirmed by an NOE interaction between the methyl group at C-2' (δ 2.07) and the signal originating from C*H*$_3$-1 (Figure 61a), which proved that these two spin systems are on the same side of the molecule, thereby revealing that the absolute configuration of the two stereogenic centers at C-1 and C-3 had not changed by the metabolic conversion.

Authentic reference material of the presumed metabolite was synthesized by treatment of dioncophylline A (**8**) with BBr_3 leading to a mixture of 5'-*O*-demethyldioncophylline A (**47**), 4'-*O*-demethyldioncophylline A (**49**), 4,5'-*O,O*-didemethyldioncophylline A (**50**). The partial synthetic products were separated from each other by treatment with preparative HPLC. Coelution of the metabolite with each of the synthetic products, permitted assignment of the metabolite to be 5'-*O*-demethyldioncophylline A (**47**), and excluded that any other theoretical possible *O*-demethylation products had been biotransformed. The assignment of the metabolite was further corroborated by direct NMR comparison, which showed only one set of signals of a 1:1 mixture of the metabolite and the reference material. The conclusion of the major metabolic product of dioncophylline A (**8**) to represent 5'-*O*-demethyldioncophylline A (**47**) is in agreement with the assumption drawn from previously biotransformation studies of the alkaloid.[46]

The mass spectrum of the faster eluting metabolite suggested addition of an oxygen atom to dioncophylline A (**8**). The low rate of formation of the metabolite prevented the isolation of sufficient amounts for NMR experiments, so that the exact structure could not be determined. However, the imaginable structure of habropetaline A (**37**, Figure 62), was excluded since authentic reference material (isolated as described in Chapter 5.2.5), did not coelute with the metabolite.

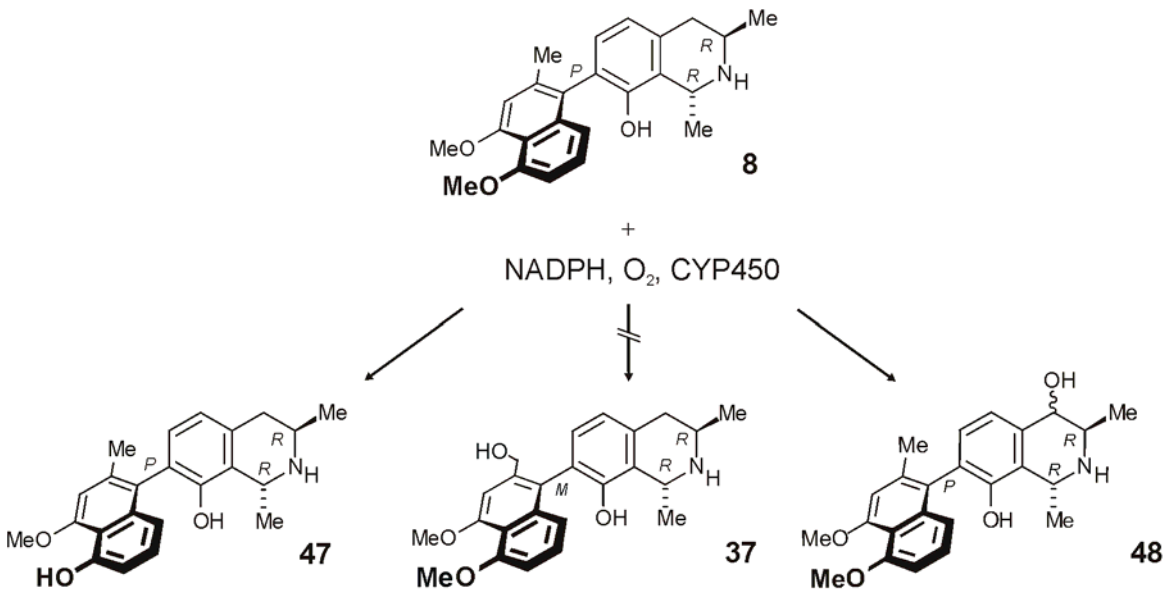

Figure 62. Metabolic conversion of dioncophylline A (**8**) to the major metabolite 5'-demethyldioncophylline A (**47**), habropetaline A (**37**) being excluded by co-elution, and a minor second metabolite **48** oxidized on the isoquinoline moiety of the molecule, presumably in the 4-position.

Oxygenation of a carbon atom at the aromatic rings was considered unlikely, since the UV spectrum of the metabolite and that of dioncophylline A (**8**) were identical. According to experience from other aromatic compounds,[239] the presence of additional phenolic OH groups should modify the UV spectrum of the naphthylisoquinoline. As deduced from the mass spectrum, the metabolite should possess a 4-hydroxylated isoquinoline portion like, *e.g.*, that of dioncophyllinol B (**38**), and should hence be represented by structure **48** (Figure 62). One of the most intensive signal in the mass spectra of the naphthylisoquinoline alkaloids is the peak of the naphthyl moiety, *e.g.*, with *m/z* 202 for dioncophylline A (**8**) (both oxygen atoms are methylated) and *m/z* 188 for **47** and dioncophyllinol B (**38**) (one free hydroxyl group) (Figure 62 and 36). Since the mass spectrum of **48** has a peak of *m/z* 202 (Figure 60), the naphthyl moiety of **48** must have remained unaltered compared to the naphthyl moiety of the parent compound **8**. Thus, the addition of oxygen must have occurred on the isoquinoline moiety of the molecule. The loss of water (*m/z* 18) from the molecular ion only occurs for dioncophyllinol B (**38**) and **48**, but not for **8** or **47**. Taking also into account that the benzylic position is favored for cytochrome P450 mediated oxidations,[240] structure **48** is the most probable one for the second metabolite formed.

Kinetic constants for the formation of **47** in rat liver microsomes were determined by M. Sieber as K_M of 32 nmol/L and v_{max} of 20 pmol mL^{-1} mg^{-1} min^{-1} suggesting a relatively low rate of oxidation of dioncophylline A (**8**) (rates determined for the 6-β-hydroxylation of testosterone in the microsome batches used were K_M = 30 nmol/mL and v_{max} = 1200 pmol mL^{-1} mg^{-1} min^{-1}).

8.2.3 Incubation of Dioncophylline C (6) and Dioncopeltine A (7)

The HPLC-UV and HPLC-MS analyses of the incubation mixtures of dioncophylline C (**6**) and dioncopeltine A (**7**) showed no indications for biotransformation. Thus, it can be concluded that the compounds are stable to phase 1 metabolism reactions caused by rat liver microsomes, which indicates that these naphthylisoquinoline alkaloids may be useful candidates for novel antimalarial drugs.

8.3 Phase 2 Metabolism Study of Dioncophyllines A (8) and C (6) and Dioncopeltine A (7)

8.3.1 Liver Microsomal Incubation Assay for Phase 2 Glucuronidation Investigations

Identical concentrations and conditions as for the phase 1 experiments were used for the carry out of the phase 2 glucuronidation experiments. The reactions were initiated by addition of uridine-diphosphoglucuronic acid (UDPGA) and terminated by adding cold methanol. After centrifugation, supernatants from the incubation solutions were analyzed by HPLC-UV and HPLC-MS methods described in Chapter Ex. 1.3.

8.3.2 HPLC-UV and HPLC-MS Analyses of the Phase 2 Glucuronidation Experiments

The HPLC-UV analyses of the samples from the phase 2 glucuronidation experiments indicated the formation of time and protein dependent glucuronidation products for all of the naphthylisoquinoline alkaloids tested. For both, dioncophylline A (**8**) and dioncopeltine A (**7**), one new peak was identified and for dioncophylline C (**6**) two new peaks were identified. The "new" peaks were all faster eluting in reversed-phase HPLC than the naphthylisoquinoline alkaloid which they originated from.

HPLC-MS analyses revealed the new peaks to correspond to mono-glucuronidation products of dioncophylline A (**8**) and dioncopeltine A (**7**), and for dioncophylline C (**6**) both a mono- and a di-glucuronidation product (Figure 63).

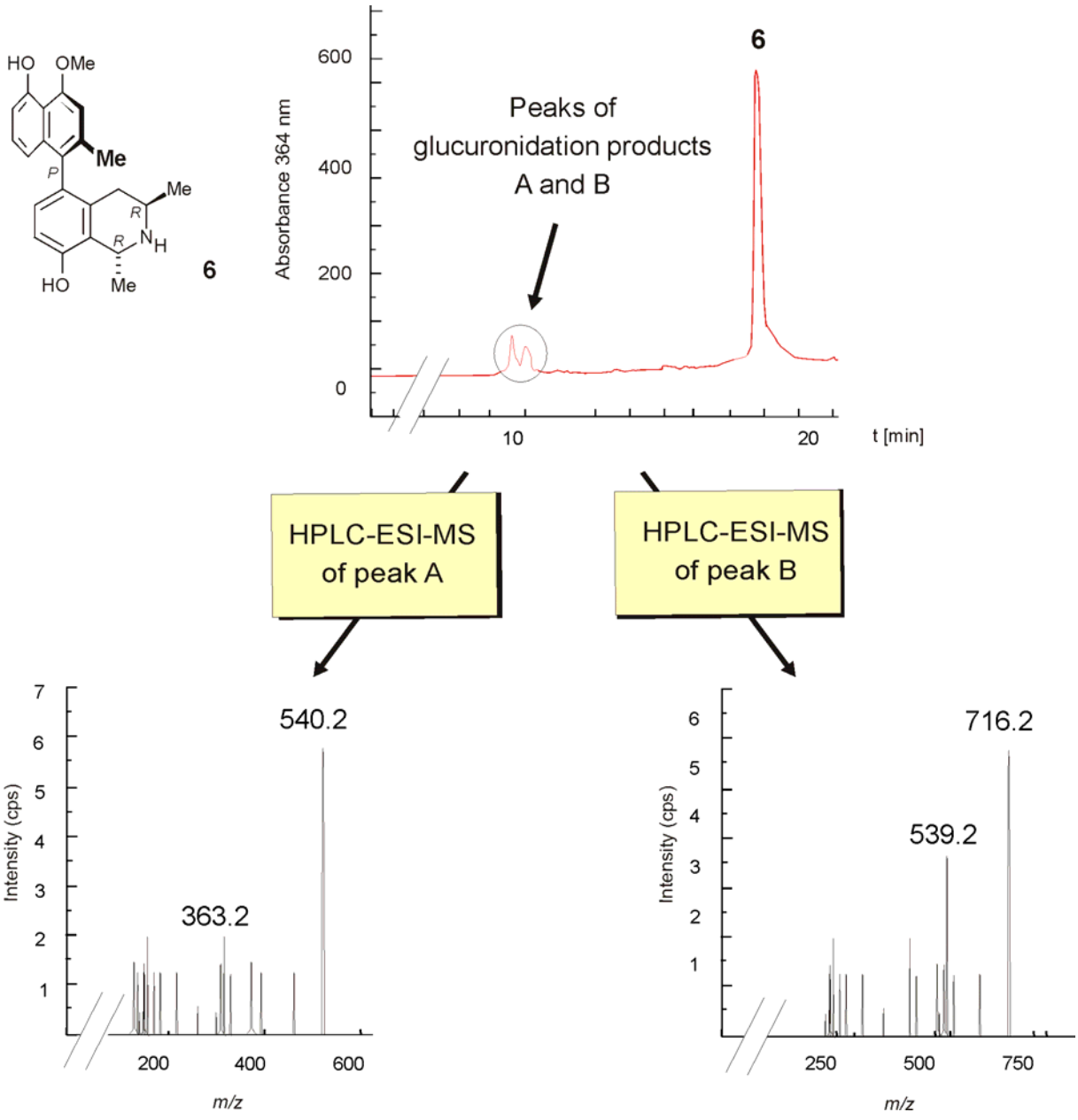

Figure 63. HPLC-UV (306 nm) and HPLC-MS analysis using a reversed-phase column of a solution from the glucuronidation incubation experiments, exemplarily for dioncophylline C (**6**) and the two glucuronide metabolites peaks A and B eluting earlier.

As for the phase 1 investigations HPLC-MS/MS analyses revealed the most intensive signal in the mass spectra of the glucuronide product of dioncophylline A (**8**) to be the peak of the naphthyl moiety, *e.g. m/z* 202, which indicated the glucuronidation site to be in the isoquinoline moiety of the phase 2 metabolite.

Furthermore, the HPLC-MS/MS analyses of monoglucuronide products of dioncopeltine A (**7**) and dioncophylline C (**6**) revealed the intensive signal of the respective naphthyl moieties in each of the chromatograms, (*i.e.*, *m/z* 204 and 188), to be replaced by a peak corresponding to one molecular unit lower (Figure 64). Thereby clearly indicating that the glucuronidation site of both of these phase 2 metabolic products to be located in the naphthyl moiety. The same signal for fragmentation was seen for the HPLC-MS/MS analyses of the diglucuronide product of dioncophylline C (**6**).

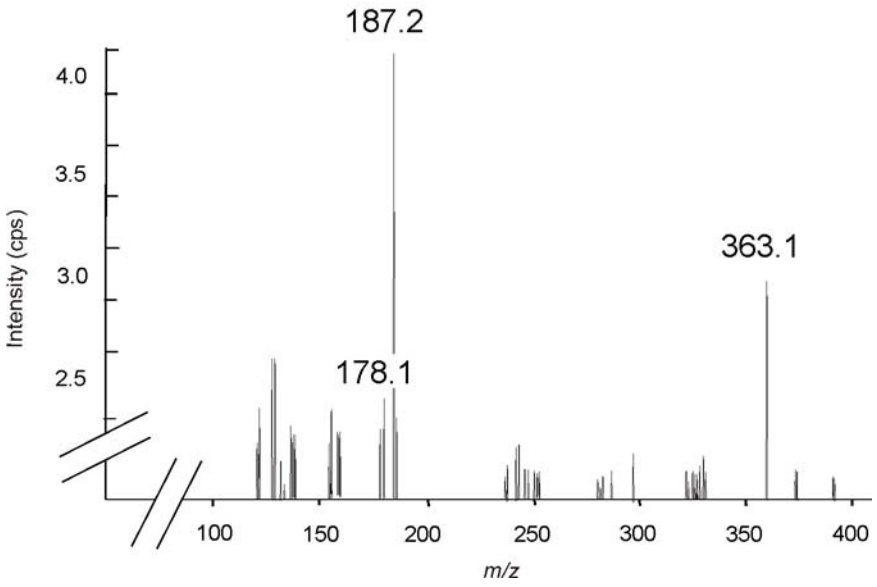

Figure 64. Mass spectrum of the monoglucuronide metabolite of **6** ($[M+H]^+$ = 540.2). The structure is indicated from HPLC-MS/MS data. The peak at *m/z* 187 corresponds to the naphthalene moiety of the molecule, the signal at *m/z* = 363 indicates a loss of glucuronic acid from the molecular ion.

Taking these findings into account combined with the fact that glucuronidation of phenolic hydroxyl groups is favored over primary hydroxyl functions[226,228] and that only very few examples of *N*-glucuronide products of secondary amines are known, reveals that the structures **51**–**54** are the most probable ones for the metabolic glucuronides of the naphthylisoquinoline alkaloids biotransformed (Figure 65).

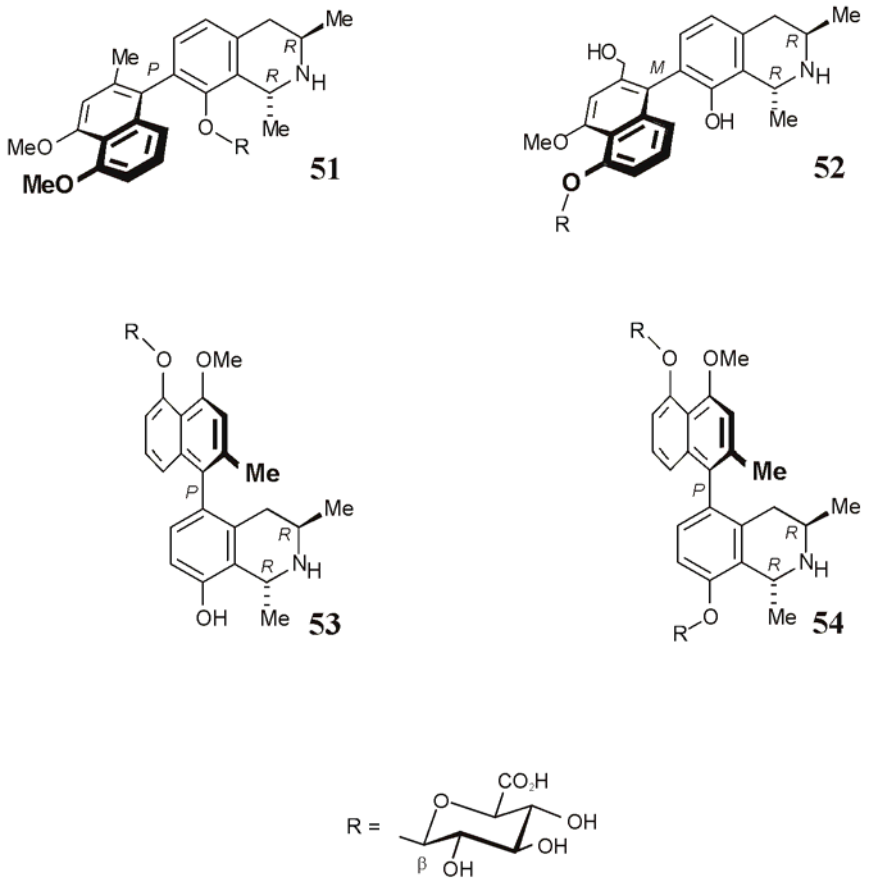

Figure 65. The presumable structures as indicated by HPLC-MS/MS analysis of the phase 2-glucuronide metabolites: **51** of dioncophylline A (**8**), **52** of dioncopeltine A (**7**), and **53** and **54** of dioncophylline C (**6**).

Interestingly, only one of the possible two mono-*O*-glucuronide metabolites of dioncophylline C (**6**) was detected, but it cannot be excluded that the two products coeluted. However, there was no indication of an additional monoglucuronide product and thus it is assumed that the *O*-glucuronidation selectively takes place first in the naphthyl moiety and then in the isoquinoline moiety.

Likewise, for the analyses of dioncopeltine A (**7**) only one monoglucuronide product was detected and no indication was found of the presence of additional *O*-glucuronide products (spectra not shown). Thus, it is assumed that the glucuronidation of dioncopeltine A (**7**) selectively leads to compound **52**.

8.4 *In Vivo* Pharmacokinetic Profile of Dioncophylline A (**8**)

In cooperation with the group of Prof. Dr. W. Dekant the pharmacokinetics of dioncophylline A (**8**) was studied.[241]

None of the phase 1 and phase 2 metabolites identified *in vitro*, could be detected in plasma, urine nor faeces samples of the *in vivo* experiment, despite targeted search by HPLC-MS/MS for diagnostic fragments indicative for these compounds.

The results of the pharmacokinetic study carried out by the group of Prof. Dr. W. Dekant suggest that an oral application will probably not result in therapeutically efficient blood concentrations of dioncophylline A (**8**), whereas the data of the intravenous application reveal a promising administration route. The pharmacokinetic profile of dioncophylline A (**8**), studied as a model substance for the naphthylisoquinoline alkaloids, indicates that these compounds may be useful candidates for a novel antimalarial drug.[241]

9 Concluding Remarks

After a decade of disappointingly few lead compounds progressing into clinical trials deduced from alternative drug discovery methods such as rational drug design and combinatorial chemistry, several pharmaceutical companies revive the search for new plant-derived drug candidates. Thus, secondary plant metabolites historically have been and still remain to be an important source of potential new pharmaceuticals.

The naphthylisoquinoline alkaloids comprise an intriguing class of natural products possessing a broad range of bioactivities, which makes them promising candidates as lead structures in the search for urgently needed new drugs against widespread fatal diseases like malaria, leishmaniasis, Chagas' disease, and African sleeping sickness. Thus, the search for further new compounds of this type and the exploration of their mode of action is potentially rewarding.

This thesis deals with the isolation and structural elucidation of bioactive naphthylisoquinoline alkaloids and related analogs. The mode of action of the antiplasmodial activity exhibited by the naphthylisoquinoline alkaloids was explored and compared to that of the antimalarial drug chloroquine (**2**). Furthermore, the phase 1 and 2 metabolism of dioncophyllines A (**8**) and C (**6**) and dioncopeltine A (**7**) were investigated.

In detail the following results have been obtained:

- From the leaves of the recently discovered East African liana *A. tanzaniensis* six naphthylisoquinoline alkaloids were isolated, among them the already known compound ancistrotectoriline (**15**), which had previously been isolated from *A. tectorius*. However, the absolute configuration at C-1 and C-3 of **15**, had been assigned only tentatively in the literature. Ruthenium(III)-catalyzed periodate oxidation of the compound isolated from *A. tanzaniensis* confirmed the configuration at the two stereogenic carbons as 1*S*,3*S,* as previously assumed. A direct NMR comparison with authentic reference material isolated from *A. tectorius* showed a single set of signals for a 1:1 mixture as a final prove that ancistrotectoriline (**15**) is occurring in both *A. tectorius* and *A. tanzaniensis*. Two of the isolated compounds were found to be new; ancistrotanzanine B (**13**) and 6-*O*-methylancistrocladinine (**14**), the former displaying highly antileishmanial activity.

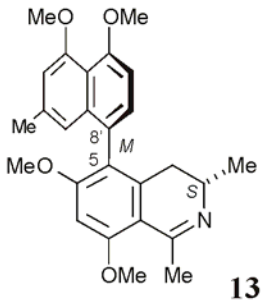

13

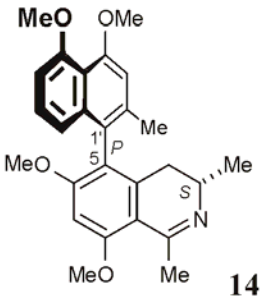

14

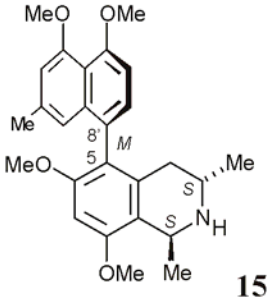

15

- The leaves of a botanical yet undescribed *Ancistrocladus* species, collected by Prof. Dr. V. Mudogo in the Democratic Republic of Congo in the habitat Yeteto near the town Ikela, were analyzed for naphthylisoquinoline alkaloids for the first time, in close cooperation with S. Pedersen. The isolation work led to the first identification of an *N*,C-coupled naphthyldihydroisoquinoline alkaloid; ancistrocladinium B (**22**), which was isolated as a 46:54 mixture of two configurationally semi-stable atropo-diastereomers. The novel alkaloid **22** represents a hitherto unprecedented *N*,6'-coupling type; the absolute configuration at the axis of each atropo-diastereomer was determined by M. Reichert, who performed extensive quantum chemical CD calculations. The Gibbs free energy at 25 ºC for the isomerization barrier of the two atropo-diastereomers was determined to be just above <100 kJ mol^{-1}, *i.e.*, above the defined energy barrier of well-separable stable atropisomers.

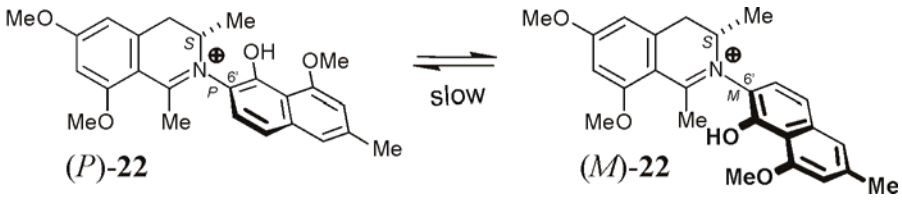

(*P*)-**22** (*M*)-**22**

Phytochemical investigation of the roots of the Congolese *Ancistrocladus* species (habitat Yeteto), performed in cooperation with J. Spuziak and Prof. Dr. V. Mudogo, afforded five new derivatives of known naphthylisoquinoline alkaloids, namely 5'-*O*-demethylhamatine (**26**), 5'-*O*-demethylhamatinine (**28**), 6-*O*-demethylancistroealaine A (**30**), 6,5'-*O*,*O*-didemethylancistroealaine A (**31**), and 5-*epi*-6-*O*-methylancistrobertsonine A (**32**), along with six known naphthylisoquinoline alkaloids.

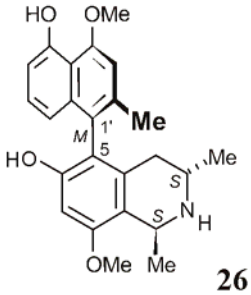

26

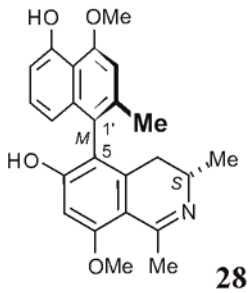

28

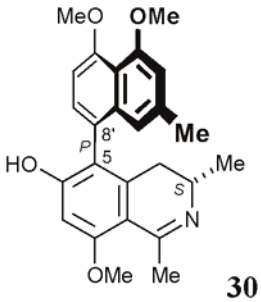

30

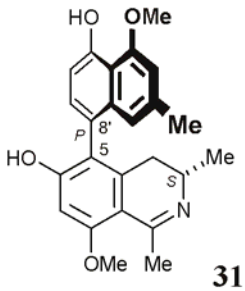

31

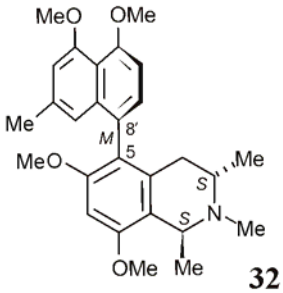

32

All of the compounds isolated from the botanical yet undescribed Congolese *Ancistrocladus species*, have an oxygen function at C-6 and the *S*-configuration at C-3. These phytochemical characteristics show close relations of the species to the known members of Ancistrocladaceae from Central, and East Africa, as well as from South-East Asia. The variety of the compounds isolated indicate that the plant from the new location of the Democratic Republic of Congo deserve probably the rank of a new species and is a rich source of naphthylisoquinoline alkaloids.

- For the large scale isolation of bioactive naphthylisoquinoline alkaloids from *Triphyophyllum peltatum*, the new liquid-liquid chromatographic method, Fast Centrifugal Partition Chromatography (FCPC), was used. This led to the development of an efficient and time saving protocol for the purification of dioncophyllines A (**8**), and C (**6**), and dioncopeltine A (**7**) in 100 mg to gram quantities.

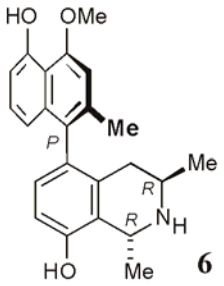

6

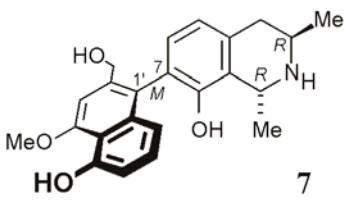

7

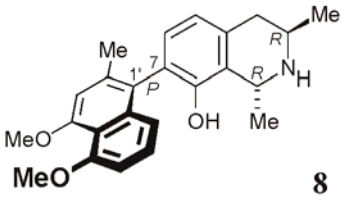

8

- The antiplasmodial activity guided purification of ^{60}Co irradiated samples containing commercially available naphthylisoquinoline related substances, afforded the isolation of the irradiation products 3,4-dihydro-1-isoquinolinone (**43**), 3,4-dihydro-1-isoquinolineamine (**44**), and 1,2,3,4-tetrahydro-1,2-diazirino-isoquinoline (**45**). The compounds were found to be more active than the starting material, although only exhibiting weak antiplasmodial activity against *P. falciparum*. The γ-ray synthesis method was proven to be a suitable tool for the generation of small compound libraries. Thus, the aim to achieve highly active antiplasmodial products by the method seems possible, judged from the first promising results obtained.

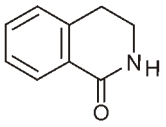

43

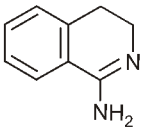

44a

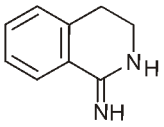

44b

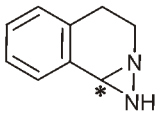

* Racemic mixture **45**

- The effect on the absorption spectrum of FPIX (**9**) due to complex formation with the naphthylisoquinoline alkaloids dioncophyllines A (**8**) and C (**6**), dioncopeltine A (**7**) korupensamine A (**46**), and ancistrocladine (**35**) was examined by a titration study. Job's plot analyses by UV-spectroscopy determined the stoichiometry for the complex formation of FPIX (**9**) and naphthylisoquinoline alkaloids to be 2:1. Furthermore, the dissociation constants for the complexation with FPIX (**9**) were determined for each of the naphthylisoquinoline alkaloids investigated. Dioncophylline C (**6**) and dioncopeltine A (**7**) were found to possess dissociation constants, which are comparable to the one reported for the antimalarial drug chloroquine (**2**).

  The ability of ESI to transfer noncovalent solution-phase assemblies intact into the gas phase, was conducted on solution mixtures of naphthylisoquinoline alkaloid and FPIX (**9**), as well as on mixtures of chloroquine (**2**) and FPIX (**9**). The mass spectrometry analyses revealed several peaks, which corresponded to the complex formation of FPIX (**9**) to the respective ligands investigated. The most interesting results obtained were the detection of peaks corresponding to the complex formation between a chelated dimer of FPIX (**9**) and dioncophylline C (**6**)

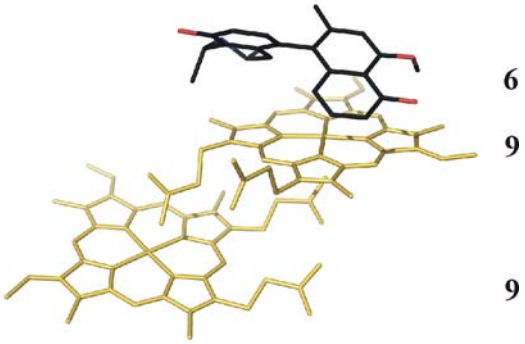

and of peaks corresponding to a double protonated tetramer of FPIX (**9**) – consisting of two chelated μ-oxo dimers of FPIX (**9**) – in complex formation with two molecules of chloroquine (**2**).

The naphthylisoquinoline alkaloids dioncophyllines A (**8**) and C (**6**), dioncopeltine A (**7**), ancistrocladine (**35**), and korupensamine A (**46**) were investigated for their activity to inhibit β-hematin formation by a recently developed high-through put screening assay using UV spectroscopy. Whereas ancistrocladine (**35**) was found to be inactive in the molar concentration investigated, the additional naphthylisoquinoline alkaloids were proven to be strong inhibitors of the β-hematin formation. The determined IC_{50} values displayed by these alkaloids were found to be comparable to the ones reported for the antimalarial drugs amodiaquine (**10**) and chloroquine (**2**), the most active compounds tested with the assay.

- In cooperation with M. Sieber two phase 1 metabolism products of dioncophylline A (**8**) were identified. Coelution in combination with HPLC-MS/MS, NMR, and CD investigations assigned the major metabolic product as 5'-*O*-demethyldioncophylline A (**47**). The minor metabolic product was only present in small amounts, which disabled an unambiguous structural characterization of the compound. However, as deduced from the mass spectrometry analyses and exclusion of a possible metabolic oxidation product by coelution with authentic reference material, the metabolite should possess a 4-hydroxylated isoquinoline portion and is assumed to be represented by structure **48**. Dioncophylline C (**6**) and dioncopeltine A (**7**) were found to be stable to phase 1 metabolism reactions caused by rat liver microsomes.

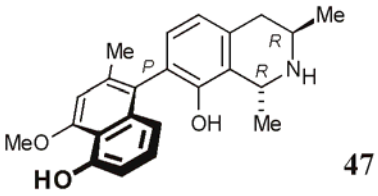

47

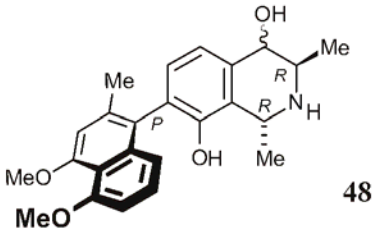

48

HPLC-UV analyses of the samples from the phase 2 glucuronidation incubations of dioncophylline A (**8**), dioncophylline C (**6**) and dioncopeltine A (**7**) revealed the formation of glucuronide products for all of the naphthylisoquinoline alkaloids investigated. HPLC-MS/MS analyses indicated these metabolic products to be represented by the structures **51**-**54**.

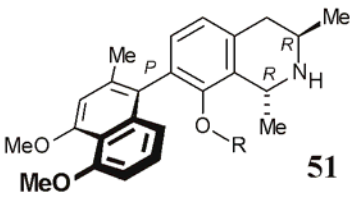

51

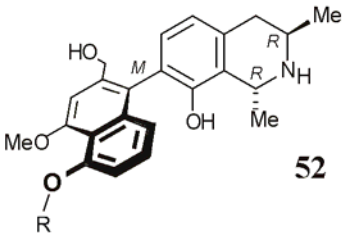

52

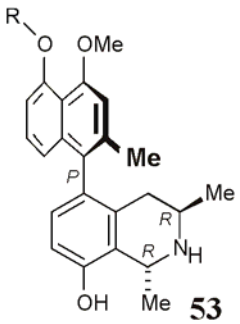

53

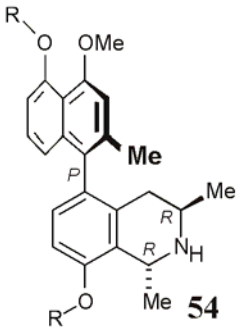

54

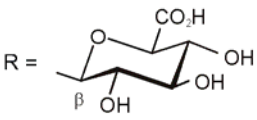

10 Zusammenfassung

Nach einem Jahrzehnt mit entäuschend wenigen Substanzen abgeleitet von alternativen Drug Disvovery Progammen, wie zum Beispiel dem Rational-Drug-Design und der kombinatorischen Chemie, die in der klinische Prüfung aufgenommen wurden, haben mehere Pharmazeutische Gesellschaften die "traditionelle" Suche nach neuen Arzneimittel-Kandidaten in Pflanzen wieder aufgenommen. Sekundäre Pflanzeninhaltstoffe sind deshalb nach wie vor eine wichtige Quelle potenzieller neuer Arzneistoffen.

Naphthylisochinolin-Alkaloide stellen eine faszinierende Klasse von Sekundärmetaboliten dar, die ein breites Wirkspektrum aufweisen und somit viel versprechende Leit-Struktur-Kandidaten für die Suche nach dringend erforderlichen neuen Arzneimittel gegen weit verbreitete tödliche tropische Krankheiten, wie Malaria, Leishmaniose, der Chagas-Krankheit und der Afrikanische Schlafenkrankheit. Die Isolierung weiterer neuer Verbindungen dieser Substanzklasse, sowie die Aufklärung ihrer Wirkmechanismen sind somit lohnende Ziele.

In der vorliegenden Dissertation wurden biokative Naphthylischinolin-Alkaloide und verwandte Analoga isoliert und deren Struktur aufgeklärt. Der Wirkmekanismus der antiplasmodialen Aktivität der Naphthylischinolin-Alkloide wurde untersucht und mit dem des Malaria-Arzneitmittels Chloroquine (**2**) verglichen. Des weiteren wurde der Phase 1 und 2 Metbolismus von Dioncophyllin A (**8**), C (**6**) und von Dioncopeltin A (**7**) untersucht.

Im Einzelnen wurden folgende Ergebnisse erzielt:

- Aus Blättern der ostafrikanischen Lianenart *Ancistrocladus tanzaniensis* wurden sechs Naphthylischinolin-Alkaloide isoliert, darunter Ancistrotectorilin (**15**) die bereits aus *A. tectorius* isoliert wurde. Allerdings wurde die Konfiguration von C-1 und C-3 von **15** nur zögernd aufgeklärt. Mit Hilfe von Ruthenium(III)-katalysiertem oxidativen Abbau der isolierten Substanz konnte die publizierte absolute Konfiguration an C-1 zu *S* und an C-3 zu *S* bestätigt werden. Der endgültige Beweis der Identität der zwei Substanzen wurde durch Aufnahme eines NMR-Spektrums einer Mischung der isolierten Verbindung mit authentischem Referenz-Material, isoliert aus *A. tectorius* gegeben, da nur ein einziger Singal satz detektiert wurde. Zwei der isolierten Substanzen waren neu: Ancistrotanzanin B (**13**) und *O*-Methylancistrocladinin (**14**), wobei die erstgenannte Verbindung zeigte hervorragende antileishmaniale Wirkung.

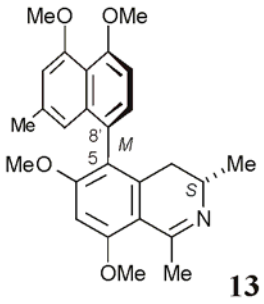

13

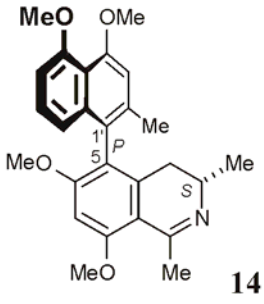

14

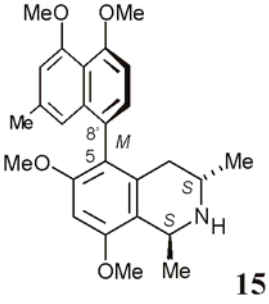

15

Von einer botanisch bisher unbeschriebenen *Ancistrocladus* Art, gesammelt von Prof. Dr. V. Mudogo in der Demokratischen Republik Kongo bei Yeteto, in der Nähe der Stadt Ikela, wurden die Blätter in Zusammenarbeit mit S. Pedersen auf ihren Inhalt an Naphthylischinolin-Alkloiden phytochemisch untersucht. Dabei konnte das erste *N*,C gekuppelte Naphthyldihydroisochinolin-Alkaloid, Ancistrocladinium B (**22**), isoliert werden, welches in einem 46:54 Gemisch zweier konfigurativ stabiler Atropo-Diastereomere vorlag. Ancistrocladinium B (**22**) ist das erste Naphthylisochinolin-Alkaloid mit *N*,8'-Kupplung. Die Konfiguration an der Achse wurde von M. Reichert durch quantenchemische CD-Rechnungen ermittelt. Die Gibbs frei Energi bei 25 ºC für die Isomerisierungs-Barriere der Atropo-Diastereomere konnte gerade zu >100 kJ mol^{-1} bestimmt werden, d.h. ist höher als die definierte Energie-Barriere gut trennbarer stabiler Atropisomere.

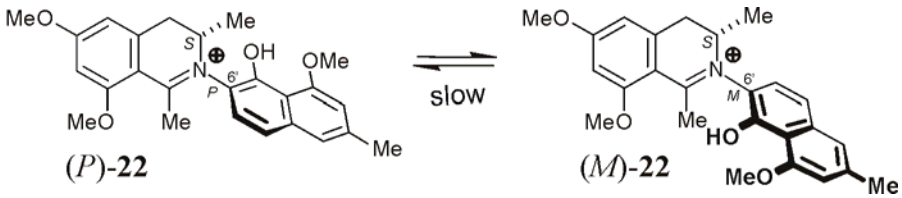

(*P*)-**22** (*M*)-**22**

- Die phytochemische Untersuchung der Wurzeln der Kongolesischen *Ancistrocladus* Art (Fundort Yeteto) wurde in Kooperation mit J. Spuziak und Prof. Dr. V. Mudogo ausgeführt und ergab die Isolierung von fünf unbekannten Derivaten bereits bekannter Naphthylisochinolin-Alkaloide: 5'-*O*-Demethylhamatin (**26**), 5'-*O*-Demethylhamatinin (**28**), 6-*O*-Demethylancistroealain A (**30**), 6,5'-*O*,*O*-Didemethylancistroealain A (**31**) und 5-*epi*-6-*O*-Methylancistrobertsonine A (**32**). Parallel dazu wurden sechs bereits bekannte Naphthylisochinolin-Alkaloide identifiziert.

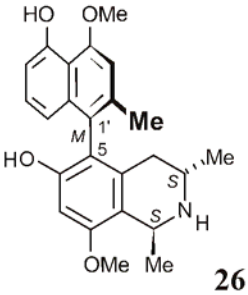

26

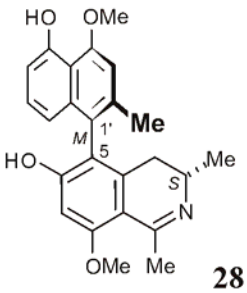

28

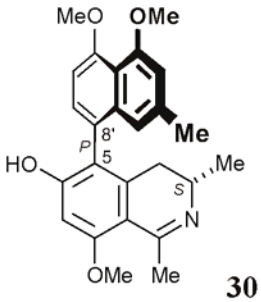

30

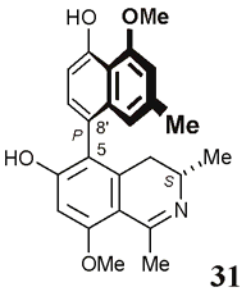

31

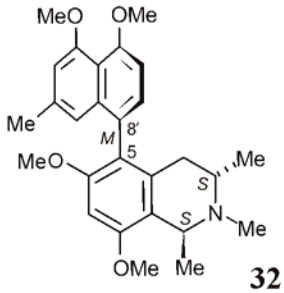

32

- Für die Isolierung von grösseren Mengen bioaktiver Naphthylisochinolin-Alkloide, wurde die Fast Centrifugal Partition Chromatography (FCPC) - eine neue flüssig-flüssig-chromatographischen Methode – benützt. So konnte ein effizientes und zeitsparendes Protokoll für die Isolierung von Dioncophyllin A (**8**), C (**6**), sowie Dioncopeltin A (**7**) in 100 mg bis Gram Massstaben entwickelt werden.

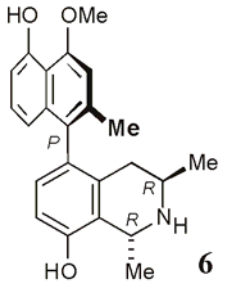

6

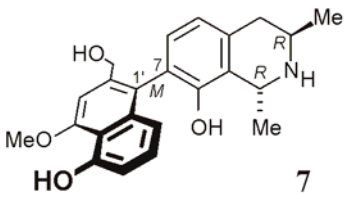

7

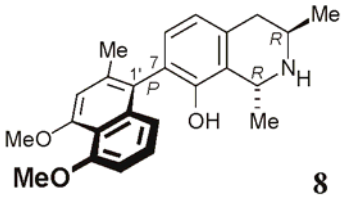

8

- Die bioaktivitätsgeleitete Reinigung antiplasmodialer ^{60}Co bestrahlter Proben – kommerziel verfügbarer Naphthylisochinolin abgeleiteter Substanzen – führte zur Isolierung verschiedener Bestrahlungs-Produkte, nämlich 3,4-Dihydro-1-Isochinolinon (**43**), 3,4-Dihydro-1-isochinolineamin (**44**), und 1,2,3,4-Tetrahydro-1,2-Diazirino-Isochinolin (**45**). Die isolierten Substanzen waren jeweils aktiver als die Edukte, zeigten aber trotzdem nur antiplasmodiale Wirksamkeit im mittleren Berreich. Die γ-Ray-Synthese-Methode sollte also zur Herstellung kleiner Substanz-Bibliotheken geeignet sein. Das Ziel hoch wirksame, antiplasmodiale Substanzen zu erhalten kann nach diesen ersten vielversprechenden Ergebnissen, als plausibel bezeichnet werden.

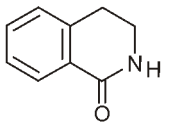

43

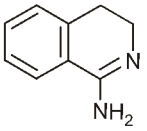

44a

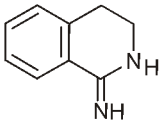

44b

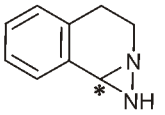

* Racemic mixture **45**

- Die Auswirkung der Komplexbildung unterschiedlicher Naphthylisochinolin-Alkloide – Dioncophylline A (**8**) und C (**6**), Dioncopeltin A (**7**), Korupensamin A (**46**), und Ancistrocladin (**35**) – auf das Absorptions-Spektrum von FPIX (**9**) wurde mittels eines Titrationsexperimentes, unter Anwendung von UV Spektroskopie, untersucht. Durch Job's Plot Analysen konnte so die Stöchiometrie der Komplex-Bildung zwischen FPIX (**9**) und Naphthylisochinolin-Alkaloide zu 2:1 bestimmt werden. Weiterhin konnten die einzelnen Dissoziationskonstanten für die Komplexierung von FPIX (**9**) mit den untersuchten Naphthylisochinolin-Alkaloiden errechnet werden. Die für Dioncophyllin C (**6**) und Dioncopeltin A (**7**) bestimmten Dissoziationskonstanten sind mit der in der Literatur für das antimalariale Arzneitmittel Chloroquine (**2**) vergleichbar. Die Möglichkeit durch ESI nicht kovalent gelöste Komponenten intakt in die Gas-Phase zu transferieren, wurden auf Lösungs-Gemische von Naphthylischinolin-Alkaloiden und FPIX (**9**) sowie auf Lösungs-Gemische von Chloroquine (**2**) und FPIX (**9**) angewandt. Die massenspektroskopischen Analysen ergaben mehrere Peaks, die der Komplex-Bildung von FPIX (**9**) mit den einzeln untersuchten Liganden entsprachen. Die interessantesten Ergebnisse waren dabei die Entdeckung von Peaks, die die Komplex-Bildung zwischen einem chelatisierten Dimer von FPIX (**9**) mit Dioncophyllin C (**6**),

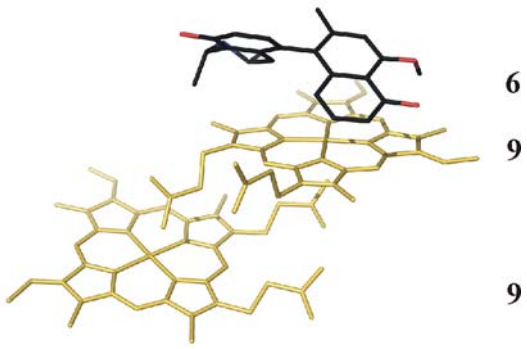

sowie zwischen einem doppelt protonierten Tetramer von FPIX (**9**) – bestehend aus zwei chelatisierten μ-oxo Dimeren von FPIX (**9**) – mit zwei Molkülen Chloroquine (**2**) entsprachen.

Die Naphthylisochinolin-Alkaloide Dioncophylline A (**8**) und C (**6**), Ancistrocladin (**35**), Korupensamin A (**46**) sowie Dioncopeltin A (**7**) wurden mittels eines neu entwickelten high-through put screening Assays unter Anwendung der UV Spektroskopie, auf ihre Hemmungung der β-Hematin Bildung untersucht. Dabei zeigte sich Ancistrocladin (**35**) inaktiv, wohingegen die anderen Verbindungen hervorragende Hemmung ausbildeten. Die bestimmten IC_{50} Werte dieser Alkaloide waren mit denen für die antimalariale Arzneimittel Amodiaquine (**10**) und Chloroquine (**2**) in der Literatur angegebenen Werte vergleichbar.

- Zwei Phase 1 Metabolite von Dioncophyllin A konnten in Kooperation mit M. Sieber identifiziert werden. Die Struktur des Haupt-Metabolismus-Produktes konnte durch Koelution, HPLC-MS/MS, NMR und CD Untersuchungen als 5'-*O*-demethyldioncophyllin A (**47**) bestätigt werden. Der in geringeren Mengen gebildete Metabolit war nur in <Milligram Mengen vorhanden. Daher konnte dessen Struktur nicht eindeutig aufgeklärt werden. Allerdings konnte durch massenspektroskopische Analysen eine Hydroxylierung postuliert werden; eine Oxidation von Dioncophyllin A (**8**) zur Habropetalin A (**37**) konnte des weiteren durch Koelution ausgeschlossen werden. Daher wurde eine Hydroxylierung in 4-Posotion von Substanz **48** vermutet. Weiterhin wurde festgetellt, dass Dioncophyllin C (**6**) und Dioncopeltin A (**7**) nicht von Rattenlebermikrosomen Phase 1 metabolisiert wird.

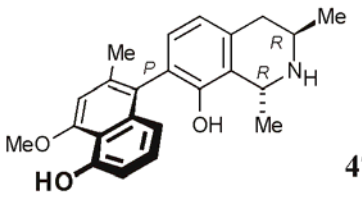

47

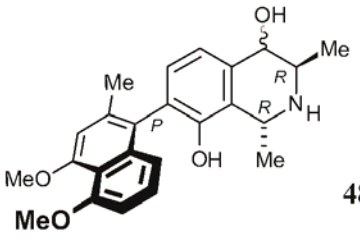

48

Die Bildung von Glucuronide Phase 2 Metabolisme Produkte von Dioncophyllin A (**8**) und C (**6**) sowie Dioncopeltin A (**7**) konnte mittels HPLC-UV Analysen von Phase 2 Glucuronidierungs-Inkubationen gezeigt werden. Weitere HPLC-MS/MS Analysen ergab die Vermutung, dass die Metaboliten die Strukturen **51**-**54** besitzen.

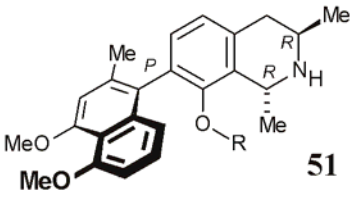
Me
P
R
R
NH
Me
MeO
O
R
MeO
Me

51

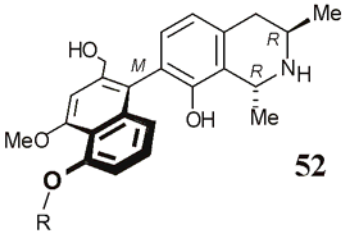
HO
M
R
R
NH
Me
MeO
OH
Me
O
R

52

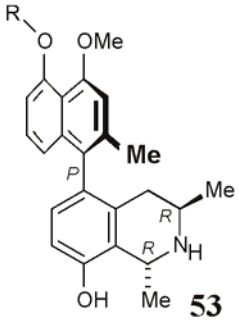
R
O
OMe
Me
P
Me
R
R
NH
OH
Me

53

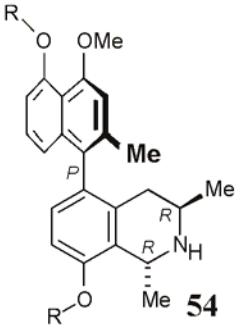
R
O
OMe
Me
P
Me
R
R
NH
R
O
Me

54

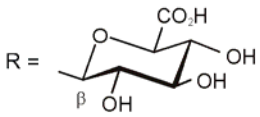
R =
CO2H
O
OH
OH
β
OH

Experimental Section

1 General Aspects

1.1 Analytical Apparatures

Melting point (mp): Melting points were determined on a *Reichert-Jung* Thermovar-Kofler-Heiztisch-microscope and are uncorrected.

Ultraviolet spectroscopy (UV): The UV-spectra were measured at RT with a *Varian* Cary 50 Conc UV-Visible Spectrophotometer. The UV spectra of solution media was measured as background. *Varian*-Cary-WinUV-Simple-scan-Application software was used for processing of the measurements.

Infrared spectroscopy (IR): The IR spectra were measured on a *Jasco* FT/IR-410 spectrometer. The spectra were recorded at RT. $\tilde{\nu}$ refers to the wavelength number. The intensity of the absorption bands is given by: s = strong, m = middle, w = weak and br = broad.

Nuclear magnetic resonance spectroscopy (^1H NMR, ^{13}C NMR): The ^{1}H NMR (400 MHz, 600 MHz) and ^{13}C NMR (100 MHz, 150 MHz,) spectra were recorded at room temperature on either a *Bruker* AMX 400 or on a DMX 600 spectrometer. The chemical shifts of the signals are given in units on the δ-scale, with reference to $\delta_{TMS} = 0$. Calibration of the spectra was carried out by means of an internal standard using the trace protons from the deuterated solvent, for ^{1}H NMR: $\delta(CDCl_3) = 7.26$; $\delta(CD_3OD) = 3.31$; δ-Aceton-$d_6 = 2.05$; δ-DMSO-$d_6 = 2.50$, and for ^{13}C NMR: $\delta(CDCl_3) = 77.01$; $\delta(CD_3OD) = 49.15$; δ-Aceton-$d_6 = 29.82$; δ-DMSO-$d_6 = 39.51$. Processing of the spectra was carried out using XWIN-NMR-software from *Bruker*. Signal multiplicity is described using the following abbreviations: singlet = s, doublet = d, doublet of doublets = dd, triplet = t, doublet of triplets = dt, quartet = q, multiplet = m. The coupling constants are given in Hertz (Hz), where ^nJ describes the number of bonds.

Mass spectroscopy (MS): Electronic ionization (EI) and high resolution electronic ionization (HREIMS) mass spectra were determined on a *Finnigan* MAT 8200 apparatus with an

ionization potential of 70 eV. The bracketed numbers give the intensity of the signals relative to the base peak (I = 100%). Electro spray ionization (ESI) and high resolution electro spray ionization HRMS (ESI) mass spectra were recorded on a *Bruker Daltonics* microTOF focus, for calculation of the respective mass values of the isotopic distribution, the software modul IsotopePattern of the software Compass 1.1 from *Bruker Daltonics* was used. ESI-MS/MS were recorded on a *Finigan* LCQ ion trap mass spectrometer equipped with a custom-built nano-electrospray ion source (ESI parameters: 2.0 kV; capillary voltage, 42 V; tube lens offset, 30 V; the electron multiplier at -950 V; no sheat or auxiliary gas). HPLC-ESI-MS analyses were performed on an *Agilent* 1100 Series System consisting of an HPLC pump, an MSD Ion Trap mass spectrometer (capillary temperature: 350 °C; ESI-voltage: 3500 V; N_2 as the heat gas), and a diode-array detector (DAD) (all *Agilent Technologies*).

GC-MSD: For the GC-MSD analysis a *Hewlett Packard* 5890 II gas chromatograph was used with a *Hewlett Packard* Ultra 2 (cross linked 5% Ph Me silicone 25 m x 0.32 mm x 0.52 µm Film) capillary column connected to a *Hewlett Packard* 59822B ionization gauge controller and a mass selective detector called *Hewlett Packard* 5917A.

Optical rotation: The optical rotation values were measured on a *Jasco* P-1020-polarimeter at the sodium-D-line (λ = 589 nm).

Circular dichroism (CD): The CD spectra were measured at RT on a *Jasco* J-715 spectropolarimeter with quartz crystal cells. The CD spectra were measured 3 times in the interval from 200 nm to 400 nm using the software *Jasco*-Borwin Version 1.50 and processed with the *Jasco* spectra manager software. The differential absorptions coefficient $\Delta\varepsilon$ [cm^2/mol] at different wavelengths λ [nm] was determined in the given solvent. For baseline correction a blank sample of eluent was measured.

1.2 Other Apparatures

Grounding of plant material: Air-dried plant material was ground using a *Retsch*-SM1 impact mill with a wire netting of 1 mm hole size.

Freeze-drying: For freeze-drying a *Christ*-Alpha 1-4 equipped with a *vacUUbrand* RZ 8 high vacuum pump was used.

Kryomat: For low temperature reactions the desired temperature was achieved using a *Kryomat*-400.

1.3 Chromatographical Methods

Thin Layer Chromatography (TLC): All reactions were followed by TLC controls using *Merck* aluminium foil silica gel 60 F_{254} plates. TLC control of substances containing nitrogen was undertaken in an NH_3 atmosphere. To detect substances on the TLC plates, fluorescent light at either 254 nm or 365 nm, development in iodine chamber, and staining with 5% sulphuric acid in methanol, Ekkards reagent, or Draggendorff reagent was used.

Preparative thin layer chromatography (PTLC): 20x20-cm-silica gel 60 F_{254} plates from *Merck* with a concentration zone and a layer thickness of 1 or 2 mm were used.

Column chromatography: The silica gel used was from *Merck* (0.063-0.2 mm), for use with compounds containing nitrogen the silica gel was deactivated by addition of 7.5% (by mass) NH_3. For gelchromatography Sephadex LH-20 was used.

High Pressure Liquid Chromatography (HPLC): Analytical HPLC was carried out using equipment from *Jasco*; pump PU-1580, degassing unit DG-1580, auto sampler AS-2055 Plus, mixer LG-1580, column oven CO-1560, diodearray detector MD-2010 Plus, furthermore a fluorescence detector from *Shimadzu* and a evaporative light scattering detector (ELSD) Sedex 75 from *Sedere* was online coupled. Processing of the measurements was done using the Borwin software from *Jasco*. Unless otherwise noted the HPLC-UV, HPLC-MS, HPLC-CD experiments were carried out using a Symmetry-C_{18} column (*Waters*; 4.6 x 250 mm, 5 µm) with mobile phases consisting of H_2O + 0.05% TFA (A), MeCN + 0.05% TFA (B); flow: 1 mL/min, 0.8 mL/min respectively; binary gradient: 0 min 5% B, 30 min 70% B, 35 min 100% B, 40 min 100% B, 41 min 5% B, 46 min 5% B. For the HPLC-NMR experiments a Symmetry-C_{18} column (*Waters*; 4.6 x 250 mm, 5 µm) was likewise used with the mobile

phases: D_2O + 0.05% TFA (A), MeCN + 0.05% TFA (B). Preparative HPLC was carried out using in online connected a *Waters*-600E pump, a *Rheodyne*-7125i injector, and a *Waters*-996 diodearray detector. For processing of the measurements and controlling the Millenium Software Version 2.15 from *Waters* was used. The chromatographical separations were carried out on a SymmetryPrep-C_{18} column (*Waters*; 19 x 300 mm, 7 µm) with the gradient: H_2O + 0.05% TFA (A), MeCN + 0.05% TFA (B); flow: 11 mL/min; 0 min 20% B, 20 min 55% B, 25 min 100% B, 30 min 100% B, 31 min 20% B, 35 min 20% B. MeCN fractions from the preparative HPLC were evaporated *in vacuo*. For separation of the TFA in the remaining aqueous solution adsorbens was added and the solution was subsequently eluted on a LiChrolut® RP-18E (*Merck*, with 500 mg RP-18 material). After washing with water the compounds bound to the adsorbens were eluted by the use of methanol.

HPLC-CD: For HPLC-CD coupling experiments, the J-715 CD spectrometer was equipped with a PU-1580 pump from *Jasco*, a LG-980-02S ternary gradient unit, a 3725i *Rheodyne* injector valve, an ERC-7215 UV detector hyphenated to a J-715 spectropolarimeter with a 5 mm standard flow cell, and the Borwin chromatographic software from *Jasco*. The CD measurements (190-400 nm), were carried out in *stop-flow* mode, using a Rheodyne 7010 injection valve, connected to a Besta motor-driven valve "H" (*Besta*, Wilhelmshafen, Germany). UV chromatograms were monitored at 254 nm. The values are given in milli-degree (Φ).

Fast centrifugal partition chromatography (FCPC): For liquid-liquid chromatography a FCPC apparatus from *Kromaton* was used, equipped with a 200 or 1000 mL rotor, and connected online to a P-400 pump from *Latek*, a Pro Star 320 UV detector from *Varian* with a SuperPrep Dual flow cell (4 mm and 0.15 mm). The samples were injected using 3725i-injectior valve (*Rheodyne*) with a 20 or 100 mL sample loop. The outlet of the UV detector was connected to a fraction collector FC-1 (*Dynamax*). Unless otherwise noted the method used was: UV detection 254 nm; flow 15 mL min^{-1}; 900 rpm, descending mode; stationary phase, *n*-hexane–EtOAc (8:2), mobile phase, MeOH–H_2O (8:2), retention rate 75%.

2 Phytochemical Investigation of Leaves from *Ancistrocladus tanzaniensis*

2.1 Extraction and Isolation

Leaves of *A. tanzaniensis* were collected in the Uzungwa Mountains in Tanzania, in 2000 by H. Ndangalasi and F. Mbago. A voucher specimen has been deposited at the Bringmann Herbarium with the code: no. 42. The air-dried material (200 g) was ground and sequentially extracted with petroleum ether, CH_2Cl_2, and MeOH. The CH_2Cl_2 phase was concentrated in vacuo to give 9.4 g of crude extract, 3 g of which were redissolved in MeOH, filtrated using a 0.2 µm PTFE syringe filter (*Phenomenex*), and subsequently injected onto the preparative HPLC in 750 µL injection doses. The chromatographical isolation using the standard gradient and the Symmetry-C_{18} column (Chapter Ex. 1.3) afforded **18** (40.5 mg, t_R = 18.8 min), **16** (12.1 mg, t_R = 19.8 min), **13** (6.5 mg, t_R = 20.7 min), **14** (5.5 mg, t_R = 21.0 min), **15** (3.2 mg, t_R = 22.1 min), **17** (4.5 mg, t_R = 19.8 min).

2.2 Ancistrotanzanine B (13)

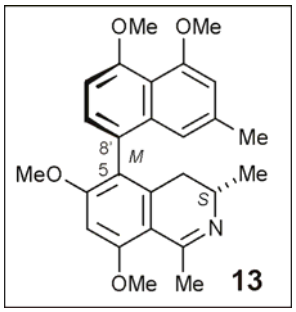

Yellow amorphous powder (6.5 mg).

$[\alpha]_D^{20}$ = +44.0 (c = 0.01, MeOH).

UV/Vis (MeOH): λ_{max} (log ε) = 230 (1.89), 305 (1.42) nm.

CD (CH_3CN): λ_{max} ($\Delta\varepsilon$) = 215 (–17.1), 230 (+9.5), 245 (-8.0), 259 (+3.2), 320 (+3.0) nm.

Table 16. NMR data of ancistrotanzanine B (**13**) in $CDCl_3$.

Position	^{13}C [ppm]	^{1}H [ppm]	HMBC	NOESY	COSY (J_{HH} [Hz])
1	173.9				
3	47.6	3.79 *m*	4, 5, 9, 10, 3-CH_3	4_{eq}, 3-CH_3	4_{ax}, 4_{eq}, 3-CH_3
4_{ax}	31.5	2.21 *dd*	3, 5, 9, 10, 3-CH_3	4_{eq}, 3-CH_3, 1'	4_{eq} (17.1), 3 (8.4)
4_{eq}	31.5	2.60 *dd*	3, 9, 10, 3- CH_3	4_{ax}, 3	4_{eq} (17.1), 3 (5.7)
5	122.7				
6	165.9				
7	94.0	6.54 *s*	5, 6, 8, 9	8-OCH_3, 6-OCH_3	
8	163.5				
9	108.4				
10	140.2				
1'	123.4	6.51 *s*	2', 3', 8', 9', 10', 2'-CH_3	2'-CH_3, 3-CH_3, 4_{ax}	3', 2'-CH_3
2'	137.1				
3'	108.9	6.70 *s*	1', 9', 10'	2'-CH_3, 4'-OCH_3	1', 2'-CH_3
4'	157.7				
5'	157.5				
6'	105.0	6.84 *d*	8'	7', 5'-OCH_3	7' (7.9)
7'	128.8	7.06 *d*	5'	6'	6' (7.9)
8'	116.1				
9'	135.8				
10'	123.3				
1-CH_3	24.5	2.86 *s*	1, 9	8-OCH_3	
3-CH_3	17.2	1.23 *d*	3, 4	3, 4_{ax}, 1', 2'-CH_3	3 (8.8)
6-OCH_3	56.3	3.80 *s*	6	H-7	
8-OCH_3	56.2	4.06 *s*	8	H-7, 1-CH_3	
2'-CH_3	22.1	2.33 *s*	1', 2', 3'	1', 3', CH_3-3	1', 3'
4'-OCH_3	56.4	3.98 *s*	4'	3'	
5'-OCH_3	56.6	4.00 *s*	5'	6'	

IR (NaCl): $\tilde{\nu}$ = 2962 (m), 2921 (w), 2855 (br), 1583 (s), 1261 (m), 1116 (s), 801 (m) cm^{-1}.

MS (EI = 70 eV): m/z (%) = 419 (100) $[M]^+$, 404 (50) $[M\text{-}CH_3]^+$, 209.5 (7) $[M]^{2+}$.

HRMS (ESI): calcd. for $C_{26}H_{29}NO_4$ $[M]^+$: 419.2097; found 419.2099.

2.3 6-*O*-Methylancistrocladinine (14)

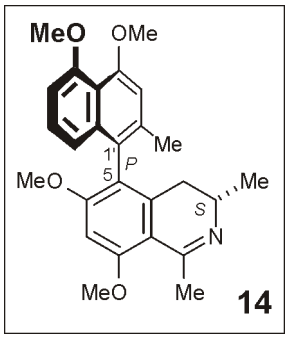

Colorless amorphous powder (5.5 mg).

$[\alpha]_D^{20} = -31.0$ ($c = 0.04$, MeOH).

UV/Vis (MeOH): λ_{max} (log ε) = 231 (0.22), 303 (0.04) nm.

CD (CH_3CN): λ_{max} ($\Delta\varepsilon$) = 211 (+17.1), 231 (–10.6), 254 (–1.2), 296 (–1.9) nm.

Table 17. NMR data of 6-*O*-methylancistrocladinine (**14**) in $CDCl_3$.

Position	^{13}C [ppm]	^{1}H [ppm]	HMBC	NOESY	COSY (J_{HH} [Hz])
1	174.4				
3	48.0	3.75 *m*	4, 5, 9, 10, 3-CH_3	4_{eq}, 3-CH_3	4_{ax}, 4_{eq}, 3-CH_3
4_{ax}	31.4	2.24 *dd*	3, 5, 9, 10, 3-CH_3	4_{eq}, 3-CH_3, 2'-CH_3	3 (9.9), 4_{eq} (17.4)
4_{eq}		2.42 *dd*	3, 9, 10, 3- CH_3	4_{ax}, 3, 8'	3 (5.4), 4_{ax} (16.8)
5	121.6				
6	166.6				
7	94.1	6.56 s	5, 6, 8, 9	8-OCH_3, 6-OCH_3	
8	164.3				
9	108.7				
10	140.6				
1'	122.0				
2'	135.9				
3'	108.3	6.79 *s*	1', 9', 10'	2'-CH_3, 4'-OCH_3	
4'	157.3				
5'	158.0				
6'	106.0	6.66 *d*	8'	7', 5'-OCH_3	7' (8.4)
7'	127.5	7.23 *dd*	5', 9'	6', 8'	6' (7.2), 8' (8.3)
8'	116.9	6.82 *d*	7', 6', 1'	7', 4_{eq}	7' (7.8)
9'	136.0				
10'	116.5				
1-CH_3	24.6	3.07 *s*	1, 9	8-OCH_3	
3-CH_3	17.5	1.25 *d*	3, 4	3, 4_{ax}	3 (6.4)
6-OCH_3	56.4	3.80 *s*	6	H-7	
8-OCH_3	56.2	4.06 *s*	8	H-7, 1-CH_3	
2'-CH_3	20.4	2.06 *s*	1', 2', 3'	3', 4_{ax}	
4'-OCH_3	56.6	3.99 *s*	4'	3'	
5'-OCH_3	56.4	4.02 *s*	5'	6'	

IR (NaCl): $\tilde{\nu}$ = 2921 (m), 2855 (m), 1583 (m), 1261 (m), 1116 (m) cm^{-1}.

MS (EI = 70 eV): *m/z* (%) = 419 (100) $[M]^+$, 404 (48) $[M\text{-}CH_3]^+$, 388 (12) $[M\text{-}OCH_3]^+$, 209.5 (6) $[M]^{2+}$.

HRMS (ESI): calcd. for $C_{26}H_{29}NO_4$ $[M]^+$: 419.2097; found 419.2095.

2.4 Ancistrotectoriline (15)

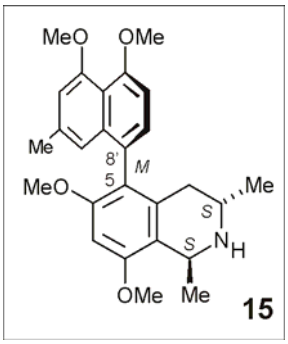

Colorless amorphous powder (3.2 mg).

$[\alpha]_D^{20}$ = +5.67 (c = 0.1, MeOH).

Lit.: +1.34 (c = 0.75, $CHCl_3$).[114]

UV/Vis (MeOH): λ_{max} (log ε) = 231 (1.86), 305 (1.43) nm.

CD (CH_3CN): λ_{max} ($\Delta\varepsilon$) = 202 (–12.6), 209 (+0.6), 240 (–17.9) nm.

^{1}H NMR (400 MHz, MeOD): δ = 1.08 (d, J = 6.1 Hz, 3 H, 3-CH_3), 1.56 (d, J = 6.5 Hz, 3 H, 1-CH_3), 2.22 (dd, J = 11.9, 17.8 Hz, 1 H, 4-H_{ax}), 2.32 (s, 3 H, 2'-CH_3), 2.40 (dd, J = 17.8, 4.0 Hz, 1 H, 4-H_{eq}), 3.35 (m, 1 H, 3-H), 3.61 (s, 3 H, 6-OCH_3), 3.90 (s, 3 H, 8-OCH_3), 3.95 (s, 3 H, 4'-OCH_3), 3.98 (s, 3 H, 5'-OCH_3), 6.48 (s, 1 H, 7-H), 6.66 (s, 1 H, 3'-H), 6.66 (s, 1 H, 1'-H), 6.82 (d, J = 7.6 Hz, 1 H, 6'-H), 7.10 (d, J = 7.6 Hz, 1 H, 7'-H).

^{13}C NMR (100 MHz, MeOD): δ = 18.4 (1-Me), 18.5 (3-Me), 21.7 (2'-Me), 31.6 (C-4), 44.0 (C-3), 47.4 (C-1), 55.4 (8-OMe), 56.2 (6-OMe), 56.4 (4'-OMe), 56.6 (5'-OMe), 94.1 (C-5), 105.0 (C-8'), 109.0 (C-3'), 116.0 (C-10), 117.5 (C-1'), 118.2 (C-9), 121.3 (C-7), 126.3 (C-9'), 126.5 (C-8'), 128.0 (C-7'), 136.3 (C-2'), 152.0 (C-4'), 156.1 (C-8), 156.8 (C-5'), 157.3 (C-6).

IR (NaCl): $\tilde{\nu}$ = 2962 (m), 2923 (m), 2851 (s), 1260 (m), 1207 (m), 1115 (m), 800 (w) cm^{-1}.

MS (EI = 70 eV): m/z (%) = 421 (100) $[M]^+$, 406 (45) $[M\text{-}CH_3]^+$, 390 (12) $[M\text{-}OCH_3]^+$, 346 (15), 210.5 $[M]^{2+}$ (6).

HRMS (ESI): calcd. for $C_{26}H_{31}NO_4$ $[M]^+$: 421.2253; found 421.2240.

The spectroscopic data are in good agreement with those previously published.[114]

Additionally a HPLC coelution was carried out with an authentic sample.[242]

2.5 Ancistrotanzanine C (16)

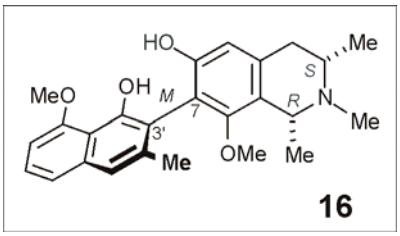

Colorless amorphous powder (12.1 mg).

$[\alpha]_D^{20}$ = –75.5 (c = 0.01, $CHCl_3$).

UV/Vis (MeOH): λ_{max} (log ε) = 231 (0.74), 307 (0.07) nm.

CD (CH_3CN): λ_{max} ($\Delta\varepsilon$) = 220 (+26.8), 238 (–17.6), 265 (–17.2), 322 (–8.1), 337 (–10.9) nm.

^{1}H NMR (400 MHz, $CDCl_3$): δ = 1.26 (d, J = 6.2 Hz, 3H, CH_3-3), 1.45 (d, J = 6.5 Hz, 3H, CH_3-1), 2.18 (s, 3H, CH_3-2'), 2.49 (s, 3H, CH_3-N), 2.56 (m_c, 1H, H-3), 2.63 (dd, J = 15.5, 10.2 Hz, 1H, H_{ax}-4), 2.73 (dd, J = 15.5, 3.3 Hz, 1H, H_{eq}-4), 3.33 (s, 3H, OCH_3-8), 3.84 (q, J = 6.5 Hz, 1H, H-1), 4.03 (s, 3H, OCH_3-5'), 6.58 (s, 1H, H-5), 6.76 (d, J = 8.0, 1.4 Hz, 1H, H-6'), 7.29 (s, 1H, H-1'), 7.34 (dd, J = 7.3, 8.3 Hz, 1H, H-7'), 7.38 (d, J = 8.3, 1.4 Hz, 1H, H-8').

^{13}C NMR ($CDCl_3$): δ = 20.3 (2'-Me), 21.4 (3-Me), 23.4 (1-Me), 37.9 (C-4), 41.8 (N-Me), 55.5 (C-3), 56.1 (5'-OMe), 57.0 (C-1), 60.2 (8-OMe), 103.7 (C-6'), 109.7 (C-5), 113.4 (C-10'), 114.7 (C-7), 115.0 (C-3'), 119.8 (C-1'), 121.2 (C-8'), 124.2 (C-9), 126.5 (C-7'), 136.6 (C-9'), 138.6 (C-2'), 137.4 (C-10), 156.1 (C-5'), 152.0 (C-4'), 152.1 (C-8), 155.7 (C-6).

IR (NaCl): $\tilde{\nu}$ = 3381 (m), 2965 (m), 1607 (m), 1579 (s), 1362 (m), 1204 (s), 1091 (m) cm^{-1}.

MS (EI = 70 eV): m/z (%) = 407 (100) $[M]^+$, 392 (50) $[M\text{-}CH_3]^+$, 377 (17) $[M\text{-}(CH_3)_2]^+$, 376 (11) $[M\text{-}OCH_3]^+$, 203.5 (7) $[M]^{2+}$.

HRMS (ESI): calcd. for $C_{25}H_{29}NO_4$ $[M]^+$: 407.2097; found 407.2094.

2.6 Ancistrotanzanine A (17)

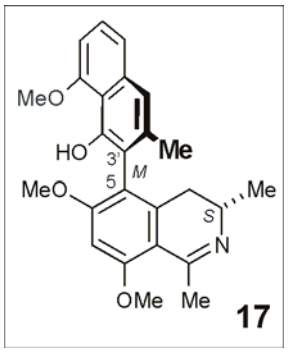

Yellow amorphous powder (4.5 mg).

$[\alpha]_D^{20}$ = +72.3 (c = 0.01, MeOH).

Lit.: +69.5 (c = 0.1, EtOH).[117]

UV/Vis (MeOH): λ_{max} (log ε) = 231 (0.81), 307 (0.21) nm.

CD (CH_3CN): λ_{max} ($\Delta\varepsilon$) = 216 (–29.7), 230 (+12.9), 243 (–16.6), 338 (+14.4) nm.

^{1}H NMR (400 MHz, $CDCl_3$): δ = 1.39 (d, J = 6.8 Hz, 3 H, 3-CH_3), 2.06 (s, 3 H, 2'-CH_3), 2.55 (m, 2 H, 4-H_{ax+eq}), 2.88 (s, 3 H, 1-CH_3), 3.86 (m, 1 H, 3-H), 3.87 (s, 3 H, 6-OCH_3), 4.05 (s, 3 H, 8-OCH_3), 4.05 (s, 3 H, 5'-OCH_3), 6.53 (s, 1 H, 7-H), 6.79 (dd, J = 7.6, 1.1 Hz, 1 H, 6'-H), 7.27 (s, 1H, 1'-H), 7.34 (dd, J = 7.3, 8.3 Hz, 1 H, 7'-H), 7.40 (dd, J = 8.3, 1.0 Hz, 1 H, 8'-H), 9.51 (s, 1 H, 4'-OH).

^{13}C NMR (100 MHz, $CDCl_3$): δ = 18.1 (3-Me), 21.3 (2'-Me), 25.2 (1-Me), 29.2 (C-4), 47.7 (C-3), 55.1 (8-OMe), 55.1 (6-OMe), 55.6 (5'-OMe), 94.3 (C-7), 105.3 (C-6'), 108.4 (C-9), 113.4 (C-10'), 117.1 (C-3'), 119.2 (C-5), 119.2 (C-1'), 121.4 (C-8'), 126.8 (C-7'), 137.4 (C-9'), 137.7 (C-2'), 141.2 (C-10), 155.7 (C-4'), 157.1 (C-5'), 165.1 (C-8), 167.0 (C-6), 175.6 (C-1).

IR (NaCl): $\tilde{\nu}$ = 3369 (s), 2957 (w), 2926 (s), 1739 (s), 1679 (s), 1201 (s), 1088 (m), 653 (m) cm^{-1}.

MS (EI = 70 eV): m/z (%) = 405 (100) $[M]^+$, 390 (31), 374 (8), 202.6 (10).

MS (ESI-pos): m/z (%) = 406 (100) $[M+H]^+$.

The spectroscopic data are in good agreement with those previously published.[117]

2.7 *O,N*-Dimethylancistrocladine (18)

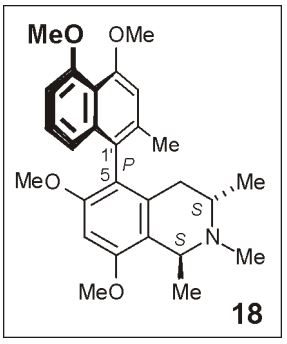

Pale-yellow amorphous powder (40.5 mg).

$[\alpha]_D^{20} = -25.2$ ($c = 0.05$, $CHCl_3$).

Lit.: –17.3 ($c = 0.03$, MeOH).[117]

Lit.: –21.0 ($c = 2.55$, $CHCl_3$).[243]

UV/Vis (MeOH): λ_{max} (log ε) = 235 (0.75), 303 (0.32) nm.

CD (MeOH): λ_{max} ($\Delta\varepsilon$) = 199 (+19.6), 226 (–27.6), 240 (+26.2), 285 (–1.5) nm.

^{1}H NMR (400 MHz, $CDCl_3$): δ = 1.38 (d, J = 6.5 Hz, 3H, CH_3-3), 1.79 (d, J = 6.8 Hz, 3H, CH_3-1), 2.18 (s, 3H, CH_3-2'), 2.22 (dd, J = 16.9, 3.8 Hz, 1H, H_{eq}-4), 2.61 (dd, J = 16.8, 9.2 Hz, 1H, H_{ax}-4), 2.96 (d, J = 4.5 Hz, 3H, CH_3-N), 3.02 (m_c, 1H, H-3), 3.67 (s, 3H, OCH_3-6), 3.96 (s, 3H, OCH_3-8), 3.98 (s, 3H, OCH_3-5'), 4.01 (s, 3H, OCH_3-4'), 4.62 (q, J = 6.5 Hz, 1H, H-1), 6.58 (s, 1H, H-7), 6.62 (dd, J = 8.4, 1.0 Hz, 1H, H-8'), 6.79 (dd, J = 8.2, 0.9 Hz, 1H, H-6'), 6.81 (s, 1H, H-3'), 7.19 (dd, J = 8.4, 7.9 Hz, 1H, H-7').

^{13}C NMR (100 MHz, $CDCl_3$): δ = 18.7 (3-Me), 19.7 (1-Me), 20.8 (2'-Me), 30.8 (C-4), 43.2 (N-Me), 55.9 (8-OMe), 56.4 (6-OMe), 56.8 (4'-OMe), 56.9 (5'-OMe), 59.9 (C-3), 60.4 (C-1), 94.8 (C-7), 105.9 (C-6'), 109.3 (C-3'), 113.2 (C-9), 117.1 (C-10'), 117.2 (C-8'), 120.3 (C-5), 123.4 (C-1'), 127.0 (C-7'), 133.2 (C-10), 136.3 (C-9'), 136.4 (C-2'), 156.6 (C-4'), 156.7 (C-8), 158.1 (C-5'), 158.5 (C-6)

IR (NaCl): $\tilde{\nu}$ = 2925 (m), 2852 (m), 2359 (m), 1674 (s), 1584 (s), 1261 (m), 1202 (s), 1129 (s) cm^{-1}.

MS (EI = 70 eV): *m/z* (%) = 435 (8) $[M]^+$, 420 (100), 390 (8).

MS (ESI-pos): *m/z* (%) = 436 (100) $[M+H]^+$.

HRMS (ESI): calcd. for $C_{27}H_{33}NO_4$ $[M]^+$: 435.2409; found 435.2407.

The spectroscopic data are in good agreement with those previously published.[117]

3 Isolation of Naphthylisoquinoline Alkaloids from the Congolese *Ancistrocladus* Species Collected in the Habitat Yeteto (Ancistrocladaceae)

3.1 Isolation of Naphthylisoquinoline Alkaloids from the Leaves

Air dried leaves from the Congolese *Ancistrocladus* speceis collected near Ikela (200 g) were ground and extracted exhaustively with CH_2Cl_2/MeOH (6:4). The solvent was removed under reduced pressure to give a combined organic extract (10 g). The extract was partioned between *n*-hexane and H_2O/MeOH (1:9). Evaporation of the aqueous phase to dryness afforded a residue (4 g), which was subsequently submitted to FCPC using a two-phase solvent system consisting of $CHCl_3$/EtOAc/MeOH/H_2O (5:3:5:3). The lower phase served as the stationary phase (flow rate 15 mL min^{-1}, rotational speed 900 min^{-1}, descending mode, retention rate 75%). After ca. 140 min, the stationary phase was flushed out in reversed mode by using MeOH, and concentrated under reduced pressure to give 450 mg of a residue. By applying preparative HPLC on a SymmetryPrep C_{18} column (19X300 mm, 5 µm, Waters) with a flow rate of 10.0 mL min^{-1} and a solvent system consisting of (A) H_2O (10% MeOH, 0.05% trifluoroacetic acid) and (B) MeOH (10% H_2O, 0.05% trifluoroacetic acid) to this residue, 10 mg of compound **25** (retention time 12.9 min), and 12 mg of compound **22** were isolated. The latter one was achieved in a 46:54 atropisomeric mixture with retention times of 17.2 min and 18.4 min for (*P*)-**22** and (*M*)-**22**, respectively. For this separation a linear gradient from 50% B at 0 min to 65% B at 20 min was used.

The resolution of the atropisomers (*P*)-**22** and (*M*)-**22** by HPLC-CD were performed using a Symmetry C18 column (4.6X250 mm, 5 µm, Waters) and a reduced flow rate of 0.9 mL min^{-1}. The gradient and the solvent system were exactly the same as for the preparative separation.

3.1.1 Ancistrocladinium B (22)

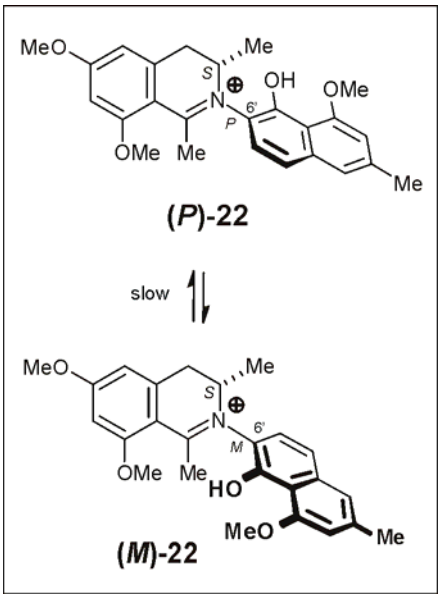

Pale yellow crystals (0.5 mg)

M.p. ≥ 230 °C (n-heptane)

$[\alpha]_D^{20} = +28$ ($c = 0.02$, MeOH)

UV/Vis (MeOH): λ_{max} (log ε) = 227 (0.94), 346 (0.34) nm.

CD (MeOH): λ_{max} ($\Delta\varepsilon$) = 211 (+7.8), 228 (+13.2), 240 (–6.1) nm.

IR (NaCl): $\tilde{\nu}$ = 3330, 2925, 1690, 1612, 1580, 1555, 1460, 1380, 1310, 1280, 1200, 1170, 1125, 1090, 960, 841, 800 cm^{-1}.

MS (EI = 70 eV): *m/z* (%) = 406 (38) [M^+], 390 (100) [$M\text{-}CH_4^+$].

HRMS (ESI): calcd. for $C_{25}H_{28}NO_4^+$ $[M]^+$: 406.20153; found 406.20183.

3.1.1.1 *P*-Ancistrocladinium B [(*P*)-22]

CD (MeOH-H_2O, recorded online, by LC-CD): λ_{max} ($\Delta\varepsilon$) = 214 (+6.4), 230 (–3.5), 238 (+2.3), 311 (–4.4) nm.

^{1}H NMR (600 MHz, DMSO-d_6): δ = 1.11 (d, ^3J = 6.9 Hz, 3 H, CH_3-3), 2.47 (s, 3 H, CH_3-2'), 2.56 (s, 3 H, CH_3-1), 3.04 (dd, ^2J = 16.9 Hz, ^3J = 1.9 Hz, 1 H, H_{eq}-4), 3.71 (dd, ^2J = 16.9 Hz, ^3J = 6.1 Hz, 1 H, H_{ax}-4), 3.97 (s, 3 H, OCH_3-6), 4.00 (s, 3 H, OCH_3-8), 4.04 (s, 3 H, OCH_3-4'), 4.49 (ddq, 1 H, H-3), 6.76 (s, 1 H, H-7), 6.81 (s, 1 H, H-5), 6.99 (s, 1 H, H-3'), 7.36 (s, 1 H, H-1'), 7.51 (d, 1 H, ^3J = 8.9 Hz, H-8'), 7.62 (d, 1 H, ^3J = 8.9 Hz, H-7'), 10.16 (s, 1 H, OH-5').

^{13}C NMR (150 MHz, DMSO-d_6): δ = 14.00 (3-Me), 21.56 (2'-Me), 22.92 (1-Me), 33.29 (C-4), 56.28 (4-OMe), 56.38 (6-OMe), 56.65 (8-OMe), 59.00 (C-3), 97.89 (C-7), 107.67 (C-5), 108.18 (C-3'), 109.16 (C-9), 112.28 (C-10'), 119.93 (C-8'), 119.96 (C-1'), 121.25 (C-6'), 124.51 (C-7'), 136.50 (C-9'), 138.83 (C-2'), 140.61 (C-10), 147.65 (C-5'), 156.26 (C-4'), 163.63 (C-8), 167.81 (C-6), 174.54 (C-1).

3.1.1.2 *M*-Ancistrocladinium B [(*M*)-22].

CD (MeOH-H_2O, recorded online, by LC-CD): λ_{max} ($\Delta\varepsilon$) = 215 (–7.7), 228 (+5.2), 239 (–6.4), 322 (+3.6) nm.

^{1}H NMR (600 MHz, DMSO-d_6): δ = 1.19 (d, ^3J = 6.9 Hz, 3 H, CH_3-3), 2.47 (s, 3 H, CH_3-2'), 2.50 (s, 3 H, CH_3-1), 3.12 (dd, ^2J = 16.9 Hz, ^3J = 1.9 Hz, 1 H, H_{eq}-4), 3.49 (dd, ^2J = 16.9 Hz, ^3J = 6.1 Hz, 1 H, H_{ax}-4), 3.98 (s, 3 H, OCH_3-6), 4.01 (s, 3 H, OCH_3-8), 4.05 (s, 3 H, OCH_3-4'), 4.36 (ddq, 1 H, H-3), 6.75 (s, 1 H, H-7), 6.81 (s, 1 H, H-5), 6.99 (s, 1 H, H-3'), 7.36 (s, 1 H, H-1'), 7.44 (d, 1 H, ^3J = 8.9 Hz, H-8'), 7.54 (d, 1 H, ^3J = 8.9 Hz, H-7'), 10.06 (s, 1 H, OH-5').

^{13}C NMR (150 MHz, DMSO-d_6): δ = 14.58 (3-Me), 21.56 (2'-Me), 23.58 (1-Me), 33.29 (C-4), 56.35 (4'-OMe), 56.43 (6-OMe), 56.70 (8-OMe), 57.77 (C-3), 97.96 (C-7), 107.83 (C-5), 107.99 (C-3'), 109.35 (C-9), 113.06 (C-10'), 118.94 (C-8'), 119.96 (C-1'), 121.76 (C-6'), 124.62 (C-7'), 136.58 (C-9'), 138.57 (C-2'), 140.51 (C-10), 147.65 (C-5'), 156.26 (C-4'), 164.00 (C-8), 167.99 (C-6), 174.66 (C-1).

3.1.2 Ancistrocladinium A (25)

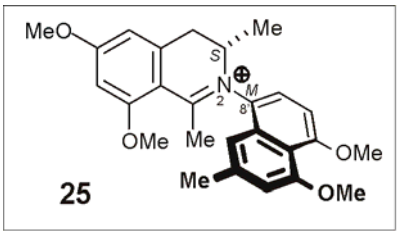

Pale-yellow amorphous powder (1.5 mg).

$[\alpha]_D^{20}$ = –5.1 (c = 0.02, MeOH)

Lit.: –6 (c = 0.05, MeOH).[132]

UV/Vis (MeOH): λ_{max} (log ε) = 214 (2.73), 325(2.69), 335 (1.65) nm.

CD (MeOH): λ_{max} ($\Delta\varepsilon$) = 230 (+6.96), 243 (–1.74) nm.

^{1}H NMR (400 MHz, CD_3OD): δ = 1.39 (d, J = 7.0 Hz, 3H, CH_3-3), 2.59 (s, 3H, CH_3-1), 2.50 (s, 3H, CH_3-2'), 3.24 (dd, J = 17.0, 2.0 Hz, 1H, H_{eq}-4), 3.96 (dd, J = 17.0, 6.0 Hz, 1H, H_{ax}-4), 4.39 (m_c, 1H, H-3), 3.98 (s, 3H, OCH_3-4'), 4.02 (s, 3H, OCH_3-5'), 4.07 (s, 3H, OCH_3-6), 4.11 (s, 3H, OCH_3-8), 6.83 (s, 1H, H-7), 6.84 (s, 1H, H-5), 7.02 (d, J = 8.0 Hz, 1H, H-7'), 7.03 (s, 1H, H-3'), 7.29 (s, 1H, H-1'), 7.70 (d, J = 8.0 Hz, 1H, H-8').

IR (NaCl): $\tilde{\nu}$ = 2955 (m), 2925 (m), 2848 (m), 1682 (s), 1585 (m), 1458 (m), 1438 (s) 1417 (s), 1204 (s), 1130 (s) cm^{-1}.

MS (EI = 70 eV): *m*/*z* (%) = 420 (10) $[M]^+$, 419 (29) $[M-H]^+$, 404 (100) $[M-CH_4]^+$.

HRMS (ESI): calcd. for $C_{26}H_{30}NO_4^+$ $[M]^+$: 420.2175; found 420.2175.

The spectroscopic data are in good agreement with those previously published.[132]

3.2 Isolation of Naphthylisoquinoline Alkaloids from the Roots

560 g of lyophilized root material of a Congolese *Ancistrocladus* species (habitat: Yeteto) were powdered and sequentially extracted with *n*-hexane, CH_2Cl_2, and MeOH-H_2O (9:1). The CH_2Cl_2 and MeOH-H_2O were concentrated *in vacuo* to give 20 g and 15 g of crude extract, respectively. The extract was further resolved by FCPC and sequenced in fractions eluting between 550-650, 650-850, 850-1100, 1150-1500 mL, the solvent was evaporated *in vacuo* and the remaining residues were further purified by preparative HPLC using the condition described in Chapter Ex. 1.3 yielding; 5.5 mg of compound **27** (t_R = 17.1 min), and 6.7 mg of compound **29** (t_R = 20.1 min); 2.5 mg of compound **26** (t_R = 17.8 min), and 3.3 mg of compound **31** (t_R = 19.2 min); 7.7 mg of compound **30** (t_R = 18.5 min), and 4.8 mg of compound **32** (t_R = 20.1 min); 2.7 mg of compound **35** (t_R = 17.3 min), and 3.3 mg of compound **34** (t_R = 17.7 min), respectively. The resolution by FCPC of the CH_2Cl_2 extract was collected in fractions eluting between 250-280, 600-850, 900-1050, 1550-1750 mL, the solvent was evaporated *in vacuo* and the remaining residues were further purified by preparative HPLC yielding; 11.2 mg of compound **20** (t_R = 20.4 min); 8.6 mg of compound **21** (t_R = 19.8 min), 7.1 mg of compound **28** (t_R = 19.0 min), respectively.

3.2.1 5'-*O*-Demethylhamatine (26)

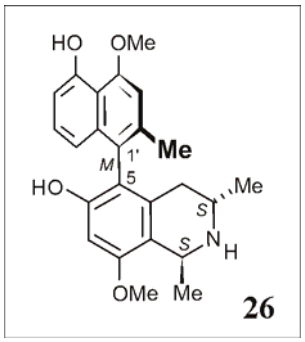

Colorless amorphous solid (2.5 mg).

$[\alpha]_D^{20} = +26$ (c = 0.10, MeOH).

UV/Vis (CH_2Cl_2): λ_{max} (log ε) = 235 (1.02), 309 (0.42), 337 (0.34) nm.

CD (MeOH): λ_{max} ($\Delta\varepsilon$) = 211 (+7.8), 228 (+13.2), 240 (–6.1) nm.

^{1}H NMR (400 MHz, MeOD): δ = 1.19 (d, J = 6.3 Hz, 3H, CH_3-3), 1.63 (d, J = 6.7 Hz, 3H, CH_3-1), 2.09 (dd, J = 17.9, 4.9 Hz, 1H, H_{ax}-4), 2.14 (s, 3H, CH_3-2'), 2.39 (dd, J = 18.0, 11.7 Hz, 1H, H_{eq}-4), 3.68 (m_c, 1H, H-3), 3.93 (s, 3H, OCH_3-8), 4.13 (s, 3H, OCH_3-4'), 4.77 (q, 1H, 6.8 Hz, H-1), 6.61 (s, 1H, H-7), 6.64 (dd, J = 8.3, 1.0 Hz, 1H, H-8'), 6.72 (dd, J = 7.6, 1.0 Hz, 1H, H-6'), 6.94 (s, 1H, H-3'), 7.14 (dd, J = 8.3, 7.7 Hz, 1H, H-7').

^{13}C NMR (100 MHz, MeOD): δ = 18.8 (1-Me), 19.3 (3-Me), 20.7 (2'-Me), 33.0 (C-4), 45.2 (C-3), 49.3 (C-1), 56.2 (8-OMe), 56.9 (4'-OMe), 99.0 (C-7), 108.3 (C-3'), 110.6 (C-6'), 114.5 (C-9), 115.4 (C-10'), 117.0 (C-8'), 118.6 (C-5), 126.1 (C-1'), 128.9 (C-7'), 132.9 (C-10), 137.5 (C-9'), 136.9 (C-2'), 156.4 (C-5'), 157.2 (C-6), 157.4 (C-4'), 157.9 (C-8).

IR (NaCl): $\tilde{\nu}$ = 2937 (m), 2848 (w), 1680 (m), 1610 (s), 1447 (m), 1427 (m), 1392 (s), 1363 (s), 1204 (s), 1136 (s), 838 (m), 801 (w) cm^{-1}.

MS (EI = 70 eV): m/z (%) = 393 (9) $[M]^+$, 378 (100) $[M\text{-}CH_3]^+$, 362 (5) $[M\text{-}OCH_3]^+$.

HRMS (ESI): calcd. for $C_{24}H_{27}NO_4$ $[M]^+$: 393.1940; found 393.1929.

3.2.2 5'-*O*-Demethylhamatinine (28)

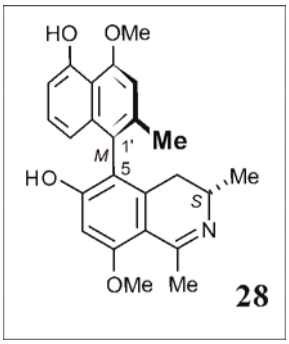

Colorless amorphous solid (7.1 mg).

$[\alpha]_D^{20} = +25$ (c = 0.10, MeOH).

UV/Vis (CH_2Cl_2): λ_{max} (log ε) = 235 (1.05), 311 (0.34), 321 (0.34), 335 (0.30) nm.

CD (MeOH): λ_{max} ($\Delta\varepsilon$) = 213 (–6.1), 230 (+6.9), 245 (–4.7) nm.

^{1}H NMR (400 MHz, MeOD): δ = 1.20 (d, J = 6.3 Hz, 3H, CH_3-3), 2.16 (s, 3H, CH_3-2'), 2.23 (dd, J = 17.0, 10.6 Hz, 1H, H_{ax}-4), 2.51 (dd, J = 16.9, 5.4 Hz, 1H, H_{eq}-4), 2.79 (s, 3H, CH_3-1), 3.77 (m_c, 1H, H-3), 4.05 (s, 3H, OCH_3-8), 4.13 (s, 3H, OCH_3-4'), 6.62 (dd, J = 8.3, 1.0 Hz, 1H, H-8'), 6.70 (s, 1H, H-7), 6.74 (dd, J = 7.6, 1.0 Hz, 1H, H-6'), 6.94 (s, 1H, H-3'), 7.18 (dd, J = 8.3, 7.8 Hz, 1H, H-7').

^{13}C NMR (100 MHz, MeOD): δ = 18.1 (3-Me), 20.6 (2'-Me), 24.9 (1-Me), 32.9 (C-4), 49.1 (C-3), 56.8 (8-OMe), 56.9 (4'-OMe), 99.7 (C-7), 108.1 (C-3'), 109.4 (C-9), 110.9 (C-6'), 115.2 (C-10'), 116.8 (C-8'), 121.4 (C-5), 124.9 (C-1'), 129.2 (C-7'), 137.0 (C-2'), 137.5 (C-9'), 142.6 (C-10), 156.5 (C-5'), 157.7 (C-4'), 166.1 (C-8), 168.5 (C-6), 175.0 (C-1).

IR (NaCl): $\tilde{\nu}$ = 2917 (m), 2851 (w), 1681 (m), 1626 (s), 1609 (s), 1447 (m), 1426 (w), 1358 (s), 1325 (s), 1203 (s), 1133 (s), 842 (m), 801 (m) cm^{-1}.

MS (EI = 70 eV): m/z (%) = 392 (100) $[M+H]^+$, 391 (73) $[M]^+$, 376 (33) $[M-CH_3]^+$, 360 (6) $[M-OCH_3]^+$.

HRMS (ESI): calcd. for $C_{24}H_{25}NO_4$ $[M]^+$: 391.1784; found 391.1779.

3.2.3 6-*O*-Demethylancistroealaine A (30)

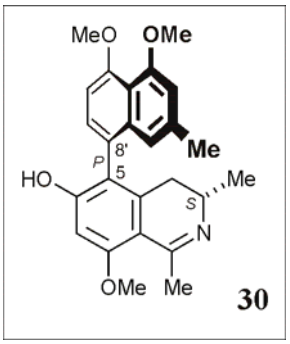

Colorless amorphous solid (7.7 mg).

$[\alpha]_D^{20} = -63.2$ (c = 0.10, MeOH).

UV/Vis (CH_2Cl_2): λ_{max} (log ε) = 232 (1.06), 316 (0.34), 321 (0.35), 335 (0.33) nm.

CD (MeOH): λ_{max} ($\Delta\varepsilon$) = 213 (+9.2), 231 (–7.2), 244 (+5.5) nm.

^{1}H NMR (400 MHz, MeOD): δ = 1.25 (d, J = 6.7 Hz, 3H, CH_3-3), 2.33 (s, 3H, CH_3-2'), 2.41 (dd, J = 16.8, 5.9 Hz, 1H, H_{eq}-4), 2.48 (dd, J = 16.9, 11.2 Hz, 1H, H_{ax}-4), 2.80 (s, 3H, CH_3-1), 3.70 (m_c, 1H, H-3), 3.94 (s, 3H, OCH_3-4'), 3.96 (s, 3H, OCH_3-5'), 4.05 (s, 3H, OCH_3-8), 6.68 (s, 1H, H-7), 6.71 (s, 1H, H-1'), 6.82 (s, 1H, H-3'), 6.94 (d, J = 8.1 Hz, 1H, H-6'), 7.11 (dd, J = 8.0 Hz, 1H, H-7').

^{13}C NMR (100 MHz, MeOD): δ = 18.1 (3-Me), 22.2 (2'-Me), 24.8 (1-Me), 33.6 (C-4), 49.5 (C-3), 56.9 (8-OMe), 56.9 (5'-OMe), 57.1 (4'-OMe), 99.4 (C-7), 106.6 (C-6'), 108.8 (C-9), 110.3 (C-3'), 117.6 (C-10'), 118.1 (C-1'), 122.7 (C-5), 125.0 (C-8'), 130.8 (C-7'), 137.3 (C-9'), 138.5 (C-2'), 142.7 (C-10), 159.0 (C-5'), 159.0 (C-4'), 165.9 (C-8), 167.8 (C-6), 175.8 (C-1).

IR (NaCl): $\tilde{\nu}$ = 2925 (m), 2849 (m), 1675 (m), 1624 (s), 1582 (s), 1454 (w), 1410 (m), 1380 (m), 1353 (s), 1325 (s), 1295 (m), 1201 (m), 1133 (s), 1099 (m), 834 (w), 800 (m) cm^{-1}.

MS (EI = 70 eV): m/z (%) = 405 (100) $[M]^+$, 390 (45) $[M\text{-}CH_3]^+$, 374 (10) $[M\text{-}OCH_3]^+$.

HRMS (ESI): calcd. for $C_{25}H_{27}NO_4$ $[M]^+$: 405.1940; found 405.1939.

3.2.4 6,5'-*O*,*O*-Didemethylancistroealaine A (31)

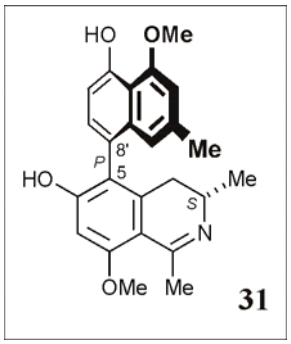

Colorless amorphous solid (7.7 mg).

$[\alpha]_D^{20} = -68.6$ (c = 0.14, MeOH).

UV/Vis (CH_2Cl_2): λ_{max} (log ε) = 235 (1.15), 313 (0.47), 321 (0.48), 335 (0.45) nm.

CD (MeOH): λ_{max} ($\Delta\varepsilon$) = 213 (+8.9), 231 (–4.7), 244 (+3.8) nm.

^{1}H NMR (400 MHz, MeOD): δ = 1.26 (d, J = 6.7 Hz, 3H, CH_3-3), 2.34 (s, 3H, CH_3-2'), 2.41 (dd, J = 16.9, 5.9 Hz, 1H, H_{eq}-4), 2.48 (dd, J = 16.9, 11.2 Hz, 1H, H_{ax}-4), 2.79 (s, 3H, CH_3-1), 3.70 (m_c, 1H, H-3), 4.04 (s, 3H, OCH_3-8), 4.10 (s, 3H, OCH_3-4'), 6.67 (s, 1H, H-7), 6.72 (s, 1H, H-1'), 6.80 (d, J = 7.8 Hz, 1H, H-6'), 6.83 (s, 1H, H-3'), 7.05 (dd, J = 7.8 Hz, 1H, H-7').

^{13}C NMR (100 MHz, MeOD): δ = 18.2 (3-Me), 22.3 (2'-Me), 24.8 (1-Me), 33.7 (C-4), 49.5 (C-3), 56.8 (8-OMe), 57.0 (4'-OMe), 99.4 (C-7), 108.7 (C-9), 110.4 (C-6'), 115.0 (C-10'), 118.8 (C-1'), 122.6 (C-5), 123.1 (C-8'), 131.7 (C-7'), 136.7 (C-9'), 138.2 (C-2'), 142.8 (C-10), 155.4 (C-5'), 158.2 (C-4'), 165.9 (C-8), 168.1 (C-6), 175.7 (C-1).

IR (NaCl): $\tilde{\nu}$ = 2925 (m), 2852 (m), 1681 (m), 1580 (s), 1453 (w), 1400 (m), 1356 (w), 1328 (s), 1299 (m), 1263 (m), 1201 (m), 1131 (s), 835 (w), 800 (m) cm^{-1}.

MS (EI = 70 eV): m/z (%) = 392 (99) $[M+H]^+$, 391 (100) $[M]^+$, 376 (40) $[M-CH_3]^+$, 360 (7) $[M-OCH_3]^+$.

HRMS (ESI): calcd. for $C_{24}H_{25}NO_4$ $[M]^+$: 391.1784; found 391.1780.

3.2.5 5-*epi*-6-*O*-Methylancistrobertsonine A (32)

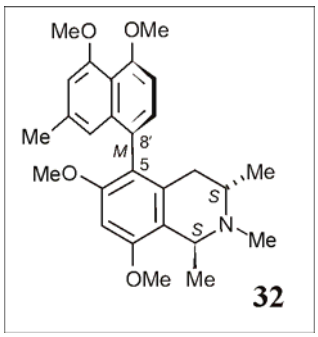

32

Colorless amorphous solid (4.8 mg).

$[\alpha]_D^{20}$ = +1.2 (*c* = 0.09, MeOH).

UV/Vis (CH_2Cl_2): λ_{max} (log ε) = 237 (1.29), 307 (0.40), 321 (0.33), 337 (0.26) nm.

CD (MeOH): λ_{max} ($\Delta\varepsilon$) = 227 (+11.1), 240 (–8.0) nm.

^{1}H NMR (400 MHz, MeOD): δ = 1.07 (d, *J* = 6.8 Hz, 3H, CH_3-3), 1.52 (d, *J* = 6.8 Hz, 3H, CH_3-1), 2.00 (dd, *J* = 17.8, 11.5 Hz, 1H, H_{ax}-4), 2.27 (s, 3H, CH_3-2'), 2.50 (dd, *J* = 18.3, 4.3 Hz, 1H, H_{eq}-4), 2.54 (s, 3H, CH_3-*N*), 3.54 (m_c, 1H, H-3), 3.65 (s, 3H, OCH_3-6), 3.98 (s, 3H, OCH_3-8), 3.93 (s, 3H, OCH_3-4'), 3.95 (s, 3H, OCH_3-5'), 4.49 (q, *J* = 6.8 Hz, 1H, H-1), 6.57 (s, 1H, H-1'), 6.72 (s, 1H, H-7), 6.77 (s, 1H, H-3'), 6.93 (d, *J* = 8.0, 1.0 Hz, 1H, H-6'), 7.09 (d, *J* = 7.9, 1.0 Hz, 1H, H-7').

^{13}C NMR (100 MHz, MeOD): δ = 17.4 (1-Me), 18.2 (3-Me), 22.1 (2'-Me), 31.7 (C-4), 35.9 (*N*-Me), 49.4 (C-3), 56.3 (8-OMe), 56.5 (6-OMe), 57.0 (4'-OMe), 57.2 (5'-OMe), 58.0 (C-1), 95.4 (C-7), 107.0 (C-6'), 110.0 (C-3'), 116.9 (C-9), 117.6 (C-10'), 118.3 (C-1'), 122.3 (C-5), 127.5 (C-8'), 129.8 (C-7'), 131.9 (C-10), 137.7 (C-9'), 137.8 (C-2'), 158.0 (C-5'), 158.2 (C-8), 158.8 (C-4'), 159.4 (C-6).

IR (NaCl): $\tilde{\nu}$ = 2926 (s), 2854 (s), 1693 (s), 1585 (s), 1454 (w), 1387 (w), 1326 (s), 1255(s), 1204 (m), 1138 (w), 1096 (m), 1079 (w), 839 (w), 801(w) cm^{-1}.

MS (EI = 70 eV): *m*/*z* (%) = 435 (2) $[M]^+$, 420 (100) $[M\text{-}CH_3]^+$, 404 (7) $[M\text{-}OCH_3]^+$.

HRMS (ESI): calcd. for $C_{26}H_{30}NO_4$ $[M\text{-}CH_3]^+$: 420.2175; found 420.2171.

3.2.6 Ancistroealaine A (20)

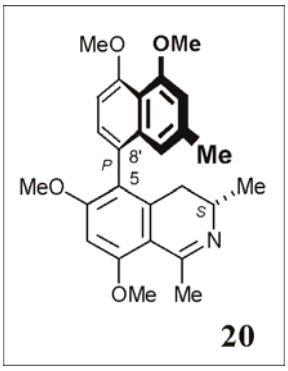

Yellow amorphous powder (11.2 mg).

$[\alpha]_D^{20} = -52.6$ (c = 0.10, MeOH).
Lit.: –34.3 (c = 0.15, MeOH).[30]

UV/Vis (CH_2Cl_2): λ_{max} (log ε) = 237 (1.11), 307 (0.50), 336 (0.45) nm.

CD (MeOH): λ_{max} ($\Delta\varepsilon$) = 213 (+19.6), 231 (–10.1), 242 (+8.8) nm.

^{1}H NMR (400 MHz, MeOD): δ = 1.25 (d, J = 6.3 Hz, 3H, CH_3-3), 2.30 (s, 3H, CH_3-2'), 2.42 (dd, J = 16.2, 5.4 Hz, 1H, H_{eq}-4), 2.50 (dd, J = 17.1, 11.0 Hz, 1H, H_{ax}-4), 2.82 (s, 3H, CH_3-1), 3.71 (m_c, 1H, H-3), 3.82 (s, 3H, OCH_3-6), 3.92 (s, 3H, OCH_3-4'), 3.94 (s, 3H, OCH_3-5'), 4.14 (s, 3H, OCH_3-8), 6.62 (s, 1H, H-1'), 6.79 (s, 1H, H-3'), 6.80 (s, 1H, H-7), 6.91 (d, J = 7.8 Hz, 1H, H-6'), 7.05 (d, J = 8.1 Hz, 1H, H-7').

IR (NaCl): $\tilde{\nu}$ = 2916 (m), 2851 (w), 1681 (m), 1626 (s), 1609 (s), 1447 (m), 1426 (w), 1358 (s), 1325 (s), 1203 (s), 1133 (s), 842 (m), 801 (m) cm^{-1}.

MS (EI = 70 eV): m/z (%) = 419 (100) $[M]^+$, 404 (48) $[M\text{-}CH_3]^+$, 388 (23) $[M\text{-}OCH_3]^+$.

HRMS (ESI): calcd. for $C_{26}H_{29}NO_4$ $[M]^+$: 419.2097; found 419.2093.

3.2.7 Hamatine (27)

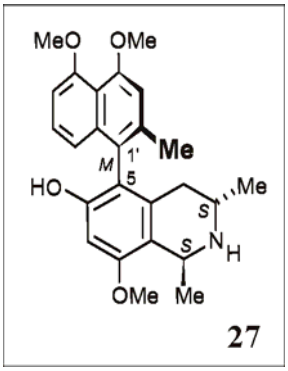

Colorless amorphous solid (3.3 mg).

$[\alpha]_D^{20} = +10.5$ (c = 0.10, MeOH).
Lit.: +16.0 (c = 0.32, $CHCl_3$).[119]

UV/Vis (CH_2Cl_2): λ_{max} (log ε) = 237 (1.18), 307 (0.37), 321 (0.32) 335 (0.28) nm.

CD (MeOH): λ_{max} ($\Delta\varepsilon$) = 225 (+9.3), 241 (–5.2) nm.

^{1}H NMR (400 MHz, MeOD): δ = 1.19 (d, J = 6.2 Hz, CH_3-3), 1.64 (3H, d, J = 6.5 Hz, CH_3-1), 2.06 (1H, dd, J = 16.8, 5.1 Hz, H_{ax}-4), 2.13 (3H, s, CH_3-2'), 2.38 (1H, dd, J = 17.5, 10.7 Hz, H_{eq}-4), 3.69 (1H, m_c, H-3), 3.93 (3H, s, OCH_3-8), 3.93 (3H, s, OCH_3-5'), 3.97 (3H, s, OCH_3-4'), 4.78 (1H, q, 6.8 Hz, H-1), 6.61 (1H, s, H-7), 6.77 (1H, dd, J = 8.3, 1.0 Hz, H-8'), 6.87 (1H, dd, J = 7.6, 1.0 Hz, H-6'), 6.93 (1H, s, H-3'), 7.19 (1H, dd, J = 8.3, 7.7 Hz, H-7').

IR (NaCl): $\tilde{\nu}$ = 2940 (m), 2844 (m), 1679 (s), 1608 (s), 1586 (s), 1453 (w), 1392 (w), 1363 (s), 1261 (m), 1202 (s), 1130 (w), 1112 (m), 1077 (w), 834 (m), 800 (m) cm^{-1}.

MS (EI = 70 eV): m/z (%) = 408 (100) $[M+H]^+$, 407 (65) $[M]^+$, 392 (68) $[M-CH_3]^+$, 376 (21) $[M-OCH_3]^+$.

HRMS (ESI): calcd. for $C_{25}H_{29}NO_4$ $[M]^+$: 407.2097; found 407.2089.

The spectroscopic data are in good agreement with those previously published.[115,119,146]

3.2.8 Hamatinine (29)

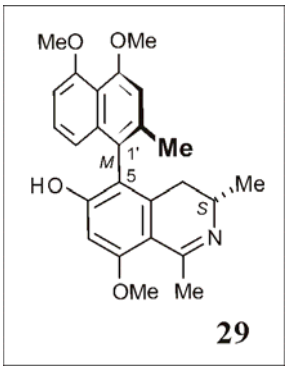

29

Yellow amorphous powder (6.7 mg).

$[\alpha]_D^{20}$ = +69.7 (c = 0.10, MeOH).

UV/Vis (CH_2Cl_2): λ_{max} (log ε) = 237 (1.08), 310 (0.37), 321 (0.36), 336 (0.31) nm.

CD (MeOH): λ_{max} ($\Delta\varepsilon$) = 213 (–6.1), 230 (+6.9) nm.

^{1}H NMR (400 MHz, MeOD): δ = 1.20 (d, J = 6.2 Hz, 3H, CH_3-3), 2.15 (s, 3H, CH_3-2'), 2.21 (dd, J = 17.0, 10.6 Hz, 1H, H_{ax}-4), 2.46 (dd, J = 16.0, 5.4 Hz, 1H, H_{eq}-4), 2.80 (s, 3H, CH_3-1), 3.75 (m_c, 1H, H-3), 3.93 (s, 3H, OCH_3-5'), 3.98 (s, 3H, OCH_3-4'), 4.05 (s, 3H, OCH_3-8), 6.67 (dd, J = 8.2, 1.0 Hz, 1H, H-8'), 6.71 (s, 1H, H-7), 6.89 (dd, J = 8.0, 0.8 Hz, 1H, H-6'), 6.92 (s, 1H, H-3'), 7.23 (dd, J = 8.0, 8.1 Hz, 1H, H-7').

IR (NaCl): $\tilde{\nu}$ = 2933 (m), 2839 (m), 1682 (s), 1568 (s), 1446 (w), 1371 (w), 1326 (s), 1261 (m), 1201 (s), 1128 (w), 1094 (w), 835 (m), 811 (m) cm^{-1}.

MS (EI = 70 eV): *m/z* (%) = 405 (100) $[M]^+$, 390 (53) $[M\text{-}CH_3]^+$, 374 (18) $[M\text{-}OCH_3]^+$, 202.5 (9) $[M]^{2+}$.

HRMS (ESI): calcd. for $C_{25}H_{27}NO_4$ $[M]^+$: 405.1940; found 405.1942.

The spectroscopic data are in good agreement with those previously published.[113]

3.2.9 6-*O*-Methylhamatinine (21)

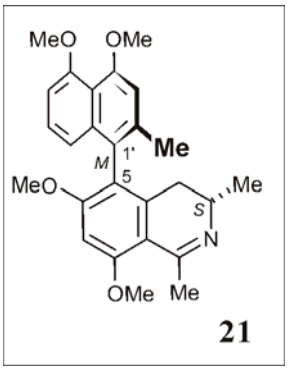

Yellow amorphous powder (8.6 mg).

$[\alpha]_D^{20}$ = +5.6 (*c* = 0.10, MeOH).
Lit.: +28.0.[244]

UV/Vis (CH_2Cl_2): λ_{max} (log ε) = 235 (0.98), 307 (0.38), 321 (0.35), 335 (0.34) nm.

CD (MeOH): λ_{max} ($\Delta\varepsilon$) = 213 (+5.6), 242 (–2.0) nm.

^{1}H NMR (400 MHz, MeOD): δ = 1.19 (d, *J* = 6.3 Hz, 3H, CH_3-3), 2.09 (s, 3H, CH_3-2'), 2.22 (dd, *J* = 17.1, 11.0 Hz, 1H, H_{ax}-4), 2.53 (dd, *J* = 16.2, 5.4 Hz, 1H, H_{eq}-4), 2.82 (s, 3H, CH_3-1), 3.75 (m_c, 1H, H-3), 3.92 (s, 3H, OCH_3-5'), 3.96 (s, 3H, OCH_3-4'), 4.15 (s, 3H, OCH_3-8), 6.68 (dd, *J* = 8.1, 0.9 Hz, 1H, H-8'), 6.86 (s, 1H, H-7), 6.86 (dd, *J* = 8.2, 0.9 Hz, 1H, H-6'), 6.90 (*s*, 1H, H-3'), 7.20 (dd, *J* = 8.0, 8.1 Hz, 1H, H-7').

IR (NaCl): $\tilde{\nu}$ = 2931 (m), 2849 (m), 1681 (s), 1633 (s), 1581 (w), 1462 s, 1438 (w), 1293 (m), 1262 (w), 1202 (s), 1129 (m), 970 (s), 830 (m) cm^{-1}.

MS (EI = 70 eV): *m/z* (%) = 421 (100) $[M]^+$, 406 (42) $[M\text{-}CH_3]^+$, 401 (22) $[M\text{-}2(CH_3)]^+$, 400 (33) $[M\text{-}OCH_3]^+$.

HRMS (ESI): calcd. for $C_{26}H_{31}NO_4$ $[M]^+$: 421.2253; found 421.2254.

The spectroscopic data are in good agreement with those previously published.[244]

3.2.10 6-*O*-Demethylancistrobrevine A (34)

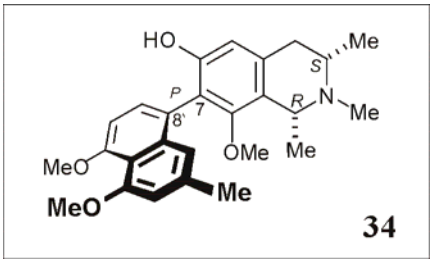

Light brown amorphous solid (3.3 mg).

$[\alpha]_D^{20}$ = +55.5 (*c* = 0.12, MeOH).

Lit.: -80 (EtOH).[22]

Ancistrobrevine A: Lit.: +54 (EtOH).[22]

UV/Vis (CH_2Cl_2): λ_{max} (log ε) = 237 (1.57), 310 (0.54), 320 (0.49), 336 (0.39) nm.

CD (MeOH): λ_{max} ($\Delta\varepsilon$) = 202 (+12.8), 216 (–7.1), 239 (+4.8) nm.

^{1}H NMR (400 MHz, MeOD): δ = 1.30 (d, *J* = 6.1 Hz, 3H, CH_3-3), 1.47 (d, *J* = 6.4 Hz, 3H, CH_3-1), 2.33 (s, 3H, CH_3-2'), 2.45 (dd, *J* = 16.9, 5.0 Hz, 1H, H_{eq}-4), 2.56 (dd, *J* = 16.9, 8.0 Hz, 1H, H_{ax}-4), 2.50 (s, 3H, CH_3-*N*), 2.68 (m_c, 1H, H-3), 3.02 (s, 3H, OCH_3-8), 3.93 (s, 3H, OCH_3-4'), 3.96 (s, 3H, OCH_3-5'), 6.48 (s, 1H, H-5), 6.77 (s, 1H, H-3'), 6.91 (s, 1H, H-1'), 6.94 (d, *J* = 8.1 Hz, 1H, H-6'), 7.22 (d, *J* = 8.0 Hz, 1H, H-7').

^{13}C NMR (100 MHz, MeOD): δ = 21.0 (3-Me), 22.2 (2'-Me), 23.0 (1-Me), 38.7 (C-4), 41.9 (*N*-Me), 57.0 (5'-OMe), 57.1 (C-3), 57.2 (4'-OMe), 59.4 (C-1), 60.5 (8-OMe), 107.0 (C-6'), 110.0 (C-3'), 111.0 (C-5), 117.5 (C-10'), 119.7 (C-1'), 121.3 (C-7),124.6 (C-9), 125.6 (C-8'), 131.1 (C-7'), 137.5 (C-2'), 137.6 (C-10), 137.9 (C-9'), 155.6 (C-6),157.7 (C-8), 158.3 (C-5'), 158.6 (C-4').

IR (NaCl): $\tilde{\nu}$ = 2957 (m), 2923 (m) 2850 (m), 1682 (s), 1611 (s), 1585 (s), 1454 (w), 1413 (m), 1384 (w), 1332 (s), 1262 (m), 1171 (s), 1142 (w), 1093 (m), 1072 (m) 827 (m) cm^{-1}.

MS (EI = 70 eV): *m*/*z* (%) = 421 (2) $[M]^+$, 406 (100) $[M\text{-}CH_3]^+$, 390 (6) $[M\text{-}OCH_3]^+$.

HRMS (ESI): calcd. for $C_{25}H_{28}NO_4$ $[M\text{-}CH_3]^+$: 406.2018; found 406.2017.

3.2.11 Ancistrocladine (35)

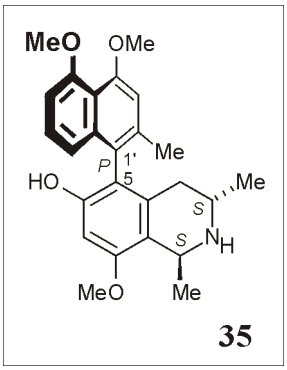

35

Colorless amorphous solid (2.7 mg).

$[\alpha]_D^{20} = -19.0$ ($c = 0.10$, MeOH).

Lit.: –21.0 ($c = 0.86$, $CHCl_3$).[119]

UV/Vis (CH_2Cl_2): λ_{max} (log ε) = 237 (1.21), 307 (0.35), 321 (0.31), 335 (0.27) nm.

CD (MeOH): λ_{max} ($\Delta\varepsilon$) = 227 (–8.3), 241 (+3.8) nm.

^{1}H NMR (400 MHz, MeOD): δ = 1.21 (d, J = 6.0 Hz, 3H, CH_3-3), 1.65 (d, J = 6.2 Hz, 3H, CH_3-1), 2.11 (s, 3H, CH_3-2'), 2.14 (dd, J = 17.2, 4.8 Hz, 1H, H_{ax}-4), 2.27 (dd, J = 17.0, 11.2 Hz, 1H, H_{eq}-4), 3.63 (m_c, 1H, H-3), 3.93 (s, 3H, OCH_3-8), 3.93 (s, 3H, OCH_3-5'), 3.97 (s, 3H, OCH_3-4'), 4.77 (q, J = 6.5 Hz, 1H, H-1), 6.61 (1H, s, H-7), 6.85 (dd, J = 8.3, 1.0 Hz, 1H, H-8'), 6.88 (dd, J = 7.8, 0.9 Hz, 1H, H-6'), 6.92 (s, 1H, H-3'), 7.23 (dd, J = 7.9, 8.1 Hz, 1H, H-7').

IR (NaCl): $\tilde{\nu}$ = 2937 (m), 2845 (m), 1681 (s), 1593 (s), 1453 (w), 1392 (w), 1361 (s), 1336 (s), 1260 (m), 1203 (s), 1129 (w), 1078 (w), 834 (m), 801 (m) cm^{-1}.

MS (EI = 70 eV): m/z (%) = 408 (88) $[M+H]^+$, 407 (100) $[M]^+$, 392 (63) $[M-CH_3]^+$, 377 (15) $[M-2(CH_3)]^+$, 376 (32) $[M-OCH_3]^+$.

HRMS (ESI): calcd. for $C_{25}H_{29}NO_4$ $[M]^+$: 407.2097; found 407.2090.

The spectroscopic data are in good agreement with those previously published.[115,119,150]

4 Isolation of Naphthylisoquinoline Alkaloids from *Triphyophyllum peltatum* (Dioncophyllaceae)

4.1 Isolation of Naphthylisoquinoline Alkaloids from the Roots of *T. peltatum*

6 kg of air dried roots of *T. peltatum* were powdered and pre-extracted with *n*-hexane. The plant material was subsequently macerated for 7 days with 15 L MeOH-1N HCl (1:1) at room temp. with ultrasonic assistance. After removal of MeOH under reduced pressure the aqueous solution was re-extracted first with $CHCl_3$ (3 L) and following with CH_2Cl_2 (4 L). Evaporation of the two organic phases yielded respectively 15 g and 5 g of brownish crude extracts. These were further submitted to FCPC using a two-phase solvent system consisting of $CHCl_3$/EtOAc/MeOH/H_2O (8:2:8:2) + 0.1% TFA. The aqueous phase served as the stationary phase.

The $CHCl_3$ extract was resolved in 19 FCPC runs. The mobile phase was sequenced in fractions eluting between 500-700, and 850-900 mL. The pooled fractions were evaporated *in vacuo* and gave 8.9 g enriched in **8**, and 150 mg enriched in **24**, respectively.

The CH_2Cl_2 extract was resolved in 12 FCPC runs. The mobile phase was sequenced in fractions eluting between 150-300, 330-380 mL. The pooled fractions were evaporated *in vacuo* and gave 800 mg enriched in **6**, and 100 mg enriched in **36**, respectively. The stationary phase was flushed out in reversed mode after about 90 min using MeOH, and concentrated under reduced pressure to give 350 mg enriched in **7**.

The enriched fractions were found to contain the respective naphthylisoquinoline alkaloids in purity ~80% as estimated by NMR. For further improvement of the purity the fractions were conducted to preparative HPLC using the conditions described in Chapter Ex. 1.3.

4.1.1 Dioncophylline C (6)

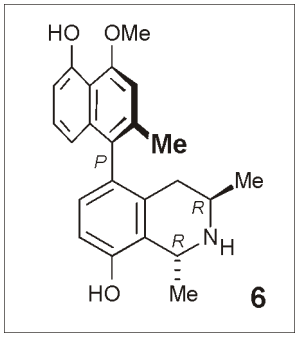

Colorless amorphous powder.

$[\alpha]_D^{20}$ = +21.2 (c = 0.2, $CHCl_3$).

Lit.: +19.2 (c = 0.52, $CHCl_3$).[130]

UV/Vis (MeOH): λ_{max} (log ε) = 231 (1.56), 305 (1.24) nm.

CD (MeOH): λ_{max} ($\Delta\varepsilon$) = 205 (–19.1), 231 (+17.8), 257 (–0.3), 282 (+0.7), 303 (–1.1) nm.

^{1}H NMR (400 MHz, MeOD): δ = 1.00 (d, J = 6.4 Hz, 3 H, 3-CH_3), 1.53 (d, J = 6.7 Hz, 3 H, 1-CH_3), 1.90 (dd, J = 17.0, 4.4 Hz, 1 H, 4-H_{ax}), 2.03 (dd, J = 17.0, 10.9 Hz, 1 H, 4-H_{eq}), 2.08 (s, 3 H, 2'-CH_3), 3.19 (m, 1 H, 3-H), 4.11 (s, 3 H, 4'-OCH_3), 4.47 (q, 1 H, 1-H), 6.66 (dd, J = 8.5, 1.2 Hz, 1 H, 6'-H), 6.69 (dd, J = 7.7, 0.8 Hz, 1 H, 8'-H), 6.72 (d, J = 8.0 Hz, 1 H, 6-H), 6.74 (d, J = 8.0 Hz, 1 H, 7-H), 6.87 (s, 1 H, 3'-H), 7.13 (dd, J = 8.5, 7.7 Hz, 1 H, 7'-H).

^{13}C NMR (100 MHz, MeOD): δ = 20.5 (1-Me), 20.7 (3-Me), 22.0 (2'-Me), 35.9 (C-4), 43.0 (C-3), 48.6 (C-1), 56.7 (4'-OMe), 94.1 (C-5), 107.9 (C-3'), 110.3 (C-6'), 113.6 (C-7), 114.8 (C-1'), 117.7 (C-8'), 127.6 (C-9'), 128.6 (C-7'), 129.9 (C-10), 131.3 (C-10'), 135.0 (C-9), 135.6 (C-2'), 137.6 (C-6), 154.3 (C-8), 155.8 (C-4'), 156.5 (C-5').

MS (EI = 70 eV): m/z (%) = 364 (15) $[M+H]^+$, 363 (22) $[M]^+$, 349 (32), 348 (100) $[M-CH_3]^+$.

HRMS (ESI): calcd. for $C_{23}H_{25}NO_3$ $[M]^+$: 363.1834; found 363.1831.

The spectroscopic data are in good agreement with those previously published.[130]

4.1.2 Dioncopeltine A (7)

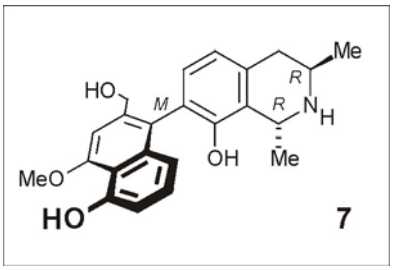

Colorless amorphous powder.

$[\alpha]_D^{20}$ = –15.2 (c = 0.15, $CHCl_3$).

Lit.: –13.1 (c = 0.53, $CHCl_3$).[129]

UV/Vis (MeOH): λ_{max} (log ε) = 233 (1.45), 307 (1.17) nm.

CD (CH_3CN): λ_{max} ($\Delta\varepsilon$) = 200 (+15.1), 222 (–37.8), 238 (+30.3), 260 (+1.5), 303 (–2.1) nm.

^{1}H NMR (400 MHz, MeOD): δ = 1.24 (d, J = 6.2 Hz, 3 H, 3-CH_3), 1.43 (d, J = 6.5 Hz, 3 H, 1-CH_3), 2.49 (dd, J = 16.3, 10.9 Hz, 1 H, 4-H_{ax}), 2.73 (dd, J = 16.8, 3.9 Hz, 1 H, 4-H_{eq}), 3.35 (m, 1 H, 3-H), 4.11 (s, 3 H, 4'-OCH_3), 4.42 (q, 1 H, 1-H), 4.53 (s, 2 H, CH_2OH) 6.75 (dd, J = 8.5, 1.2 Hz, 1 H, 6'-H), 6.69 (dd, J = 7.7, 0.8 Hz, 1 H, 8'-H), 6.72 (d, J = 8.0 Hz, 1 H, 6-H), 6.74 (d, J = 8.0 Hz, 1 H, 7-H), 6.87 (s, 1 H, 3'-H), 7.13 (dd, J = 8.5, 7.7 Hz, 1 H, 7'-H).

^{13}C NMR (100 MHz, MeOD): δ = 21.6 (1-Me), 23.2 (3-Me), 38.4 (C-4), 42.4 (C-3), 48.6 (C-1), 55.9 (4'-OMe), 62.4 (2'- CH_2OH), 104.0 (C-7), 110.2 (C-3'), 114.8 (C-1'), 117.9 (C-6'), 119.9 (C-5), 123.4 (C-8'), 126.5 (C-9'), 127.2 (C-7'), 128.8 (C-10'), 129.7 (C-10), 136.1 (C-9), 137.4 (C-2'), 140.5 (C-6), 152.6 (C-8), 155.5 (C-4'), 156.2 (C-5').

MS (EI = 70 eV): *m*/*z* (%) = 379 (20) $[M]^+$, 364 (100) $[M\text{-}CH_3]^+$.

HRMS (ESI): calcd. for $C_{23}H_{25}NO_4$ $[M]^+$: 379.1784; found 379.1782.

The spectroscopic data are in good agreement with those previously published.[129]

4.1.3 Dioncophylline A (8)

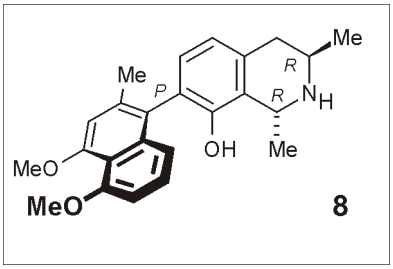

8

Colorless amorphous powder.

$[\alpha]_D^{20}$ = –15.7 (*c* = 0.1, $CHCl_3$).
Lit.: –14.9 (*c* = 1.0, $CHCl_3$).[245]

UV/Vis (MeOH): λ_{max} (log ε) = 231 (1.05), 306 (0.52) nm.

CD (CH_3CN): λ_{max} ($\Delta\varepsilon$) = 198 (+3.1), 224 (–27.8), 244 (+20.3) nm.

^{1}H NMR (400 MHz, MeOD): δ = 1.17 (d, *J* = 6.2 Hz, 3 H, 3-C*H*$_3$), 1.37 (d, *J* = 6.3 Hz, 3 H, 1-C*H*$_3$), 2.07 (s, 3 H, 2'-C*H*$_3$), 2.43 (dd, *J* = 16.5, 11.0 Hz, 1 H, 4-H_{ax}), 2.74 (dd, *J* = 16.5, 3.8 Hz, 1 H, 4-H_{eq}), 3.27 (m, 1 H, 3-H), 3.98 (s, 3 H, 4'-OC*H*$_3$), 4.05 (s, 3 H, 5'-OC*H*$_3$), 4.33 (q, 1 H, 1-H), 6.64 (s, 1 H, 3'-H), 6.66 (d, *J* = 7.6 Hz, 1 H, 8'-H), 6.73 (d, *J* = 7.9 Hz, 1 H, 5-H), 6.75 (d, *J* = 7.9 Hz, 1 H, 6'-H), 6.77 (d, *J* = 8.2 Hz, 1 H, 6-H), 7.14 (dd, *J* = 8.0, 7.9 Hz, 1 H, 7'-H).

^{13}C NMR (100 MHz, MeOD): δ = 20.9 (1-Me), 21.5 (3-Me), 22.7 (2'-Me), 37.2 (C-4), 41.2 (C-3), 47.3 (C-1), 56.2 (4'-OMe), 56.8 (5'-OMe), 105.3 (C-7), 106.8 (C-5), 110.2 (C-6), 114.0 (C-1'), 116.9 (C-8'), 121.0 (C-3'), 122.2 (C-7'), 124.2 (C-6'), 128.4 (C-10), 128.4 (C-9), 135.1 (C-10'), 135.9 (C-9'), 136.2 (C-2'), 149.8 (C-8), 154.6 (C-5'), 156.4 (4').

MS (EI = 70 eV): *m/z* (%) = 377 (78) $[M]^+$, 362 (100) $[M\text{-}CH_3]^+$, 346 (28) $[M\text{-}OCH_3]^+$.

HRMS (ESI): calcd. for $C_{24}H_{27}NO_3$ $[M]^+$: 377.1991; found 377.1989.

The spectroscopic data are in good agreement with those previously published.[245]

4.1.4 Dioncophylline B (24)

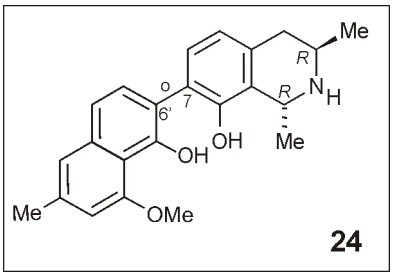

Colorless amorphous powder.

$[\alpha]_D^{20} = -29.7$ ($c = 0.1$, $CHCl_3$).

Lit.: –37.6 ($c = 0.37$, $CHCl_3$).[131]

UV/Vis (MeOH): λ_{max} (log ε) = 231 (0.95), 305 (0.43) nm.

^{1}H NMR (400 MHz, MeOD): δ = 1.24 (d, J = 6.3 Hz, 3 H, 3-CH_3), 1.51 (d, J = 6.7 Hz, 3 H, 1-CH_3), 2.42 (dd, J = 17.1, 10.8 Hz, 1 H, 4-H_{ax}), 2.45 (s, 3 H, 2'-CH_3), 2.72 (dd, J = 17.0, 4.3 Hz, 1 H, 4-H_{eq}), 3.30 (m, 1 H, 3-H), 3.98 (s, 3 H, 4'-OCH_3), 4.48 (q, 1 H, 1-H), 6.66 (d, J = 1.4 Hz, 1 H, 3'-H), 6.73 (d, J = 7.9 Hz, 1 H, 5-H), 7.09 (d, J = 8.0 Hz, 1 H, 6-H), 7.18 (m, 1 H, 1'-H), 7.30 (d, J = 8.0 Hz, 1 H, 8'-H), 7.35 (d, J = 8.2 Hz, 1 H, 7'-H).

^{13}C NMR (100 MHz, MeOD): δ = 21.0 (1-Me), 21.7 (2'-Me), 22.2 (3-Me), 36.7 (C-4), 43.2 (C-3), 48.3 (C-1), 56.4 (4'-OMe), 107.2 (C-3'), 109.5 (C-6'), 112.2 (C-7), 119.5 (C-8'), 121.0 (C-1'), 121.4 (C-5), 123.6 (C-2'), 128.6 (C-6), 129.1 (C-9'), 131.1 (C-7'), 135.3 (C-10), 136.2 (C-10'), 136.3 (C-9), 149.5 (C-5') 150.9 (C-8) 155.8 (4').

MS (EI = 70 eV): *m/z* (%) = 363 (72) $[M]^+$, 348 (100) $[M\text{-}CH_3]^+$.

HRMS (ESI): calcd. for $C_{23}H_{25}NO_3$ $[M]^+$: 363.1834; found 363.1834.

The spectroscopic data are in good agreement with those previously published.[131]

4.1.5 Dioncolactone A (36)

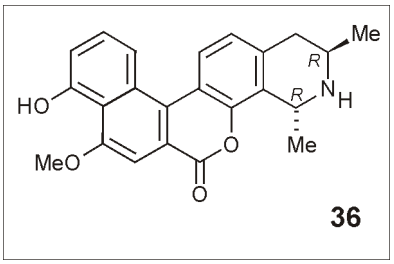

Yellow amorphous powder.

$[\alpha]_D^{20} = -45.2$ ($c = 0.1$, $CHCl_3$).

Lit.: −64.0 ($c = 0.26$, CH_3Cl_3).[129]

UV/Vis (MeOH): λ_{max} (log ε) = 230 (1.27), 311 (0.76) nm.

^{1}H NMR (400 MHz, MeOD): δ = 1.25 (d, J = 6.6 Hz, 3 H, 3-CH_3), 1.52 (d, J = 6.7 Hz, 3 H, 1-CH_3), 2.50 (dd, J = 16.9, 11.0 Hz, 1 H, 4-H_{ax}), 2.80 (dd, J = 17.0, 4.2 Hz, 1 H, 4-H_{eq}), 3.39 (m, 1 H, 3-H), 4.05 (s, 3 H, 4'-OCH_3), 4.52 (q, 1 H, 1-H), 6.91 (d, J = 8.2 Hz, 1 H, 5-H), 7.05 (d, J = 8.2 Hz, 1 H, 6'-H), 7.42 (s, 1 H, 3'-H), 7.47 (dd, J = 7.7, 8.1 Hz, 1 H, 6'-H), 8.05 (d, J = 7.9 Hz, 1 H, 6-H), 8.11 (d, J = 8.0 Hz, 1 H, 8'-H), 7.15 (s, 1 H, 3'-H), 7.20 (dd, J = 8.0, 8.4 Hz, 1 H, 7'-H).

MS (EI = 70 eV): m/z (%) = 376 (9) $[M+H]^+$, 375 (26) $[M]^+$, 374 (29) $[M-H]^+$, 360 (100) $[M-CH_3]^+$.

HRMS (ESI): calcd. for $C_{23}H_{21}NO_4$ $[M]^+$: 375.1471; found 375.1469.

The spectroscopic data are in good agreement with those previously published.[129]

4.2 Isolation of Naphthylisoquinoline Alkaloids from the Leaves of *T. peltatum*

12 kg of air dried leaves and twigs from *T. peltatum* were powdered and sequential extracted with *n*-hexane, $CHCl_3$, CH_2Cl_2, $CHCl_3$-MeOH (9.1), and CH_2Cl_2-MeOH (9.1). The solvents were evaporated under reduced pressure and gave 20 g of a brown residue from the CH_2Cl_2 extract, and 12 g of dark brown residue $CHCl_3$-MeOH (9.1). 200 mg of the former and 150 mg of the latter were resolved directly using preparative HPLC and the conditions described in Chapter Ex. 1.3 and gave 12 mg of **38** (t_R = 22.1 min), and 2 mg of **33** (t_R = 22.8 min), respectively.

4.2.1 Habropetaline A (37)

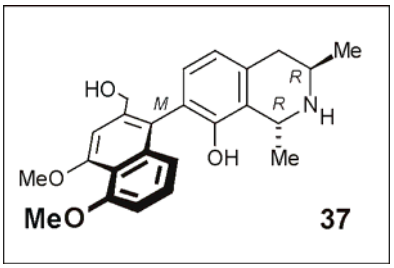

Light yellow amorphous powder.

$[\alpha]_D^{20} = -27.2$ ($c = 0.1$, MeOH).

Lit.: −16.5 ($c = 0.1$, MeOH).[169]

UV/Vis (MeOH): λ_{max} (log ε) = 233 (0.92), 305 (0.56) nm.

CD (CH_3CN): λ_{max} ($\Delta\varepsilon$) = 222 (–20.1), 239 (+12.3), 264 (+1.4), 282 (+2.9), 304 (–0.9) nm.

^{1}H NMR (400 MHz, MeOD): δ = 1.27 (d, J = 6.3 Hz, 3 H, 3-CH_3), 1.51 (d, J = 6.8 Hz, 3 H, 1-CH_3), 2.55 (dd, J = 16.8, 10.8 Hz, 1 H, 4-H_{ax}), 2.79 (dd, J = 17.0, 4.5 Hz, 1 H, 4-H_{eq}), 2.08 (s, 3 H, 2'-CH_3), 3.35 (m, 1 H, 3-H), 3.91 (3H, *s*, OCH_3-5′), 3.99 (s, 3 H, 4'-OCH_3), 4.41 d, J = 3.9 Hz, CH_2OH-2', 4.47 (q, 1 H, 1-H), 6.81 (d, J = 7.6 Hz, 1 H, 6-H), 6.88 (dd, J = 7.7, 0.8 Hz, 1 H, 6'-H), 6.94 (dd, J = 8.0, 0.9 Hz, 1 H, 8'-H), 7.15 (s, 1 H, 3'-H), 7.20 (dd, J = 8.0, 8.4 Hz, 1 H, 7'-H).

^{13}C NMR (100 MHz, MeOD): δ = 20.5 (1-Me), 21.9 (3-Me), 37.9 (C-4), 43.2 (C-3), 48.6 (C-1), 56.8 (5'-OMe), 57.1 (4'-OMe), 63.2 (2'- CH_2OH), 106.9 (C-6'), 107.2 (C-3'), 113.6 (C-7), 118.5 (C-4'), 120.2 (C-8'), 121.5 (C-5), 123.6 (C-7), 126.1 (C-1'), 127.5 (C-7'), 128.4 (C-8), 131.1 (C-6), 136.0 (C-4), 138.4 (C-8'), 140.2 (C-2'), 152.4 (C-8), 158.5 (C-4'), 158.5 (C-5').

MS (EI = 70 eV): *m*/*z* (%) = 393 (42) $[M]^+$, 378 (68) $[M\text{-}CH_3]^+$, 378 (100) $[M\text{-}CH_3\text{-}H_2O]^+$.

HRMS (ESI): calcd. for $C_{24}H_{27}NO_4$ $[M]^+$: 393.1940; found 393.1938.

The spectroscopic data are in good agreement with those previously published.[169]

4.2.2 Dioncophyllinol B (38)

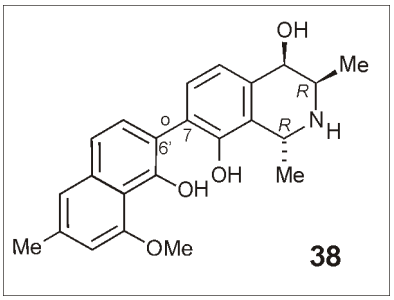

Colorless amorphous powder.

$[\alpha]_D^{20}$ = +25 (*c* = 0.2, MeOH).

Lit.: +17 (*c* = 0.05, $CHCl_3$).[246]

UV/Vis (MeOH): λ_{max} (log ε) = 231 (0.97), 305 (0.62) nm.

CD (CH_3CN): λ_{max} ($\Delta\varepsilon$) = 200 (–12.1), 220 (+7.5), 240 (–0.3), 285 (+5.4), 328 (+1.1) nm.

^{1}H NMR (400 MHz, MeOD): δ = 1.41 (d, *J* = 6.6 Hz, 3 H, 3-CH_3), 1.58 (d, *J* = 6.8 Hz, 3 H, 1-CH_3), 2.48 (s, 3 H, 2'-CH_3), 3.51 (dq, *J* = 6.5, 2.0 Hz, 1 H, 3-H), 4.05 (s, 3 H, 4'-OCH_3), 4.23 (d, *J* = 2.1, 1 H, 4-H), 4.46 (q, 1 H, 1-H), 6.69 (s, 3 H, 3'-H), 7.08 (d, *J* = 7.9 Hz, 1 H, 5-H), 7.28 (d, *J* = 7.5 Hz, 6-H), 7.31 (d, *J* = 8.5 Hz, 8'-H), 7.33 (d, *J* = 8.4 Hz, 7'-H).

^{13}C NMR (100 MHz, MeOD): δ = 17.5 (3-Me), 19.5 (1-Me), 22.0 (2'-Me), 47.9 (C-3), 49.0 (C-1), 48.6 (C-1), 56.8 (4'-OMe), 68.8 (C-4), 107.8 (C-3'), 113.3 (C-10'), 119.1 (C-6'), 120.0 (C-8'), 121.3 (C-1'), 122.4 (C-5), 127.6 (C-7), 128.5 (C-9), 129.6 (C-6), 131.0 (C-7'), 136.4 (C-2'), 136.8 (C-9'), 137.9 (C-10), 149.3 (C-5'), 150.3 (C-8), 156.1 (C-4').

MS (EI = 70 eV): *m*/*z* (%) = 379 (12) $[M]^+$, 364 (100) $[M\text{-}CH_3]^+$, 348 (15) $[M\text{-}OCH_3]^+$.

HRMS (ESI): calcd. for $C_{23}H_{25}NO_4$ $[M]^+$: 379.1784; found 379.1783.

The spectroscopic data are in good agreement with those previously published.[246]

5 γ-Ray Synthesis of Antimalarial Compounds

5.1 γ-Ray Irradiation of Samples

Solutions (4 mL, 300 mM) of 1,2,3,4-tetrahydroisoquinoline (**39**), benzylamine (**40**), 3-hydroxy-benzyl-alcohol (**41**), and 3-methoxy-benzyl-alcohol (**42**) and mixtures of two compounds in equimolar concentrations, in a MeOH-water 9:1 mixture were exposed to γ-rays from a ^{60}Co source, Gammacell 220 *Atomic Energy of Canada Ltd.*. The irradiation was performed at PPS Laboratories (Paul Scherrer Institute, Villigen, Switzerland), by A. Wuhrmann. The solutions were irradiated in glass containers with screw-type plastic caps at room temperature and air atmosphere. The dose rate was maintained at 2.22 kGy/h, and the total dose applied was 50 kGy or 500 kGy.

5.2 Antiplasmodial Activity Screening

The antiplasmodial activity was determined using the chloroquine (**2**) sensitive 3D7 strain of *P. falciparum* (sensitive to all known drugs) in Copenhagen by Prof. S. B. Christensen and coworkers. A modification of the [^{3}H]-hypoxanthine incorporation assay was used.[185] In brief, infected human red blood cells were exposed to serial drug dilutions in microtiter plates for 48 h at 37 °C in a gas mixture with reduced oxygen and elevated CO_2 levels. [^{3}H]-hypoxanthine was added to each well and after further incubation for 24 h the wells were harvested on glass fiber filters and counted in a liquid scintillation counter. The estimated IC_{50} values of the fractions were determined by testing at intervals of 5-50 μg/mL. The assays were run in duplicate and repeated at least once.

5.3 Bioactivity Guided Isolation of Antiplasmodialy Active γ-Ray Irradiation Products

The irradiated samples containing **39** and the mixture **39** + **40** were each fractionated in one run by direct injection of the irradiated sample into the FCPC, using the solvent system as described in Chapter Ex. 1.3. The eluents were collected in 10 mL fractions, which were analyzed by HPLC-UV, using the conditions described in Chapter Ex. 1.3. This enabled the division of the chromatographical eluent of **39** into seven compound containing fractions and the one of the mixture **39** + **40** into eleven fractions. The solvent of these fractions were evaporated and the remaining residues were subsequently screened for their antiplasmodial activity. The screening revealed two of these obtained residues from the irradiated solutions of **39** and three from the mixture of **39** + **40** to display higher antiplasmodial activity than the

starting compounds. The residues of the these fractions were chosen for further work-up; all other fraction residues were discarded. For the further deconvolution the residues were resolved by preparative HPLC, using the standard conditions described in Chapter Ex. 1.3, analyzed by HPLC-UV and HPLC-MS, and subsequently pooled into four subfractions each containing only one pure compound. The solvent of the subfractions was evaporated and the remaning residues were screened for their activity against *P. falciparum*.

The screening revealed that three of the four residues obtained from the subfractions contained antiplasmodially active compounds. From these residues the chromatographic isolation using the standard gradient and the preparative Symmetry-C_{18} column (Chapter Ex. 1.3) afforded **43** (2.5 mg, t_R = 14.8 min), **44** (1.1 mg, t_R = 16.9 min), **45** (1.5 mg, t_R = 18.7 min).

5.4 3,4-Dihydro-1-Isoquinolinone (43)

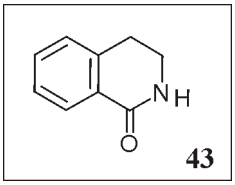

43

Colorless amorphous powder (2.5 mg).

M.p. 63 °C (CH_3CN/H_2O).
Lit.: 57-59 °C (EtOAc/ H_2O),[187] 67-69 °C (cyclohexane).[247]

UV/Vis (MeOH): λ_{max} (log ε) = 210 (1.92), 250 (0.83) nm.

^{1}H NMR (400 MHz, MeOD): δ = 2.81 (d, J = 6.3 Hz, 2 H, H_2-4), 3.43 (d, J = 6.4 Hz, 2 H, H_2-3), 7.26 (dd, J = 7.9, 8.2 Hz, 1 H, H-7), 7.29 (d, J = 8.0 Hz, 1 H, H-5), 7.44 (dd, J = 7.8, 8.0 Hz, 1 H, H-6), 7.89 (d, J = 7.9 Hz, 1 H, H-8).

^{13}C NMR (100 MHz, MeOD): δ = 28.4 (C-4), 32.9 (C-3), 125.6 (C-5), 126.6 (C-7), 129.8 (C-6) 134.4 (C-9), 135.3 (C-10), 135.8 (C-8), 173.9 (C-1).

IR (NaCl): $\tilde{\nu}$ = 3428 (s), 3335 (m), 2851 (s), 1805 (s), 1675 (s), 1645 (m), 1415 (s), 1190 (m), 1120 (m), 940 (m), 854 (w) cm^{-1}.

MS (EI = 70 eV): m/z (%) = 147 (100) $[M]^+$, 91 (55), 45 (38).

HRMS (ESI): calcd. for C_9H_9NO $[M]^+$: 147.0684; found 147.0682.

5.5 3,4-Dihydro-1-Isoquinolineamine (44)

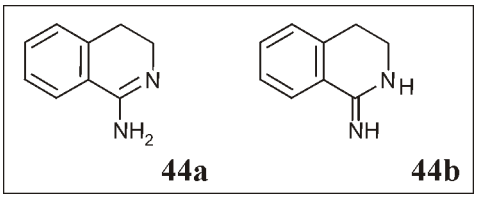

44a **44b**

Colorless crystals (1.4 mg).

M.p. 128 °C (CH_3CN/H_2O).
Lit.: 133-134 °C.[190]

UV/Vis (MeOH): λ_{max} (log ε) = 210 (1.67), 248 (0.74) nm.

^{1}H NMR (400 MHz, MeOD): δ = 2.94 (d, J = 6.8 Hz, 2 H, H_2-4), 3.50 (d, J = 6.6 Hz, 2 H, H_2-3), 7.30 (d, J = 8.1 Hz, 1 H, H-5), 7.35 (dd, J = 8.0, 8.0 Hz, 1 H, H-7), 7.48 (dd, J = 7.9, 8.1 Hz, 1 H, H-6), 7.93 (d, J = 8.0 Hz, 1 H, H-8).

^{13}C NMR (100 MHz, MeOD): δ = 29.4 (C-4), 37.3 (C-3), 126.1 (C-7), 127.9 (C-5), 128.3 (C-8), 128.8 (C-9), 130.1 (C-6), 138.0 (C-10), 168.5 (C-1).

IR (NaCl): $\tilde{\nu}$ = 3405 (m), 2860 (s), 1795 (s), 1775 (s), 1690 (s), 1660 (s), 1415 (s), 1122 (m), 920 (m) cm^{-1}.

MS (EI = 70 eV): m/z (%) = 145 (75) $[M]^+$, 121 (100), 98 (33).

HRMS (ESI): calcd. for $C_9H_9N_2$ $[M]^+$: 145.0766; found 145.0762.

5.6 1,2,3,4-Tetrahydro-1,2-Diazirino-Isoquinoline (45)

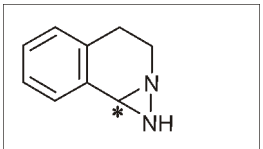

* Racemic mixture **45**

Colorless amorphous powder (1.2 mg).

M.p. 96 °C (CH_3CN/H_2O).

UV/Vis (MeOH): λ_{max} (log ε) = 210 (1.67), 269 (0.74) nm.

^{1}H NMR (400 MHz, MeOD): δ = 2.92 (m, 2 H, H_2-4), 3.08 (m, 2 H, H_2-3), 5.22 (br s, 1 H, H_2-3), 7.05-7.12 (m, 4 H, H-5, H-6, H-7, H-8).

^{13}C NMR (100 MHz, MeOD): δ = 25.8 (C-4), 65.6 (C-3), 72.5 (C-1), 124.9 (C-7), 125.6 (C-5), 126.1 (C-6), 126.3 (C-8), 135.2 (C-10), 136.0 (C-9).

IR (NaCl): $\tilde{\nu}$ = 3330 (m), 3293 (s), 2855 (s), 1805 (s), 1770 (s), 1580 (m), 1430 (s), 1162 (m), 1185 (m), 950 (m) cm^{-1}.

MS (EI = 70 eV): *m*/*z* (%) = 145 (25) $[M]^+$, 130 (100) $[M-NH]^+$, 103 (26).

HRMS (ESI): calcd. for $C_9H_9N_2$ $[M]^+$: 145.0766; found 145.0762.

6 Antimalarial Drug–Heme Interactions

6.1 Materials

2,2,6,6-Tetramethylpiperidine 1-oxyl (TEMPO), bovine serum albumin (BSA), sodium dodecyl sulfate (SDS), *o*-phenyl-diamine (OPD), phosphate buffer, HEPES buffer, chloroquine (**2**) disphosphate salt, and hemin chloride (>98%) were purchased from *Sigma-Aldrich*. The naphthylisoquinoline alkaloids investigated were purified by preparative HPLC using the standard method (Chapter Ex. 1.3) as TFA salts with a purity of over 98% as estimated by NMR. D_2O and NaOD were purchased from *Euroiso-top*. All other reagents were analytical grade or better.

6.2 CD Spectroscopy

Circular dichroism spectra of aqueous solutions of dioncophylline C (**6**) and FPIX (**9**) were recorded on a Jasco J-715 spectrometer as described in Chapter Ex. 1.1.

For the experiments in pure aqueous medium stock solutions of FPIX (**9**) were prepared by solving hemin chloride in 0.05 M NaOH assisted by ultrasonic assistance (30 min), in a concentration of 10 mM. The FPIX (**9**) stock solutions were prepared daily and prior to use centrifuged with 150 × g for 10 min. The exact concentration in the supernatant was determined by a standard curve prepared on the analytical HPLC using the chromolith column and method (Chapter Ex. 1.3). Stock solutions of dioncophylline C (**6**) were prepared in H_2O in a concentration of 10 mM. Aliquots of the two stock solutions were mixed and diluted with H_2O and adjusted with 0.05 M NaOH to give a pH of 10.5 and a concentration of 1.5 mM dioncophylline C (**6**) and 1.5 mM of FPIX μ-oxo dimer (**11**) in the final sample solution. Subsequently the solution was transferred to a 0.2 mm quartz cell.

6.2.1 CD Spectroscopy of Mixtures of Dioncophylline C (6) and FPIX (9) (1:1, 2 mM)

CD (H_2O, pH 10.5): $\Delta\varepsilon_{210}$ –5.9, $\Delta\varepsilon_{235}$ +5.5, $\Delta\varepsilon_{320}$ –1.1, $\Delta\varepsilon_{400}$ –2.9.

6.3 UV

UVspectra were recorded on a *Varian* Cary 50 Conc UV Visible Spectrophotometer as described in Chapter Ex. 1.1.

For the UV experiments stock solutions of FPIX (**9**) were prepared daily by solving hemin chloride in 0.01 M NaOH in a concentration of 1.68 mM and subsequently diluted with H_2O PBS (10 mM, pH 6.5) to give a final concentration of 0.168 mM. Stock solutions of dioncophylline A (**8**), dioncophylline C (**6**), dioncopeltine A (**7**), korupensamine A (**46**), and ancistrocladine (**35**) were prepared in H_2O buffered with PBS (10 mM, pH 6.5) in a concentration of 0.168 mM.

6.3.1 Job's Plot

For the Job's plot determination test solution of 0, 0.4, 0.525, 0.6, 0.7, 0.8, 1.05, 1.3, 1.4, 1.5, 1.575, 1.8 and 2.1 mL of the 0.168 mM naphthylisoquinoline alkaloid stock solutions were brought to a final volume (V_T) of 2.1 mL by the addition of the 0.168 mM FPIX (**9**) stock solution. The extinction at 365 nm was measured.

6.3.2 Binding Constant

Titrations of 2 mL of the FPIX (**9**) solution with the naphthylisoquinoline alkaloid stock solutions in titration steps of 10 µL in the molar equivalent range of 0-8 relative to FPIX (**9**), were monitored as UV/Vis spectra and by the decrease of the absorbance at 365 nm. Final spectra were recorded about 10 min after each addition, when sequentially recorded spectra varied by less than 0.001 absorbance units at 365 nm. Difference absorption spectra derived from titration FPIX (**9**) ranged in intensity from ≥ 0.010 a.u. to ≤ 0.04-0.08 a.u. Digested titration data were corrected for dilution and corresponding binding isotherms were analyzed using a nonlinear curve fitting model.

6.4 Mass Spectrometry Experiments

6.4.1 Sample Preparation

Stock solutions were prepared daily of FPIX (**9**) using hemin chloride and contained 5 mM in MeOH with one drop of amoniak added to 1 mL of stock soltution, while those of chloroquine (**2**), dioncophylline A (**8**), dioncophylline C (**6**), dioncopeltine A (**7**), korupensamine A (**46**), and ancistrocladine (**35**), contained 5 mM of the drug in MeOH:H_2O (3:1; vol/vol). Mixtures of the drugs with FPIX (**9**) were prepared in different drug:FPIX (**9**) ratios starting from the stock solutions, and subsequently diluted with a stock solution to give a mixture MeOH:H_2O (3:1; vol/vol) in the final sample. The final pH of the solutions was measured to be about 7. Drug-FPIX (**9**) mixtures with a molar concentration ratio 1:1 contained 250 µM drug and 250 µM FPIX (**9**) in MeOH:H_2O (3:1; vol/vol); for the drug:FPIX

(**9**) mixtures with a concentration ratio 1:2 the concentration of the drug was 125 μM, while that of FPIX (**9**) was 250 μM in MeOH:H_2O (3:1; vol/vol). The final mixtures were subjected to electrospray ionization mass spectrometry or to collision-induced dissociation tandem mass spectrometry.

6.4.2 Mass Spectrometry

ESI MS and HRMS (ESI) mass spectra were recorded on a Bruker Daltonics microTOF focus (Chapter Ex. 1.1).

6.4.3 Mass Spectroscopy of FPIX (9)

MS (ESI-pos): *m/z* (%) = 616 (79) $[M (\mathbf{9})]^+$, 1231 (100) $[M (\mathbf{12})]^+$, 1249 (58) $[M (\mathbf{11})]^+$.

6.4.4 Mass Spectroscopy of Chloroquine (2) – FPIX (9) (1:1)

MS (ESI-pos): *m/z* (%) = 320 (100) $[M (\mathbf{2})]^+$, 616 (33) $[M (\mathbf{9})]^+$, 935 (48) $[M (\mathbf{2}) + M (\mathbf{9})\text{-}H]^+$, 1231 (15) $[M (\mathbf{12})]^+$, 1249 (42) $[M (\mathbf{11})]^+$, 1551 (10) $[M (\mathbf{2}) + M (\mathbf{12})\text{-}H]^+$, 1568 (57) $[M (\mathbf{2}) + M (\mathbf{11})\text{-}H]^+$.

6.4.5 Mass Spectroscopy of Dioncophylline C (6) – FPIX (9) (1:1)

MS (ESI-pos): *m/z* (%) = 364 (46) $[M (\mathbf{6})+H]^+$, 616 (42) $[M (\mathbf{9})]^+$, 979 (100) $[M (\mathbf{6}) + M (\mathbf{9})]^+$, 1231 $[M (\mathbf{12})]^+$ (12), 1594 (13) $[M (\mathbf{6}) + M (\mathbf{12})+H]^+$.

6.4.6 Mass Spectroscopy of Dioncopeltine A (7) – FPIX (9) (1:1)

MS (ESI-pos): *m/z* (%) = 380 (11) $[M (\mathbf{7}) +H]^+$, 616 (17) $[M (\mathbf{9})]^+$, 995 (100) $[M (\mathbf{7}) + M (\mathbf{9})]^+$, 1610 (18) $[M (\mathbf{7}) + M (\mathbf{12})+H]^+$.

6.4.7 Mass Spectroscopy of Dioncophyline A (8) – FPIX (9) (1:1)

MS (ESI-pos): *m/z* (%) = 378 (58) $[M (\mathbf{8})+H]^+$, 616 (34) $[M (\mathbf{9})]^+$, 993 (100) $[M (\mathbf{8}) + M (\mathbf{9})]^+$, 1231 (15) $[M (\mathbf{12})]^+$, 1609 (34) $[M (\mathbf{8}) + M (\mathbf{12})+2H]^+$.

6.4.8 Mass Spectroscopy of Korupensamine A (46) – FPIX (9) (1:1)

MS (ESI-pos): *m*/*z* (%) = 380 (27) [M (**46**)+H]$^+$, 616 (25) [M (**9**)]$^+$, 995 (100) [M (**46**) + M (**9**)]$^+$, 1610 (9) [M (**46**) + M (**12**)+H]$^+$.

6.4.9 Mass Spectroscopy of Ancistrocladine (35) – FPIX (9) (1:1)

MS (ESI-pos): *m*/*z* (%) = 408 (65) [M (**35**)+H]$^+$, 616 (33) [M (**9**)]$^+$, 1023 (100) [M (**35**) + M (**9**)]$^+$, 1642 (7) [M (**35**) + M (**12**)+2H]$^+$.

6.5 Spin State Determination, Evans Experiments

For the experiments in pure aqueous medium stock solutions of FPIX (**9**) were prepared by solving hemin chloride in 0.05 NaOD in D_2O by ultrasonic assistance (30 min), in a concentration of 10 mM. For the experiments MeOD stock solutions of FPIX (**9**) were prepared by solving hemin chloride in MeOD, in a concentration of 10 mM. The FPIX (**9**) stock solutions were prepared daily and prior to use centrifuged by 150 × g for 10 min and subsequently the exact concentration in the supernatant was determined by a standard curve prepared on the analytical HPLC using the chromolith column and method (Chapter Ex. 1.3). Stock solutions of chloroquine (**2**) were prepared in a concentration of 10 mM in D_2O for the experiments in aqueous medium and in MeOD:D_2O (9:1; vol/vol) for the experiments in MeOD. Stock solutions of dioncophylline C (**6**) and dioncopeltine A (**7**) were prepared in D_2O in a concentration of 10 mM.

For the spin state determination experiments a coaxial NMR tube system (WILMAD, *Wilmad-LabGlass*, Buena, NJ, USA) was used. The inner capillary contained 100 µL of an 1 mM 3-(trimethylsilyl)propionic acid-d_4 sodium salt (TSP) solution in D_2O for naphthylisoquinoline alkaloids adjusted to pH 10.5 with 10 mM NaOD and for chloroquine (**2**) with PBS (10 mM pH 6.5 or 9). For determination of the geometry factor the outer capillary contained 1 mM TSP and the standard radical molecule 2,2,6,6-tetramethylpiperidine 1-oxyl (TEMPO) in a concentration of 2 mM. For the actual spin state determination experiments aliquots of the aqueous stock solutions of FPIX (**9**) and of naphthylisoquinoline alkaloids or chloroquine (**2**) were mixed in Eppendorf tubes to give a concentration in the final sample of 1.0 mM FPIX µ-oxo dimer (**11**) and predetermined titration steps of the naphthylisoquinoline alkaloids or chloroquine (**2**) in the range of 0-8 molar equivalents. A stock solution of TSP in D_2O (100 mM) was prepared, and aliquots thereof were added to the samples to give a final concentration of 1 mM TSP. A solution of

D_2O adjusted to pH 10.5 with 10 mM NaOD for the samples with naphthylisoquinoline alkaloids, and with PBS (10 mM, pH 6.5 or 9) for the samples with chloroquine (**2**), was added to give a total sample volume of 500 μL. Argon was gently bubbled through the samples for 30 min to eliminate the paramagnetic oxygen impurities. Subsequently 300 μL of the samples were transferred to the outer tube of a coaxial tube system. Samples in MeOD were prepared accordingly.

6.6 β-Hematin Formation

6.6.1 Preparation of 12.9 M Acetate

NaOAc trihydrate (63.14 g) was suspended in 47.28 mL of glacial acetic acid. Gentle warming at 60 °C with vigorous stirring resulted in complete dissolution. The viscous solution had a volume of 100 mL and a measured pH of 5.0. The pH is critical to the success of the assay and it is equally important that the NaOAc remains dissolved. The solution is supersaturated at room temperature, so upon standing, NaOAc precipitates. This occurs rapidly if pipettes contaminated with NaOAc are used or if no septum is used while pipetting the solution.

6.6.2 Assay for β-Hematin Inhibition

FPIX (**9**) stock solutions (1.680 mM) were prepared by dissolving hemine chloride in 0.1 M NaOH (used within 60 min of preparation). Series of stock solutions of dioncophylline A (**8**), dioncophylline C (**6**), dioncopeltine A (**7**), korupensamine A (**46**), and ancistrocladine (**35**), were prepared by dissolving the naphthylisoquinoline alkaloids in MeOH (84 mM), and subsequently pipetting aliquots thereof and dilute with MeOH to obtain solutions in concentrations predetermined to give 0.01-10 equivalents relative to FPIX (**9**) in the final samples.

15.2 μL of the FPIX (**9**) stock solution were dispensed in a series of Eppendorf tubes (25.3 nmol/Eppendorf tube). Each tube contained 1.52 μL of one of the prepared series of stock solutions of the naphthylisoquinoline alkaloids. After mixing, 8.81 μL of the 12.9 M acetate solution (pH 5.0) preincubated in a thermostated bath at 60 °C were added. The final FPIX (**9**) concentration in the solution was 1 mM and the pH was 4.5 (N.B. achievement of this final pH is critical to the success of the assay). The reaction mixtures were incubated at 60 °C for 60 min. Subsequently, the samples were quenched at room temperature by adding 675 μL of 5% (vol/vol) pyridine (200 mM Hepes, pH 8.2) to buffer the mixtures to a final pH between

7.2 and 7.5. This was followed by adding 825 μL of 5% (vol/vol) pyridine solution (20 mM Hepes, pH 7.5). The solutions were shaken to ensure complete dissolution of FPIX (**9**) and subsequently centrifuged at 150 × g for 5 min. The supernatants were carefully transferred to a cuvette without disturbing the precipitate. The absorbance was measured at 405 nm. The sigmodial dose response curve was analyzed by nonlinear least squares fitting using *GraphPad* prism to determine the number of equivalents of drug required to inhibit β-hematin formation by 50% (IC_{50}).

7 Metabolism Study of Naphthylisoquinoline Alkaloids

7.1 Rat Liver Microsomes

Rat liver microsomes were either purchased by *In Vitro Technologies* or kindly provided by Prof. Dr. W. Dekant's group who prepared them as described in the literature.[248] All liver microsomes used originated from the strain Sprague-Dawly rat. The liver microsomes were stored at –80 °C.

7.2 General Phase 1 and Phase 2 Microsomal Incubation

The complete incubation systems (final volume 1000 µL) contained rat liver microsomal protein (0.8–4 mg/mL), 0.1 M phosphate buffer (pH 7.4) and an NADPH-generating system consisting of 25 mM glucose-6-phosphate, 1 mM $NADP^+$ and 0.5 IU/mL glucose-6-phosphate dehydrogenase. For phase 2 incubations 1.9 mg/mL UDPGA and 100 µg/mL were additionally added.

Before pursuing new experiments as control for the enzyme activity of new batches the rate constants were determined for the formation of 6-β-hydroxylation; standard deviations of 10% were accepted within K_M = 30 nmol/mL and v_{max} = 1200 pmol mL^{-1} mg^{-1} min^{-1}.

7.3 Time Dependent Incubation

For determination of the time dependent biotransformation the microsomal incubations using the general procedure were stopped in predetermined time intervals of 0, 10, 20, 30 min. Additionally, a control was carried out after 30 min incubations without the NADPH generating system.

7.4 Substrate Dependent Incubation

For determination of the substrate dependent biotransformation the microsomal incubations were carried out in predetermined concentrations of 826, 821, 806, 781, 756, and 731 0.1 M phosphate buffer (pH 7.4), and 5.0, 10.0, 25.0, 50.0, 75.0, and 100.0 µL of a naphthylisoquinoline alkaloid stock solution (0.25 M). The reactions were stopped after 20 min. Additionally a control experiment was carried out by incubating for 20 min without the NADPH generating system.

7.5 Enzyme Dependent Incubation

For the determination of the enzyme dependent biotransformation aliquots of a rat liver stock solution (17.59 mg/mL protein) were added to the incubation mixtures to give concentrations of 1.0, 2.0, 3.0, 4.0, 6.0, and 8.0 mg/mL protein. The reactions were stopped after 20 min.

7.6 Phase 1 Investigation of Dioncophylline A (**8**)

The system was preincubated for 5 min at 37 °C, then dioncophylline A (**8**) (concentrations from 13.1 µM to 262 µM) was added and the mixture incubated for 10 to 30 min. The reaction was terminated by adding 1 mL cold methanol (–20 °C). After centrifugation, supernatants of the incubation solutions were analyzed by HPLC-UV. The control incubations were carried out using the same conditions without the NADPH-generating system. Since the metabolites and dioncophylline A (**8**) have identical UV-spectra and presumably similar extinction coefficients, the metabolite formation was quantified by comparison of the peak areas with calibration curves for dioncophylline A (**8**).

HPLC-UV, HPLC-MS analyses of the incubation mixtures and coelution with authentic reference material carried out using the method described in Chapter Ex. 1.3, enabled the identification of the phase 1 metabolites **47** (t_R = 24.3 min) and **48** (t_R = 22.5 min). Separation by preparative HPLC using the method described in Chapter Ex.1.3 gave 0.15 mg and 0.04 mg of the two metabolites, respectively.

7.6.1 5'-*O*-Demethyldioncophylline A (47)

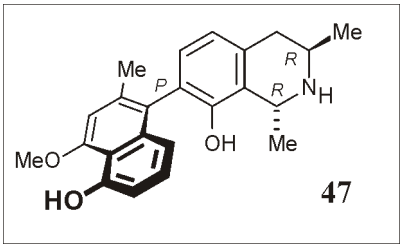

47

Colorless amorphous powder (0.15 mg).

HPLC-UV/Vis: λ_{max} (log ε) = 231 (1.10), 305 (0.52) nm.

HPLC-MS (ESI-pos): *m*/*z* (%) = 364 (40), 332 (30), 202 (35), 188 (100).

^{1}H NMR, CD, and $[\alpha]_D^{20}$ spectroscopic data were identical to the ones reported for the synthetically prepared authentic reference material reported in Chapter Ex. 8.7.1.

7.6.2 Phase 1 Metabolite (48)

Colorless amorphous powder (0.04 mg).

HPLC-UV/Vis: λ_{max} (log ε) = 231 (1.15), 242 (0.58) nm.

HPLC-MS (ESI-pos): *m*/*z* (%) = 376 (10), 362 (100), 202 (40).

7.7 Synthesis of 5'-*O*-Demethyldioncophylline A (47), 4'-*O*-Demethyldioncophylline A (49), and 4',5'-*O*,*O*-Didemethyldioncophylline A (50)

To a solution of 20.0 mg (53 µmol) dioncophylline A (**8**) in 10 mL abs. CH_2Cl_2, 27 mg (107 µmol) BBr_3 were added at –72 °C and the mixture was stirred for 10 min. Then 4 mL MeOH were added slowly. The reaction mixture was allowed to reach ambient temperature, and the solvent was removed in vacuo. The residue was purified by preparative reversed-phase HPLC using the method described in Chapter Ex. 1.3, yielding **47** (20%), 4.0 mg of **49** (21%), and 8.6 mg of **50** (44%).

7.7.1 5'-*O*-Demethyldioncophylline A (47)

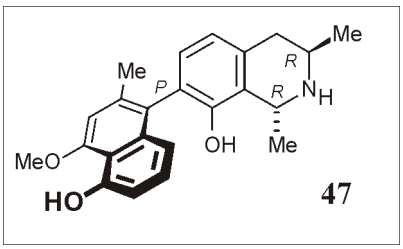

47

Colorless amorphous powder (3.2 mg).

$[\alpha]_D^{20}$ = –15.5 (*c* = 0.2, $CHCl_3$).

Lit.: –11.1 (*c* = 0.015, $CHCl_3$).[238]

UV/Vis (MeOH): λ_{max} (log ε) = 231 (1.14), 306 (0.58) nm.

CD (CH_3CN): λ_{max} ($\Delta\varepsilon$) = 198 (+2.2), 224 (–19.8), 244 (+15.7) nm.

^{1}H NMR (400 MHz, MeOD): δ = 1.15 (d, *J* = 6.3 Hz, 3 H, 3-C*H*$_3$), 1.36 (d, *J* = 6.2 Hz, 3 H, 1-C*H*$_3$), 2.07 (s, 3 H, 2'-C*H*$_3$), 2.44 (dd, *J* = 16.5, 11.0 Hz, 1 H, 4-H$_{ax}$), 2.73 (dd, *J* = 16.5, 3.8 Hz, 1 H, 4-H$_{eq}$), 3.27 (m, 1 H, 3-H), 3.99 (s, 3 H, 4'-OC*H*$_3$), 4.32 (q, 1 H, 1-H), 6.65 (s, 1 H, 3'-H), 6.67 (d, *J* = 7.7 Hz, 1 H, 8'-H), 6.73 (d, *J* = 7.9 Hz, 1 H, 5-H), 6.76 (d, *J* = 7.7 Hz, 1 H, 6'-H), 6.77 (d, *J* = 8.0 Hz, 1 H, 6-H), 7.13 (dd, *J* = 7.9, 7.9 Hz, 1 H, 7'-H).

^{13}C NMR (100 MHz, MeOD): δ = 20.7 (1-Me), 21.1 (3-Me), 22.7 (2'-Me), 37.2 (C-4), 41.5 (C-3), 47.5 (C-1), 56.0 (4'-OMe), 107.1 (C-5), 110.4 (C-6), 113.8 (C-1'), 116.9 (C-8'), 121.0 (C-3'), 122.4 (C-7'), 124.5 (C-6'), 128.3 (C-9), 128.4 (C-10), 135.3 (C-10'), 136.0 (C-9'), 136.2 (C-2'), 149.7 (C-8), 154.5 (C-5'), 156.2 (4').

MS (EI = 70 eV): *m/z* (%) = 363 (23) $[M]^+$, 349 (33) $[M+H-CH_3]^+$, 348 (100) $[M-CH_3]^+$, 333 (18) $[M-2(CH_3)]^+$.

HRMS (ESI): calcd. for $C_{23}H_{25}NO_3$ $[M]^+$: 363.1834; found 363.1837.

The spectroscopic data are in good agreement with those previously published.[238,249]

7.7.2 4'-*O*-Demethyldioncophylline A (49a/49b)

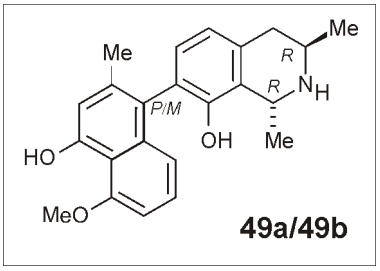

49a/49b

Colorless amorphous powder (2.5 mg).

UV/Vis (MeOH): λ_{max} (log ε) = 231 (1.20), 306 (0.65) nm.

^{1}H NMR (400 MHz, MeOD): δ = 1.24 (d, *J* = 6.3 Hz, 3 H, 3-C*H*$_3$), 1.26 (d, *J* = 6.3 Hz, 3 H, 3-C*H*$_3$), 1.45 (d, *J* = 6.3 Hz, 3 H, 1-C*H*$_3$), 1.48 (d, *J* = 6.4 Hz, 3 H, 1-C*H*$_3$), 2.05 (s, 3 H, 2'-C*H*$_3$), 2.07 (s, 3 H, 2'-C*H*$_3$), 2.63-2.70 (m, 2 H, 4-H$_{ax}$),* 2.80-2.85 (m, 2 H, 4-H$_{eq}$),* 3.37 (m, 2 H, 3-H),* 4.05 (s, 3 H, 5'-OC*H*$_3$), 4.43-4.46 (m, 2 H, 1-H),* 6.64 (d, *J* = 7.5 Hz, 1 H, 8'-H), 6.66 (d, *J* = 7.6 Hz, 1 H, 8'-H), 6.69 (s, 1 H, 3'-H), 6.70 (s, 1 H, 3'-H), 6.75 (d, *J* = 7.9 Hz, 1 H, 6'-H), 6.76 (d, *J* = 7.9 Hz, 1 H, 6'-H), 6.83 (d, *J* = 7.8 Hz, 2 H, 5-H),* 6.88 (d, *J* = 8.0 Hz, 2 H, 6-H),* 7.06 (dd, *J* = 8.0, 7.9 Hz, 1 H, 7'-H), 7.07 (dd, *J* = 8.0, 7.9 Hz, 1 H, 7'-H).

^{13}C NMR (100 MHz, MeOD): δ = 19.9 (1-Me), 20.1 (1-Me), 21.5 (3-Me), 21.8 (3-Me), 22.5 (2'-Me),* 36.2 (C-4),* 44.2 (C-3),* 48.3 (C-1),* 56.8 (5'-OMe),* 105.9 (C-8'), 106.0 (C-8'), 106.8 (C-5),* 110.2 (C-6),* 111.7 (C-3'), 111.8 (C-3'), 114.5 (C-9'),* 117.2 (C-6'),* 122.0 (C-10),* 124.3 (C-1'),* 126.4 (C-7),* 127.4 (C-7'),* 130.1 (C-9),* 132.8 (C-6),* 135.6 (C-2'),* 137.9 (C-10'),* 150.2 (C-8),* 152.4 (4')* 155.6 (C-5').*

*: These signals overlapped for the two isomers.

MS (EI = 70 eV): *m*/*z* (%) = 363 (27) $[M]^+$, 348 (100) $[M\text{-}CH_3]^+$.

HRMS (ESI): calcd. for $C_{23}H_{25}NO_3$ $[M]^+$: 363.1834; found 363.1836.

7.7.3 4',5'-*O*,*O*-Didemethyldioncophylline A (50a/50b)

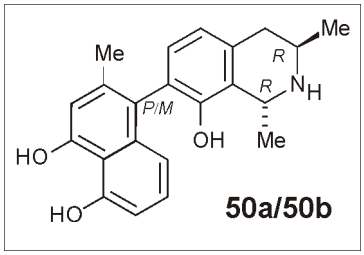

Colorless amorphous powder (6.5 mg).

UV/Vis (MeOH): λ_{max} (log ε) = 231 (1.06), 306 (0.49) nm.

^{1}H NMR (400 MHz, MeOD): δ = 1.43 (d, *J* = 6.4 Hz, 3 H, 3-C*H*$_3$), 1.45 (d, *J* = 6.3 Hz, 3 H, 3-C*H*$_3$), 1.55 (d, *J* = 6.3 Hz, 3 H, 1-C*H*$_3$), 1.60 (d, *J* = 6.4 Hz, 3 H, 1-C*H*$_3$), 2.06 (s, 3 H, 2'-C*H*$_3$), 2.08 (s, 3 H, 2'-C*H*$_3$), 2.83-2.92 (m, 2 H, 4-H$_{ax}$),* 3.12-3.17 (m, 2 H, 4-H$_{eq}$),* 3.84 (m, 2 H, 3-H),* 4.43-4.46 (m, 2 H, 1-H),* 6.65 (d, *J* = 7.7 Hz, 1 H, 8'-H), 6.66 (d, *J* = 7.6 Hz, 1 H, 8'-H), 6.67 (d, *J* = 7.9 Hz, 1 H, 6'-H), 6.68 (d, *J* = 7.9 Hz, 1 H, 6'-H), 6.70 (s, 1 H, 3'-H), 6.72 (s, 1 H, 3'-H), 6.85 (d, *J* = 7.8 Hz, 2 H, 5-H),* 6.92 (d, *J* = 8.0 Hz, 2 H, 6-H),* 7.07 (dd, *J* = 8.1, 7.9 Hz, 1 H, 7'-H), 7.11 (dd, *J* = 8.0, 8.0 Hz, 1 H, 7'-H).

^{13}C NMR (100 MHz, MeOD): δ = 18.1 (1-Me), 19.1 (1-Me), 20.3 (3-Me),* 20.7 (2'-Me),* 35.2 (C-4),* 45.3 (C-3),* 50.0 (C-1),* 107.9 (C-8'), 108.0 (C-8'), 110.8 (C-3'),* 115.2 (C-9'),* 117.2 (C-6'),* 121.2 (C-5),* 121.8 (C-10),* 125.2 (C-1'),* 125.8 (C-7),* 127.8 (C-7'),* 132.4 (C-9),* 133.0 (C-6),* 137.9 (C-2'),* 138.1 (C-10'),* 151.9 (C-8),* 155.4 (4')* 155.7 (C-5').*

*: These signals overlapped for the two isomers.

MS (EI = 70 eV): *m*/*z* (%) = 349 (14) $[M]^+$, 334 (100) $[M\text{-}CH_3]^+$.

HRMS (ESI): calcd. for $C_{22}H_{23}NO_3$ $[M]^+$: 349.1678; found 349.1681.

The spectroscopic data are in good agreement with those previously published.[249]

7.8 Phase 2 Glucuronidation Investigations of Dioncophylline A (8), Dioncopeltine A (7), and Dioncophylline C (6)

The system was preincubated for 5 min at 37 °C, subsequently the respective naphthylisoquinoline alkaloid (concentrations from 13.1 µM to 262 µM) was added and the mixture incubated for 10 to 30 min. The termination and work up of the reactions, as well as the control incubations were carried out as described for the phase 1 incubations (Chapter Ex. 7.6).

7.8.1 Phase 2 Glucuronidation Investigations of Dioncophylline A (8)

HPLC-UV, HPLC-MS analyses of the incubation mixture carried out using the method described in Chapter Ex. 1.3, allowed the identification of the phase 2 glucuronide **51** (t_R = 16.4 min).

7.8.1.1 Phase 2 Glucuronide Metabolite (51) (Presumably: Dioncophylline A-8-*O*-glucuronide)

HPLC-UV/Vis: λ_{max} (log ε) = 231 (1.15), 306 (0.56) nm.

HPLC-MS (ESI-pos): *m*/*z* (%) = 377 (40), 202 (100), 178 (52).

7.8.2 Phase 2 Investigation of Dioncopeltine A (7)

HPLC-UV, HPLC-MS analyses of the incubation mixture carried out using the method described in Chapter Ex. 1.3, allowed the identification of the phase 2 glucuronide **52** (t_R = 14.8 min).

7.8.2.1 Phase 2 Glucuronide Metabolite (52) (Presumably: Dioncopeltine A-5'-*O*-glucuronide)

HPLC-UV/Vis: λ_{max} (log ε) = 231 (1.45), 312 (0.72) nm.

HPLC-MS (ESI-pos): *m*/*z* (%) = 379 (25), 203 (100), 178 (65).

7.8.3 Phase 2 Investigation of Dioncophylline C (6)

HPLC-UV, HPLC-MS analyses of the incubation mixture carried out using the method described in Chapter Ex. 1.3, allowed the identification of the phase 2 glucuronide **53** (t_R = 15.6 min), **54** (t_R = 16.5 min).

7.8.3.1 Phase 2 Glucuronide Metabolite (53) (Presumably: Dioncophylline C-5'-*O*-glucuronide)

HPLC-UV/Vis: λ_{max} (log ε) = 231 (1.45), 306 (0.86) nm.

HPLC-MS (ESI-pos): *m*/*z* (%) = 363 (57), 187 (100), 178 (65).

7.8.3.2 Phase 2 Glucuronide Metabolite (54) (Presumably: Dioncophylline C-5'-*O*,*O*-diglucuronide)

HPLC-UV/Vis: λ_{max} (log ε) = 231 (1.24), 306 (0.56) nm.

HPLC-MS (ESI-pos): *m*/*z* (%) = 539 (15) 362 (10), 187 (100), 178 (65).

References and Annotations

[1] G. B. Mahady; Global harmonization of herbal health claims; *J. Nutr.* **2001**, *131*, 1120s–1123s.

[2] P. Talalay, P. Talalay; The importance of using scientific principles in the development of medicinal agents from plants; *Acad. Med.* **2001**, *76*, 238–247.

[3] M. M. Cowan; Plant products as antimicrobial agents; *Clin. Microbiol. Rev.* **1999**, *12*, 564–582.

[4] Z. X. Shen; Recent research and development in traditional Chinese medicine in China in *Report of the third meeting of directors of WHO collaborating centers for traditional medicine*; WHO Publications Office, Geneva Switzerland **1996**, 7–13.

[5] G. B. Mahady; Medicinal Plants for the prevention and treatment of bacterial infections; *Cur. Pharm. Design* **2005**, *11*, 2405–2427.

[6] J. R. Vane, R. M. Botting; The mechanism of action of aspirin; *Thromb. Res.* **2003**, *110*, 255–258.

[7] X. Slavatella, E. Giralt; NMR-based methods and strategies for drug discovery; *Chem. Soc. Rev.* **2003**, *32*, 365–372.

[8] S. W. Homans; NMR spectroscopy tools for structure-aided drug design; *Angew. Chem.* **2003**, *43*, 290-300; *Angew. Chem. Int. Ed.* **2004**, *43*, 290–300.

[9] A. Lee, J. G. Breitenbucher; The impact of combinatorial chemistry on drug discovery; *Curr. Opin. Drug Discovery Dev.* **2003**, *6*, 494–508.

[10] S. S. Young, N. Ge; Design of diversity and focused combinatorial libraries in drug discovery; *Curr. Opin. Drug Discovery Dev.* **2004**, *7*, 318–324.

[11] G. A. Cordell; Natural products in drug discovery – creating a new vision; *Phytochem. Rev.* **2003**, *1*, 261–273.

[12] G. Folkers, U. Kessler; Random Chemistry: Look for the unexpected; *Curr. Drug Discovery* **2003**, 33–36.

[13] P. Kapkova, E. Heller, M. Unger, G. Folkers, U. Holzgrabe; Random chemistry as a new tool for the generation of small compound libraries: development of a new acetylcholinesterase inhibitor; *J. Med. Chem.* **2005**, *48*, 7496–7499.

[14] G. M. Cragg, J. Newman; Biodiversity: a continuing source of novel drug leads; *Pure Appl. Chem.* **2005**, *77*, 7–24.

[15] S. Class; Pharma overview; *Chem. Eng. News* **2002**, *80*, 39–49.

[16] N. R. Farnsworth, R. O. Akerle, A. S. Bingel, D. D. Soejarto, Z. Guo; Medicinal plants in therapy; *Bull. WHO* **1985**, *63*, 965–981.

[17] W. H. Wernsdorfer, H. Nödel; Molecular markers for drug resistance in malaria: use in treatment, diagnosis and epidemiology; *Curr. Opin. Infect. Dis.* **2003**, *16*, 553–558.

[18] http//:www.who.int

[19] A. D. Buss, R. D. Waigh; Natural products as leads for new pharmaceuticals; in *Burgers medicinal chemistry and drug discovery*; 5th ed., (Hrsg. I. M. E. Wolff), John Willey, New York **1995**, *vol. 1*, 983–1033.

[20] H. Meimberg, P. Dittrich, G. Bringmann, J. Schlauer, G. Heubl; Molecular phylogeny of Caryophyllidae s.l. based on matK sequences with special emphasis on carnivorous taxa; *Plant Biol.* **2000**, *2*, 218–228.

[21] N. Ruangrungsi, V. Wongpanich, P. Tantivatana, H. J. Cowe, P. J. Cox, S. Funayama, G. A. Cordell; Ancistrotectorine a new naphthylisoquinoline alkaloid from *Ancistrocladus tectorius*; *J. Nat. Prod.* **1985**, *48*, 529–535.

[22] G. Bringmann, F. Pokorny; The naphthylisoquinoline alkaloids; in *The Alkaloids*, (Hrsg.: G. A. Cordell), Academic Press, New York, **1995**, *vol. 46*, 127-271.

[23] T. R. Govindachari, P. C. Parthasarathy, T. G. Rajagopalan, H. K. Desai, G. Kartha, S.–M. Lai Chen, K. Nakanishi; Absolute stereochemistry of ancistrocladine and ancistrocladinine; *J. Chem. Soc., Perkin Trans. 1* **1974**, *12*, 1413–1417.

[24] G. Bringmann, M. Wohlfarth, H. Rischer, M. Grüne, J. Schlauer; A new biosynthetic pathway to alkaloids in plants: acetogenic isoquinolines; *Angew. Chem.* **2000**, *112*, 1523–1525; *Angew. Chem. Int. Ed.* **2000**, *39*, 1464–1466.

[25] G. Bringmann, C. Günther, M. Ochse, O. Schupp, S. Tasler; Biaryls in nature: a multi-facetted class of stereochemically, biosynthetically, and pharmacologically intriguing secondary metabolites; in *Progress in the Chemistry of Organic Natural Products*; (Hrsg.: W. Herz, H. Falk, G. W. Kirby, R. E. Moore, C. Tamm), Springer: Wien, **2001**, *Vol. 82*, 1–249.

[26] S. C. Sharma, Y. N. Shukla, J. S. Tandon; Alkaloids and terpenoids of *Ancistrocladus heyneanus*, *Sagittaria sagittifolia*, *Lyonia formosa* and *Hedychium spicatum*; *Phytochemistry* **1975**, *14*, 578–579.

[27] K. P. Manfredi, J. W. Blunt, J. H. Cardellina II, J. B. McMahon, L. L. Pannell, G. M. Cragg, M. R. Boyd; Novel alkaloids from the tropical plant *Ancistrocladus abbreviatus* inhibit cell killing by HIV-1 and HIV-2; *J. Med. Chem.* **1991**, *34*, 3402–3405.

[28] M. R. Boyd, Y. F. Hallock, J. H. Cardellina II, K. P. Manfredi, J. W. Blunt, J. B. McMahon, R. W. Buckheit, G. Bringmann, M. Schäffer, G. M. Cragg, D. W. Thomas, J. G. Jato; Anti-HIV michellamines from *Ancistrocladus korupensis*; *J. Med. Chem.* **1994**, *37*, 1740–1745.

[29] J. B. McMahon, M. J. Currens, R. J. Gulakowski, R. W. Buckheit, C. Lackman-Smith, Y. F. Hallock, M. R. Boyd; Michellamine B, a novel plant alkaloid, inhibits human immunodeficiency virus-induced cell killing by at least two distinct mechanisms; *Antimicrob. Agents Chemother.* **1995**, *39*, 484–488.

[30] G. Bringmann, A. Hamm, C. Günther, M. Michel, R. Brun, V. Mudogo; Ancistroealaines A and B, two new bioactive naphthylisoquinolines, and related naphthoic acids from *Ancistrocladus ealaënsis*; *J. Nat. Prod.* **2000**, *63*, 1465–1470.

[31] A. Ponte-Sucre, J. H. Faber, T. Gulder, I. Kajahn, S. E. H. Pedersen, M. Schultheis, G. Bringmann, H. Moll; Activity of Naphthylisoquinoline Alkaloids and Synthetic Analogs Against *Leishmania major*; *Antimicrob. Agents Chemother*. **2007**, *51*, 188–194.

[32] G. Bringmann, U. Holzgrabe, V. Hörr, G. Stich; Antitrypanosomal naphthylisoquinoline alkaloids and related compounds; *Pharmazie* **2003**, *58*, 343–346.

[33] G. Bringmann, J. Holenz, L. Aké Assi, C. Zhao, K. Hostettmann; Molluscicidal activity of naphthylisoquinoline alkaloids from *Triphyophyllum* and *Ancistrocladus* species; *Planta Med.* **1996**, *62*, 556–557.

[34] G. Bringmann, J. Holenz, L. Aké Assi, K. Hostettmann; Molluscicidal activity (*Biomphalaria glabrata*) of dioncophylline A – structure activity investigations; *Planta Med.* **1998**, *64*, 485–486.

[35] G. François, M. van Looveren, G. Timperman, B. Chimanuka, L. Aké Assi, J. Holenz, G. Bringmann; Larvicidal activity of the naphthylisoquinoline alkaloid dioncophylline A against the malaria vector *Anopheles stephensi*; *J. Ethnopharmacol.* **1996**, *54*, 125–130.

[36] C. Grimm, P. Proksch, S. Gramatzki, C. Schneider, G. Bringmann; Deleterious effects of naphthylisoquinoline alkaloids on survival and growth of *Spodoptera littoralis*; *Planta Med.* **1992**, *58 (Suppl. 1)*, 630.

[37] G. Bringmann, S. Gramatzki, C. Grimm, P. Proksch; Feeding deterrency and growth retarding activity of the naphthylisoquinoline alkaloid dioncophylline A against *Spodoptera littoralis*; *Phytochemistry* **1992**, *31*, 3821–3825.

[38] G. Bringmann, S. Gramatzki, C. Müller, P. Proksch; Structure-activity relationships of naphthylisoquinoline alkaloids: feeding experiments with the herbivorous insect *Spodoptera littoralis*; *Planta Med.* **1993**, *59 (Suppl. 1)*, 624.

[39] G. Bringmann, J. Holenz, B. Wiesen, B. W. Nugroho, P. Proksch; Dioncophylline A as a growth-retarding agent against the herbivorous insect *Spodoptera littoralis*: structure-activity relationships; *J. Nat. Prod.* **1997**, *60*, 342–347.

[40] G. Bringmann, M. Rübenacker, E. Ammermann, G. Lorenz, L. Aké Assi; Dioncophyllines A and B as fungicides; European Patent EP 0515 856 A1, 2 December **1992**.

[41] G. François, G. Bringmann, C. Dochez, C. Schneider, G. Timperman, L. Aké Assi; Activities of extracts and naphthylisoquinoline alkaloids from *Triphyophyllum peltatum*, *Ancistrocladus abbreviatus* and *Ancistrocladus barteri* against *Plasmodium berghei* (Anka strain) *in vitro*; *J. Ethnopharmacol.* **1995**, *46*, 115–120.

[42] G. François, G. Timperman, J. Holenz, L. Aké Assi, T. Geuder, L. Maes, J. Dubois, M. Hancoq, G. Bringmann G; Naphthylisoquinoline alkaloids exhibit strong growth-inhibiting activities against *Plasmodium falciparum* and *P. berghei in vitro* – structure-activity relationships of dioncophylline C; *Ann. Trop. Med. Parasitol.* **1996**, *90*, 115–123.

[43] G. François, G. Timperman, W. Eling, L. Aké Assi, J. Holenz, G. Bringmann; Naphthylisoquinoline alkaloids against malaria: evaluation of the curative potentials of dioncophylline C and dioncopeltine A against *Plasmodium berghei in vivo*; *Antimicrob. Agents Chemother.* **1997**, *41*, 2533–2539.

[44] G. François, B. Chimanuka, G. Timperman, J. Holenz, J. Plaizier-Vercammen, L. Aké Assi, G. Bringmann; Differential sensitivity of erythrocytic stages of the rodent malaria parasite *Plasmodium chabaudi* to dioncophylline B, a highly active naphthylisoquinoline alkaloid; *Parasitol. Res.* **1999**, *85*, 935–941.

[45] G. François, G. Bringmann, J. D. Phillipson, L. Aké Assi, C. Dochez, M. Rübenacker, C. Schneider, M. Wéry, D. C. Warhurst, G. C. Kirby; Activities of extracts and naphthylisoquinoline alkaloids from *Triphyophyllum peltatum*, *Ancistrocladus abbreviatus* and *A. barteri* against *Plasmodium falciparum in vitro*; *Phytochemistry* **1994**, *35*, 1461–1464.

[46] G. Bringmann, S. Gramatzki, R. God, P. Proksch; Enzymatic biotransformation of naphthylisoquinoline alkaloids: first hints at the metabolism of dioncophylline A; *Planta Med.* **1992**, *58 (Suppl. 1)*, 577–578.

[47] A. Rajapakse, N. J. Tiethner-Hooker, S. S. Farid; Modeling of biopharmaceutical drug development pathway and portfolio management; *Comput. Chem. Eng.* **2005**, *29*, 1357–1368.

[48] M. Danhof, J. W. Mandema, A. Hoogerkamp, R. A. Mathot; Pharmacokinetic-pharmacodynamic modeling in pre-clinical investigations: principles and perspectives; *J. Europ. Drug Res.* **1993**, *18*, 41–47.

[49] J. Molzon; The common technical document: the changing face of new drug application; *Nature Reviews: Drug discovery* **2003**, *2*, 71–74

[50] R. W. Snow, C. A. Guerra, A. M. Noor, H. Y. Myint, S. I. Hay; The global distribution of clinical episodes of *Plasmodium falciparum* malaria; *Nature* **2005**, *434*, 214–217.

[51] R. F. Loeb, W. M. Clarke, G. R. Coateney, L. T. Coggeshall, F. R. Dieuaide, A. R. Dochez, E. G. Hakansson, E. K. Marshall, S. C. Marvel, O. R. McCoy, J. J. Sapero, W. H. Serbell, J. A. Shannon, G. A. Carden; Activity of a new antimalarial agent, chloroquine; *J. Am. Med. Assoc.* **1946**, *130*, 1069–1070.

[52] M. Foley, L. Tilley; Quinoline antimalarials: mechanisms of action and resistance; *Int. J. Parasitol.* **1997**, *27*, 231–240.

[53] P. Schlagenhauf, A. Tschopp, R. Johnson, H. D. Nothdurft, B. Beck, E. Schwartz, M. Herold, B. Krebs, O. Veit, R. Allwinn, R. Steffen; Tolerability of malaria chemoprophylaxis in non-immune travellers to sub-Saharan Africa multicentre, randomised, double blind, four arm study, *BMJ* **2003***, 327*, 1078–1083.

[54] M. Foley, M., L. Tilley; Quinoline antimalarials: mechanisms of action and resistance and prospects for new agents; *Pharmacol. Ther.* **1998**, *79*, 55–87.

[55] World Health Organization, *International travel and health 2005*. WHO: Geneva, 2005. http://www.who.int/ith/en/

[56] R. Banerjee, D. E. Goldberg; The Plasmodium food vacuole; in *Antimalarial Chemotherapy*, (Ed.: P. J. Rosenthal), Humana Press, Totowa, New Jersey, **2001**, 43–63.

[57] S. Pagola, P. W. Stephens, D. S. Bohle, A. D. Kosar, S. K. Madsen; The structure of malaria pigment β-haematin; *Nature* **2000**, *404*, 307–310.

[58] P. Loria, S. Miller, M. Foley, L. Tilley; Inhibition of the peroxidative degradation of haem as the basis of action of chloroquine and other quinoline antimalarials; *Biochem. J.* **1999**, *339*, 363–370.

[59] T. J. Egan, K. K. Ncokazi; Quinoline antimalarials decrease the rate of β-hematin form; *J. Inorg. Biochem.* **2005**, *99*, 1532–1539.

[60] C. R. Chonga, D. J. Sullivan Jr.; Inhibition of heme crystal growth by antimalarials and other compounds: implications for drug discovery; *Biochem. Pharmacol.* **2003**, *66*, 2201–2212.

[61] L. M. B. Ursos, P. D. Roepe; Chloroquine resistance in the malarial parasite, *Plasmodium falciparum*; *Med. Res. Rev.* **2002**, *22*, 465–491.

[62] A. Chai, R. Chevli, C. Fitch; Ferriprotoporphyrin IX fulfills the criteria for identification as the chloroquine receptor of malaria parasites; *Biochemistry* **1980**, *19*, 1543–1549.

[63] A. F. G. Slater, A. Cerami; Inhibition by chloroquine of a novel haem polymerase enzyme activity in malaria trophozoites; *Nature* **1992**, *355*, 167–169.

[64] A. F. G. Slater; Chloroquine: Mechanism of drug action and resistance in *Plasmodium falciparum*; *Pharmacol. Ther.* **1993**, *57*, 203–235.

[65] C. A. Homewood, J. M. Jewsbury, M. L. Chance; The pigment formed during haemoglobin digestion by malaria and schistosomal parasites; *Comp. Biochem. Physiol.* **1972**, *43B*, 517–523.

[66] A. Yayon, Z. I. Cabantchik, H. Ginsburg; Susceptibility of human malaria parasites to chloroquine is pH dependent; *Proc. Natl. Acad. Sci. USA* **1985**, *82*, 2784–2788.

[67] H. Ginsburg, T. G. Geary; Current concepts and new ideas on the mechanism of action of quinoline containing antimalairals; *Biochem. Pharmacol.* **1987**, *36*, 1567–1576.

[68] S. N. Cohen, K. O. Phifer, K. L. Yielding; Complex formation between chloroquine and ferrihæmic acid in vitro, and its side effect on the antimalarial action of chloroquine; *Nature* **1964**, 805–806.

[69] A. C. Chou, R. Chevli, C. D. Fitch; Ferriprotoporphyrin IX fulfills the criteria for identification as chloroquine receptor of malaria parasites; *Biochem.* **1980**, *19*, 1543-1549.

[70] T. J. Egan; Interactions of quinoline antimalarials with hematin in solution; *J. Inorg. Biochem*. **2006**, *100*, 916–926.

[71] J. Silver, B. Lukas; Mössbauer studies on protoporphyrin IX iron(III) solutions; *Inorg. Chim. Acta* **1983**, *78*, 219–224.

[72] L. Cheng, J. Lee, D. R. Powell, G. B. Richter-Addo; μ-Oxo-bis[(protoporphyrin IX dimethyl ester)iron(III)]; *Acta Crystallogr.* **2004**, *E60*, m1340–m1342.

[73] T. J. Egan; Physico-chemical aspects of hemozoin (malaria pigment) structure and formation; *J. Inorg. Biochem.* **2002**, *91*, 19–26.

[74] A. D. Wright, H. Wang, M. Gurrath, G. M. König, G. Kocak, G. Neumann, P. Loria, M. Foley, L. Tilley; Inhibition of heme detoxification processes underlies the antimalarial activity of terpene isonitrile compounds from marine sponges; *J. Med. Chem*. **2001**, *44*, 873–885.

[75] V. A. Pashynska, H. Van den Heuvel, M. Claeys, M. V. Kosevich; Characterization of noncovalent complexes of antimalarial agents of the artemisinin-type and FE(III)-heme by electrospray mass spectrometry and collisional activation tandem mass spectrometry; *J. Am. Soc. Mass Spectrom.* **2004***, 15*, 1181–1190.

[76] T. J. Egan, W. W. Mavuso, D. C. Ross, H. M. Marques; Thermodynamic factors controlling the interaction of quinoline antimalarial drugs with ferriprotoporphyrin IX; *J. Inorg. Biochem.* **1997**, *68*, 137–145.

[77] G. Blauer; Optical activity of ferriheme-quinine complexes; *Biochem. Int.* **1983**, *6*, 777–782.

[78] G. Blauer; Interaction of ferriprotoporphyrrin IX with the antimalarials amidoquine and halofantrine; *Biochem. Int.* **1988**, *17*, 729–734.

[79] S. Auparakkitanon, W. Noonpakdee, R. K. Ralph, W. A. Denny, P. Wilairat; Antimalarial 9-anilinoacridine compounds directed hematin; *Antimicrob. Agents Chemother.* **2003**, *47*, 3708–3712.

[80] J. Simplicio; Hemin monomers in micellar sodium laryl sulfate. A spectral and equilibrium study with cyanide; *Biochem.* **1971**, *11*, 2525–2528.

[81] T. J. Egan, K. K. Ncokazi; Effects of solvent composition and ionic strength on the interaction of quinoline antimalarials with ferriprotoporphyrin IX; *J. Inorg. Biochem.* **2004**, *98*, 144–152.

[82] J. Simplicio, K. Schwenzer; Hemin intercalated in micellar cetyltrimethylammonium bromide and trixton X-1 kinetic, spectral, and equilibrium study with cyanide; *Biochem.* **1973**, *12*, 1923–1929

[83] J. Simplicio, K. Schwenzer, F. Maenpa; Kinetics of cyanate and imidazole binding to hemin in micelles; *J. Am. Chem. Soc.* **1975**, *97*, 7319–7326.

[84] J. Hodgkinson, R. B. Jordan; Solvent exchange rates from iron(III) and iron(III)-porphyrin systems; *J. Am. Chem. Soc.* **1973**, *95*, 763–768.

[85] L. Rusnak, R. B. Jordan; Solvent-exchange rates from manganese(III) protoporphyrin IX dimethyl ester by nuclear magnetic resonance line broadning; *Inorg. Chem.* **1972**, *11*, 196–199.

[86] T. J. Egan, R. Hunter, C. H. Kaschula, H. M. Marques, A. Misplon, J. C. Walden; Structure-function relationships in aminoquinolines: effect of amino and chloro groups on quinoline-hematin complex formation, inhibition of β-hematin formation, and antiplasmodial activity; *J. Med. Chem*. **2000**, *43*, 283–291.

[87] C. H. Kaschula, T. J. Egan, R. Hunter, N. Bascilico, S. Parapini, D. Taramelli, E. Pasini, D. Monti; Structure-activity relationships in 4-aminoquinoline antiplasmodials. The role of the group at the 7-position; *J. Med. Chem.* **2002**, *45*, 3531–3539.

[88] G. S. Collier, J. M. Pratt, C. R. De Wet, C. F. Tshabalala; Studies on haemin in dimethyl sulphoxide/water mixtures; *Biochem. J.* **1979**, *179*, 281–289.

[89] S. Moreau, B. Perly, J. Biguet; Interaction of chloroquine with ferriprotoporphyrin IX. Nuclear magnetic resonance study; *Biochimie* **1982**, *64*, 1015–1025.

[90] S. Moreau, B. Perly, C. Chachaty, C. Deleuze; A nuclear resonance study of the interactions of antimalarial drugs with porphyrins; *Biochim. Biophys. Acta* **1985**, *840*, 107–116.

[91] I. Constantinidis, J. D. Satterlee; UV-visible and carbon NMR studies of quinine binding to urohemin I chloride and uroporphyrin I in aqueous solution; *J. Am. Chem. Soc.* **1988**, *110*, 927–932.

[92] I. Constantinidis, J. D. Satterlee; UV-visible and carbon NMR studies of chloroquine binding to urohemin I chloride and uroporphyrin I in aquoeous solution; *J. Am. Chem. Soc.* **1988**, *110*, 4391–4395.

[93] A. Leed, K. DuBay, L. M. B. Ursos, D. Sears, A. C. de Dios, P. D. Roepe; Solution structures of antimalarial drug-heme complexes; *Biochemistry* **2002**, *41*, 10245–10255.

[94] A. C. de Dios, L. B. Casabianca, A. Kosar, P. D. Roepe; Structure of the amodiaquine-FPIX μ-oxo-dimer solution complex at atomic resolution; *Inorg. Chem.* **2004**, *43*, 8078–8084.

[95] A. C. de Dios, R. Tycko, L. M. B. Ursos, P. D. Roepe ; NMR Studies of chloroquine-ferriprotoporphyrin IX complex ; *J. Phys. Chem. A* **2003***, 107*, 5821–5825.

[96] C. Portela, C. M. M. Afonso, M. M. M. Pinto, M. J. Ramos; Definition of an electronic profile of compounds with inhibitory activity against hematin aggregation in malaria parasite; *Bioorg. Med. Chem.* **2004**, *12*, 3313–3321.

[97] C. Portela, C. M. M. Afonso, M. M. M. Pinto, M. J. Ramos; Receptor-drug association studies in the inhibition of the hematin agrregation process of malaria; *FEBS lett.* **2003**, *547*, 217–222.

[98] T. J. Egan; Haemozoin formation as a target for the rational design of new antimalarials; *Drug Des. Rev. Online* **2004**, *1*, 93–110.

[99] M. J. Dascombe, M. G. B. Drew, H. Morris, P. Wilairat, S. Auparakkitanon, W. A. Moule, S. Alizadeh-Shekalgourabi, P. G. Evans, M. Lloyd, A. M. Dyas, P. Carr, F. M. D. Ismail; Mapping antimalarial pharmacophores as a useful tool for the rapid discovery of drugs effective *in vivo*: design, construction, characterization, and pharmacology of metaquine; *J. Med. Chem.* **2005**, *48*, 5423–5436.

[100] P. A. Adams, P. A. M. Berman, T. J. Egan, P. J. Marsh, J. Silver; The iron environment in heme and heme-antimalarial complexes of pharmacological interest; *J. Inorg. Biochem.* **1996**, *63*, 69–77.

[101] H. Abu-Soud, J. Silver; Intermediate spin protoporphyrin(IX) iron(III) complexes; *Inorg. Chim. Acta* **1998**, *52*, 61–66.

[102] G. Blauer, M. Akkawi, W. Fleischhacker, R. Hiessböck; Synthesis and optical properties of the chloroquine enantiomers and their complexes with ferriprotoporphyrin IX in aqueous solution; *Chirality* **1997**, *10*, 556–563.

[103] T. Frosch, B. Küstner, S. Schlücker, A. Szeghalmi, M. Schmitt, W. Kiefer, J. Popp; *In vitro* polarization-resolved resonance Raman studies of the interaction of hematin with the antimalarial drug chloroquine; *J. Raman Spectrosc.* **2004***, 35*, 819–821.

[104] S. Cîntă Pînzaru, N. Peica, B. Küstner, S. Schlücker, M. Schmitt, T. Frosch, J. H. Faber, G. Bringmann, J. Popp; FT-Raman and NIR-SERS characterization of the antimalarial drugs chloroquine and mefloquine and their interaction with hematin; *J. Raman Spectrosc.* **2006**, *37*, 326–334.

[105] B. R. Wood, S. J. Langford, B. M. Cooke, J. Lim, F. K. Glenister, M. Duriska, J. K. Unthank, D. McNaughton; Resonance raman spectroscopy reveals new insight into the electronic structure of β-hematin and malaria pigment, *J. Am. Chem. Soc*. **2004**, *126*, 9233–9239.

[106] J. H. Faber; Isolation and structural elucidation of antiplasmodial compounds from *Ancistrocladus tanzaniensis*; Master Thesis, Danish University of Pharmaceutical Sciences, Copenhagen, **2001**

[107] C. M. Taylor, R. E. Gereau, G. M. Walters; Revision of Ancistrocladus Wall. Ancistrocladaceae; *Ann. Missouri Bot. Gard.* **2005**, *92*, 360–399.

[108] R. E. Gereau; Typification of names in *Ancistrocladus* Wallich (Ancistrocladaceae); *Novon* **1997**, *7*, 242–245.

[109] M. Cheek, C. Frimodt-Møller, V. Hørlyck; A new submontane species of *Ancistrocladus* from Tanzania; *Kew Bull.* **2000**, *55*, 207–212.

[110] G. Bringmann, R. God, M. Schäffer; An improved degradation procedure for determination of the absolute configuration in chiral isoquinoline and β-carboline derivatives; *Phytochemistry* **1996**, *43*, 1393–1403.

[111] I thank Mrs. Michaela Schraut for performing the oxidative degradation.

[112] T. R. Govindachari, P. C. Parthasarathy, H. K. Desai; Ancistrocladine, a minor alkaloid from *Ancistrocladus heyneanus*; *Indian J. Chem.* **1971**, *9*, 1421–1422.

[113] H. A. Nguyen, A. Porzel, H. Ripperger, G. Bringmann, M. Schäffer, R. God, V. S. Tran, G. Adam; Naphthylisoquinoline alkaloids from *Ancistrocladus cochinchinensis*; *Phytochemistry* **1997**, *45*, 1287–1291.

[114] C.–P. Tang, Y.–P. Yang, Y. Zhong, Q.–X. Zhong, H.–M. Wu, Y. Ye; Four new naphthylisoquinoline alkaloids from *Ancistrocladus tectorius*; *J. Nat. Prod.* **2000**, *63*, 1384–1387.

[115] G. Bringmann, R. Zagst, H. Reuscher, L. Aké Assi; Ancistrobrevine B, the first naphthylisoquinoline alkaloid with a 5,8'-coupling site, and related compounds from *Ancistrocladus abbreviatus*; *Phytochemistry* **1992**, *31*, 4011–4014.

[116] G. Bringmann, M. Dreyer, M. Michel, F. S. K. Tayman, R. Brun; Ancistroheynine B and two further 7,3'-coupled naphthylisoquinoline alkaloids from *Ancistrocladus heyneanus* Wall.; *Phytochemistry* **2004**, *65*, 2903–2907.

[117] G. Bringmann, M. Dreyer, J. H. Faber, P. W. Dalsgaard, D. Stærk, J. W. Jaroszewski, H. Ndangalasi, F. Mbago, R. Brun, S. B. Christensen; Ancistrotanzanine C and related 5,1'- and 7,3'-coupled naphthylisoquinoline alkaloids from *Ancistrocladus tanzaniensis*; *J. Nat. Prod.* **2004**, *67*, 743–748.

[118] I thank Dr. M. Dreyer for providing reference material of ancistrotanzanine A and *O*,*N*-dimethylancistrocladine, which he had previously isolated from *A. tanzaniensis*.

[119] G. Bringmann, F. Teltschik, M. Schäffer, R. Haller, S. Bär, M. A. Robertson, M. Isahakia; Ancistrobertsonine A and related naphthylisoquinoline alkaloids from *Ancistrocladus robertsoniorum*; *Phytochemistry* **1998**, *47*, 31–35.

[120] G. Bringmann, F. Teltschik, M. Michel, S. Busemann, M. Rückert, R. Haller, S. Bär, A. Robertson, R. Kaminsky; Ancistrobertsonines B, C, and D as well as 1,2-didehydroancistrobertsonine D from *Ancistrocladus robertsoniorum*; *Phytochemistry* **1999**, *52*, 321–332.

[121] G. Bringmann, K. Messer, R. Brun, V. Mudogo; Ancistrocongolines A-D, new naphthylisoquinoline alkaloids from *Ancistrocladus congolensis*; *J. Nat. Prod.* **2002**, *65*, 1096–1101.

[122] J. Léonard; Ancistrocladaceae; *Bull. Soc. Bot. Belg.* **1949**, *82*, 27–40.

[123] The botanical description of the plant species is in progress.

[124] S. E. H. Pedersen; Isolation of naphthylisoquinoline alkaloids from the leaves of *Ancistrocladus ikela*; Master Thesis, Danish University of Pharmaceutical Sciences, Copenhagen, **2004**.

[125] G. Bringmann, M. Dreyer, H. Kopff, H. Rischer, M. Wohlfarth, H. A. Hadi, R. Brun; *Ent*-Dioncophylleine A, and related dehydrogenated isoquinoline alkaloids, the first Asian Dioncophyllaceae-type naphthylisoquinoline alkaloids, from the "new" plant species *Ancistrocladus benomensis*; *J. Nat. Prod.* **2005**, *68*, 686–690.

[126] G. Bringmann, M. Dreyer, J. H. Faber, P. W. Dalsgaard, D. Stærk, J. W. Jaroszewski, H. Ndangalasi, F. Mbago, R. Brun, M. Reichert, K. Maksimenka, S. B. Christensen; Ancistrotanzanine A, the first 5,3'-coupled naphthylisoquinoline alkaloid, and two further, 5,8'-linked related compounds from the newly described species *Ancistrocladus tanzaniensis*; *J. Nat. Prod.* **2003**, *66*, 1159–1165.

[127] G. Bringmann, M. Dreyer, H. Rischer, K. Wolf, H. A. Hadi, R. Brun, H. Meimberg, G. Heubl; Ancistrobenomin A, the first naphthylisoquinoline oxygenated at Me-3, and related 5,1'-coupled alkaloids, from the "new" plant species *Ancistrocladus benomensis*; *J. Nat. Prod.* **2004**, *67*, 2058–2062.

[128] G. Bringmann, K. Messer, K. Wolf, J. Mühlbacher, M. Grüne, R. Brun, A. M. Louis; Dioncophylline E from *Dioncophyllum tholonnii*, the first 7,3'-coupled dioncophyllaceous naphthylisoquinoline alkaloid; *Phytochemistry* **2002**, *60*, 389–397.

[129] G. Bringmann, M. Rübenacker, P. Vogt, H. Busse, L. Aké Assi, K. Peters, H. G. von Schnering; Dioncopeltine A and dioncolactone A: alkaloids from *Triphyophyllum peltatum*; *Phytochemistry* **1991**, *30*, 1691–1696.

[130] G. Bringmann, M. Rübenacker, R. Weirich, L. Aké Assi; Dioncophylline C from the roots of *Triphyophyllum peltatum*, the first 5,1'-coupled Dioncophyllaceae alkaloid; *Phytochemistry* **1992**, *31*, 4019–4024.

[131] G. Bringmann, M. Rübenacker, T. Geuder, L. Aké Assi; Dioncophylline B, a naphthylisoquinoline alkaloid with a new coupling type from *Triphyophyllum peltatum*; *Phytochemistry* **1991**, *30*, 3845–3847.

[132] G. Bringmann, I. Kajahn, M. Reichert, S. E. H. Pedersen, J. H. Faber, T. Gulder, R. Brun, S. B. Christensen, A. Ponte-Sucre, H. Moll, G. Heubl, V. Mudogo; Ancistrocladinium A and B, the first *N*,*C*-coupled naphthyldihydroisoquinoline alkaloids, from a Congolese *Ancistrocladus* species; *J. Org. Chem.* **2006**, *71*, 9348–9356.

[133] G. Bringmann, K. Messer, M. Wohlfarth, J. Kraus, K. Dumbuya, M. Rückert; HPLC-CD-on-line coupling in combination with HPLC-NMR und HPLC-MS/MS for the determination of the full absolute stereostructure of new metabolites in plant extracts; *Anal. Chem.* **1999**, *71*, 2678–2686.

[134] G. Bringmann, J. Mühlbacher, M. Reichert, M. Dreyer, J. Kolz, A. Speicher; Stereochemistry of isoplagiochin C, a macrocyclic bisbibenzyl from liverworts; *J. Am. Chem. Soc.* **2004**, *126*, 9283–9290.

[135] J. M. Wanjohi, A. Yenesew, J. O. Midiwo, M. Heydenreich, M. G. Peter, M. Dreyer, M. Reichert, G. Bringmann; Three dimeric anthracene derivatives from the fruits of *Bulbine abyssinica*; *Tetrahedron* **2005**, *61*, 2667–2674.

[136] J. J. P. Stewart; Optimization of parameters for semiempirical methods I. method; *J. Comput. Chem.* **1989**, *10*, 209–220.

[137] a) A. D. Becke; A new mixing of hartree-fock and local density-functional theories; *J. Chem. Phys.* **1993**, *98*, 1372–1377. b) A. D. Becke; The role of exact exchange; *J. Chem. Phys.* **1993**, *98*, 5648–5652.

[138] A. A. Frost, R. G. Pearson; Kinetik und Mechanismen homogener chemischer Reaktionen; Verlag Chemie GmbH, Weinheim/Bergstr. **1964**, 173–174.

[139] L. Ernst; Isolierbare Konformationsisomere; *Chemie Uns. Zeit* **1983**, *17*, 21–30.

[140] S. E. Boiadjiev, D. A. Lightner; Atropisomerism in monopyrroles; *Tetrahedron: Asymmetry* **2002**, *13*, 1721–1732.

[141] Clayden, J.; Greeves, N.; Warren, S.; Wothers; *Organic Chemistry*; Oxford University Press, Oxford, **2001**, p. 450.

[142] G. Bringmann, C. Rummey; 3D-QSAR Investigations on antimalarial naphthylisoquinoline alkaloids, by comparative molecular similarity indices analysis (CoMSIA), based on different alignment approaches; *J. Chem. Inf. Comput. Sci.* **2003**, *43*, 304–316.

[143] N. Stiefl, G. Bringmann, C. Rummey, K. Baumann; Evaluation of extended parameter sets for the 3D-QSAR technique MaP: implications for interpretability and model quality exemplified by antimalarially active naphthylisoquinoline alkaloids; *J. Comput-Aided Mol. Des.* **2003**, *17*, 347–365.

[144] G. Bringmann, M. Wohlfarth, H. Rischer, J. Schlauer, R. Brun; Extract screening by HPLC coupled to MS-MS, NMR, and CD: a dimeric and three monomeric naphthylisoquinoline alkaloids from *Ancistrocladus griffithii*; *Phytochemistry* **2002**, *61*, 195–204.

[145] Z. Chen, B. Wang, K. Qin, B. Zhang, Q. Su, Q. Lin; Isolation and identification of alkaloids from *Ancistrocladus tectorius*; *Yaoxue Xuebao* **1981**, *16*, 519–523.

[146] T. R. Govindachari, P. C. Parthasarathy, T. G: Rajagopalan, H. K. Desai, K. S. Ramachandran, E. Lee; Hamatine, a new isoquinoline alkaloid from *Ancistrocladus hamatus*; *Indian J. Chem.* **1975**, *13*, 641–643.

[147] G. Bringmann, J. H. Faber, J. Spuziak, S. E. H. Pedersen, T. Gulder, G. Heubl, S. Brøgger Christensen, R. Brun, V. Mudogo; Six novel naphthylisoquinoline alkaloids and a related benzopyranonecarboxylic acid from a Congolese *Ancistrocladus* species; *Phytochemistry*, submitted.

[148] T. R. Govindachari, P. C. Parthasarathy, H. K. Desai, M. T. Saindane; On the absolute stereochemistry of hamatine; *Indian J. Chem.* **1977**, *15B*, 871–872.

[149] G. Bringmann, S. Busemann; Quantumchemical calculation of CD spectra: the absolute configuration of biologically active natural products; in *Natural Product Analysis* (Hrsg.: P. Schreier, M. Herderich, H.–U. Humpf, W. Schwab), Friedr. Vieweg & Sohn Verlagsgesellschaft mbH, Wiesbaden **1998**, 195–211.

[150] T. R. Govindachari, P. C. Parthasarathy; Ancistrocladine, a novel isoquinoline alkaloid from *Ancistrocladus heyneanus* Wall.; *Indian J. Chem.* **1970**, *8*, 567–569.

[151] N. H. Anh, A. Porzel, H. Ripperger, G. Bringmann, M. Schäffer, R. God, T. V. Sung, G. Adam; Naphthylisoquinoline alkaloids from *Ancistrocladus cochinchinensis*; *Phytochemistry* **1997**, *45*, 1287-1291.

[152] G. Bringmann, R.–M. Pfeifer, P. Schreiber, K. Hartner, M. Schraut, M. Breuning; The 'lactone method': enantioselective preparation of novel P,N-biaryl ligands and their use in the synthesis of the biarylic alkaloids, ancistrotanzanine B and ancistroealaine A; *Tetrahedron* **2004**, *60*, 4349–4360.

[153] G. Bringmann, A. Hamm, M. Schraut; Atroposelective biaryl coupling with chiral catalysts: total synthesis of the antileishmanial naphthylisoquinoline alkaloids ancistrotanzanine B and ancistroealaine A.; *Org. Lett.* **2003**, *5*, 2805–2808.

[154] T. Frosch, M. Schmitt, K. Schenzel, J. H. Faber, G. Bringmann, W. Kiefer, J. Popp; *In-vivo* localization and identification of the antiplasmodial active alkaloid dioncophylline A in the tropical liana *Triphyophyllum peltatum* by a combination of fluorescence, FTIR Raman microscopy and DFT calculations; *Biopolym. Biospectrosc.* **2006**, *82*, 295–300.

[155] R. Schmid; Die systematische Stellung der Dioncophyllaceen; *Bot. Jahrb. Syst.* **1964**, *83*, 1–56.

[156] H. K. Airy Shaw; On the Dioncophyllaceae, a remarkable new family of flowering plants; *Kew Bull*. **1951**, *3*, 327–347.

[157] G. Bringmann, M. Wenzel, H. Bringmann, J. Schlauer, L. Aké Assi; Die "Teilzeit-fleischfressende" Pflanze *Triphyophyllum peltatum* (Dioncophyllaceae): Nutzung der Fangorgane zur Erforschung der Alkaloidbildung; *Der Palmengarten* **1996**, *60*, 32–37.

[158] G. Bringmann, G. François, L. Aké Assi, J. Schlauer; The alkaloids from *Triphyophyllum peltatum* (Dioncophyllaceae); *Chimia* **1998**, *52*, 18–28.

[159] G. Bringmann, D. Feineis; Novel antiparasitic biaryl alkaloids from Westafrican Dioncophyllaceae plants; *Act. Chim. Thérapeut.* **2000**, *26*, 151–171.

[160] Doris Feineis, unpublished results **2005**.

[161] http://www.kromaton.com

[162] A. P. Foucault, P. Durand, E. Camacho Frias, F. Le Goffic; Bisphatic mixture of water, dimethylsulfoxide, and tetrahydrofuran for use in centrifugal partition chromatography; *Anal. Chem.* **1993**, *65*, 2150–2154.

[163] A. P. Foucault; Countercurrent chromatography; *Anal. Chem.* **1991**, *63*, 569A–579A.

[164] Y. Ito; Golden rules and pitfalls in selecting optimum conditions for high-speed counter current chromatography; *J. Chromatogr. A*. **2005**, *1065*, 145–168.

[165] A. Berthod, B. Billardello; Test to evaluate countercurrent chromatographs. Liquid stationary phase and chromatographic resolution; *J. Chromatogr. A*. **2000**, *902*, 323–335.

[166] J.–H. Renault, J.–M. Nuzillard, O. Intes, A. Maciuk; Solvent system in *Countercurrent chromatography. The support-free liquid stationary phase*; A. Berthod, Ed.; Elsvier, Amsterdam **2002**, 49–83.

[167] G. Lang, Isolierung und Charakterisierung neuer Naturstoffe aus Schwamm-assoziierten Mikroorganismen, Dissertation, Universität Würzburg, **2004**.

[168] G. Bringmann, J. R. Jansen, A. Hille, H. Reuscher; *Symp. Colloq. Int., Plantes Méd. Subst. Origine Nat., 6th*, Angers, France **1988**, 181–207.

[169] G. Bringmann, K. Messer, B. Schwöbel, R. Brun, L. Aké Assi; Habropetaline A, an antimalarial naphthylisoquinoline alkaloid from *Triphyophyllum peltatum*; *Phytochemistry* **2003**, *62*, 345–349.

[170] G. Bringmann, C. Günther, W. Saeb, J. Mies, R. Brun, L. Aké Assi; 8-*O*-Methyldioncophyllinol B and revised structures of other 7,6'-coupled naphthylisoquinoline alkaloids from *Triphyophyllum peltatum* (Dioncophyllaceae); *Phytochemistry* **2000**, *54*, 337–346.

[171] J. F. Wishart; Photochemistry and radiation chemistry: a perspective in *Photochemistry and Radiation Chemistry: Complementary Methods for the Study of Electron Transfer* (J. F. Wishart and D. G. Nocera); vol. 254 of *Advances in Chemistry*, Oxford University Press, Washington, DC **1998**, 1–4.

[172] S. C. Lindt; *Radiation Chemistry of Gases*; American Chemical Society Monograph Series, New York **1961**.

[173] A. Mozumder; *Fundamentals of Radiation Chemistry*; Academic Press, San Diego, London **1999**.

[174] H. Wilkinson Richter; Radiation Chemistry: Principles and applications in *Photochemistry and Radiation Chemistry: Complementary Methods for the Study of Electron Transfer*: J. F. Wishart and D. G. Nocera; vol. 254 of *Advances in Chemistry*, Oxford University Press, Washington, DC **1998**, 5–33.

[175] J. Kroh; *Early Developments in Radiation Chemistry*; Royal Society of Chemistry, Cambridge **1989**.

[176] H. Schwarz; Free radicals generated by radiolysis of aqueous solutions; *J. Chem. Edu.* **1981**, *58*, 101–105.

[177] R. J. Woods, A. K. Pikaev; *Applied Radiation Chemistry: Radiation Processing*; Wiley Interscience Publication, New York **1994**.

[178] G. Klein, R. Schüler; Oxidation of benzene by radiolytically produced OH radicals; *Radiation Phys. Chem.* **1974**, *11*, 167–171.

[179] K. Bhatia; Reactions of the radiolytically generated hydroxycyclohexadienyl radical in aqueous benzene systems; *Rad. Res.* **1974**, *59*, 537–555.

[180] M. Eberhardt; Hydroxylation and phenylation of benzene; *J. Phys. Chem.* **1974**, *78*, 1795–1797.

[181] S. Gordon, A. Van Dyken, T. Doumani; Identification of products in the radiolysis of liquid benzene; *J. Phys. Chem.* **1957**, *62*, 20–24.

[182] N. H. Sagert, R. MacFarlane, W. Kremers; Isotopic exchange; *Rad. Phys. Chem.* **1991**, *38*, 407–411.

[183] U. Kessler, Random synthesis and biological characterization of nucleoside analogs – new perspectives for drug discovery, Dissertation, Swiss Federal Institute of Technology, **2000**.

[184] A. Wuhrmann, Gamma-ray synthesis of tyrosine kinase inhibitors: a new method for the design of chemical inhibitors, Dissertation, Swiss Federal Institute of Technology, **2005**.

[185] R. E. Desjardins, C. J. Canfield, J. D. Haynes, J. D. Chulay; Quantitative assessment of antimalarial activity *in vitro* by a semiautomated microdilution technique; *Antimicrob. Agents Chemother*. **1979**, *16*, 710–718.

[186] E. Spath, F. Galinovsky; Dehydrogenation of hydrogenated α-pyridone derivatives; *Ber. Dtsch. Chem. Ges.* **1936**, *69B*, 2059–2061.

[187] C. Cai, J. S. Plummer, D. Conor, D. D. Holsworth, J. J. Edmunds; Synthesis of novel tricyclic aryltriazole-3-thione compounds; *Synth*. *Commun*. **2005**, *35*, 349–356.

[188] A. R. Gangloff, J. Litvak, K. Parajasingham, D. Sperandio; *3,4-Dihydroisoquinolin-1-one derivatives as inducers of apoptosis*; PCT Int. Appl. WO 2004004727, 15 January **2004**.

[189] C. Jeanmart, M. N. Messer, P. E. Simon; Antitussive 3,4-dihydro-1-substituted-isoquinolines; South African Appl. SFXXAB ZA 6901552, 9 October **1969**.

[190] G. D. Diana, B. W. Hinshaw, H. E. Lape; Synthesis and antihypertensive activity of 1-amino-3,4-dihydroisoquinolines; *J. Med. Chem*. **1977**, *20*, 449–452.

[191] H. Beaton, P. Hamley, D. J. Nicholls, A. C. Tinker, A. V. Wallace; 3,4-Dihydro-1-isoquinolineamines: A novel class of nitric oxide synthase inhibitors with a range of isoform selectivity and potency; *Bioorg. Med. Chem. Lett.* **2001**, *11*, 1023–1026.

[192] E. Schmitz; New synthesis of three ring C-N-N compounds (diaziridines); *Angew. Chem.* **1959**, *71*, 127.

[193] C. A. Lipinski, F. Lombardo, B. W. Dominy, P. J. Feeney. Experimental and computational approaches to estimate solubility and permeability in drug discovery and development settings. *Adv. Drug Delivery Rev.* **1997**, *23*, 3–25.

[194] G. François, G. Timperman, T. Steenackers, L. Aké Assi, J. Holenz, G. Bringmann; *In vitro* inhibition of liver forms of the rodent malaria parasite *Plasmodium berghei* by naphthylisoquinoline alkaloids – structure-activity relationships of dioncophyllines A and C and ancistrocladine; *Parasitol. Res.* **1997**, *83*, 673–679.

[195] Y. India, K. Shibata; The soret band of monomeric hematin and its changes on polymerization; *Biochem. Biophys. Res. Com.* **1962**, *9*, 323–327.

[196] D. C. Warhurst; The quinine-haemin interaction and its relationships to antimalarial activity; *Biochem. Pharmacol.* **1981**, *30*, 3323–3327.

[197] G. M. König, A. D. Wright, C. K. Angerhorfer; Novel potent antimalarial diterpene isocyanat, isothiocyanats, isonitriles from the tropical sponge *Cymbastela hooperi*; *J. Org. Chem.* **1996**, *61*, 3259–3267.

[198] P. MacCarthy; Simplified experimental route for obtaining Job's curves; *Anal. Chem.* **1978**, *50*, 2165.

[199] D. A. Skoog, D. M. West; Fundamentals of analytical chemistry; Holt, Rinehart and Winston, 3rd ed., New York **1976**, 553–559.

[200] K. A. Connors; Binding constants; Wiley, New York **1987**.

[201] L. Fielding; Determination of association constants (Ka) from solution NMR data; *Tetrahedron* **2000**, *56*, 6151–6170.

[202] R. Sudha, S. R. Vippagunta, A. Dorn, A. Bubendorf, R. G. Ridley, J. L. Vennerstrom; Deferoxamine: stimulation of hematin polymerization and antagonism of its inhibition by chloroquine; *Biochem. Pharmacol.* **1999**, *58*, 817–824.

[203] T. J. Egan, R. Hunter, C. H. Kaschula, H. M. Marques, A. Misplon, J. Walden; Structure-function relationships in aminoquinolines: effect of amino and chloro groups on quinoline-hematin complex formation, inhibition of β-hematin formation, and antiplasmodial activity; *J. Med. Chem*. **2000**, *43*, 283–291.

[204] Y. Reichert, unpublished results **2005**.

[205] M. Przybylski, M. O. Glocker; Electrospray mass spectrometry of biomacromolecular complexes with noncovalent interactions – new analytical perspectives for supramolecular chemistry and molecular recognition processes; *Angew. Chem. Int. Ed.* **1996**, *108*, 878–899.

[206] T. D. Veenstra; Electrospray ionization mass spectrometry in the study of biomacromolecular noncovalent interactions; *Biophys. Chem.* **1999**, *79*. 63–79.

[207] Z. Skribanek, L. Balaspiri, M. Mák; Interactions between synthetic amyloid-β-peptide (1-40) and its aggregation inhibitors studied by electrospray ionization mass spectrometry; *J. Mass Spectrom.* **2001**, *36*, 1226–1229.

[208] J. A. Loo; Studying noncovalent protein complexes by electrospray ionization mass spectrometry; *Mass Spectrom. Rev.* **1997**, *16*, 1–23.

[209] Y.–T. Li, Y.–L. Hsieh, J. D. Henion; Studies in heme binding in myoglobin, hemoglobin and cytochrome c by ion spray mass spectrometry; *J. Am. Soc. Mass Spectrom.* **1993**, *4*, 631–637.

[210] T. H. M. Jonckers, S. van Miert, K. Cimanga, C. Bailly, P. Colson, M.–C. De Pauw-Gillet, H. Van den Heuvel, M. Clayes, F. Lemiére, E. L. Esmans, J. Rozenski, L. Quirijnen, L. Maes, R. Dommisse, G. L. F. Lemiére, A. Vlietinck, L. Pieters; Synthesis, cytotoxicity, and antitrypasonomal activity of new neocyptolepine derivates; *J. Med. Chem.* **2002**, *45*, 3497–3508.

[211] K. F. Schwedhelm, M. Horstmann, J. H. Faber, Y. Reichert, G. Bringmann, C. Faber; The novel antimalarial compound dioncophylline C forms a complex with heme in solution; *ChemMedChem*, in press.

[212] K. F. Schwedhelm; Paramagnetische Relaxation in der NMR zur Aufklärung der Molekülstruktur von Antimalaria-Wirkstoffen; Diplomarbeit, Universität Würzburg, **2005**.

[213] D. F. Evans; The determination of the paramagnetic susceptibility of substances in solution by nuclear magnetic resonance; *J. Chem. Soc.* **1959**, 2003–2005.

[214] J. L. Deutsch, S. M. Poling; The determination of paramagnetic susceptibility by NMR; *J. Chem. Educ.* **1969**, *43*, 167–168.

[215] T. J. Egan, J. M. Combrinck, J. Egan, G. R. Hearne, H. M. Marques, S. Ntenteni, B. T. Sewell, P. J. Smith, D. Taylor, D. A. van Schalkwyk, J. C. Walden; Fate of haem iron in the malaria parasite *Plasmodium falciparum*; *Biochem. J.* **2002**, *365*, 343–347.

[216] A. F. G. Slater, W. J. Swiggard, B. R. Orton, W. D. Flitter, D. E. Goldberg, A. Cerami, G. B. Henderson; An iron-carboxylate bond links the heme units of malaria pigment; *Proc. Natl. Acad. Sci. USA* **1991**, 325–329.

[217] T. J. Egan, D. C. Ross, P. A. Adams; Quinoline anti-malarial drugs inhibit spontaneous formation of β-haematin (malaria pigment), *FEBS lett.* **1994**, *352*, 54–57.

[218] A. Dorn, R. Stoffel, H. Matile, A. Bubendorf. R. G. Ridley; Malarial hemozoin/β-haematin supports haem polymerization in the absence of protein, *Nature* **1995**, *374*, 269–271.

[219] D. J. Sullivan, I. Y.Gluzman, D. G. Russell, D.E. Goldberg; On the molecular mechanism of chloroquine's antimalarial action; *Proc. Natl. Acad. Sci. USA* **1996**, *93*, 11865–11870.

[220] C. D. Fitch, G. Z. Cai, Y. F. Chen., J. D. Shoemaker; Involvement of lipids in ferriprotoporphyrin IX polymerization in malaria; *Biochim. Biophys. Acta* **1999**, *1454*, 31–37.

[221] S. Parapini, N. Basilico, E. Pasini, T. J. Egan, P. Olliaro, D. Taramelli, D. Monti; Standardization of the physicochemical parameters to assess in vitro the β-haematin inhibitory activity of antimalarial drugs, *Exp. Parasitol.* **2000**, *96*, 249–256.

[222] T. J. Egan, E. Hempelmann, W. W. Mavuso; Characterisation of synthetic β-haematin and effects of the antimalarial drugs quinidine, halofantrine, desbutylhalofantrine and mefloquine on its formation; *J. Inorg. Biochem.* **1999**, *73*, 101–107.

[223] Y. Kurosawa, A. Dorn, M. Kitsujii-Shirane, H. Shimada, T. Satoh, H. Matile, W. Hofheinz, R. Masciardi, M. Kansy, R. G. Ridley, Hematin polymerization assay as a high-throughput screen for identification of new antimalarial pharmacophores; *Antimicrob. Agents Chemother.* **2000**, *44*, 2638–2644.

[224] J. Ziegler, L. Pasierb, K. A. Cole, D. W. Wright; Metalloporphyrin probes for antimalarial drug action; *J. Inorg. Biochem.* **2003**, *96*, 478–486.

[225] K. K. Ncokazi, T. J. Egan; A colometric high-throughput β-hematin inhibition screening assay for use in the search for antimalarial compounds; *Anal. Biochem.* **2005**, *338*, 306–319.

[226] G. G. Gibson, P.Skett; Introduction to Drug Metabolism; Nelson Thornes Publishers, 3rd ed.; United Kingdom **2001**, 1–36.

[227] L. W. Wormhoudt, J. N. M. Commandeur, N. P. E. Vermeulen; Genetic polymorphisms of human *N*-acetyltransferase, epoxide hydrolase enzymes: relevance to xenobiotic metabolism and toxicity; *Crit. Rev. Toxicol.* **1999**, *29*, 59–124

[228] M. J. Derelanko, M.A. Hollinger; Handbook of Toxicology; CRC Press; West Palm Beach **1995**, 539–579.

[229] K. M. L. Crommentuyn, J. H. M. Schellens, J. D. van den Berg, J. H. Beijnen; In-vitro metabolism of anti-cancer drugs, methods and application: paclitaxel, docetaxel, tamoxifen and ifosfamide; *Cancer Treat. Rev.* **1998**, *24*, 345–366.

[230] D. A. Smith, B. C. Jones; Commentary: speculations on the structure activity relationship (SSAR) of cytochrome P450 enzymes; *Biochem. Pharmacol.* **1991**, 2089–2098.

[231] S. A. Wrighton, J.C. Stevens; The human hepatic cytochromes P450 involved in drug metabolism; *Crit. Rev. Tox.* **1992**, *22*, 1–21.

[232] F. C. Lu; Basic Toxicology – Fundamentals, Targets Organs and Risk Assessment; Taylor and Francis, 3rd ed.; Washington DC **1996**, 27–39.

[233] E. F. A. Brandon, C. D. Raap, I. Meijerman, J. H. Beijnen, J. H. D. Schellens; An update on in vitro test methods in human hepatic drug biotransformation research: pros and cons; *Toxicol. Appl. Pharmacol.* **2003**, *189*, 233–246.

[234] N. Plant; Strategies for using in vitro screens in drug metabolism; *Drug Discovery Today* **2004**, *9*, 328–336.

[235] M. V. S. Varma, Y. Ashokraj, C. S. Dey, R. Panchagunla; P-glycoprotein inhibitors and their screening: a perspective from bioavailability enhancement; *Pharm. Res.* **2003**, *48*, 347–359.

[236] A. Braun, S. Hämmerle, K. Suda, B. Rothen-Rutishauser, M. Günthert, S. D. Krämer, H. Wunderlei-Allenspach; Cell cultures as tools in biopharmacy; *Eur. J. Pharm. Sci.* **2000**, *11*, S51–S60.

[237] V. Bickert; Identifizierung und Charackterisierung eines Metaboliten von Dioncophyllin A; F-Praktikums-Bericht, Universität Würzburg, **2001**, 1–25.

[238] G. Bringmann, W. Saeb, R. God, M. Schäffer, G. François, K. Peters, E.–M. Peters, P. Proksch, K. Hostettmann, L. Aké Assi; 5'-*O*-demethyldioncophylline A, a new antimalarial alkaloid from *Triphyophyllum peltatum*; *Phytochemistry* **1998**, *49*, 1667–1673.

[239] F. Santavy; The effect of hydroxy, methoxy and methylenedioxy groups on the ultraviolet spectra of aromatic and heterocyclic compounds — Alkaloids; *Heterocycles* **1980**, *14*, 1159–1172.

[240] O. M. Bakke, R. R. Scheline; Hydroxylation of aromatic hydrocarbons in the rat; *Toxicol. Appl. Pharmacol.* **1970**, *16*, 691–700.

[241] M. Sieber, W. Dekant, J. H. Faber, G. Bringmann; Biotransformation and pharmacokinetics of the antiplasmodial naphthylisoquinoline alkaloid dioncophylline A; *Xenobiotica* **2006**, *36*, 750–762.

[242] I thank Dr. Y. Ye's group for providing an authentic sample of ancistrotectoriline, isolated from *A. tectorius*.[114]

[243] T. R. Govindachari, P. C. Parthasarathy; Ancistrocladine, a new type of isoquinoline alkaloid from *Ancistrocladus heyneanus*; *Tetrahedron* **1971**, *27*, 1013–1026.

[244] M. A. Rizzacasa, M. V. Sargent; The total synthesis of (-)-*O*-methylancistrocladine and (+)-*O*-methylhamatine and their enantiomers; *J. Chem. Soc. Perkin Trans. 1* **1991**, *4*, 845–854.

[245] G. Bringmann, M. Rübenacker, J. R. Jansen, D. Scheutzow, L. Aké Assi; On the structure of the Dioncophyllaceae alkaloids dioncophylline A (″triphyophylline″) and ″*O*-methyl-triphyophylline″; *Tetrahedron Lett.* **1990**, *31*, 639–642.

[246] G. Bringmann, M. Wenzel, M. Ruckert, K. Wolf, S. Busemann, M. Schäffer, L. Aké Assi; Dioncophyllinol D, the first 4-hydroxylated naphthylisoquinoline alkaloid, from the leaves of *Triphyophyllum peltatum*; *Heterocycles* **1998**, *47*, 985–990.

[247] K. Yu. Koltunov, G. K. Surya Prakas, G. Rasul, G. A. Olah; Superacidic activation of 1- and 3-isoquinolinols and their electrophilic reactions; *J. Org. Chem.* **2002**, *67*, 8943–8945.

[248] W. Völkel, N. Wolf, M. Derelanko, W. Dekant; Slow oxidation of acetoxime and methylethyl ketoxime to the corresponding nitronates and hydroxyl nitronates by liver microsomes from rats, mice and humans; *Toxicol. Sci.* **1999**, *47*, 144–150.

[249] W. Saeb, Synthese biologisch aktiver mono- und dimerer Naphthylisochinolin-Alkaloide sowie Isolierung und Strukturaufklärung von Naturstoffen aus tropischen Heilpflanzen, Dissertation, Universität Würzburg, **2001**.